Enhancement of the mechanical performance of semi-crystalline polyamides by tailoring the intermolecular interaction in the amorphous phase

Naji Hussein

N° d'ordre 2013ISAL0140
Année 2013

Thèse

Enhancement of the mechanical performance of semi-crystalline polyamides by tailoring the intermolecular interaction in the amorphous phase

Présentée devant
L'institut national des sciences appliquées de Lyon

Pour obtenir
Le grade de docteur

Formation doctorale
Ingénierie des Matériaux Polymères et Composites

École doctorale
École Doctorale Matériaux de Lyon

Par
Naji Hussein
(Ingénieur)

Soutenue le 09 Décembre 2013 devant la Commission d'examen

Jury MM.

P. Cassagnau	Professeur (LMPB-UCBL 1)
L-A. Fillot	Docteur (Solvay-R&I centre-Lyon), Correspondant industriel
G-H. Hu	Professeur (INPL-ENSIC Nancy), Rapporteur
L. Laiarinandrasana	Professeur (CNRS) (Mines ParisTech)
D. Long	Directeur de recherche (CNRS) (LPMA), Directeur de thèse
Y. Marco	Directeur de recherche (LBMS-ENSTA Bretagne), Rapporteur
R. Seguela	Directeur de recherche (CNRS) (INSA de Lyon)

Abstract

The use of polyamides in the automotive industry has grown significantly over the last years with the demand to reduce vehicle weight and also to increase fuel efficiency. Polyamide 66 having excellent chemical resistance, mechanical strength and toughness becomes the largest engineering thermoplastic used in automotive components. These latter are often submitted to repeated stress during service and their mechanical properties decline progressively until the failure. E. Mourglia-Seignobos (thesis 2009), pointed out that damage of polyamide 66 involves voids nucleation and growth in the amorphous phase. In order to improve the durability of this material, we tailored the cohesive energy of its amorphous phase by introducing phenolic moieties offering strong intermolecular H-bonds interactions.

We proposed a preparation method of block copolyamides containing aliphatic polyamide 66 and phenolic groups (PA6HIA) by reactive extrusion. Microstructural characterizations pointed out that crystalline properties of resulting copolymers are not significantly altered at low PA6HIA content and that reactive extrusion is more appropriate than the in-situ copolymerization for the preparation of these materials. We showed that PA66/6HIA copolyamides having undisturbed crystalline features exhibit superior mechanical performance than the standard PA66, particularly longer lifetime under cyclic loading.

The results of this work put in evidence the impact of the amorphous phase on the ultimate properties of semi-crystalline polymers in one hand, and open the way to a better increase of the durability of these materials by improving their crystalline features in another hand.

Key words: Semi-crystalline polymer, Polyamide, Hydrogen bond, Block copolymer, Reactive extrusion, Microstructure, Free surface energy, Amorphous phase, Crystallite size perfection, Cavitation, Impact, Fatigue, Failure.

Résumé

L'utilisation du Polyamide 66 dans l'industrie automobile est en forte croissance car il offre à un bon compromis légèreté/propriétés mécaniques pour les applications de structure. A noter que pendant le service d'un véhicule, les pièces en polyamides sont souvent soumises à des sollicitations mécaniques très sévères aboutissant à une dégradation progressive du matériau. Récemment. E. Mourglia-Seignobos (thèse 2009), a montré que l'endommagement du polyamide 66 implique des mécanismes de cavitation et de microcraquelure dans la phase amorphe. Afin d'améliorer la durabilité de ce matériau, nous avons modifié la cohésion de sa phase amorphe via l'introduction de fonction phénolique à forte interactions intermoléculaires.

Nous proposons une méthode de préparation de copolyamides bloc, à base du polyamide 66 et des noyaux phénoliques, par extrusion réactive. Nous montrons que, contrairement à la co-polycondensation classique, la structure cristalline de ces copolymères n'a pas été significativement modifiée, surtout à faible taux de PA6HIA. Les propriétés mécaniques et particulièrement la tenue en fatigue de ces copolymères dépassent largement celles du PA66.

Les résultats obtenus mettent en évidence l'impact de la cohésion de la phase amorphe sur les propriétés ultimes de polymères semi-cristallins d'une part, et ouvrent la voie vers une meilleure augmentation de la durabilité de ces matériaux via le perfectionnement de leur phase cristalline d'autre part.

Contents

Aim and outline of the thesis

This PhD work was carried out at the "Laboratoire des Polymères et Matériaux Avancés (LPMA)", a joint research unit between the CNRS and Solvay (UMR 5268). This study was done within the framework of development of sustainable polyamide based materials for structural applications in the automotive industry.

Polyamide is known for its balance of stiffness, strength and toughness as well as for its chemical resistance to hydrocarbon products. Accordingly, neat and glass fiber reinforced polyamides, being lighter, have been widely used to replace the metal in engineering applications. In such applications, the polymeric parts are often submitted to repeated stresses and their mechanical properties decline progressively leading to failure at relatively low stresses. In a previous work, done by E. Mourglia-Seignobos, at the LPMA (2009), the drop of mechanical properties under continuous loading was explained in terms of a damage accumulation mechanism, mainly by voids nucleation and microcracking, which triggers for a given damage level at a given stress the ultimate failure.

Thus, it could be considered to reduce the damage occurring under loading either by preventing the voids nucleation or by repairing the generated microcracks in order to get sustainable and durable solutions based on polymeric materials. Many works have been conducted on polymeric material in order to develop a crack repair capability of these materials. Of particular interest, we can note the inclusion of microcapsules containing a "healing agent" or the introduction of functions with reversible bonds in the polymeric chains that contributes to the healing of voids and microcracks. In the case of polyamides, it is reported that voids nucleation is limited because of their high surface energy which mainly originates from the H-bonds interactions. This means that polyamide materials experience already self-healing processes thanks to the reversible H-bonds network between the amide groups. Thus, the main challenge is to fine tune these intermolecular interactions without altering the other molecular aspects of the polyamide materials. Indeed, from an applicative point of view, it is important to enhance the long term durability of polyamide without deteriorating other performances such as toughness, impact resilience and chemical resistance.

In this work we will try to reduce the damage accumulation in PA66 by enhancing its intrinsic ability to self-healing in order to improve the mechanical performances of polyamide-based materials. In fact, we plan to enhance the cohesive energy of polyamide by the introduction of auto-associative functions, notably phenolic functions offering strong H-bonds interactions. We expect that increasing the energy coming from the H-bonds interactions may reduce the damage developed under loading. Taking into consideration that polyamide 6,6 is a semi-crystalline polymer composed of a rigid crystalline phase and an amorphous phase in which voids nucleation exclusively occurs, it is reasonable to think that modifying the inter-chains interactions in the amorphous phase should have a major influence on the durability of PA6,6.

In order to reach our goal, segmented block copolymers based on polyamide 66 segments and semi-aromatic segments bearing the phenolic functions were synthesized. The effect of

phenolic moieties content and their distribution along the copolymer chains on the physical, thermal and mechanical properties of these copolymers was studied. Differences in the mechanical behavior of the studied samples have been correlated with the observed changes of the molecular characteristics, the crystalline phase and the interlamellar amorphous layers. This work is presented in this manuscript composed of four chapters.

Firstly, a literature review focused on the synthesis and processing of polyamides is presented in the **chapter 1**. A brief description of the microstructure and physical properties of polyamide 66 is given. In the second part of this chapter, the mechanical properties and the failure mechanisms are discussed in the light of the microstructural parameters. This review allowed us to define a strategy for reaching our objective of PA66 fatigue lifetime enhancement. In the **second chapter**, an overall description of the materials and characterization techniques used in this work is presented.

The **third chapter** of this thesis deals with the preparation of semi-crystalline copolyamides with highly cohesive amorphous phase. In this respect, phenolic functions offering strong H-bond interactions were incorporated into the PA66 segment by reactive melt blending. Firstly, the suitable experiment conditions, established at laboratory scale, to incorporate the phenolic group in the amorphous phase without significantly alteration of the crystalline phase are detailed. The preparation of modified polyamide was carried out over a wide composition and the microstructure of the samples was characterized. Then, the reactive extrusion of semi-crystalline modified polyamide 66 at larger scale is described as well as further processing preparation (injection molding).

The **fourth chapter** focuses on the effect of incorporation of strongly associative groups (phenol) on the microstructure and the mechanical properties of the modified polyamide. Firstly, we describe how the phenolic ring alters the amorphous phase (chain mobility) and the crystalline phase (fraction, thickness and perfection) of the modified PA66. On the basis of the analysis of the molecular microstructure, the relationship between the thermal properties and the molecular characteristics of these materials is discussed. In the second part of this chapter, the tensile, impact strength properties and long term mechanical properties are studied. In order to better understand the mechanical performance of modified polyamide, damage mechanisms and deformation processes at the microscopic and nanoscopic scale were characterized. Then, the response of the studied materials under mechanical solicitation is correlated to their molecular and structural features. **Finally,** the general conclusions drawn from the present PhD work are underlined.

1

Introduction

Chapter I: Introduction

Polyamides are widely used as technical polymers, touching applications ranging from synthetic fibers for clothing and end-use market for the general public to industrial and structural applications. Recent report published by Global Industry Analysts (GIA) announces that the global world market for nylon is expected to reach 6.6 million tons by the year 2015. They state that this market growth is primarily driven by the excellent properties offered by nylon and the increasing demand from textiles end-use market, building and automotive industry [1], especially in Asia. In fact, the global world consumption of polyamide resins had exceeded 5.8 million tons in 2010. It is worth noting that 2.4 million tons (around 41 %) of the polyamide resins were used as engineering thermoplastic polymers in several applications (industry, automotive…) as shown in Figure 1.

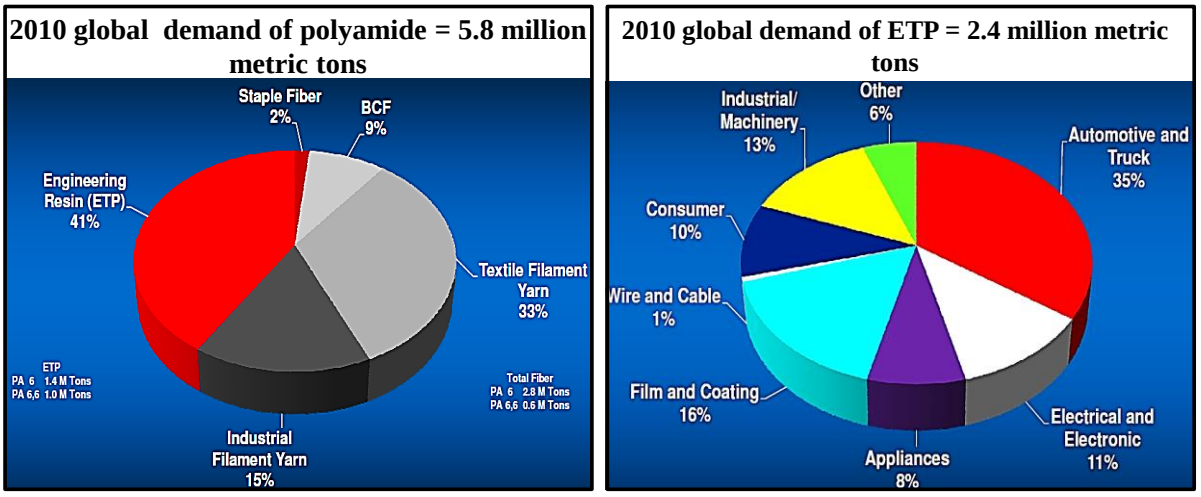

Figure 1: 2010 global demand of : (a) Polyamide;(b) Engineering thermoplastic polyamide (ETP), reprinted from [2]

In this work, we are interested in the polyamide used in the automotive industry, particularly for structural parts located under the hood such as air intake manifolds, cooling system parts, oil pump housings, fuel rails, thermostat components and others. It should be noted that these automotive components are mainly made from glass fiber reinforced and rubber toughened polyamide 66 and/or polyamide 6. Recently, temperatures in the engine compartment have been rising because of reduced space and more powerful engines. Consequently, use of polymers with higher temperature performance such as semiaromatic polyamides (PPA) increased, particularly inside the engine compartment. At high temperatures, the superior stiffness of PPA materials compared to PA66 and PA6 was related to the incorporation of

aromatic ring in the aliphatic structure which enhances the physical properties such as glass transition, aging resistance and solvent resistance.

In order to have a deep understanding of the relationship between the chemistry and the end-use properties of polyamide based materials, this chapter will be mainly focused on the description of the microstructure, mechanical properties and the fracture mechanisms of semi-crystalline polymers. Firstly, a literature review giving fundamental information on the synthesis, processing and microstructure of polyamides, particularly of polyamide 66 is presented. Then, the damage and failure mechanism under static and dynamic load are discussed in the light of various parameters, including molecular architecture, crystallinity and morphology in order to underline the relationship between the microstructure of the polymer and its mechanical properties. In a second part, we state the applicative and scientific issues of this thesis and then we explain the adopted strategy in this work to improve the performance of polyamide-based materials, in particular their sustainability. Finally, on the basis of the literature review and the proposed strategy, the conduct plan of this PhD work is presented.

I. State of the art

To become familiar with the chemical and the structural characteristics of polyamides, basics on polyamides synthesis and processing are presented in a first part, the microstructure and main features of the semi-crystalline polyamide 66 being also described. In a second part, the static and the dynamic mechanical properties as well as the damage mechanism will be described as a function of the microstructure.

Part I: Chemistry, processing and microstructure

1. Polyamides

Polyamides are synthetic polymers that contain an amide group, -CONH-, as a recurring part of the macromolecular chain. These polymers which were first synthesized by Carthors in 1933 and commercialized by Dupont in 1939 as Nylon 66 market for artificial fibers, have experienced considerable development for numerous other applications such as engineering plastics.

1.1. Nomenclature

Polyamides are conventionally identified by the number of carbon atoms in the used monomer. Two monomers are often needed, a diamine and a diacid monomers. Consequently, polyamides are designated by two numbers: the first one corresponds to the number of carbon in the diamine and the second one to that in the diacid. Sometimes acid and

amine functions are carried by the same monomer. In this case, the name is designated by a single digit as is the case of polyamide 6 and polyamide 11.

It should be noted that polyamides can be classified into three groups as a function of the nature of the segments that separate the amide functions: aliphatic, aromatic and semi-aromatic polyamides. The latter group corresponds to the combination of aromatic and aliphatic functionalities.

1.2. **Synthesis of polyamides**

Despite the great diversity of polyamides products, it likely seems that most of them are prepared by polyamidation (polycondensation) between carboxylic acid and amine functions, releasing water as by-product (Figure 2-a). Polyamides made from lactam or aminoacid are mainly prepared by opening ring polymerization and anionic polymerization as shown in Figure 2-b.

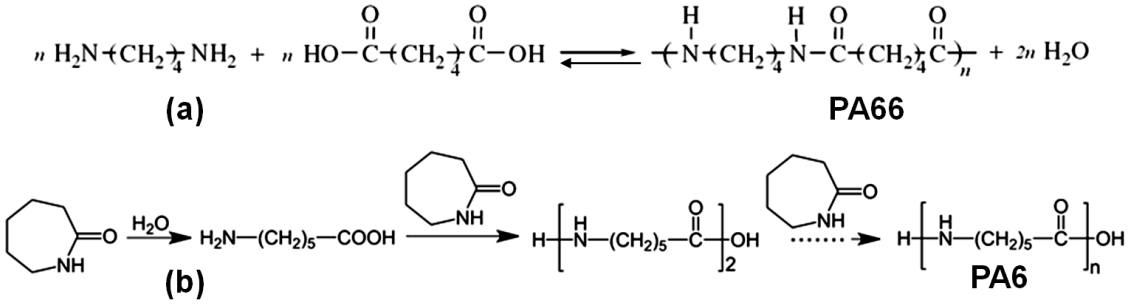

Figure 2: Polycondensation reaction in the case of: (a) PA66-polycondensation; (b) PA6 opening ring polymerization

The emergence of new polyamides markets such a high melting temperature polyamides contributed to the development of new polyamidation techniques such as interfacial polycondensation, solid state polycondensation and other exotic techniques that were never been used at the industrial scale. In this section, the most important polyamidation techniques are presented.

1.2.1. Bulk polyamidation

Bulk polyamidation is the most commonly used industrial method to produce polyamides. The polycondensation reaction is often carried out under pressure at high temperature (between 150 and 300 ° C in the case of polyamide 66). Firstly, the monomers (diacid and diamine or caprolactam) are dissolved in aqueous solution, forming “Nylon salt” as shown in equation (1). Note that in the case of lactam such as caprolactam, the Nylon 6 salt is prepared by heating a mixture of lactam and water at about 270°C in order to hydrolyze the lactam molecule to aminoacid.

$$HOOC - R - COOH \; + \; H_2N - R'' - NH_2 \overset{\text{w:w)}}{\leftrightarrow} {}^{-}COO - R - COO^{-} \; + \; {}^{+}H_3N - R'' - NH_3^{+} \quad (1)$$

The pH of the “Nylon salt” should be adjusted to control the initial stoichiometry of reactive functions. It has to be noted that an equimolar quantities of ionic salt of amine and acid

functions allows the obtaining of a polycondensation conversion close to 100% and then the formation of polyamide chains of high molecular weight.

The polyaddition reaction is then started in a closed reactor under pressure; it may be carried out in batch or in continuous process. Usually, the reactor is heated with a heat transfer fluid following ramp temperatures in order to accelerate the polycondensation reaction between the ionic diacid and diamine salts. Close to 200°C, the polymerization kinetics becomes significant and then polyaddition occurs progressively as long as the water content is relatively low. This latter evaporates at high temperature, resulting in a significant increase of the pressure up to several bars.

As the amidation reaction is in equilibrium with the hydrolysis reaction (see Figure 2-a), the released water has to be extracted from the reaction medium in order to move the equilibrium toward the formation of high molecular weight polymers. Therefore, the reaction medium is depressurized to a pressure slightly above atmospheric pressure. This operation is very difficult and requires a control of the speed of water vapor withdrawal to avoid a loss of monomer or polymer deposition on the reactor walls. Then, the polycondensation is done in the melt between 250 and 290°C at a pressure below atmospheric pressure. During this phase, called the finishing step, the viscosity of the reaction medium increases significantly during the last stages of the reaction, limiting the diffusion of the macromolecular chains and thus slowing down the reaction. Consequently, the temperature of the reactor should be set up sufficiently above the melting temperature of the polymer, to achieve a high conversion degree, without exceeding the polymer degradation temperature.

1.2.2. Anionic polymerization

Polyamide 6 is mainly prepared by opening polymerization in the presence of water at high temperature as described in Figure 2-b. Another common way to prepare polyamide 6, by anionic polymerization, has been also developed. The mechanism of anionic polymerization was described by Reimschuessel in 1977 [3]. It consists in a two steps synthesis: an initiation step (anion formation) followed by a propagation phase (polyaddition), Firstly, a lactam anion which is primary reactive specie is formed by reaction of lactam with a strong base. The lactam anion reacts then with a second lactam to give an anionic dimer and subsequently polyaddition occurs rapidly until reaching high conversion degree. It should be noted that the polymerization kinetic is extremely dependent on the specific initiators used and that the conversion to high molecular mass can be roughly instantaneous in the case of certain initiator. As a result, anionic polymerization was recently used in reactive injection molding (RIM) process for making low-volume pieces of polyamide 6.

1.2.3. Polyamidation in solution

It is often used for the synthesis of aromatic polyamides having high melting temperatures. It consists in dissolving the initial monomers in miscible solvents which usually contains a driving agent of the polymer. The used solvents are commonly organic solvents containing cationic metal such as calcium chloride or lithium salt. This technique is carried out at low temperature and requires additional steps of crystallization and purification of the synthesized polyamide. Note that this technique has attracted much academic interest but it is not widely used in industrial processes.

1.2.4. Interfacial polycondensation

Usually, interfacial polymerization is used for the synthesis of aromatic polyamides from high reactive monomers such as diacid chloride and diamine. It is carried out at low temperature by dissolving reactive monomers in different immiscible solvents. The polymerization takes place only at the interface of the biphasic mixture of solvents (between the aqueous phase and the organic phase). The contact surface between the two phases should be renewed as the polycondensation reaction progresses. Unlike polymerization in solution, the prepared polyamide is insoluble in the solvent mixture and then precipitate in solid form.

1.2.5. Solid state polycondensation

Solid state polycondensation (SSP) is widely used for the preparation of high molecular mass polyamides. It is a subcase of bulk polyamidation, it consists in the reaction between reactive ends functions of polyamides chains at the solid state. In fact, the initially solid material is heated at a temperature lower than melting temperature but high enough for polyaddition reaction to occur. As for bulk polycondensation, the formed condensates (water) should be removed in order to get high molecular weight. Therefore SSP is commonly carried out under primary vacuum with a passing inert gas to accelerate the diffusion process of water from the bulk to the surface of the polymer.

It is interesting to state that polyamidation reactions take place in regions containing an important ends function concentration and where the chain mobility is high enough to allow reactions to occur [4]. Therefore, reactions mainly take place in the amorphous phase as schematically presented in Figure 3. In fact, during solidification from the melt, oligomeric chains and most of the reactive end groups (up to 95 %) are excluded from the crystalline phase.

As the polyaddition reaction proceeds, the ends functions concentration and then the associated polyamidation equilibrium is changed. This leads to a continuous drop of the kinetic of post-condensation reactions. Moreover, the reactive chain end mobility in the amorphous phase gradually decreases as a consequence of the molecular weight increase. The aforementioned changes imply the formation of polyamide chains with different lengths, resulting in a broad molecular weight distribution at the end of the SSP. Diffusion process, temperature heterogeneities as well as condensate removal conditions may also broaden the molecular mass distribution. It is believed that when polyamide is processed (injection molding, blow molding …), the molecular mass distribution returns to narrower distribution as a result of ends functions equilibrating by exchange reactions in the melt [5].

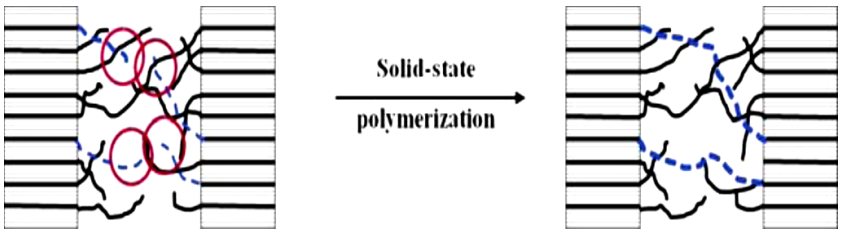

Figure 3: Scheme of solid-state polymerization reactions in the amorphous regions of polyamide [5]

1.3. **Copolymerization**

Copolymers are polymers that are synthesized with more than one kind of monomer or repeat unit as opposed to homopolymers that contain only one repeat unit. The distribution of the monomers along the copolymer chains depends on many factors such as the synthesis procedure and the reactivity ratio between the monomers that define the selective addition of these monomers. Based on the monomer arrangement along the chain, copolymers can be classified into: random copolymer, alternating copolymer, gradient and block copolymer.

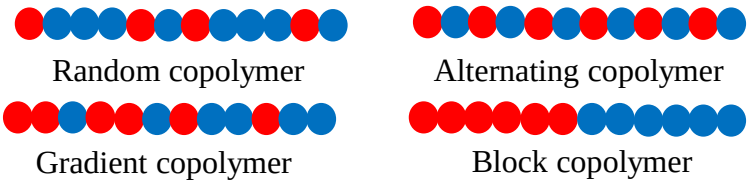

Figure 4: Monomers distribution in different types of copolymers

As shown in Figure 4, a random copolymer consists in a statistical distribution of the monomers along the chain copolymer. In contrast, an alternating copolymer presents a periodic interchange between the first and the second repetition unit. On the other hand, gradient copolymers exhibit a gradual change in monomer composition from predominantly one species to predominantly the other. Finally, a block copolymer is composed of two or more homopolymer subunits of each monomer. Block copolymers are interesting because they can form periodic nanostructures and they can combine the properties of the initial homopolymers.

1.3.1. Random copolymer

The most common technique for the synthesis of random copolyamides is the bulk co-polycondensation whereby the monomers (acids and diamine) or their derivate are mixed in aqueous solution to prepare the Nylon salt. Similarly to bulk polycondensation, the co-polyaddition is processed at high temperature and pressure until reaching the desired viscosity. The resulting copolymer consists generally in a random copolymer as schematized in Figure 5. The overall composition of this copolymer is often close to that of the initial monomer mixture, as a consequence of the high degree of conversion reached (~100%).

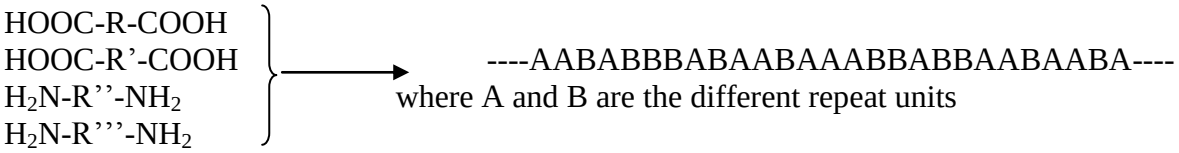

Figure 5 : Synthesis of random copolymers by direct co-polycondensation

It was noticed that if one of the co-monomer does not crystallize in a crystalline structure similar to that of the first monomer, such as the case of PA6/66, PA8/12, PA6/69 and PA6/MXDI, the resulting copolymers exhibits a crystallization ability and a crystallinity fraction lower than that of the corresponding homopolymers. This results in a lower melting temperature as well as a lower mechanical modulus [6]. Moreover, random copolymers containing a monomer that is unable to crystallize, such as isophthalic acid derivates, exhibit

an important drop of crystallinity fraction and elastic modulus as the concentration of this component increases. On the other hand, copolymers based on terephthalic acid that co-crystallizes with the first monomer such as PA66/6T and PA46/4T show a monotonically increase of the glass transition and melting temperatures with the fraction of the terptalic component [7]. These copolymers have high mechanical performance, low water uptake and high thermal stability. Consequently, manufacturing techniques of polyamides copolymers with large amount of terephthalic acid have been developed over the last years [8].

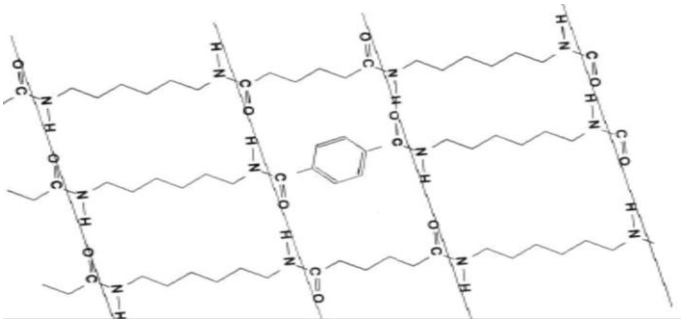

Figure 6: Replacement of adipic acid with terephthalic acid in the crystal of PA66/6T

The presence of terephthalic monomer in the crystal of PA66 and PA6T is related to the fact that the distance between the functional groups (amides) remains constant when the adipic acid is replaced by the terphatlic acid. Moreover, the terphtalic acid adopts the same orientation of its co-monomer (adipic acid) in the crystal lattice as shown in Figure 6 [7,9].

1.3.2. Alternating copolymers

Alternating polyamides copolymers are synthesized following a two steps procedure [10]. Firstly, p-nitrophenylester of the diacid is prepared by reaction of p-nitreophenol with acid derivate. In the second step, the diamine is converted to diamide by reaction of hexamethylene diamine with dichloride acid derivate. Subsequently, the copolymerization reaction is started through direct reaction between the nitro phenyl ester and the diamide as described in Figure 7. This reaction is usually carried out in organic solvent like 1,2,4-trichlorbezene at temperature ranging from 100-200°C to avoid the monomer exchange called hereafter as transamidation reactions.

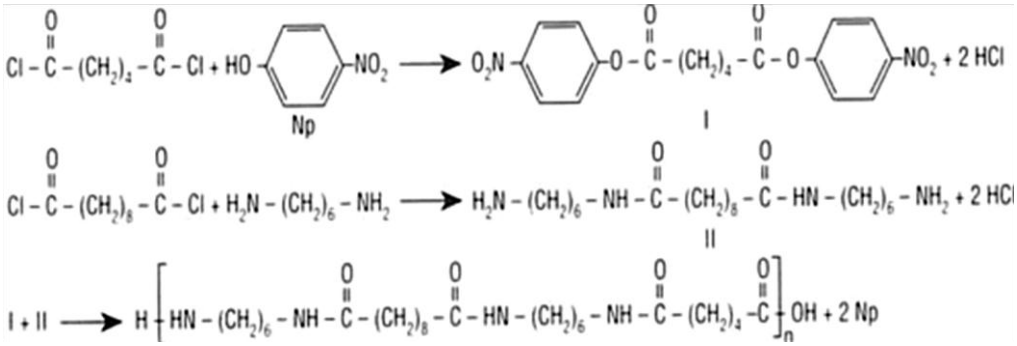

Figure 7: Synthesis steps of alternating PA66/610 copolymers

Since the co-monomers are periodically interchanged, the repeat unit in alternating copolymers is longer and more regular than that in random copolymer. Consequently, in the

case of crystallisable polyamides, alternating copolymers may be arranged easily and could crystallize more efficiently than random ones, resulting in a higher crystalline fraction and a higher melting temperature (~ 50°C higher) [10,11].

1.3.3. Block copolymers

The preparation of block copolymers is well established in the case of radical polymerization due to the recent development of living polymerization techniques, notably atom transfer free radical polymerization (ATRP), reversible addition fragmentation chain transfer (RAFT), ring-opening metathesis polymerization (ROMP), and living cationic or living anionic polymerizations. However, for polycondensates substrates, the preparation of block copolymer is more difficult and less controlled due to different rival reactions such as hydrolysis and exchange reactions at high temperature.

Block copolyamides can be prepared by the reaction of prepolyamides of relatively low molecular weight in a two-stage polycondensation. Firstly, amino-ended and carboxylic–ended prepolyamides are separately prepared by heating monomer mixtures in which an excess amount of diamine (or carboxylic acid) is added to the Nylon salt, at temperature ranging from 270 to 290 °C. The prepared prepolyamides are then mixed together in order to let occur the reaction between the ends functions of the prepolyamides that lead to the formation of block copolyamides.

Since the prepared prepolyamides are solids at room temperature, the second step should be carried out either by dissolving both prepolyamides in a common solvent and then heating the mixture solution, or by melting the solid blend under nitrogen at reduced pressure [12]. In the first case, the block length of the copolymer is well controlled and is very close to that of the initial homopolyamide. However, this technique requires polymer precipitation in a second solvent and additional purification steps [13]. On the other hand, melting prepolyamides implies exchanges reactions between prepolyamides chains resulting in a gradual conversion of prepolyamides into copolyamide. The extent and the kinetics of these reactions are dependent on many factors such as time and temperature, moisture content and the ends functions concentration. It may be noted that at long melt polycondensation and high temperature, the occurrence of exchange reactions is very important, leading to the formation of random copolyamides.

Another technique for the preparation of block copolyamides consists in the synthesis of oligomeric components in separate compartments of a flask and then breaking the glass partition separating the two components to get contact between oligomers [14]. This technique has not found a big success at the industrial scale and kept limited to academic studies.

To resume, melt-polycondensation is considered to be the most practical and efficient technique to prepare block copolyamides of many different monomers. It is very attractive way from an industrial point of view as it can be carried out in batch or in a continuous process. Indeed, melt-polycondensation is generally done on extruders since they offer the possibility of removing the released water as well as the incorporation of some additives such as fillers and glass fibers. However, extrusion conditions should be controlled (time, temperature and moisture level) to avoid the formation of a random copolyamide (see 1.4.3)

1.4. Polyamides processing

1.4.1. Blending

The growing number of polymer applications particularly in the automotive industry has led to an increased interest in developing a range of new polyamides. Mixing polymers together is a way to combine complementary properties (for instance high stiffness, high impact and high tensile strength) and to get a new material widely useful in a large range of applications [15,16].

One of the important concerns in blending is the miscibility or compatibility of the blend components. Most of the popular blend systems like polycondensates/polyolefins are immiscible due to their small mixing entropy and their high interfacial tension. However, for polycondensates/polyphenols and polycondensates/polycondensates systems, a partial compatibility can be achieved through strong interactions between the components such as hydrogen bonding, ion-dipole and dipole-dipole interactions [17–28]. Many researches on the miscibility between two polycondensates have been carried out based on a mean-field interaction model [17,26–31]. But it was well established that PA6/PA12 and PA6/PA12,12 blends exhibit phase separation even though hydrogen bonds may form between the components [32,33]. And there are also some contradictory conclusions on the miscibility between PA6 and PA66. For example, Wei et al. reported a partial miscibility between the PA66 and PA6 coalesced from their common cyclodextrin inclusion complex. They mentioned also that the initial miscibility of the blend was not enhanced after melting [34]. On the other hand, Ong et al. found a single glass transition temperature for the PA6/PA66 blend. They state that this result is fully consistent with the predicted miscibility based on the cohesive energy density and interactions parameters calculations[35].

Similarly, there is some disagreement on the miscibility of poly(hexamethyleneisophthalamide) PA6I and PA66 blends. According to Brisson et al, DSC scans of PA66/PA6I blends reveal a clear transition in the range of the glass transition temperature of pure PA6I, suggesting the immiscibility of these systems. They reported also that heating above the melting point of both polymers followed by rapid quenching did not alter their immiscibility [36]. This conclusion was excluded by Ellis who showed that PA66 is miscible with PA6I in all proportions [37].

1.4.2. Extrusion and injection

Polyamides can be processed by all common melt processing techniques such as extrusion and injection molding. Note that polyamides can be readily extruded in conventional extrusion conditions over a wide temperature range without significant degradation due to its good thermal stability. Various screw and temperature profiles may be set up as a function of the polyamide crystalline fraction, melt viscosity, and the additives introduced in the formulation. A particular attention may be paid to the processing conditions (e.g. moisture level, time, impurities…) to optimize the physical properties of the end-shaped component.

Since polyamide has polar groups (amides) able to interact with water molecules, it is of great importance to remove absorbed water of polyamide. At high temperature, particularly in the molten state, water degrades the molecular weight of chains by hydrolyzing the amide groups

distributed along the polyamide chains. For this reason, polyamide pellets are commonly dried by heating at temperature above Tg (around 100°C) under primary vacuum coupled with an adequate gas flow in order to accelerate water diffusion through the bulk to the surface.

It should be noted that overdrying polyamide may lead to higher molecular weight by means of post condensation reactions in the melt. This change is often manifest by an increase of the melt viscosity during the processing. Accordingly, water level is commonly kept around 0.15%, which corresponds to water content in equilibrium with the ends groups concentration in classic polyamides.

Similarly to extrusion process, most of polyamides can be processed in standard injection molding conditions. Remember that the melt viscosity of polyamide, like other polymers, is very dependent on the shear rate. For instance, increasing the shear rate from 100 to 400 s^{-1} divides by 2.2 the melt viscosity of polyamide 66 at a given temperature. Accordingly, injection molding is usually performed at high speed injection (high shear rate) to correctly fill the mold. As polyamides are generally semi-crystalline polymers, some processing parameters such as temperature and pressure mold should be accurately controlled. For instance, it was found that high temperature mold favours the formation of high crystalline fraction while low temperature mold reduces the crystalline fraction [38]. In general, the mold temperature set in the case of polyamide 66 injection molding should be in the range 60-80 °C.

Finally, polyamides, especially high viscosity polyamides, can be also processed by extrusion and injection blow molding to make tubes and hollow parts such as tanks.

1.4.3. Exchanges reactions in the melt

It is known that polycondensates, such as polyesters, polycarbonates, and polyamides are chemically very reactive during melt processing. In fact, blends of polycondensates bearing reactive functional groups, give rise in the molten state to exchange reactions [39–71]. These exchange reactions can yield block, segmented or random copolymers exhibiting properties (molecular mass distribution, crystallinity, miscibility and morphology) that can be different from that of the original blends [28,54–58]. And thanks to these exchange reactions, non-miscible blends can be compatibilized by the creation of copolymers at the interface between the phases during melt extrusion. It has to be noted that processing conditions of blending strongly affect the extent of these exchange reactions and then the compatibility between the blend components. In the case of miscible blends, there are intimate contacts between the components at the molecular scale and then transreactions (exchange reactions) occur to large extent resulting in changes of the macromolecular chains.

The exchange reactions during the melt mixing process have been the object of many researches. It has been shown that the transreactions occur mainly by direct exchange between two functional groups located inside the polymer chain (referred as the inner functional group). The contribution of the reactive-chain-end groups in the reaction during the melt mixing process was often neglected [28,52–54,56–58,60–62]. In the past few years, some researchers were interested in the role of the reactive chain end (referred as the outer group) in the exchange reactions. They revealed that the inner-inner exchange occurs typically in polyesters and polycarbonates blends, whereas amides exchange reactions (inner-

inner) are not observed [47–51,63–65]. Moreover, they concluded that only acidolysis processes (outer-inner exchange) was found to occur in the melt blends of polyamides [49,63,66]. Similarly, Zimmerman and Miller[46,55], reported that amide-amide exchange reactions are not observed at temperatures below 320°C and that only acidolysis reactions are involved. It was also reported that exchange reactions may be accelerated by the presence of a catalyst [41–45] or by the reactive terminal groups (NH2 and COOH) that are originally present in the polymers, or generated in situ by thermal and hydrolytic degradation reactions [39–71].

It is worth noting that exchange reactions were also attracting a lot of interest from the synthesis point of view. In fact, the synthesis of copolymers from reactive blending of the homopolymers has now become an alternative way to the usual copolymerization reactions started from the monomers [39–41,46].

1.5. **Polyamides reinforcement**

Reinforcing polymers enhances their mechanical properties and then allows their use in increasingly demanding applications such as metal replacement, leading to weight reduction opportunities. In the case of polyamides, fibers such as glass fiber and carbon fibers are widely used. Mineral particles and glass beads are also used as fillers reinforcers. Fibers and/or fillers are generally introduced into the polyamide matrix during the compounding step. Indeed, pellets polyamide containing glass fibers with a given aspect ratio are commercially available. Care during further processing steps is necessary to avoid excessive fibers fragmentation.

It should be noted that the important factors for controlling polyamide reinforcement are: reinforcer aspect ratio, fiber strength, stiffness, orientation and concentration. The coupling between the polyamide matrix and the reinforcer (fiber or filler) affects the polymer shearing at the matrix-reinforcer interface and then plays an important role in the load transfer from the matrix to the reinforcer. Accordingly, the final properties of a reinforced polymer are strongly depending on the cohesion between the fiber/filler and the polymeric matrix. Several treatments of the fibers/fillers surface such as coating, sizing and chemical coupling have been reported in the case of polyamide reinforcement[6]. Of particular interest, the bi-functional coupling method implies a bonding agent with an alkoxsilane function at one end, which provides adhesion to the glass fiber/filler, and a functional group at the other end that is capable of reaction with the polyamide matrix.

The reinforcement of polyamide with fibers or fillers globally enhances its mechanical properties, such as stiffness, creep resistance, tensile, impact and fatigue strength [6]. Fibers often provide larger benefit effects on the mechanical properties than fillers. In contrast, fillers further improve other properties like dimensional stability and scratch resistance. But it should be kept in mind that the mechanical performances of fiber reinforced polymers are strongly dependent on the orientation of the fibers. It is commonly accepted that fibers orientation parallel to the load offers the highest stiffness and the highest strength.

2. Polyamide 66

Polyamide 66 results from the polycondensation of Hexamethylene diamine and Adipic acid or their Nylon salt following the above described techniques. The repeat unit of this polymer is presented in Figure 8.

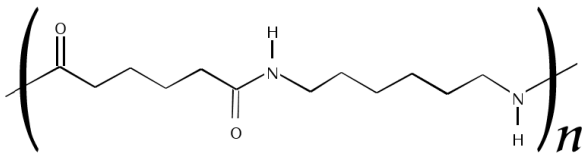

Figure 8: Repeat unit of PA66

PA66 contains amide groups periodically distributed along the polymer chain that are at the origin of the establishment of regular H-bonds between the polyamide chains. This periodicity may favor chains organization resulting in a well-ordered stacking, favoring thus their crystallization. However, the ability of polyamide chains to crystallize in not entire and then some fraction of polyamide chains remain relatively disordered. Accordingly, polyamide 66 can be considered as a two-phase material composed of a crystalline phase (ordered) and an amorphous phase (disordered). The crystalline fraction may vary from 30 to 40% as a function of the preparation conditions (processing and cooling). In the crystalline phase, the polyamide chains are well organized at different scale levels.

In this section, the conformation of chains in the crystalline phase will be presented from the nanometric scale (crystal lattice) to a larger scale (crystalline lamella), until the micrometric scale (spherulite structure). Afterward, the structure and the molecular mobility of the amorphous phase of PA66 will be described

2.1. Crystal structure of PA66

PA66 crystallizes principally into the triclinic structure which is thermodynamically stable. In this structure the chains are arranged in a zigzag conformation resulting in the formation of H bonds between the amide groups in the zigzag plane, sheets of H-bonds being then formed and stacked one over the other through van der Waals interactions. It should be noted that Bunn et al. proposed two triclinic structures, α and β, for the crystalline domains which form the sheets, where the α structure contains one chain per unit cell, and the β structure contains two [72].

Figure 9 shows the α triclinic structure of PA6,6 with the lattice parameters being a=0.49 nm, b=0.54 nm, c=1.72 nm, α=48.5°, β=77° and γ=63.5° [72]. It can be seen that the H-bonds can take place due to the one methylene shift of the adjacent molecule in the chain direction. The intermolecular H-bonds between the H-N (donor) and C=O (acceptor) of two neighboring chains is around 0.44nm. It can be also observed that intermolecular H-bonds are in the same planar sheet of the polyamide chains ((010) plane). In the plane (100), the chains are held together through van der Waals interactions with an intersheet distance of 0.37nm [73]. It is should be noticed that the chain direction (along the c-axis) in the H-bonds sheet is inclined to the basal plane (001) by an angle about 42°. As the PA66 molecules are centrosymetric,

the chains have no directionality and then parallel and antiparallel chains are equivalent, which explains the no γ form of PA66.

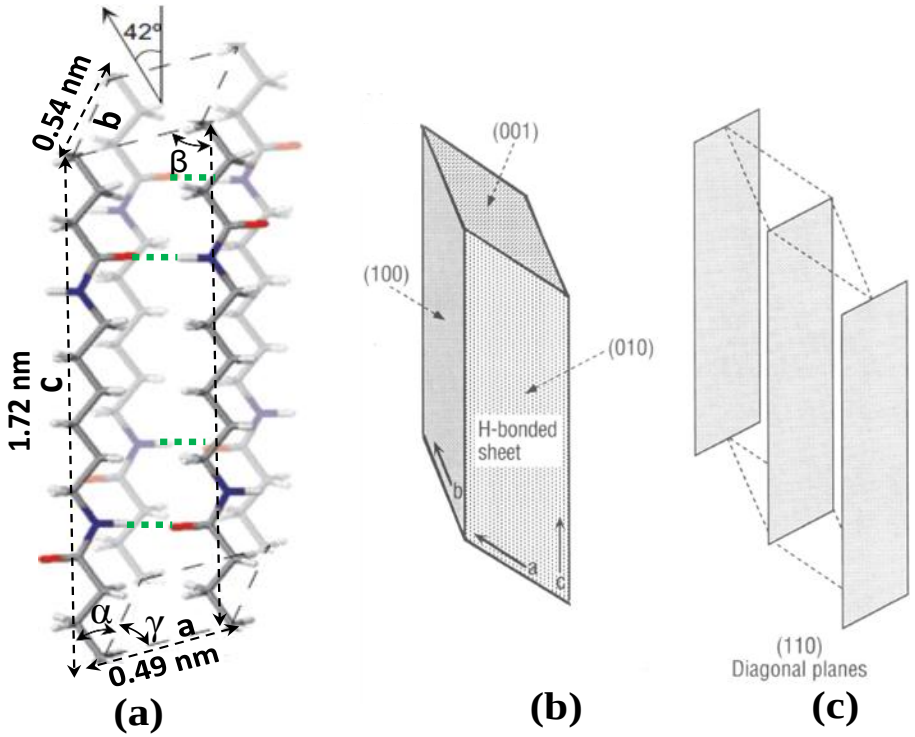

Figure 9: (a) Triclinic unit cell of PA6,6 α crystalline structure: blue is nitrogen, red is oxygen , grey is carbon and white is hydrogen; (b) representation of the (001),(100) and (010) planes (c) (110) plane

Like other polyamides, PA66 exhibits a crystalline polymorphism (different α crystalline structures) depending on the processing conditions or the crystallization method. Indeed, PA66 samples obtained from slow cooling from the melt or at high crystallization temperature crystallize into the α_{II} form ("Thermodynamic"), while rapidly melt-quenched PA6,6 samples crystallize into the α_{I} form ("Kinetic")[74]. This nonequilibrium form is characterized by a pseudo-hexagonal unit structure which tends to evolve towards the more stable α_{II} form. Another crystalline evolution called the Brill Transition [75] occurs upon heating (around 160°C) and implies phase transformation from a triclinic structure to the pseudo-hexagonal structure.

2.2. **Lamellar structure of PA66**

Lamellar structure is a layer crystal formed by folding of polymer chain during the crystallization. The morphology of this lamellar structure is somehow determined and restricted by the arrangement of the polymer chains according to the formation of H bonds between them. Note that along the a-direction the H-bond interactions between polyamide chains are formed as presented in Figure 10. It was found that chains within each lamella are tilted at 46° with respect to the fold surface, and the a-axis is the direction of greatest lamellar elongation and thus fastest crystal growth. [6].

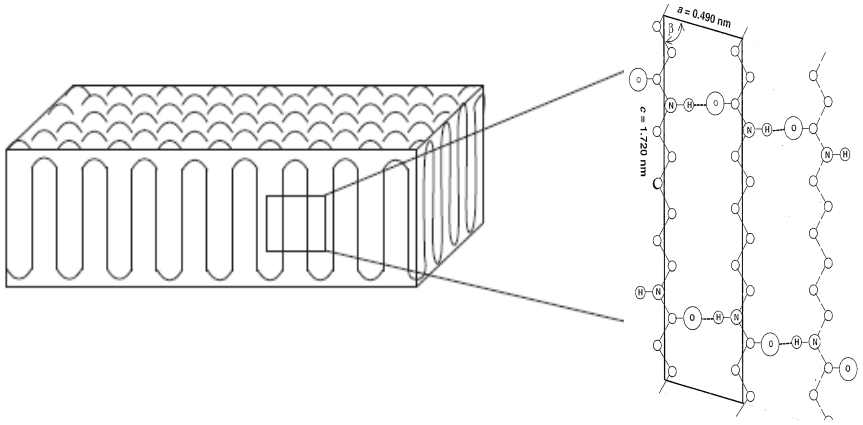

Figure 10: Packing of PA 66 chains into lamella structure

Dreyfuss et al. have suggested that in the case of PA66 crystallized from dilute solution, three and a half monomeric repeat units are needed to form one lamellar stem and then the polymer chain folds in the methylene backbone so as to form further lamellae stem as described in Figure 11 [76]. Note that chain folding similar to that seen in solution crystallized samples was also found in the case of melt-crystallized polyamide 66.

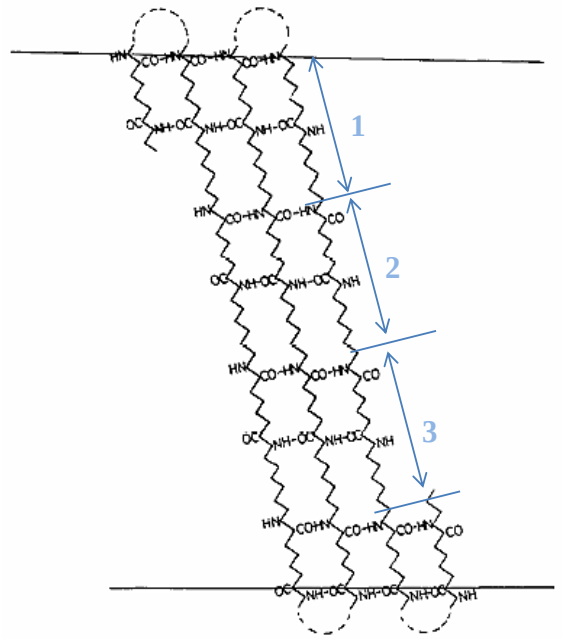

Figure 11: Ideal chain folding within a PA66 lamella, crystallized from dilute solution, composed of 3.5 repeat units corresponding to a lamellar thickness of about 5.2 nm [76]

On the other hand, it was reported that annealing of solution or melt-crystallized polyamide causes either a small decrease or a discontinuous increase of the long period. The decrease of the long spacing was associated with the improvement of the fold surface whereas the increase was explained by a lamellar thickening mechanism which involves suction of chain ends as shown in Figure 12 .

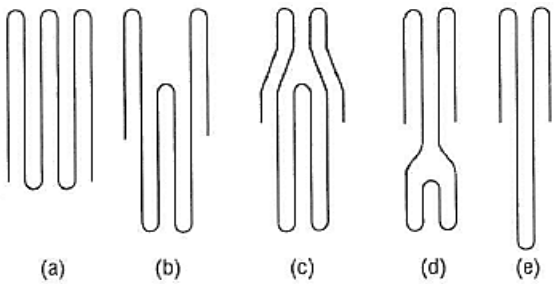

Figure 12: Schematic lamellar thickening mechanism in polyamide. The central fold in (a) recedes and is "consumed" equally (c) by its neighbors. The fold dislocation that is created will climb (d) until it leaves the layer, resulting in a fold that is twice the length of the original fold (e). Reprinted from [6].

2.3. **Spherulitic structures of PA66**

It is well established that during cooling from the melt, crystallization starts from a nucleus or an impurity and proceeds by a quasi-instantaneous radial growth of lamellae in all the directions. This leads to an isotropic structure called "spherulite" which is presented in Figure 13-a. Depending on the crystallization temperature, polyamides lamellae grow with a certain axis to produce negative or positive spherulites. The growing of these positive and negative spherulites is schematically shown in Figure 14. When the crystallization temperature is below 250°C, the spherulite grows with a radius parallel to the major axis of its component crystals resulting in a positive spherulite. However, if crystallization occurs between 250°C and 264°C, spherulite grows with a radius parallel to the minor axis favoring the formation of negative spherulite. It should be noted that negative spherulites usually have higher melting points than the positive spherulites.

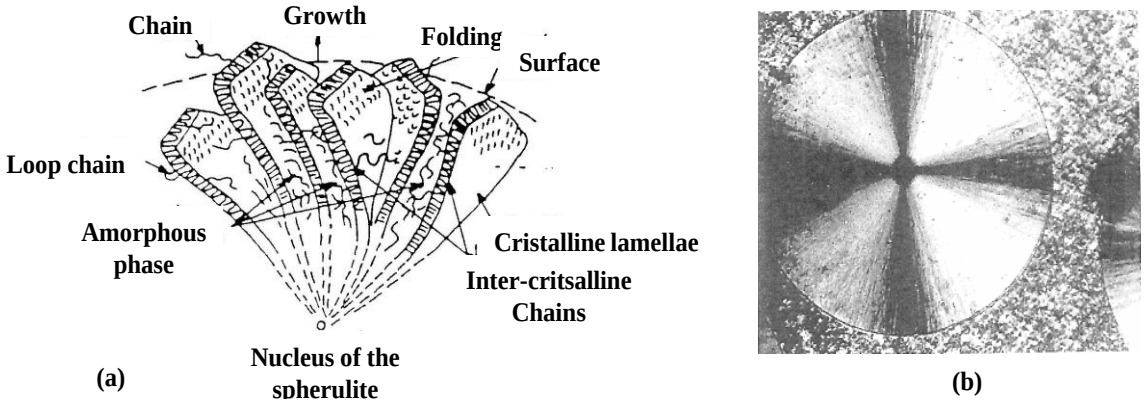

Figure 13: Spherulite structure in polyamide: (a) schematic presentation; (b) "Maltese cross"-like polyamide characteristic spherulite

The spherulitic structure can be evidenced by polarized optical microscopy as it exhibits a birefringence feature (some axis of the crystal is parallel to the spherulite radius). This birefringence produces the "Maltese cross" pattern in polyamides spherulites when polarized light propagates through the polymers' crystalline phase as shown in Figure 13-b.

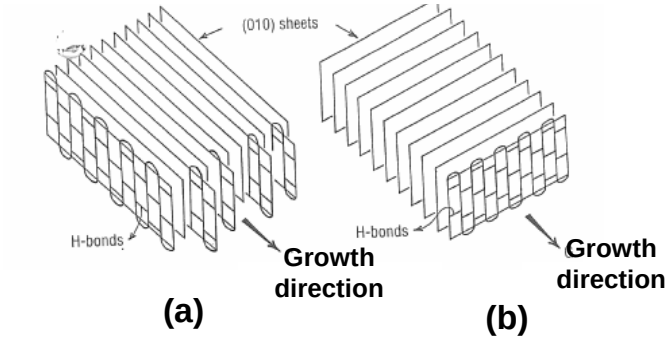

Figure 14: Schematic representation of chain folding and crystal growth in (a) positive and (b) negative spherulites.

The birefringence difference between the spherulites, mainly due to the orientation of H-bond sheets with respect to the spherulite radius, can be understood based on the spherically symmetrical arrangement of uniaxial (refractive) index ellipsoids [77]. Accordingly, spherulites show positive birefringence when the larger refraction index is in the radial direction of the spherulite whereas negative spherulites show birefringence when the larger refraction index is in the tangential direction as schematically shown in Figure 15.

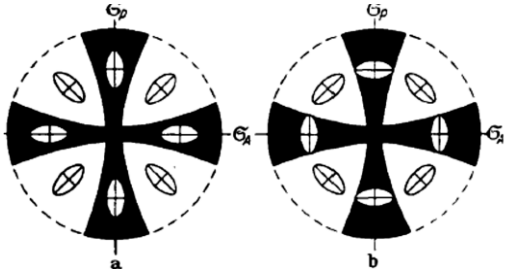

Figure 15: Schematic presentation of uniaxial ellipsoids in: (a) positive spherulite; (b) negative spherulite.

2.4. **Amorphous phase of PA66**

As mentioned earlier, polyamide 66 is a semi-crystalline polymer which could be considered as a two-phase system comprising a crystalline phase and an amorphous phase. However, several authors [78–81] have proposed the existence of a third intermediate phase composed of amorphous chains constrained by the presence of crystallites near them as shown in Figure 16. This phase is called Rigid Amorphous Fraction (RAF) so as to differentiate it from the central amorphous phase known as the Mobile Amorphous Fraction (MAF). It is assumed that in the RAF phase, polymer chains have a reduced mobility when compared to the chains belonging to the MAF region.

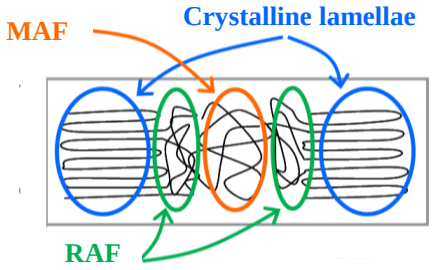

Figure 16: Schematic representation of a 3-phase polyamide composed of a crystalline phase, a mobile amorphous fraction and a rigid amorphous fraction.

2.4.1. Amorphous structure

It is supposed that chains of fully amorphous polymer exist in the state of random coil conformation without any significant organization. However, in the case of polyamide some order may exists due to particular restricted conformations induced by the H-bond interactions. Since the crystalline fraction in polyamide 66 is not so important (below 40%), structural information on the amorphous phase is essential to have a better understanding of the physical and mechanical properties of this material. One way to describe order in the amorphous phase is the X-ray diffraction on entirely amorphous polyamide. Unfortunately, it is not possible to get fully amorphous polyamide 66 even through quenching process. Note that some polyamides containing randomly aromatic rings, being 100% amorphous, can be used for structural characterization. However, the obtained information such as inter and intra-atomic distances or torsional angles for the amorphous chains may be probably different from that of the aliphatic Nylon 66 since they have a different chemical structure.

An alternative way is to get structural information by means of solid-state NMR techniques that observe selectively the signal from the amorphous and the crystalline phase. For example, it was found that a fraction of amide groups remain associated in the amorphous phase above the Tg [82]. It was also concluded that the amorphous chains prefer an extended conformation about the amide group and that intramolecular energetics define the average conformation in the amorphous phase [83].

Additional insight can be gained through the characterization of the polymer molecular relaxations and the study of the effect of water or solvent on the relaxation behaviour of the amorphous phase [81].

2.4.2. Relaxations in polyamide

The molecular mobility of the amorphous phase is generally related to chains motions that are thermally activated. With increasing temperature of the polymer, the chain motions become faster and then the physical properties of the polymer may be changed. These motions, known as molecular relaxations, can be characterized by mechanical, electrical and magnetic solicitations at a given time scale. It is generally assumed that two types of molecular relaxations occur in polymers: the main relaxation corresponding to the coordinated motion of relatively long chain segments, and the secondary relaxations related to the motion of small chain segments or molecular functions.

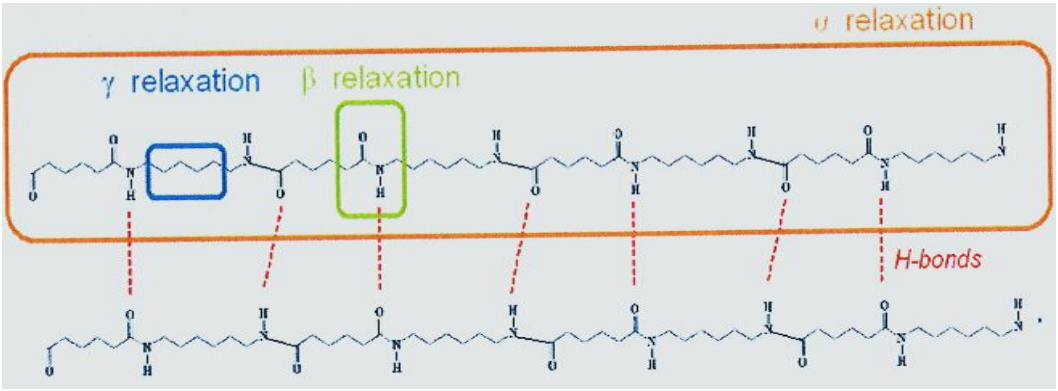

Figure 17: Schematic representation of the participation of chemical groups in polyamide relaxations

In the case of polyamide, three relaxations labeled as gamma, beta and alpha, in the order of apparition with increasing temperature, have been identified. A schematic representation of these three relaxations in the case of PA6,6 is given in Figure 17. The molecular motions involved in theses relaxation have been well described in the literature [84–88].

- The gamma relaxation (γ) corresponds to the vibrational motions of the methylene groups between the amide functions. It occurs at almost the same temperature and frequency as the γ relaxation of polyethylene (around -110°C) and its intensity increases as the monomer length of polyamide increases.

- The beta relaxation (β) is generally assigned to the rotation of the amide functions. It is assumed that the beta relaxation involves the motion of amide and/or a linked water-amide functions along the polyamide chains.

- The main relaxation (α) implies long range motion of the chain segment. It involves a cooperative motion of around 15 repeat units as described by Boyd [88] as well as by Owen et al. [87]. This relaxation is associated with the glass transition of the polymer. Since polyamides have amide groups which form inter and intra-chains H-bonds, it is reasonable to think that H-bonds are probably broken during the cooperative motion of the chain segment. Accordingly, the (α) relaxation is dependent on the chemical structure of the polyamide, especially on the amide group concentration. It was found that (α) relaxation occurs at lower temperature when the number of methylene groups increases (amide concentration decreases). In the case of polyamide 66, (α) relaxation approximately takes place at 60 – 70°C at a frequency of 1Hz.

2.5. **Water absorption**

An important feature of polyamide 66 is its high water uptake due to the important density of amide groups presents in the polymer chains. In fact, amide groups are polar functions which can be considered as sorption centers of polar molecules, and especially of water. This latter interacts with the amide groups by H-bond formation between the oxygen of water and the hydrogen of the amide group, and/or between the hydrogen of water and the oxygen of the amide groups. The second interaction is said to be stronger than the first one and is then established preferentially. Figure 18 illustrates the interaction mechanism between the water molecules and the amide groups. Two kinds of bound water are considered: firmly bound water and loosely bound water. The former one concerns the molecules that are able to form 2 H-bonds with two different carboxylic functions while the second one corresponds to the molecules that bind themselves to one amine and one carboxylic function.

It is widely accepted that crystalline phase is not accessible for water suggesting that absorbed water is mainly located in the amorphous phase [89,90]. The mechanism of water absorption in the amorphous phase was well described in the literature. According to Puffr et al. [91], water molecules firstly interact with free amide groups (non H-bonded) which constitute less than 1 % of the total number of amide groups. Secondly, water interacts with linked amides, broking the PA inter-chains H-bonds to form two H-bonds with tow carbonyl groups (Water bridges (1)) as presented in Figure 18. Water then interacts with the already hydrogen-bonded C=O groups and the hydrogen atoms of –NH groups of the amides. These water molecules (2) are sometimes called “loosely bound water”. After that, additional water

molecules can be added to already bound water molecules through further H-bond, leading to water clustering at high water concentration.

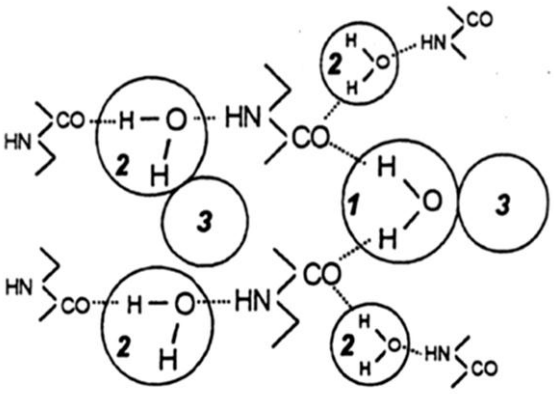

Figure 18: Mechanism of water sorption in polyamides: (1) firmly bound water, (2) loosely bound water, and (3) water clustering

The rate and the amount of water sorption are dependent on the carbons/amide ratio as well as the crystallinity content and morphology. It is well established that an increase in the crystallinity content or in the molar ratio [CH2]/[amide] results in a decrease of the water uptake [6,92].

As water interacts with the existent H-bonds network in the amorphous phase, chain motions in wet polyamide are expected to be be strongly modified. Indeed, the main relaxation (α) associated to the glass transition temperature is significantly shifted towards low temperature with increasing the moisture content. It is believed that water acts as a plasticizer which increases the chain mobility by breaking the H-bonds between the amide groups. Consequently, the properties of polyamide at solid state, particularly its dimensional stability and its mechanical properties are considerably altered [93].

Several works aiming at improving the dimensional stability and the mechanical performance of aliphatic polyamides in the presence of water have been investigated. Most of these studies involve the incorporation of aromatic functions that are less susceptible to moisture into the aliphatic backbone of Nylons. Indeed, a lot of aromatic polyamides have been developed, such as poly (phenylene terephthalamide) (PPTA), poly(hexamethylene-terephthalamide) PA6T, PA6I and poly(nonamethylene-terephthalamide) PA9T [94–98]. It is worth noting that all these polyamides except for PA9T cannot be produced by melting process due to their either high glass transition or high melting temperatures. Consequently, semiaromatic copolyamides (PPA) based on PA66 such as PA66/6T, PA66/PT and PA66/6I were synthesized from hexamethylene diamine, p-phenylenediamine, adipic acid, iso and terephthalic acid monomers [99,100]. These aromatic and semiaromatic polyamides have been known for their low water uptake, high thermal stability, chemical resistance, high strength, and high modulus [96–98,101].

Part II: Mechanical properties

In the part I, various techniques of synthesis of polyamides and copolyamides were presented. A particular focus on polyamide 66, mainly on its complex microstructure (from the atomic scale to the macroscopic scale) was also given. The mechanical properties are now investigated, a particular attention being paid to take into account the relation between the microstructure (molecular weight, amorphous and crystalline phase) and the ultimate properties of the material. The impact of the microstructure is pointed out on: firstly the static mechanical properties and secondly the long term mechanical properties, the damage mechanisms at all stages of the polyamide structure being also described.

1. Static mechanical properties

Uniaxial tensile tests are the recurrent experience to highlight the static mechanical properties of a material. It simply consists in recording the needed force to deform a solid material at a constant strain rate. The material resistance to the deformation (linear and/or viscous response) is quite complex and depends on the intrinsic properties of the polymer as well as the experiment conditions (temperature and strain rate).

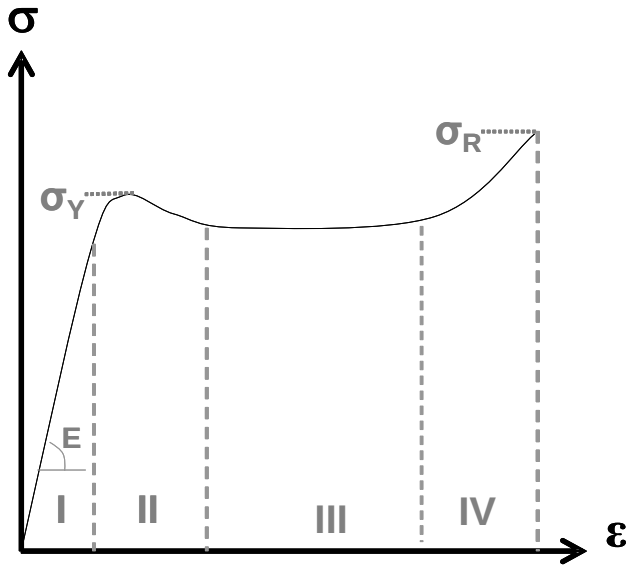

Figure 19: General Stress-strain curve for polymer ;(I) Elastic response, (II) Viscous response and Yielding, (III) Plastic flow followed by strain hardening, (E: Young's Modulus, σy: Yield stress, σ_r :Stress at rupture)

Figure 19 shows a schematic stress-strain curve of a thermoplastic polymer. As it can be seen, the stress increases linearly with strain in the first region which corresponds to the elastic behaviour (reversible deformation). As deformation increases, the response becomes nonlinear or viscoelastic (gradual recovery of deformation). The second region is characterized by irreversible deformation and subsequent yielding process. Beyond the yielding point, local deformation processes facilitated by cooperative sequential motions are involved in the viscous response of the material. In the case of a material having a low molecular mobility, failure can occur before the activation of the yielding process. Such a material, characterized by a restricted extensibility is said to be brittle. Otherwise, beyond the yield stress the material deformation proceeds and stress drops, often in association with the

formation of a neck. Necking may lead either to a subsequently failure or to a cold-drawing (notable reduction in cross-section of strained specimen). At this stage of plastic flow (region III), molecules orientate in the tensile direction, which macroscopically appears in the form of constant stress. When the polymers chains become totally stretched in the tensile direction, a stress increase before the final failure, known as strain hardening, is often observed (zone IV). In some cases, the region III goes up until high strain value resulting in ductile failure of the material. This latter is then usually considered as a tough polymer.

1.1. **Influence of the microstructure**

The macroscopic deformation of polymeric materials is a complex process which involves a number of different local phenomena ranging from the atomic scale (chains) to the microscopic scale (spherulite). A lot of studies reporting the microstructure-properties relationship of semi-crystalline polymers have been published. These studies deal essentially with the effect of crystallinity degree, morphology and crystalline structure on the mechanical properties of these polymers.

It is well established that static mechanical properties of semi-crystalline polymers are strongly affected by their crystalline fraction and morphology. In recent studies on poly (L-lactic acid), it was concluded that crystallinity causes an increase of the elastic modulus, impact and yield strength while significantly decreasing the ultimate elongation [102,103]. Similarly, Starkweather et al. [104] observed that aliphatic polyamides become more brittle (stiffness and yield stress grow up while ultimate elongation decreases) when the crystalline fraction does (see Figure 20).

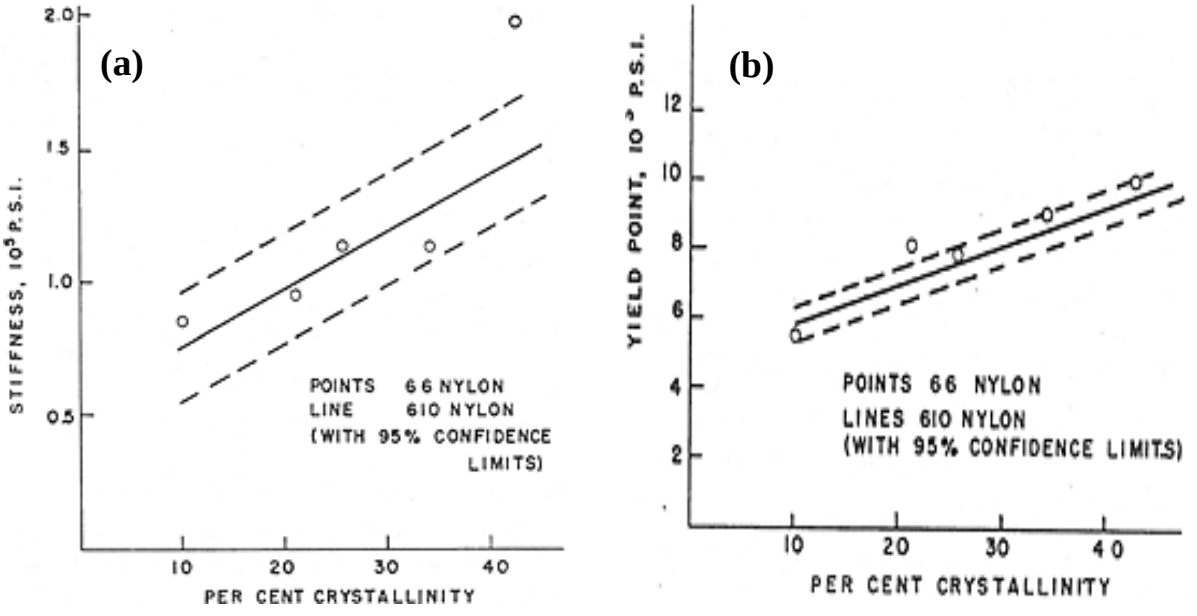

Figure 20: Stiffness (a) and yield stress (b) evolution as a function of the crystalline fraction of PA66 and PA610 [104]

Moreover, the impact of spherulite size on the mechanical properties of polymers was also investigated. Hammer et al. observed that when the spherulite size of polyacetals decreases, the impact strength and the ultimate elongation increase whereas the yield stress decreases [105]. A similar conclusion on the impact strength of linear polyethylene was also drawn by Ohlberg et al. [106]. In another works, Andrianova et al. and Way et al. observed defects and

voids formation at the boundaries between large spherulites that may cause a decrease in the ultimate elongation of isotactic polypropylene [107]. An opposite effect of spherulite size on the ultimate elongation was however found by Starkweather et al. [108]. They reported that polyamide having smaller spherulite exhibits a more brittle behaviour (lower elongation at break and tensile impact strength), and that yield strength increases as the number of spherulites increases, as shown in Figure 21.

Furthermore, it was found that increasing the lamella thickness, either by slowing the cooling from the melt or annealing treatment on solid, results in higher yield stress in the case of polyethylene materials as described by Popli et al. [109], and Pawlak [110]. In recent work, Schrauwen stated that during compressive tests on PE at room temperature, the first yield point (related to fine chain slip) and second yield stress (related to coarse chain slip) increases with the crystallinity level, or better with the lamellar thickness as shown in Figure 22 [111].

Similarly, the effect of the crystalline lattice on the mechanical properties was also investigated. Of particular interest is the study of Miri et al. conducted on the tensile properties of PA6 [112]. They concluded that polyamides 6 having α crystalline structure, considered as the densest and the thermodynamical structure, exhibit higher yield stress than those containing the γ and β crystalline form. To our knowledge, no works have been reported in the literature on the relationship between the crystal structure of the crystalline phase of PA66 and its mechanical properties.

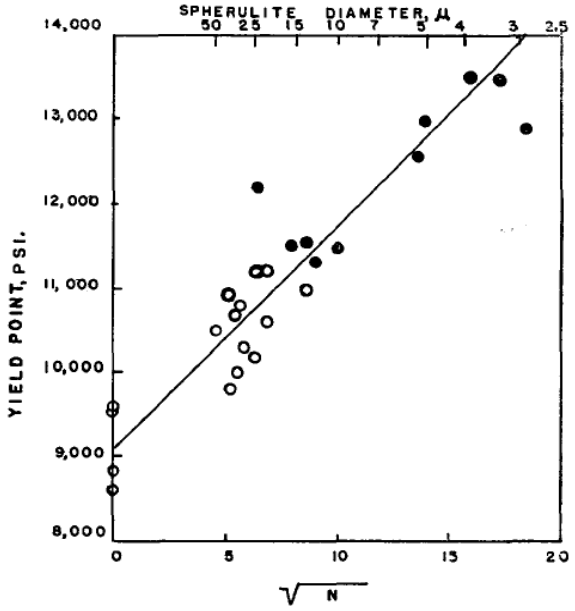

Figure 21: Effect of the spherulite diameter μ on the yield stress of: (°) compression-molded films and (•) injection-molded bars of PA6,6; N is the number of spherulite boundaries per millimeter [108]

Numerous studies have then been conducted on polymers having different molecular weight average. But in most cases, the crystalline microstructure (crystallinity degree, spherulite size and lamella thickness) changes when the molecular weight does. So, the impact of molecular weight on the mechanical properties could not be distinctly identified and at the end conclusions do not converge. For example, Stern et al. observed that the crystallinity fraction decreases and the lamellar thickness increases as the molecular weight of polypropylene increases [113]. They found also, that the elastic modulus and especially the tensile strength

increase as the molecular weight increases, probably due to the presence of strong and thick crystallites. However, they found that the ultimate strain firstly increases as Mw increases and then decreases at high molecular weight; they suggest that a ductile-to-brittle transition occurs when the molecular weight exceeds a critical value. It was also reported that increasing molecular weight decreases the spherulite growth in polyethylene. However, for a given spherulite size, it was found that the lower the average molecular weight, the greater the impact strength [106]. This result seems to be in contradiction with the work of Perego et al. which shows that impact strength rises with increasing the average molecular weight of poly(L-Lactic acid) [103].

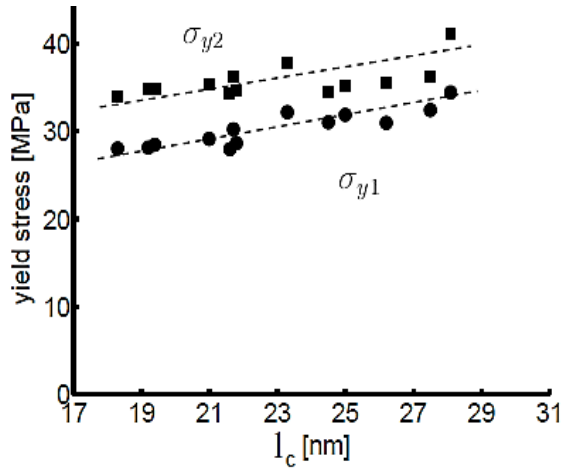

Figure 22: Relationship between lamellar thickness (lc) and the two yield stresses determined from compressive tests of PE at room temperature [111]

1.2. **Impact of the mobility chains of the amorphous phase**

The deformation of semi-crystalline polymers involves both crystalline and amorphous phases. The properties of this latter are very related to the amorphous chain mobility that depends on many factors such as intermolecular interactions, fraction of surrounding crystals and temperature. It is admitted that temperature is the most important parameter that have obvious effect on the polymer's amorphous phase molecular mobility. Indeed, the chains mobility is very low at the glassy state (below the glass temperature). It increases with temperature and becomes significantly high at the rubbery state (above the glass transition). Accordingly, the response of the amorphous phase and then mechanical behavior of the semi-crystalline polymer is expected to be dependent on the temperature.

It was reported that semi-crystalline polymers exhibit higher resistance to yield at low temperature, likely due to the slower segmental motion of polymeric chains in the glassy state. For instance, polyamide 66 exhibits brittle behavior at room temperature (high Young's modulus E and yield stress σ_Y) but as temperature increases the polymer becomes more ductile/tough (E and σ_Y drop) especially when the glass transition temperature is exceeded as shown in Figure 23. In the same way, Wang et al. reported that a more brittle behavior was observed in the case of glass fibers reinforced polyamide 6 when the temperature test decreases [114].

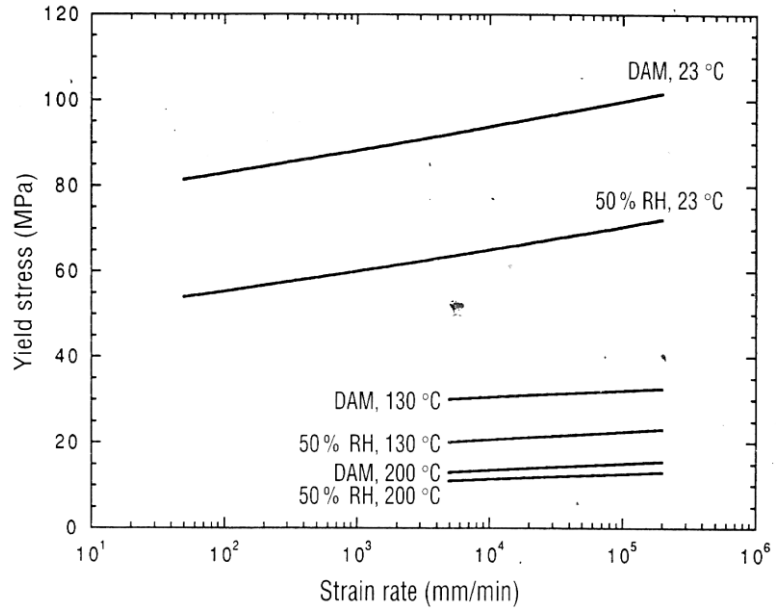

Figure 23: Effect of strain rate and temperature on the yield stress of polyamide66 [6]

Another factor should be taken into consideration in the case of polyamide is the water content. Indeed, water plasticizes polyamide by disturbing the H-bond network between the polyamides chains and then enhances the mobility chains of the amorphous phase. This results in a drop of the elastic modulus as well as of the yield stress σ_Y (see Figure 23). On the contrary, the elongation at break becomes greater, as reported in several works [6,112,115].

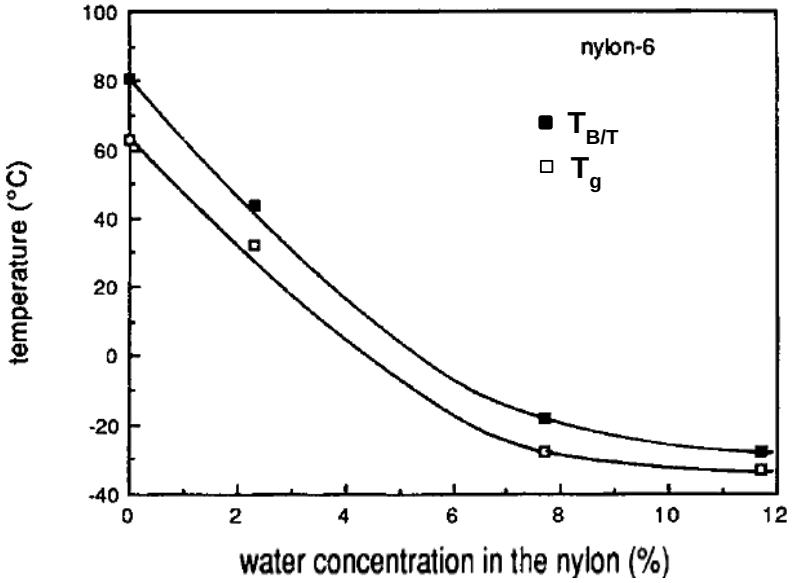

Figure 24: Evolution of Tg and $T_{B/T}$ as a function of the water concentration in PA66

It was also concluded that polyamide becomes more ductile (higher impact strength) when water is absorbed by the sample. Moreover, it was found that the brittle-tough transition temperature $T_{B/T}$ shifts towards lower temperatures with increasing the content of absorbed water [116]. This shift appears to be similar to that of the glass transition temperature T_g as illustrated in Figure 24. Furtheremore, the work of Rios et al. [81]evidenced a linear dependence between the Tg and the brittle-tough transition of various neat and chemically

modified PA66 conditionned at different humidity levels. This highlights the importance of the role of the intermolecular interactions in the amorphous phase on mechanical properties of polyamides, especially their impact properties.

1.3. **Damage mechanism**

As shown earlier, semi crystalline polymers exhibit a multi-scale structure ranging from nanometric scale to micrometric scale. Therefore, the damage mechanism of these polymers is extremely complex and involves a number of physical phenomena that cover all the scales of this structure (chains, crystalline lamellae, interphase, interlamellar amorphous phase and spherulites). Most of reported works in the literature are focused on the damage mechanism at large deformations that consists of massive rearrangement of material morphology such as chain slip of crystalline lamellae, lamellae fragmentation, martensitic phase transitions, cavitation, microcrazing and microfibrillation.

Little works have been done at small deformation level[117–119]. They found that at a low strain level, stretching favors the occurrence of different structural defects such as nanocavitation in the interlamellar amorphous layers and damage of the crystalline lamellae. The mentioned structural transformations induced by small deformations are not so pronounced as at large strains.

In this section, the reported damage mechanisms of semi-crystalline polymers at small and large strain level are detailed at the scale of the crystalline phase, amorphous phase and spherulite structure.

1.3.1. Deformation of the crystalline phase

It is well established that deformation of the crystalline structure involves three basics processes: crystal slip, twinning or phase transformation [120].

1.3.1.1. **Lamellar slip**

It is the most typical deformation mode of crystals which consists in the sliding of crystalline blocks over one another along the crystallographic plane containing the chain backbone as reported by Cowking et al. in the case of polyethylene[121–124]. It should be noted that in the case of polyamide, the slip process was observed only in the plane parallel to the hydrogen-bonded sheets [125].

Figure 25, presents the mechanism of slip proposed by Bowden et al. who state that slip phenomena implies glide of some inherent dislocation that causes displacement of one portion of the crystal with respect to another. As a function of the deformation level, the size of crystal involved in slip could be fine (Figure 25-a) or coarse (Figure 25-b).

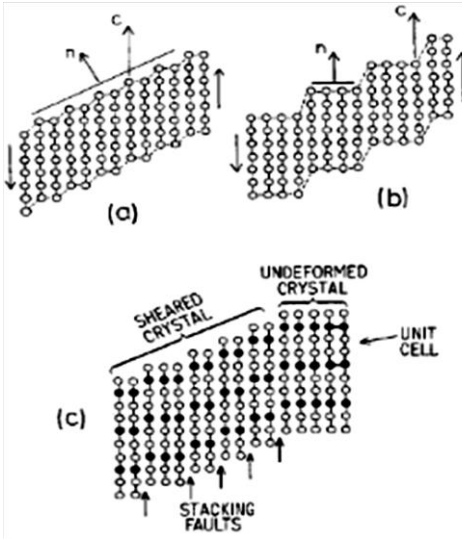

Figure 25: Schematic presentation of dislocation and slip movement in semi crystalline polymers: (a) fine slip; (b) coarser slip; (c) Shearing of a lattice by fine slip of partial dislocations (reprinted from [120] **).**

1.3.1.2. **Twinning**

Twining is the second type of plastic deformation of crystal which is supposed to occur when chains in a part of crystal move by simple shear to take up a symmetric orientation to the orientation of the rest of crystal as shown in Figure 26. This phenomena was reported to occur in semi crystalline polymers such as polyethylene[126–128], polypropylene [129] and polyamide 66 [130].

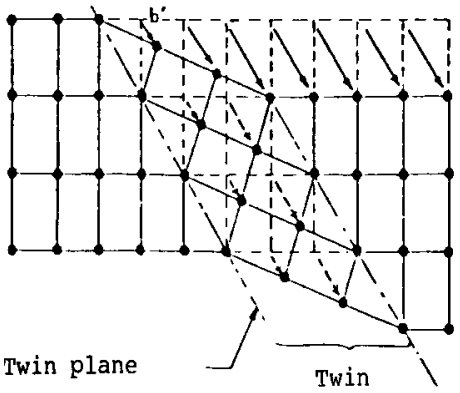

Figure 26: Illustration of twining mechanism in polymer

1.3.1.3. **Phase transformation**

High deformation level (plastic deformation) may induce a change in the chain conformation, which propagates step by step along the molecular chain inside the crystalline lamellea. Such a phase transition was observed in the case of polyethylene [128,131,132] polypropylene [133], PVDF[134], aliphatic polyamides [75] notably γ-α phase transition in the case of PA6 [135].

1.3.1.4. **Lamella fragmentation**

The deformation mechanisms described above are crystallographic processes common to all crystalline solids. A specific behavior of polymer crystals is the lamella fragmentation. The

destruction of crystalline lamellae has been widely studied in single crystals as well as bulk crystallized polymers [136–139]. Most of these works are focused on large deformation beyond the yield point. A common observation is the formation of craze which involves manifold structural transformations as cavitation, lamella twisting and folded-chain lamellae transformation into oriented microfibrillar structure. According to Peterlin's work regarding the tensile drawing of polyethylene and polypropylene, the first stage of lamella fragmentation involves coarse crystal slip and twinning (see Figure 27). An expect effect is the chains tilt toward the drawing direction. Such a tilt favors chain slip and subsequent break up of lamella into lamellar folded chain blocks [136].

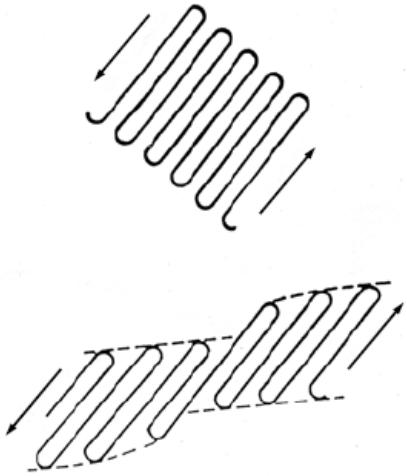

Figure 27: Peterlin's molecular model for the homogeneous shear and fragmentation of a crystalline lamella. Reprinted from [140]**.**

Recently, Detrez et al. [119] have examined the structural changes in poly (1-butene), polycaprolactone and polyamide 6 under uniaxial stretching prior to yielding. They reported that well below the yield point, a gradual fragmentation of the crystallites into smaller pieces is observed. They suggest that at low strain, lamella fragmentation is the main mechanism of damage in theses polymers without significant cavitation. It is believed that fragmentation occurs through sliding of lamella parts along interfaces between the crystalline blocks. This block sliding occurs either due to coarse chain slip and twinning, or particular disorder of the block interfaces.

1.3.2. Deformation of the amorphous phase

Deformation of semi-crystalline polymer is a process which involves the crystalline lamellae as well as the amorphous layers. It is believed that amorphous chains are solicited by the crystalline lamellae according to the basic mechanism presented in Figure 28 .

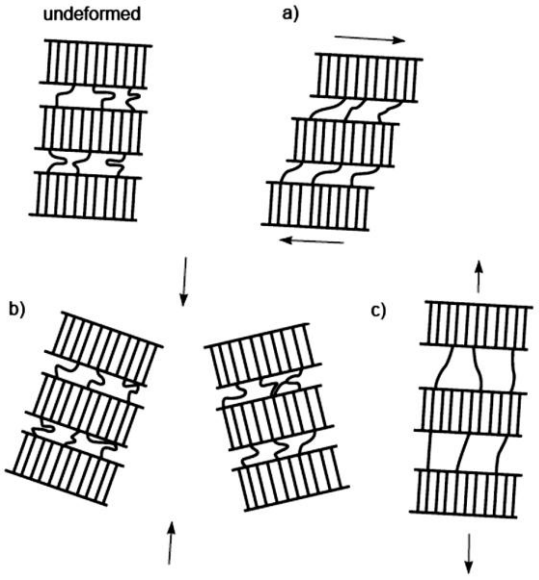

Figure 28: Deformation in amorphous regions [120]**: a) interlamellar slips; b) stack rotation; c) interlamellar separation**

According to Bowden et al. [120,138], three kinds of deformations can be identified: Interlamellar slip, lamella-stack rotation and interlamellar separation.

- The interlamellar slip is usually reversible, it occurs mainly in the early stage of deformation by shearing of the amorphous layer between the crystalline lamellae [122,123,141]. This reversibility was explained either by elastic properties of the amorphous phase or significant residual stresses in the undeformed material [123,141,142]. Pope et al. noted that [123] some irreversibility can be observed due to breaking of chains or pulling out of macromolecules from lamellae. It is interesting to note that some works reported that interlamellar slips compete with crystallographic slips in the crystalline phase [123,143].

- The second type of deformation is lamella-stack rotation (Figure 28-b). It consists in the rotation of stacks of lamellae (up to ten crystallites) under the influence of stress and implies cooperative movements of amorphous phase and crystallites. It is worth noting that this kind of movement requires a relatively easily deformable amorphous phase [122,144,145]

- The third type of deformation is the interlamellar separation (Figure 28-c) [123,142,146–148]. It consists in the separation of the lamellae oriented perpendicular to the load direction. This type of deformation depends strongly on the material structure such as the lamella size, the entanglement density of the amorphous phase and the number of tie molecules that interconnect the crystalline lamellae.

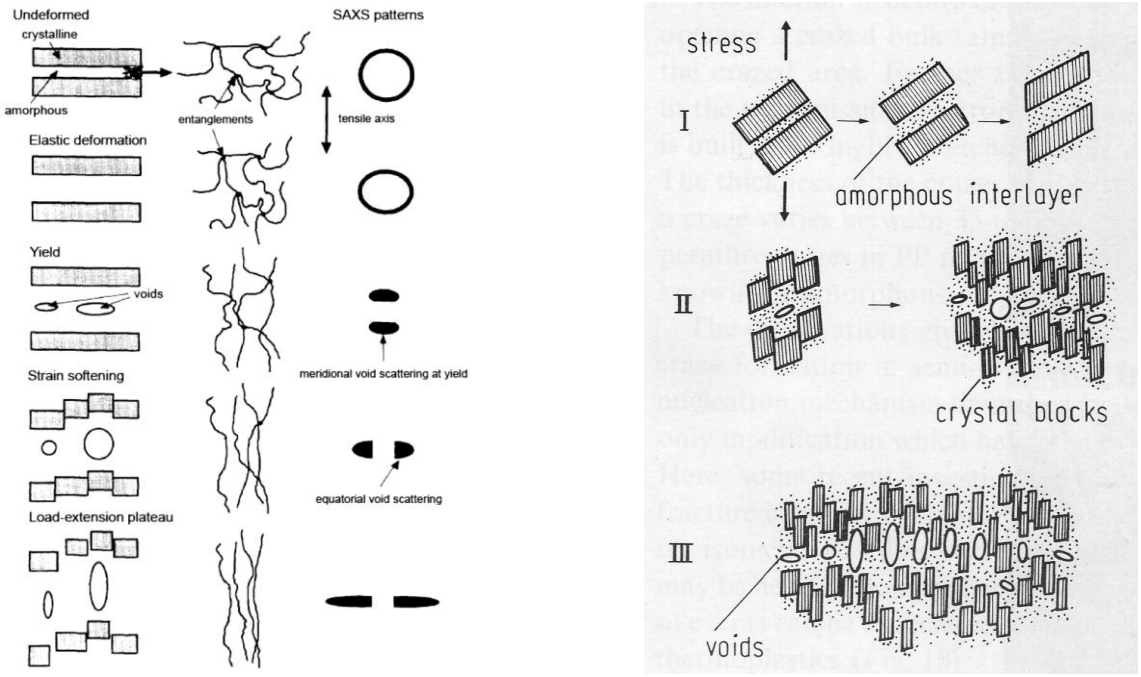

(a) **(b)**

Figure 29: Schema of cavity formation and growth in the interlamellar region during deformation of semi crystalline polymer. Reprinted from (a): Butler et al. [139] **; (b) Friedrich** [149]

At high deformation, lamellae separation is often accompanied by the formation of voids especially in the case of materials having strong and thick crystals like polypropylene and high density polyethylene. Recent works pointed out that cavitation appears in the amorphous phase just before reaching the macroscopic yield point. Voids nucleate mainly between lamellae oriented perpendicularly [139] or at an angle of approximately 45° to the load direction [149]. Figure 29 (b), illustrates the related mechanism of cavitation highlighted by X-rays scattering. At the beginning, the nucleated voids are confined between lamellae and oriented perpendicularly to the direction of deformation. As the deformation level increases, lamellae separation becomes greater, favoring further cavitation. At larger deformation, lamellae fragmentation is observed resulting in a strong extension of the nucleated cavities. These latter become stretched along the load direction.

1.3.3. Deformation of spherulites

Numerous studies were interested in the morphological changes within the spherulite structure under loading. They reported that both the intra and interlamellar domains are involved according to the elementary deformation processes described above (paragraphs I.1.3.1 and I.1.3.2). The local deformation modes are determined by orientation of lamellae stacks with respect to the main deformation axes. Taking into account that spherulite consists in radially arranged lamellae and amorphous regions, three characteristic regions differing in relative arrangement of lamellae are considered as shown in Figure 30.

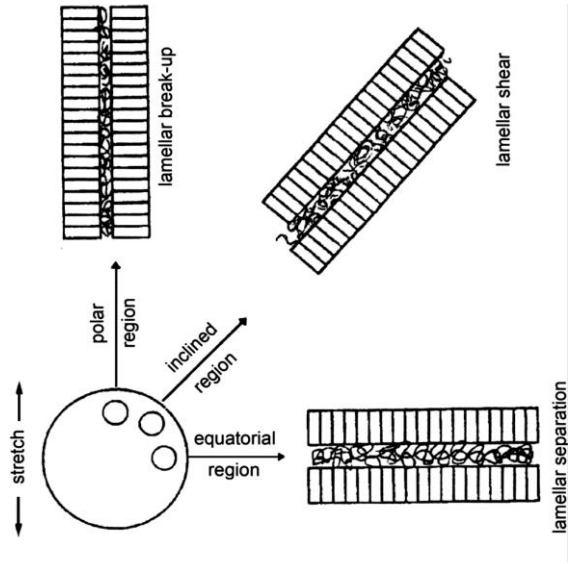

Figure 30: Schematic presentation of principal regions of spherulite during uniaxial deformation. Reprinted from [150]

- Polar region: in this spherulite region lamellae are roughly parallel to the direction of deformation. This spherulite region exhibits the highest resistance to plastic deformation involving shear, slip and rotation of stacked lamellae. At high deformation level, lamellae breaking into small block was observed [127,151].

- Equatorial region: in this region lamellae are arranged almost perpendicularly to the direction of deformation and then are submitted to the highest stress value at given strain. The mechanism involved in this region implies lamellar separation and rotation.

- Diagonal region: In this region, lamellae are oriented at an angle of approximately 45° to the load direction. In consequence, lamellar separation accompanied by shear of interlamellar amorphous layer is mainly observed. As deformation level increases, lamellar rotation in the direction of the applied load may be observed.

Many works describe the cavitation during deformation of semi crystalline polymers. Of particular intersest, Gałęski et al. [152] reported that interlamellar separation in the equatorial spherulite region is accompanied by lamellae deformation "kinking" and nanocavities formation in the amorphous phase of PA6 (Figure 31-c). Similar observations were also noted elsewhere [138,153,154]. In these works, the voids apparition was related to chain breakdown and chain pulling-out at high lamella separation. On the other hand, lamellae located in the diagonal region are brought to rotation because of intra-and interlamellar slips (Figure 31-b). On the contrary, lamellae located in the polar region are deformed mainly by shearing until crystallite fragmentation. This leads to void nucleation in the polar region at further stage of deformation as reported by Galeski et al. (Figure 31-d). The result of the complex process (plastic deformation of the crystal and cavitation in the amorphous phase) taking place in the spherulite structure is a macroscopic change in the spherulite's shape: sphere-ellipse.

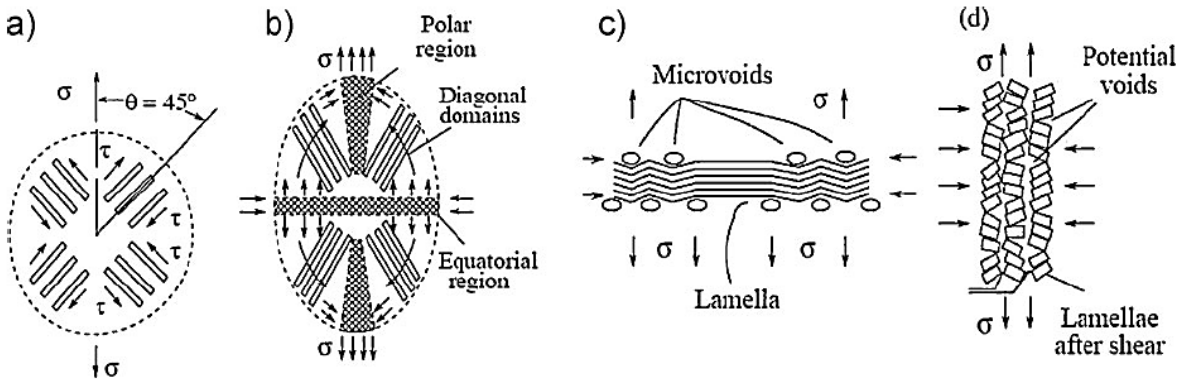

Figure 31: Deformation phenomena in the spherulite structure under uniaxial deformation: (a) crystallites of the diagonal region; (b) lamellar rotation in the diagonal region; (c) kinking of lamellae due to shear instability in the amorphous matrix in equatorial region; (d) shear instability due to chain slip in lamellae in polar regions [155].

It turned out that cavitation process under loading is very sensitive to the thermal history of the polymer [110,113,139,156–158] as well as to its microstructure such as crystal size and lamellas orientation [159]. For instance, large spherulites composed of thick lamellae of poly(1-butene) experience, prior to the yield point, intensive cavitation phenomena while small ones exhibit gradual fragmentation of the crystallites into smaller pieces [118]. Indeed, Pawlak et al. pointed out [137] that a competition between cavitation and activation of crystal plasticity is taken place during deformation. Cavitation, mainly associated with chain pulling-out and/or scission, occurs in polymers having strong and well developed crystal such as POM, PP, and HDPE or annealed samples (thick lamellae). Nevertheless, plastic deformation of crystals takes place in polymers with thin and defected crystals like LDPE. The same authors concluded that in the case of PA6 which contains more rigid crystal, nanocavitation probably occurs; nevertheless the generated voids could be quickly closed because of the high surface tension of PA6. In a related study, they do not observe any empty voids by (TEM) but only traces of damaged material (regions having lower density) between the crystalline lamellae.

A second factor influencing the cavitation process is the molecular weight of the polymer [113,156–158,160]. It is established that increasing molecular weight leads to less cavitation probably due to higher density of chains entanglement in the amorphous phase [139,160].

2. Long term mechanical properties

Long term mechanical properties or fatigue behavior of polymeric material is commonly studied through uniaxial (tensile and/or compression) or flexural cyclic loading tests. The typical cyclic load is a square, triangular or sinusoidal wave with a given amplitude, mean stress (or strain), stress ratio (minimum stress/maximum stress) and frequency as shown in Figure 32.

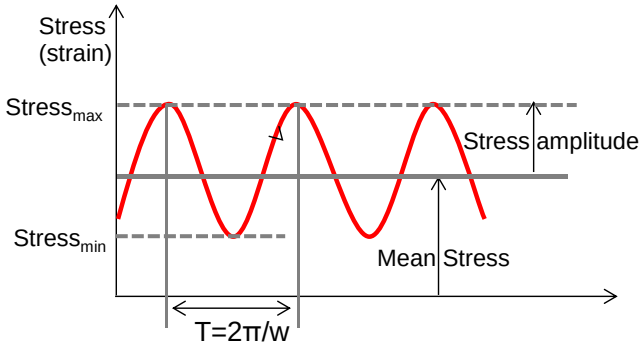

Figure 32: General parameters of fatigue test

It was reported that, under continuous load, failure occurs often at stress level lower than that observed in the case of static loading. This difference of stress at failure was related to the damage accumulation (nanocavities, submicrocracks...) that causes the ultimate failure. Depending on the applied stress level and the frequency, two modes of fatigue failure in thermoplastic polymers were identified: thermally dominated failure and mechanically dominated failure.

- The thermally dominated failure occurs primarily at relatively high stresses and frequencies. In such conditions, polymers generate significant heat, essentially by internal damping, which is not totally evacuated due to their low thermal conductivity. In consequence, the polymer temperature rises continuously throughout the test. As the temperature sample increases, the physical and mechanical properties of the polymer will be affected. This thermal softening of the material is supposed to be the main cause of the quick failure. It worth noting that some works reported that in some cases the temperature of the polymer near to failure exceeded its melting temperature [161,162].

- The mechanically dominated failure is observed at relatively low stresses and frequencies. In such conditions, the self-heating is lower and then the temperature of the sample reaches a stable value due to thermal equilibrium with the surrounding environment. This regime corresponds to the true fatigue response of the material, and in this mode the polymer can withstand a large number of cycles before failure (long fatigue lifetime).

It was assumed that mechanically dominated process involves the nucleation of damage and its subsequent growth in the form of distributed microcracks[163]. The damage initiation is generally followed by a subsequent propagation of the developed microcraks. Therefore, the total fatigue lifetime is considered as the combination of number of cycles needed to initiate damage or microcraks with the number of cycles required to propagate the obtained microcraks to a critical size causing the final failure.

Depending on the polymer nature, the total fatigue lifetime may be mainly associated either to the initiation stage or to the propagation stage. For example, PMMA exhibits a short craze initiation time but a long crack propagation stage, the latter governing predominantly its total fatigue lifetime. On the contrary, the total fatigue lifetime of semi crystalline polymers such as polyacetal and PA66 is totally governed by the initiation stage as shown in Table 1.

Material	K_{IC} (MPa/m^2)	N_i	N_p	N_{total}
Polyacetal	3.1	~4.8x10^6	186000	5x10^6
PA66	6	~2x10^7	9000	2x10^7

Table 1: Contribution of the initiation and propagation stages to the total fatigue lifetime of Polyacetal and PA66 [164]

In this section, we are interested in the effect of the microstructural parameters such as molecular weight, crystallinity and morphology on the mechanical fatigue lifetime. To begin with, their impact on the total fatigue lifetime is described in the first part and subsequently their effect on fatigue crack propagation rates will be highlighted in the second part.

2.1. Wöhler curves

The total fatigue lifetime (initiation and propagation) can be characterized following the Wöhler's procedure. It consists in applying a cyclic stress on notched or un-notched specimens and recording the number of cycles at failure. The test is often conducted on a wide range of stress levels (usually $0.3\sigma_y < \sigma_{max} < 0.65\sigma_y$) and the data are presented in the form of σ–N curves.

In general, the fatigue lifetime decreases with increasing the applied stress as a result of greater damage accumulation per cycle at higher stress. The damage magnitude and consequently the total lifetime are dependent on many factors including the test conditions (frequency, temperature, environment…) and the inherent characteristics of the material (molecular weight and microstructure).

2.1.1. Effect of the microstructure

It was pointed out that semi-crystalline polymers that contain intercrystalline linkages present superior fatigue performance than amorphous polymers. For instance, the ratios of the endurance limit (stress level below which the material has an infinite life) to tensile strength, are 0.5, 0.3, and 0.5 for polyacetal, polyamide66 and polyterafluoroethylene respectively against 0.2 for amorphous polystyrene [165]. Similarly to the static mechanical properties, many works reported that deformation and failure modes of semi-crystalline polymers under cyclic loading are dependent on their microstructure features and multi-scale morphology such as crystalline fraction, crystal lattice, crystalline lamella and spherulite .

In contrast with the huge literature reported on the relationship between the microstructure of polymer and its fatigue crack propagation resistance, a limited number of works on unnotched specimens can be found. In general, it has been reported that semi-crystalline polymers having high degree of crystallinity [166], fine and more uniform spherulites [167–169] exhibit low self-heating and excellent fatigue performance. For instance, Bareishis et al. [170], demonstrated that certain additives (stabilizers and antioxidants) enhance the

spherulite nucleation and induce some refinement in the crystal structure of polycapromaide. This contributes to an increase of the material stiffness as well as of its fatigue performance.

Furthermore, Stinskas et al. [171] studied the impact of temperature-induced structural changes on the fatigue properties of Nylon6 under stress-controlled conditions. They demonstrated that oil heating at 180°C of polyamide 6 generates uniform spherulite with monoclinic crystal packing which exhibit superior fatigue properties than the untreated PA6, which owned a less perfect spherulitic structure and a hexagonal crystalline form (see Figure 33).This improvement of fatigue lifetime was explained by the existence of more complete supermolecular and crystalline structures after heat treatment.

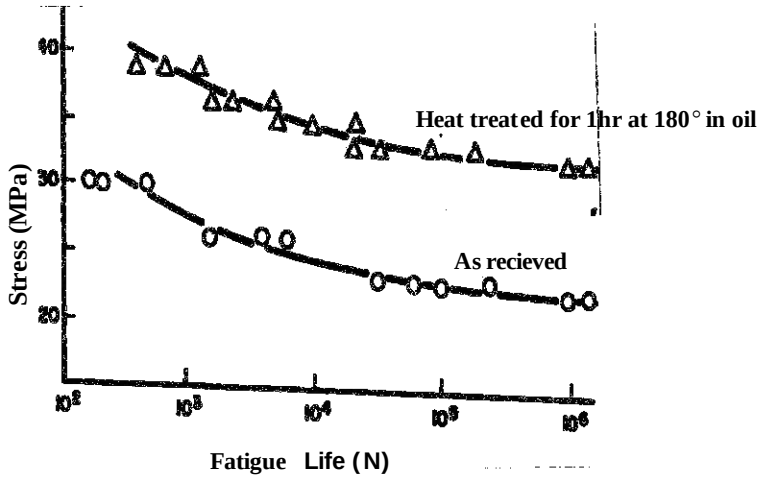

Figure 33: Effect of the crystalline microstructure on the fatigue lifetime of polyamide 6 (reprinted from Stinskas[171]**).**

2.1.2. Effect of molecular weight

Many works concerning the effect of molecular parameters on the total fatigue lifetime of amorphous polymers were investigated [172,173]. It was found that both molecular weight average and distribution strongly affect the initiation and propagation of damage during fatigue [174]. For example, the fatigue endurance limit is increased by a factor of 7 when the average molecular weight of polystyrene increases from 1.6×10^5 to 2×10^6 for a given molecular weight distribution. It was also observed that the S–N curves shift upwards and to the right, indicating a longer lifetime at the same applied stress as shown in Figure 34 [175].

Furthermore, it was found that the addition of only 1% of high molecular weight polystyrene ($Mw = 7 \times 10^5$) induced a significant increase of the total fatigue lifetime of low molecular weight polystyrene ($Mw = 10^4$) [176]. Additional studies have been conducted to identify the sensibility of the fatigue lifetime to the molecular weight distribution[177,178]. It was shown that, at the same Mn value, polymers having broad molecular weight distribution exhibit higher lifetime than polymers with narrow distribution. From a general point of view, the increase of fatigue lifetime with the molecular weight could be explained by higher entanglement density and larger orientation hardening of crazed microfibrils. Both factors imply more resistant fibrils in the craze tip, which results in a stable craze that propagates slowly and then a longer total cyclic life [172,177].

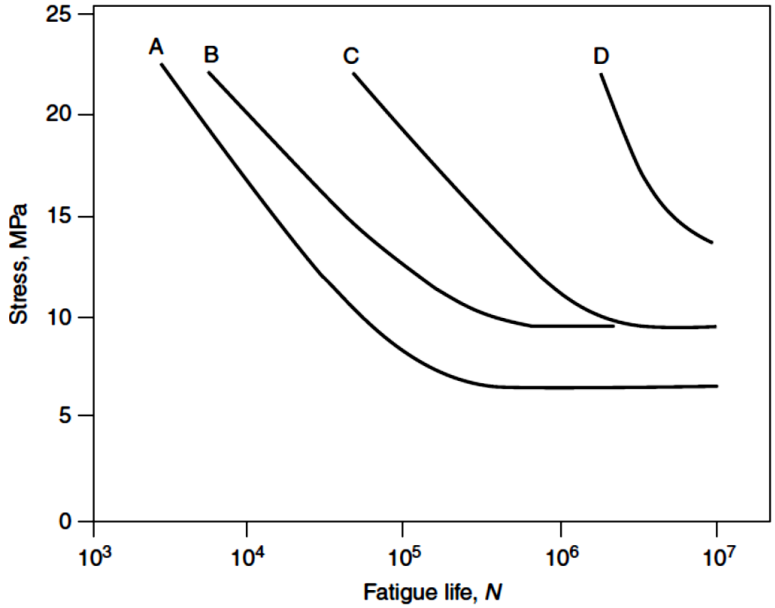

Figure 34: S-N curves of polystyrene with different Mw (A= 1.6 × 10^5, B= 3.3 × 10^5, C=8.6 × 10^5, D= 2.0 × 10^6)

Even though numerous studies have been conducted on amorphous polymers, little work has been done to elucidate the impact of molecular weight on the endurance of semi-crystalline polymers. Of particular interest, Sauer et al. reported that the fatigue lifetime of polyethylene was improved when the molecular weight was increased [175]. A similar observation (one decade improvement) was reported by Nishimura et al. on notched specimens of medium density polyethylene [179] (see Figure 35). However, Niinomi et al. stated in their work that increasing the molecular weight of ultra-high molecular weight polyethylene (UHMWPE) does not necessarily increase fatigue lifetime. They concluded that fatigue lifetime was strongly affected by the drop of the crystalline fraction rather than by the molecular weight increase, since they observed a reduction of the crystallinity degree with increasing the molecular weight [180].

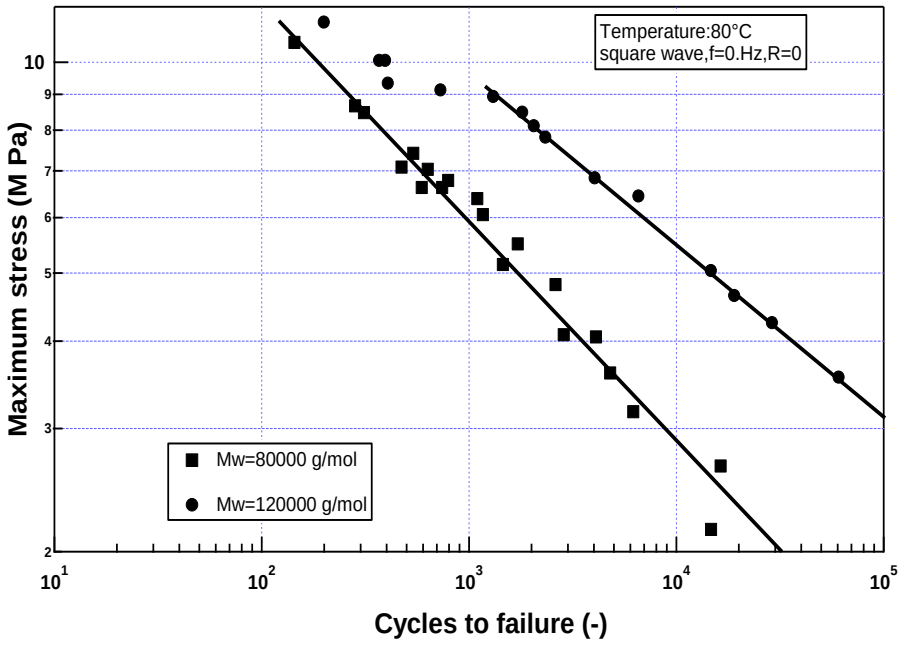

Figure 35: Effect of Mw on the fatigue behavior of medium density polyethylene

2.1.3. *Effect of moisture*

As mentioned earlier, moisture absorption obviously affects the physical and mechanical properties of polyamides. The effect of moisture on the mechanical behavior of polyamides has been well described. In general, Young's modulus and yield stress decrease, whereas impact toughness increases with increasing water content. Concerning fatigue resistance, it was reported that dry polyamides exhibit superior performance than wet polyamide under controlled cyclic stress [181–183]. For example, the S-N curves for dry and 50% RH conditioned polyamide 66 are presented in Figure 36. It can be seen that at given applied stress, dry PA66 exhibits higher lifetime than that at 50% RH. Moreover, the endurance limit is reduced by as much as 30% when polyamide 6,6 is equilibrated at 50% RH.

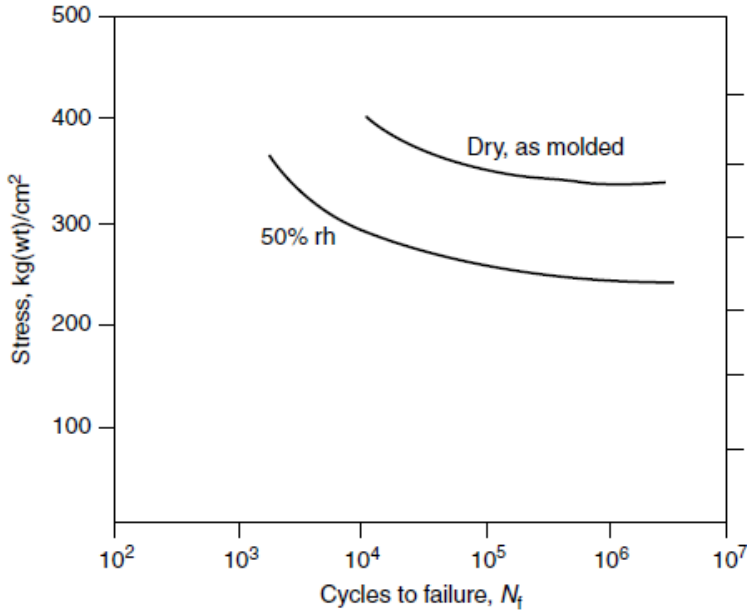

Figure 36: Wöhler curves for dry and 50% RH conditioned polyamide66. Reprinted from [6]

2.2. Fatigue Crack Propagation

Fatigue Crack Propagation (FCP) tests were developed to assess the lifetime of samples that contain an initial crack. It is assumed that when the provided mechanical work exceeds the energy required to create new crack surface, the crack propagates and then either stops or continues until the final failure [184]. For example, brittle material exhibits dramatic crack propagation rate leading to immediate failure and then short lifetime. However, the energy dissipated to propagate the crack in the case of ductile material is very important, resulting in slow crack propagation and hence long lifetime.

This energy balance is dependent on the stress intensity factor (geometry, crack length and loading conditions) as well as on the intrinsic material properties. Many studies are dealing with measuring FCP rates in polymers as a function of these different parameters. Of particular interest, the Paris Law [185] states that the relationship between the crack growth rate and the difference of stress intensity factor is a power-type law as described in equation **(2)**.

$$\frac{da}{dN} = A(\Delta K)^n \quad (2)$$

Where $\frac{da}{dN}$ is the growth rate of a crack of length a; ΔK is the difference of stress intensity factor associated with the maximum and the minimum stresses in a given cycle; A and m are constants depending on the material.

It was supposed that slow crack evolution, at a given stress level, originates from progressive subcritical crack growth prior reaching a critical size for crack propagation. The crack growth rate is dependent on numerous structural parameters such as crystallinity, morphology and molecular weight. In the following, the relationship between these parameters and the crack propagation rate is discussed.

2.2.1. Effect of the microstructure

It is interesting to underline that semi-crystalline polymers are more resistant to crack propagation than amorphous ones [175]. For instance, it was reported that FCP rates of amorphous polyamide are around three orders of magnitude higher than those observed for semi crystalline polyamide 66. Similarly, Ramirez et al. [186] reported that amorphous polyethylene terephthalate (PET) exhibits superior FCP resistance in comparison with other amorphous polymers thanks to the development of crystalline structure, that is remarkably strong, at the crack tip during the fatigue test.

Figure 37 shows the FCP rates for several semi-crystalline polymers in comparison with common amorphous polymers [174]. It can be seen that the lowest FCP rate was observed for Polyamide66 [187,188], Polyamide6[189], Polyvinylidiene fluoride (PVDF) [190] and polyacetal [191].

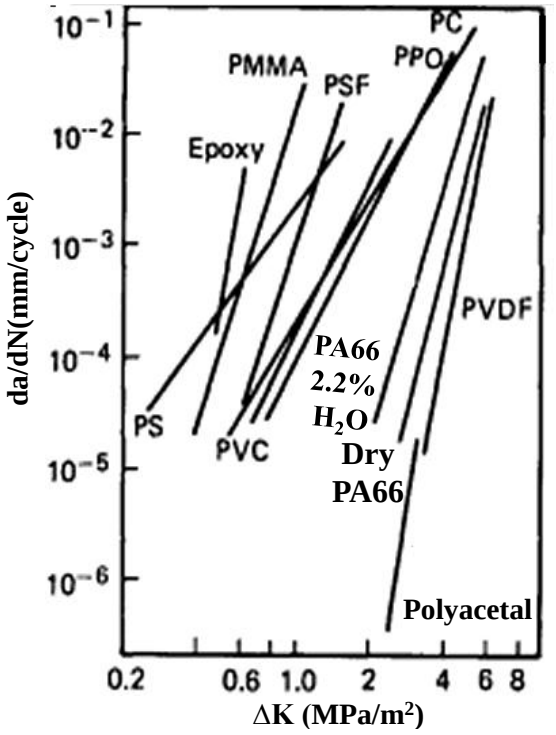

Figure 37: Comparison between the FCP rates of amorphous and semi crystalline polymers

The greater FCP resistance of semi-crystalline polymers in comparison with amorphous ones was correlated to the higher energy dissipation during the crystallite deformation as well as to the existence of strong fibrils connecting the crazes [192–194], as schematically presented in Figure 38.

Many reports concerning the effect of degree of crystallinity on the fatigue behavior of semi-crystalline polymers have been published. For instance, Wang et al. reported that recycled polyamide 46 exhibits lower elastic modulus, yield strength and FCP resistance than those of original material, likely due to a drop of the crystallinity after recycling process [195]. Moreover, Iwamoto et al. demonstrated that increasing crystallinity degree of polypropylene results in an improvement of its fatigue performance [196,197]. Concerning high density polyethylene materials, contradictory conclusions were reported. Some works pointed out that increasing the degree of crystallinity results in a decrease of the FCP rates in polyethylene [198–200] while others reported that samples having smaller degree of crystallinity exhibits a higher FCP resistance [201,202]. It should be noted that, in these works, the crystallinity effect has been investigated by means of various thermal treatment such as quenching and annealing. As consequence, the crystalline microstructure (e.g., spherulite, lamella thickness and tie molecules density) of these samples was altered at the same time as their crystallinity. This suggests that the different parameters associated to the multi-scale crystalline structure could yield different effects on the FCP resistance (enhancement or degradation).

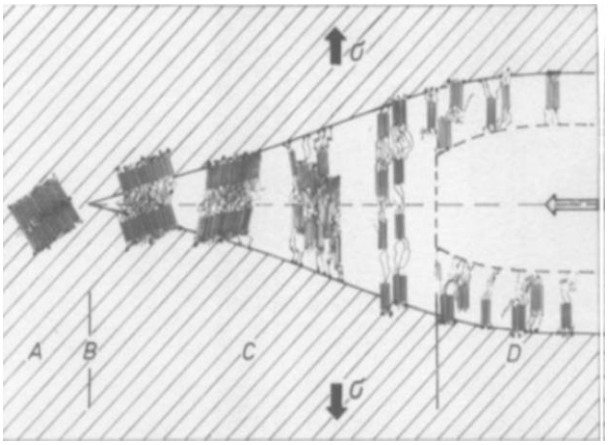

Figure 38: Stable craze of semi crystalline polymer containing fibrils structure

Strebel et al. [202], demonstrated that annealing polyethylene specimens induces a thickening of the crystalline lamellae and a crystalline fraction increase which are supposed to be favorable for fatigue resistance. However, these samples exhibit much lower resistance to the crack initiation and subsequent propagation than the quenched ones. Estimation of the entanglements number shows that the relative tie molecule concentration in annealed sample is 1.5 times lower than that in the quenched one. Thus, it was concluded that the fatigue behaviour of these samples was likely governed by a competing effect between crystallinity degree, lamellae thickness and the tie molecule density (chains connecting the crystalline lamellae). Such evidence of this competition effect was also pointed out by Ramirez et al in the case of initially amorphous PET annealed at four different temperatures for various amounts of time. They demonstrated that at any annealing temperature and at a constant value of the stress intensity factor, FCP rates decrease as annealing proceeds and then increase catastrophically. The decrease of FCP rate with annealing time was related to the crystallization of PET during the annealing treatment. However, even at high crystalline

fraction, the authors supposed that tie chains density decreases to a point that no effective entanglement network is present to link the crystallites, and then fracture readily occurs [203]. Accordingly, tie molecules density appears to play a major role in the FCP resistance of semi crystalline polymers.

Regarding the reported studies so far, it can be seen that it is difficult to make vary the crystalline content, the lamellae thickness and the tie chain density independently. As a consequence, the contribution of each parameter on the fatigue resistance could not be determined separately.

One attempt has been made to isolate the effect of tie molecule density on the FCP resistance of polybutylene terephthalate (PBT). The authors of this study prepared specimens of PBT by annealing quenched amorphous samples under controlled hydrolysis conditions [204]. They demonstrated that prepared specimens exhibited similar degree of crystallinity, supramolecular structure and lamellae thickness but different tie chain densities. At the end of their work, they confirmed again the dramatic influence of the tie molecule density on the FCP resistance of semi-crystalline polymers. To summarize, it has been established that increasing molecular weight and rapidly cooling sample from the melt induce higher concentration of tie molecule in the intercrystalline zones resulting in a higher damping capability and a superior crack growth resistance [201,202,204,205]

Finally, the effect of spherulite size and distribution on FCP response of semi crystalline polymers was studied. Friedrich et al. demonstrated that FCP resistance of isotactic polypropylene decreases as the content of large spherulites increases [206]. Moreover, Runt et al. reported that larger spherulite size and distribution appears to have a deleterious effect on fatigue properties of polyethylene [201]. In contrast, Laghouati et al. mentioned that no significant effect of spherulite size on FCP resistance of polyethylene was observed. A similar conclusion was also drawn by Yeh et al., who found that the propagating crack front is preceded by a significant zone of plastic deformation and is not expected to directly encounter the spherulites [205].

2.2.2. Effect of molecular weight

Contrary to the static properties (modulus, yield and toughness) which change little over a broad range of molecular weights, a small increase in the molecular weight Mw may result in a significant improvement of the resistance to fatigue crack propagation.

In the case of amorphous polymers, the positive effect of the molecular weight was largely described for notched Poly(methyl-methacrylate) [207], polyvinylchloride [208], polycarbonate [209,210] and polystyrene [211]. Evidence supporting the positive effect of molecular weight was also pointed out by Wellinghoff et al. They concluded that molecular weight distribution (MWD) of polystyrene containing small proportions of high molecular chains generate stable crazes and then low FCP rates [176].

In related work, Michel et al. found that the Paris law was consistent over a wide range of Mw and ΔK, the relationship between the FCP rate and the Mw being described by the following equation [212].

$$\frac{da}{dN} = A' e^{\frac{B'}{M_w}} (\Delta K)^n \quad (3)$$

where A', B' and n are constants depending on the material and test conditions.

For semi-crystalline polymers, the same trend (High molecular weight with a relatively narrow MWD implies high FCP resistance) was observed in the case of high density polyethylene [200,205,213], Polyacetal [191,214], Polyamide 66 [214] (see Figure 39) and polypropylene [215]. This improvement was related to higher tie molecules density (chain connecting the crystalline lamellae) at higher Mw, resulting in lower crack propagation. However, the increase of the crack resistance with the molecular weight is less significant than that in amorphous polymers. This was attributed to the important contribution of the crystalline structure in the crack stabilization as presented earlier.

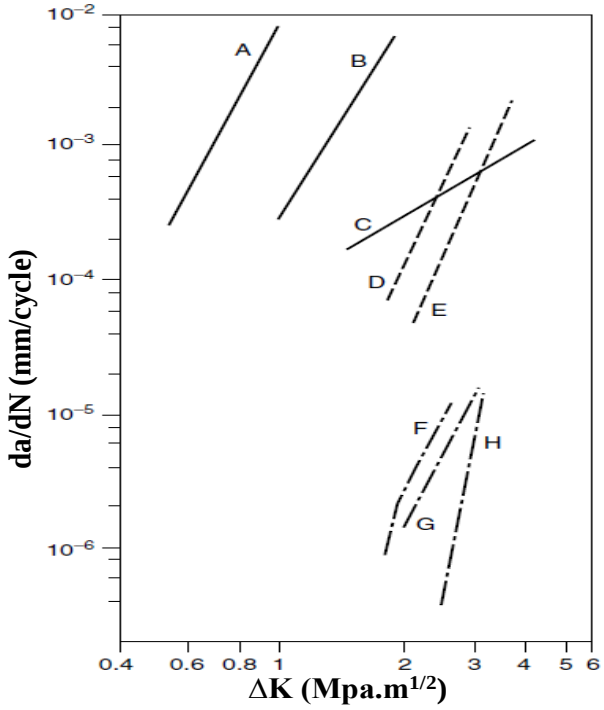

Figure 39: Fatigue crack growth rates for HDPE Mw (A = 45 000, B= 70000, C= 200000), PA66 Mn (D= 17000, E= 34000) and polyacetal Mn (F= 30000, G=40000, H= 70000) [163]

To sum up, it is assumed that FCP response is related to the breakdown of the entanglement network which includes tie molecules, that depends on the proportion of high Mw chains. Indeed, low Mw chains exhibit low resistance to chains disentanglement and then tie molecules will be rapidly extended and later pulled-out from the lamellae or broken down under cyclic loading (see Figure 40-c and f). Longer polymer chains are more entangled and then exhibit longer time for disentanglement. In addition, a high density of tie molecules distributes the load between the extended chains resulting in less chain scission. This may lead to bending and/or disintegration of the lamellae to which tie molecules are attached, resulting in the formation of resistant fibrils as schematically presented in Figure 40-d and e.

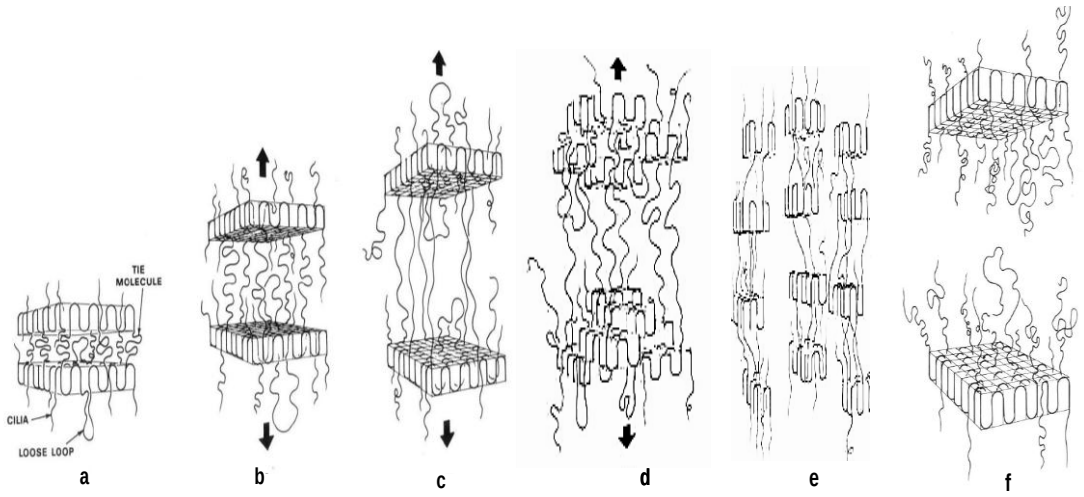

Figure 40: steps in the deformation of polyethylene under long term loading conditions: (a) Initial state; (b),(c) Lamella separation; (d), (e) strong tie molecule density leading to ductile deformation; (f) chain scission of tie molecules leading to brittle failure at low molecule molecular weight. Reprinted from Lustiger et al. [216]

2.2.3. Effect of moisture

The effect of moisture content on the FCP resistance of polyamide 66 was described by Bretz et al. [217]. They observed that FCP rate of PA66 decreases with the moisture level until a minimum corresponding to a water content around 2.5% and then increases rapidly reaching maximum value on saturation (see Figure 41-a). This behavior has been attributed to the changes of hydrogen bonds between the amide groups induced by water. At water content around 2 .5%, the local mobility of polyamide chains at the crack-tip is relatively enhanced. This increased mobility allows for crack-tip blunting as a result of the combined effects of enhanced plastic deformation and localized crack-tip heating. However, at high water content, plasticizing effect of water is very important leading to a decrease of the room-temperature modulus of the bulk material. This stiffness lowering overshadows crack-tip blunting and contributes to a general worsening of FCP behaviour as schematically illustrated in Figure 41-b.

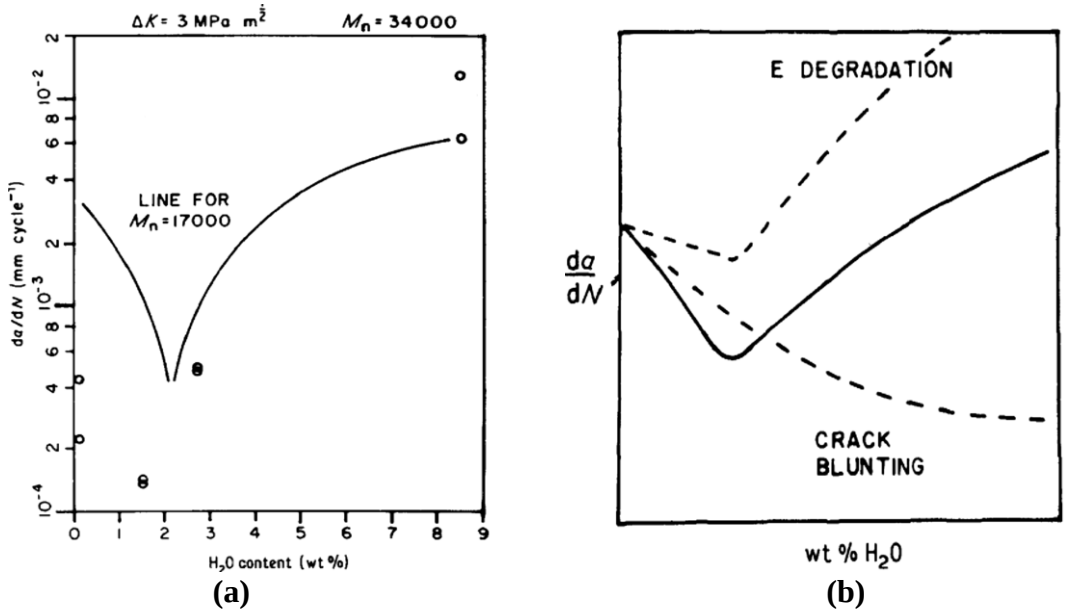

Figure 41: Schematic diagram of the effect of crack blunting and modulus degradation on crack-growth rates in nylon as a function of moisture content. Reprinted from [217]

2.3. Damage mechanism

Numerous works have been devoted to the study of the failure mechanisms that occur in polymers under cyclic loading. Most of them were carried out on glass fiber reinforced polymers and were mainly focused on the last stage of lifetime. It was well established that fatigue failure mechanism occurs as below: Damage is initiated in the matrix (polymer) near the fibre ends resulting in voids nucleation. These voids grow and coalesce into microcracks accompanied by fiber debonding. The microcraks, bridged by drawn polymer or unbroken fibers, grow until reaching a certain critical size of crack leading to specimen failure [182,183,218–221].

Recently, more attention has been paid to the former stage of fatigue. Microstructural and morphological changes (e.g. physical aging, strain hardening or softening and crystallization) in amorphous and semi crystalline polymers have been found to occur in the first stage of loading [164,222–224]. In addition, damage characterizations revealed that nano-cavitation and nano-cracking occur in the earlier stage of fatigue. As fatigue proceeds, further cavitation accompanied by growth and coalescence mechanisms were observed. For example, Small angle X-ray Scattering (SAXS) of polystyrene submitted to cyclic loading indicated that some voids are nucleating and growing following a simple exponential law [225]. Such evidence of cavitation was also proved by Yee and co-workers. They observed the formation of voids in polycarbonates with initial dimensions of 60 nm and 150-200 nm in directions parallel and perpendicular to the load direction, respectively [226,227]. In related work, they proved by Positron annihilation lifetime spectroscopy that the free volume increased with the number of fatigue cycles. They suggested that the increase of the hole size originates likely from a coalescence mechanism of nucleated voids [228]. Furthermore, Zhurkov et al. observed incipient cracks (platelet shaped nanoscopic voids) that appear at early stages and then coalesce leading to crazing before failure [229]. It should be noted that in the case of PMMA, crazes appear at relatively early stage but the total lifetime is principally related to the crazes growth [230].

Concerning semi crystalline polymers, Kausch et al. have studied the long time failure in oriented lamellar morphology, particularly in polyamide 66 fibers [231]. They concluded that thermo-mechanical scission of extended chains in the amorphous phase was the important cause of damage accumulation. Little work has been done to characterize damage mechanism in spherulitic microstructure. Of particular interest, Jones et al. pointed out that at initial stage, small crazes initiate and grow homogenously through bulk spherulitic isotactic polypropylene. With increasing the number of cycles, the number density of crazes decreases while the craze length increases. It was suggested that as the fatigue test proceeds, small crazes coalesce continually resulting in random distributed larger crazes [232].

More recently, in our laboratory, Mourglia-Seignobos et al. have described the damage mechanism in polar semi crystalline polymers especially in the case of polyamide 66 [233]. They observed nucleation of nanocavities in the interlamellar amorphous phase, mainly located in the equatorial region of spherulites. They reported that during the first stage of fatigue, the number of nanocavities increases with the number of cycles while their size remains constant. However, as the fatigue test continues, cavities grow perpendicularly to the load direction resulting in elliptic shaped voids as schematically presented in Figure 42. The size of the corresponding voids characterized by USAXS was in the range of 20 nm to 13 µm perpendicular to the load direction and of 20 nm to 2.6 µm in the load direction. It was

suggested that this process was the precursor to crazing observed by transmission electron microscopy before failure.

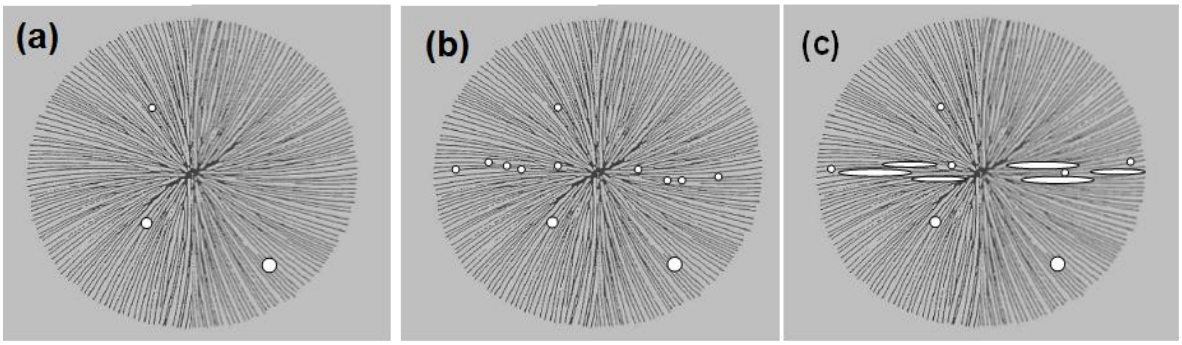

Figure 42: Schema of fatigue damage mechanism: a) initial micronic cavities (b) nucleation of nanometric cavities in the amorphous phase (c) growth of the nanometric cavities in direction perpendicular to the stress direction.

The fatigue damage presented above has also been quantitatively described. The energetic balance of cavities nucleation being evaluated on the basis of the rupture theory of elastic materials [234], which is locally applied within the amorphous phase. Accordingly, the activation energy required to create a surface has been related to the elastic energy stored in the sample and the work involved in the creation of this surface, as given in equation **(4)**.

$$\zeta(\sigma) = W_S + W_E = \pi\gamma a^2 - \frac{1}{2}\frac{\pi}{6}K\left(\frac{\mu\sigma}{E}\right)^2 a^3 \qquad (4)$$

Here W_S represents the energy required to create the surface and W_E represents the released elastic energy upon cavitation under a certain stress value.

where ζ is the activation energy of cavitation, γ is the surface free energy, a is the cavity diameter, K is the bulk modulus, E is the elastic modulus, μ is the local amplification factor defined as the ratio of the local deformation to the macroscopic deformation.

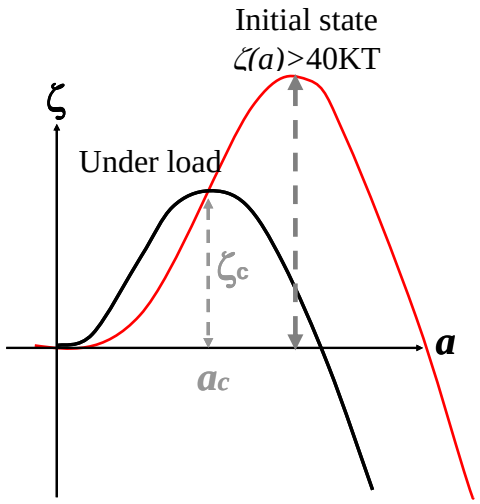

Figure 43: Potential energy of cavitation as a function of cavity diameter

They assumed that at room temperature, the activation energy of cavitation is very high and then no cavitation can be observed. When applying a force, the activation energy is reduced

and then it becomes possible to get over the maximum of the potential energy as schematically illustrated in Figure 43.

On the basis of the first derivate of the activation energy function, they determined the energy barrier needed for void nucleation under a given stress as below (5):

$$\zeta(\sigma) = \frac{64\pi}{3} \frac{\gamma^3}{K^2 \left(\frac{\mu\sigma}{E} \right)^4} \cong 60 \frac{\gamma^3}{K^2 \left(\frac{\mu\sigma}{E} \right)^4} \quad (5)$$

This energetic analysis suggests that void nucleation involves the surface free energy (γ) and the bulk modulus of the amorphous phase (K) for a given level of local deformation ($\mu \frac{\sigma}{E}$). This latter is dependent on the macroscopic applied stress as well as on the microstructure of the material (e.g. tie molecules density, lamella thickness and orientation, crystallinity degree and spherulite size).

Conclusion on the state of the art

We have seen that polyamides, used as engineering thermoplastics, can be prepared by polycondensation reaction between diamine and diacid functions. A particular attention has been paid to aliphatic polyamides and especially polyamide 66. The crystalline multi scale structure of polyamide 66 was described, and it was shown that the current organization was depending on the chemical and molecular structure of polyamide but also on the synthesis and the processing conditions. For instance polyamides having high molecular weight exhibit thick crystalline lamellae, large spherulites and most likely low crystalline fraction. Also, it was pointed out that high cooling rate from the melt implies thin lamellae, small spherulites and high crystalline fraction.

In the second part, the static mechanical properties of semi crystalline polymers and particularly of polyamides were described and the damage mechanisms were presented at all the microstructure levels. On one hand, it was shown that molecular architecture little affects the mechanical properties at low deformation (stiffness) while lamella thickness, spherulite size and crystallinity yield a stronger effect. On the other hand, the yield process was found to be dependent on all these microstructural parameters. Finally the response of material at high deformation level was attributed to associated effects of molecular weight, chain mobility and crystallinity.

The dependence of long-term mechanical properties on the microstructure has been also investigated. The general reported trend is that increasing molecular weight, crystal perfection and crystallinity fraction improves the polymer resistance to both initiation and crack propagation. However, thicker lamellae and larger spherulites may drop the fatigue lifetime because of the presence of higher defects concentration accompanied by lower tie molecules density.

As shown in this chapter, the damage mechanism at the later stage of lifetime is well described especially in the case of glass fiber reinforced polyamides. It has been reported that damage initiates in the polymer near the fiber ends, resulting in voids which grow to form microcraks that are bridged with drawn polymer and/or fibers. In the case of neat polymer, it has been observed that voids nucleate in the amorphous phase between the crystalline lamellae mainly located in the equatorial region of spherulites. In a first stage, the number of nanovoids increases with the number of cycles resulting in random distributed cavities inside the material. These cavities grow subsequently to become later elongated perpendicularly to the load direction. It was also suggested that as the fatigue test proceeds, these cavities coalesce continually resulting in crazes leading to the ultimate failure.

To sum up, it was shown that molecular weight and crystallinity of polyamide (perfection, lamellae thickness, spherulite size and fraction) first order govern its properties (physical and mechanical properties). The reported damage mechanisms are quite complex and imply both amorphous and crystalline phase which are dependent on the polyamide chemistry and processing conditions. A particular attention has been paid to damage under cyclic loading that seems likely occurs by nucleation of cavities in the amorphous phase. It was established that cavitation mechanism is governed mainly by the cohesion strength of the amorphous macromolecular chains but also by the amorphous-crystalline coupling (pulling out and chain-scission of tie molecules).

Within the framework of this thesis, we are looking to control the damage mechanism in the amorphous phase of polyamide 66 in order to enhance its fatigue lifetime. This may be achieved through tailoring the microstructural parameters of PA66 such as molecular weight, crystalline features and intermolecular interactions between the amorphous chains. Further details on the present methodology will be discussed in the following part.

II. Research objectives

1. Problem statement

The important reason for replacing metal by either reinforced or non-reinforced polymer is to achieve a good combination set of vehicle lighting and reducing fuel consumption in the objective of lowering carbon dioxide emission. And since sustainable solutions for structural parts made of polymeric materials **require long life service,** it is the objective of the present research to **enhance the long term durability** of polymeric materials, especially of **polyamides** by means of reducing the damage occurrence within the material submitted to discontinuous or continuous loading.

In the last 20 years, many works have been devoted to the enhancement of the working life and the safety of polymeric components. A part of these works were focused on developing a built-in capability of polymer to substantially recover its properties, namely its mechanical properties. This aptitude known as "**self-healing**" can be achieved through various methods such as heating favoring molecular interdiffusion, photo-induced chains recombination, living polymerization or inclusion of functions with reversible bonds interactions in the polymer chains. In this work **we will focus on the introduction of reversible interactions** since they could improve the intrinsic properties of the virgin material to dissipate energy as well as the self-repairing efficiency of the damaged material.

In general, reversible bonds are weaker than covalent bonds and for this reason multiple interactions should often be associated to get strong bonding. **Hydrogen bonds** are an interesting type of reversible bonds, because of **their strength** (stronger than dipole-dipole interactions), their directionality and their cooperative interactions. New polymeric materials based on multiple hydrogen bonding have already been studied in the literature. For instance, Lehn et al., prepared several supramolecular polymers from small molecules bearing complementary units, that are able to self-associate by three hydrogen-bonds, resulting in the formation of polymer-like chains [235–237]. An urea-based molecule has been developed by Bouteiller [238,239], permitting multiple associations. Furthermore, the ureidopyrimidinone molecule synthesized by Meijer et al. [240,241] and which is able to get four-fold hydrogen-bonds has been widely used as a monomeric unit or a grafting agent to prepare polymer chains with **strong reversible interactions** [241–246].

As most of these supramolecular systems are prepared in an organic solvent or require a purification process, they are not industrially suitable. More recently, Leibler et al. [247] have developed a molecule called amidoethyl-imidazolidinone which is expected to form hydrogen bonds by association of N-H and C=O groups. This molecule was prepared by reaction between 2-aminoethyl-imidazolidone (UDETA) and the carboxylic acid derivates of fatty acids. This molecule was then considered as a building block for the preparation of self-healing elastomers [248,249].

Up to date, there are no works reported on the **introduction/modification of Hydrogen bond systems in semi crystalline** polymers or solid materials presenting already polar groups. In this work, a particular attention is paid to polyamides since they have good compromise between processing and mechanical properties. It is worth noting that the

behaviour of these materials is strongly affected by the **number of H-bond functions** along the chains, the H-bond strength and its lifetime. Consequently, we expect to **tailor the polyamide properties** by fine-tuning these parameters. Indeed, we will attempt to introduce chemical groups that can establish **strong H-bond interactions** in order to increase the **cohesive energy of polyamide 66.** This energy increase may **delay the cavities nucleation**, **reduce the damage accumulation** under continuous load and then enhance the polymer durability.

2. Strategy

As presented earlier, **damage mechanism** in polymers, especially in the case of semi-crystalline polymers, consists mainly in the **nucleation of cavities** in the **amorphous phase**. Based on the physical model proposed by Mourglia-Seignobos et al., **the energy of cavitation** in the amorphous phase depends on two inherent parameters: the **bulk modulus** and the **free surface energy**.

$$\zeta(\sigma) \cong 60 \frac{\gamma^3}{K^2 \left(\frac{\mu \sigma}{E} \right)^4} \tag{5}$$

where ζ is the activation energy of cavitation, γ is the surface free energy, K is the bulk modulus, E is the elastic modulus, μ is the local amplification factor.

Equation (5) shows that the cohesion of the amorphous phase is firstly related to its free surface energy. Indeed, the surface tension is exercised from the very beginning of void formation, which tends to close it. In general, void is preserved if the negative pressure around it, defined by the ratio of surface tension to void size (equation (6)), is sufficiently high. Accordingly, small voids or high surface energy provide a spontaneous healing of the nucleated voids.

$$P = -2\frac{\gamma_s}{r} \tag{6}$$

Where γ_s is the surface energy and r is the size of a void.

In the case of polyamide 66, the **surface energy is relatively high** (~47x10^{-3} J/m^2) which suggests that up to certain diameter the negative pressure is not high enough to keep opened a newly nucleated void. As a consequence, **healing mechanism of nucleated voids** in polyamide 66 is supposed to be very significant. On other words, up to a critical size nanovoids are unstable, they appear and disappear immediately. Accordingly, we expect that **increasing the surface energy of the amorphous phase** of polyamide 66 could lead to an increase of the critical size of cavity nucleation and then to **a damage reduction**. This should **improve the mechanical properties** of the resulting material particularly under cyclic loading.

It is widely accepted that surface energy is the energy required to destroy the intermolecular bonds to create a new surface. Two main intermolecular interactions can be found in polyamide: van der Waals interactions (between the methylene groups) and Hydrogen-bonds between the amide groups as illustrated in Figure 44.

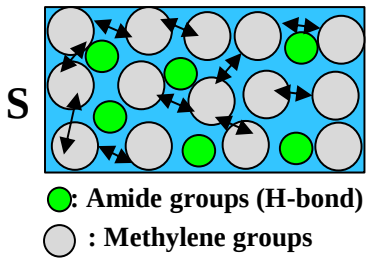

Figure 44: Schematic presentation of the intermolecular interactions (van der Waals and H-bond) in in polyamide domains of surface S

So, the surface free energy of polyamide 66 could be considered as the sum of the contribution of these two intermolecular interactions as given in equation (7).

$$\gamma_s = \gamma_{\text{van der Waals}} + \gamma_{H-bonds} \quad (7)$$

where $\gamma_{\text{van der Waals}}$ is the contribution of the methylene groups estimated at 20 mJ/m^2 at 25°C and $\gamma_{H-bonds}$ is the contribution of the Hydrogen-bonds, calculated according to equation **(8)**:

$$\gamma_{H-bonds} = \rho . b . E_H \quad (8)$$

where ρ is the density by surface unity and b is the size of function offering H-bonds interaction.

In the case of PA66, ρ is roughly estimated to 0.3 x10^{28} m^{-3}, b ~0.2nm and E_H~ 0.45.10^{-19} J. This leads to a contribution of the Hydrogen-bonds in the free surface energy of PA66 estimated at 58 % versus 42% for van der Waals interactions.

The important contribution of H-bond interactions to surface tension energy implies that it is possible to **increase the surface energy** of polyamide by **increasing the contribution of H-bond interactions**. To do this, either the density of amide groups, which are responsible of H-bonds interaction, or the **strength of the H-bonds** should be increased. It is believed that increasing the density of the H-bonds may leads to an increase of the bulk modulus since it is correlated to the density of the intermolecular interactions. A schematic representation of deformation of the amorphous chains submitted to hydrostatic stress is given in Figure 45.

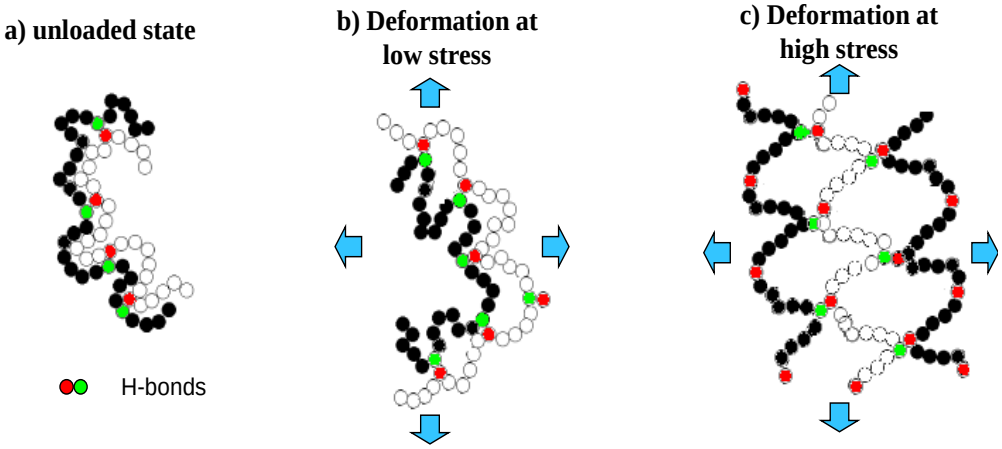

Figure 45: Deformation of the amorphous chains of PA66 at the molecular level

It can be seen that at a given deformation level, the Van de Waals interactions are first dissociated favoring the expansion of the polyamide chains (Figure 45-b). As the deformation level increases, the expansion of the amorphous chains becomes more important and then involves the H-bond interactions (Figure 45-c). Depending on the deformation level and on the distance between amide groups, a fraction of the H-bond bridges could be broken. The higher the H-bond density, the higher the resistance to chains stretching and then the higher the bulk modulus.

In order to not increase the bulk modulus of the amorphous phase that could lead to a drop of the energy barrier for void nucleation (see equation(5)), the H-bond density was not changed in the framework of this PhD, and only an **increase of the strength of the H-bond interactions** was considered. We made the assumption that the bulk modulus did not increase significantly when increasing the energy of the intermolecular interactions.

As described previously, several self-association molecules based on strong H-bond interactions have been developed. Unfortunately, most of these molecules decompose at temperature above 230°C and then could not be introduced into polyamide 66 because of its high melting temperature (~265°C). Recently, few studies have been reported on the blending of aliphatic polyamides with thermally stable sulfonamide [250–253], phenolic resins or low molecular weight hydroxylated aromatic compounds. It is well established that sulfonamides and phenolic compounds are miscible with polyamides at molecular level thanks to strong hydrogen bonds interactions between the hydroxyl of the phenol group and the amide groups of Nylons [254–263]. It has been also noticed that the tensile modulus of the resulting blends is higher than that of the originate polyamide, possibly due to the strong hydrogen bonds network in the blend and to the rigidity of the aromatic rings.

On the other hand, it was reported that the addition of phenolic components, by blending with aliphatic polyamides, affects both the crystalline and the amorphous phases of semi-crystalline polyamides (spherulite size, lamellae thickness, mobility chains…) [254–256,262]. In order to not alter the initial structure of polyamides, it could be of great interest to have an alternative way to incorporate the phenolic functions that offer strong H-bond interactions in the polyamide chains.

In this work, **we are interested** in the introduction of **phenolic groups into polyamide** backbone by means of **covalent linkage** between these groups and the polyamide chains. On one hand, as it is desired to **increase the energy of H-bond interactions** in the amorphous phase in order to prevent cavitation, these functions should be mainly located in the disordered phase. On the other hand, the interconnection between the crystalline lamellae (tie molecules) should be not disturbed, since it has a strong impact on the fatigue lifetime. In order to **introduce the phenolic** moieties in the amorphous phase **without altering** the coupling between crystalline and amorphous phases, a **block copolymer structure** is considered. In this configuration, we expect the phenolic based segments to be efficiently **anchored to the crystalline** lamellae thanks to the crystallization of polyamide 66 segments that are present on the chain, as schematically presented in Figure 46.

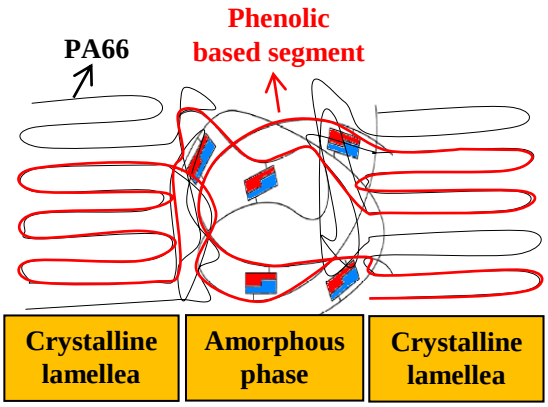

Figure 46: Schematic structure of semi-crystalline modified polyamide66

To materialize the above concept, **block copolymers of polyamide 66 and Hydroxyisophtalic** based polyamide were prepared by **reactive extrusion** within the framework of the thesis. As described in paragraph I.1.3.3, reactive melt-polycondensation can be considered as an industrial tool to prepare block copolymers. However, attention should be paid in order to limit the secondary reactions in the melt. Accordingly, we have investigated in the first part of this PhD work, the reactive melt blending of functional PA66 and phenolic materials by micro-compounding and twin screw extrusion over a broad range of compositions in order to optimize the processing conditions that favor the formation of block copolymers.

Even if the driver of this PhD work for enhancing Polyamide 66 durability was the increase of the strength of intermolecular interactions, it was shown in this chapter, that many other **microstructural parameters can** have a **significant effect** on the mechanical properties and namely the **long term properties** of polymeric semi-crystalline materials. Consequently, an accurate structural **characterization** of the prepared materials was **carried out** in order to be able **to separate** the **contribution of intermolecular interactions** modification from the other microstructural parameters (mainly molecular architecture **and crystalline features**) to the mechanical performances of polyamides and notably their **sustainability.**

2

Materials and experimental techniques

Chapter II: Materials and experimental techniques

This chapter describes the materials used in this study: Aliphatic polyamide (PA66), semi-aromatic polyamide (PA6HIA) and aliphatic semi-aromatic copolyamides (PA66/6HIA). The preparation of block PA66/6HIA copolyamides by reactive extrusion is firstly detailed (microcompounding and twin screw extrusion) and the processing technique used to prepare the specimens is then presented (Injection molding). The main experimental techniques used to check the molecular structure such as Gel Permeation Chromatography (GPC), Nuclear Magnetic Resonance (NMR) and Mass spectroscopy (MALDI-TOF) are described. Commonly used tools for the characterization of the semi-crystalline features such as Polarized Optical Microscopy (POM), Transmission electron microscopy (TEM), Small and Wide Angle X-ray Scattering and Differential Scanning Calorimetric (DSC) are then presented. The rheological characterizations of the prepared material as well as the free surface energy measurement are also described. Then, the mechanical characterizations including dynamic mechanical analysis, tensile tests, impact and fatigue tests are described. The stiffness evolution of the injection molded materials under dynamic loading is also evaluated by Digital Image Correlation (DIC). Finally, the developed damage is evidenced by using Scanning Electron Microscopy (SEM), and Small and Ultra Small Angle X-ray Scattering (SAXS and USAXS).

1. Materials components

1.1. Polyamide 66

Polyamide 66 results from the polycondensation of hexamethylene diamine and adipic acid, usually present in the ionic form known as Nylon salt, in a condensation reactor. At the end of the polycondensation reaction, the melt of PA66 is quickly cooled and then granulated in the form of pellets of 2-3mm of size. The chemical structure of polyamide 66 is given in Figure 47.

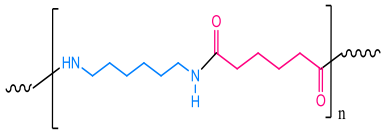

Figure 47: Chemical structure of PA66

Three grades of polyamide 66 with different molecular weight were used as references in this study. The first one denominated hereafter **PA1** is a Solvay-grade polyamide which is an amine terminated PA 66 (GTA=105 meq/Kg, GTC=32.7 meq/Kg, Mn = 10500 g/mol, Mw = 35000 g/mol). This un-equilibrated end-groups PA66 was chosen for the realization of the PA66/6HIA copolyamides that will be described later. It should be noted that **PA1** contains 20 ppm of a catalyzer called sodium hypophosphite, but in order to optimize the

copolyamides conversion, an additional amount of catalyzer was added (100 ppm in total). In the following report, the polymer noted **PA66/6HIA (100/0 w:w)** is precisely the neat PA66 **PA1** that contains 100 ppm of sodium hypophosphite.

The second PA66 grade used in the framework of this study is also a PA66 Solvay-grade (Mn = 12100 g/mol, Mw = 38200 g/mol) called hereafter **standard PA66.** A third PA66 Solvay-grade exhibiting a high molecular weight PA66, thanks to a preparation by Solid State Post-condensation (SSP) in the presence of 75 ppm of catalyst, was studied. This polymer will be called hereafter **HMw PA66** so as to differentiate it from the standard PA66. It should be noted that all the PA66 grades used in this study are semi-crystalline polymers with a glass transition temperature around 65°C and a crystalline fraction about 33 %.

1.2. **Polyamide 6HIA**

PA6HIA is a polyamide which results from the polycondensation of hexamethylene diamine and hydroxyisophthalic acid (see Figure 48). The specificity of this polyamide is that it presents a phenolic function which is able to establish strong H-bond with the amide functions. However, **PA6HIA** chains could not undergo crystallization during cooling from the melt and is still amorphous after solidification.

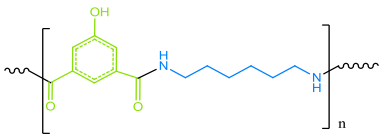

Figure 48: Chemical structure of PA6HIA

An acid terminated **PA6HIA** (GTC=385 meq/Kg, GTA=47 meq/Kg, Mn = 6500 g/mol and Mw = 13800 g/mol), was synthetized by the CRTL Solvay LSPP laboratory (Stéphane Jéol and Daniel Duchêne). At the end of the polycondensation reaction, the melt viscosity of the polyamide was not high enough to make pellets by the usual granulation techniques, and then **PA6HIA** was collected as solid coils of few centimeters of size.

As a result of its high glass transition temperature (167°C), resulting from the presence of aromatic rings and the presence of strong H-bonds between amides and phenol moieties, the solid coils were very brittle in their glassy state, and it was not possible to mold specimens of neat **PA6HIA**. Consequently, acid terminated **PA6HIA** were crushed and blended with **PA1** PA66-NH_2 at different weight compositions to get, by reactive extrusion, copolymers of **PA66/6HIA** that are now described.

1.3. **Copolyamide 66/6HIA**

PA66/6HIA copolyamides were prepared by reactive extrusion of blends composed of:

- The amine terminated PA66 described in 1.1 (**PA1**)
- The carboxyl terminated PA6HIA described in 1.2 (**PA6HIA**)

Different PA66/PA6HIA blends were prepared, containing between 0 and 40% in weight of PA6HIA. The obtained copolymers will be called hereafter **PA66/6HIA (x/y w:w)**, with x

and y the relative proportion of PA66 and PA6HIA in weight. The chemical structures of the aliphatic and semi-aromatic polyamides are presented in Table 2.The description of the preparation (extrusion and injection) and the structure of the obtained **PA66/6HIA** copolyamides will be fully detailed in chapter III.

Polyamide	Structure
PA66	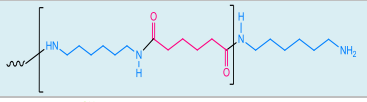
PA6HIA	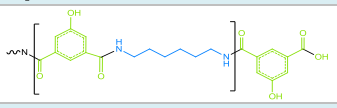
PA66/6HIA	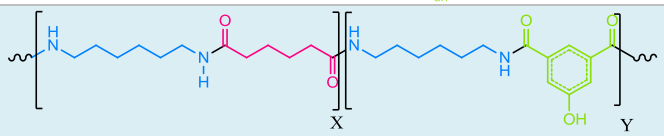

Table 2: Chemical structure of polyamides PA66, PA6HIA and PA66/HIA copolymer

A second grade of PA66/6HIA copolyamide, containing 17% wt of the 6HIA monomer, was synthesized by Stephane Jeol (LSSP laboratory) by in-situ copolycondensation of Nylon salt and HIA monomer. It should be noted that in-situ copolycondensation mainly produces random copolyamide (statistical addition of co-monomers) while reactive extrusion in well controlled conditions leads to multiblock copolyamides as pointed out in the first chapter. In the following, PA66/6HIA copolyamides prepared by in situ co-polycondensation will be designed by **i-PA66/6HIA** so as to differentiate them form copolyamides prepared by reactive extrusion called hereafter **m-PA66/6HIA**.

2. Materials preparation

2.1. Microcompounding

PA 66-NH_2 **(PA1)** and **PA6HIA** pellets were dried in a primary vacuum oven at 110°C for at least 36 h, the moisture level before the melt-blending operation, checked using a Karl Fisher device, being in the range 300/400 ppm. After that, pellets were weighed with a precision of 0.01 g and hand-mixed to form homogenous masterbatches for each of the **PA66/PA6HIA** compositions. Portions of 10 g of these masterbatches were processed with a DSM Midi 2000 Micro-compounder composed of a separable mixing compartment containing two removable conical mixing screws in co-rotating mode. On this batch mini extruder, the mixing time can be varied thanks to a recirculation channel of the melt, and the processing temperature can be adjusted in three separately controlled heating zones (see Figure 49).

PA66/PA6HIA compositions with different weight fractions of PA6HIA (from 0% to 40%) were introduced in the top of the micro-compounder by a specially designed manual injector feeder. Feeding time was set as short as possible (less than 10 s), which was especially important in the case of short residence time. Various blend compositions of **PA66** and **PA6HIA** were extruded under nitrogen flow in different processing conditions: the extrusion time varied from 90 s to 600s and the extrusion temperature varied from 290 °C to 310 °C. However, the screw speed was kept constant for all blends at 100 rpm.

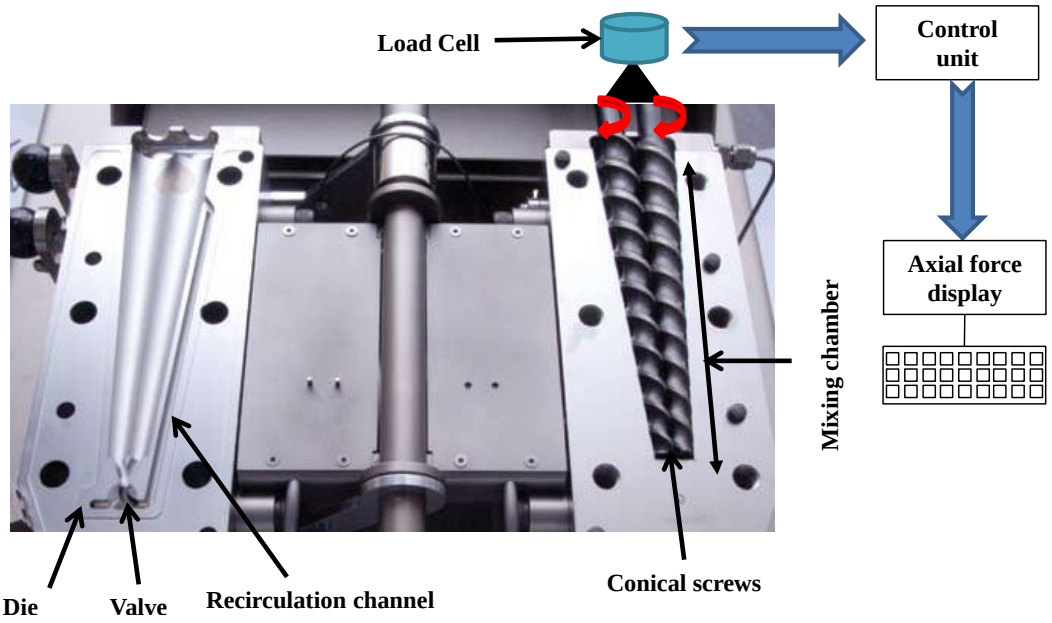

Figure 49: Presentation of cross-section of the mini-extruder and the axial force measurement

During extrusion, the force needed for the screw to push the polymer inside the mixing chamber and through the circulation channel was followed indirectly by measuring with a load sensor the opposing axial force exerted by the screw toward the top as shown in Figure 49. This force measurement gives qualitative information on the melt viscosity evolution and the rheological behavior of reactive blends during extrusion. The axial force measurements were recorded during the mixing process for all the **PA66/PA6HIA** blends as a function of time at different extrusion temperatures. Portions of 10 g of each mixture were sustained at least three times to have a steady regime and then the retained sample was introduced quickly. During the sample introduction, the axial force increases sharply and then decrease as the pellets melt. Thus, axial force data were recorded only when the axial force reached a steady value at the end of the feeding operation, to ensure that the polymer was entirely molten in the extruder. At the end of the micro compounding process, the polymer was taken out by changing the position of the valve to guide the polymer in the exit die. Then, polymer was pulled out slowly and cooled quickly in cold water in order to have solid rods before pelletizing.

2.2. **Twin screw extrusion**

As mentioned above, **m-PA66/6HIA** copolymers have been prepared by reactive extrusion of amine terminated PA66 (**PA1**) and carboxyl terminated PA6HIA **(PA6HIA**). In this way, pellets of **PA1** and **PA6HIA** were dried in a primary vacuum oven at 110°C for at least 36h before the melt-blending operation. The moisture level measured by coulometric Karl Fisher titration was in the range between 300 to 400 ppm. After that, blend compositions with different weight fractions of **PA6HIA** (from 0% to 23 %) were introduced into a Leistritz co-rotating twin screw extruder by using two feeding devices with weight precision of 1%. The used Leistritz extruder had a diameter of 34mm and ratio length on diameter L/D of 35. The barrel had ten temperature-controlled zones: eight cooled with air and two cooled with water (zones 4 and 8). The set temperature profile ranged from 285°C in the first zone to 305°C in the last zone, resulting in an extrusion temperature of 305°C at the die (temperature of the melt).

The screw profile was designed in order to have the longest residence time for maximizing the polycondensation reaction, with one « open » zone to eliminate the water produced by polycondensation reaction. The corresponding residence time at a screw speed of 200rpm and a throughput of 8 Kg/h was founded to be around 100s.

In addition to **m-PA66/6HIA** copolyamides, **standard PA66** was extruded using the same screw profile but in standard conditions. In fact, the set temperature profile was ranged from 275°C in the first zone to 290°C in the last zone resulting in a melt temperature around 290°C.

The resulting products (**m-PA66/PA6HIA** and **standard PA66**) were drawn slowly and immediately cooled down in cold water (20°C) in order to have solid rod before pelletizing.

2.3. **Injection molding**

Tensile and impacts specimens with a thickness of 4 mm were injection molded using an Arburg injection molding machine with a clamping force of 35 tons. Prior molding, polymer pellets were dried in a primary vacuum oven at 110°C for at least 24 h. The moisture level before the injection molding operation, measuring by a Karl Fisher, was in the range between 500 to 600 ppm. Figure 50 shows a schematic presentation of an injection molding machine. It is principally composed of one screw extruder which melts the polymer. This latter is carried to the mold environment by an hydraulic press coupled to the screw. At this stage, the polymer takes the form of the mold under the application of a counter-pressure imposed by an hydraulic press. Note that the mold is continuously cooled down with water to enhance the polymer solidification into the final piece which is extracted from the mold thanks to an ejecting device.

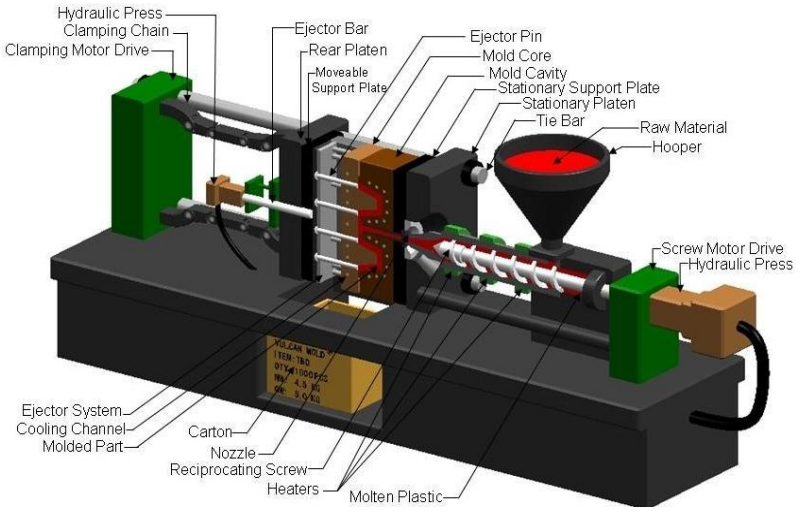

Figure 50: Schematic presentation of an injection molding machine

As melting temperature, viscosity and crystallization kinetics were very dependent upon the nature, the molecular mass, and the composition of the copolyamides, the processing conditions (injection speed, mold pressure and temperature as well as the piece retention time) were adjusted for each material in order to get proper injection molded specimens.
All the processing steps (microcompounding, extrusion and injection molding) were done in collaboration with Vincent Curtil and Michel Sorin from the Processing Facility of Solvay.

3. Experimental techniques used to characterize the microstructure

3.1. Molecular scale

3.1.1. Molecular mass distribution

The molar mass distribution of the prepared materials was determined by Gel Permeation Chromatography (GPC). The separation principle of different macromolecules is based on their size in solution expressed in terms of hydrodynamic volume. The gel stationary phase in the column contains pores which will retain molecules according to their hydrodynamic volume. Thus, macromolecules exhibiting the largest hydrodynamic volume will elute first, followed by the smallest ones as presented in Figure 51.

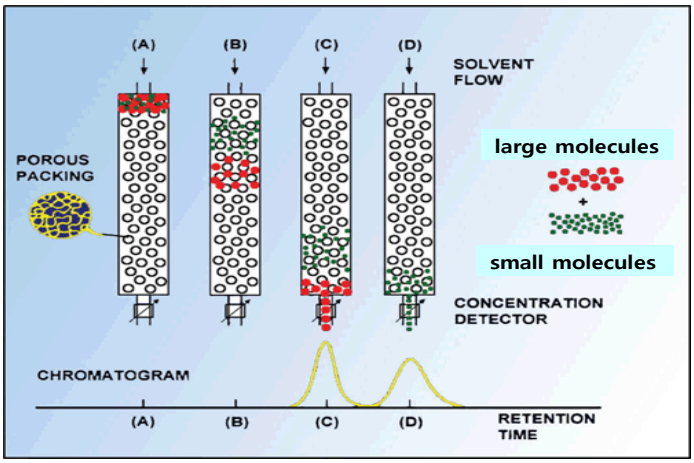

Figure 51: Schematic presentation of molecules separation by GPC

Gel permeation chromatographic analysis was carried out at room temperature on a PL GPC 120 (four columns PLGEL MIXTE C of 60 cm with particles of 5 µm) by Nadia Delon-Anik, from Solvay Analysis Department. The apparatus was equipped with auto-sampler, auto-injector, refractometer and UV detectors. The combination of the different detectors allowed a universal calibration and so the obtaining of the exact average molar masses. A mixture of Dichloromethane/Trifluroacetic anhydrous (DCM/ATFA 95:5 v/v) was used as a solvent. After 4 hours of stirring, the samples were filtered at 0.2µm and then injected in the column. The flow rate was fixed at 1 mL/min. Detection by UV2000 spectra physique was done at 254 nm and 310 nm to differentiate the not-reacted PA6HIA in the form of homopolyamide from the reacted one in the form of PA66/6HIA copolyamide. Indeed, the amide functions of PA66 and PA6HIA are detected at 254nm, while only the phenolic moieties of the PA6HIA are detected at 310nm. In order to obtain the absolute molar masses of polyamides, calibration curves with standards of narrow molecular weight distribution were done. Based on these curves, a molecular weight (Mi) was associated to each retention time (t_i) or elution volume (V_i).

Number average molar mass M_n and weight average molar mass M_w were then calculated as below:

$$M_n = \frac{\sum_i N_i M_i}{\sum_i N_i} \quad (9)$$

$$M_w = \frac{\sum_i N_i M_i^2}{\sum_i N_i M_i} \quad (10)$$

With N_i the number of macromolecules of mass M_i. M_n is more sensitive to molecules of low molecular mass, while M_w is more sensitive to molecules of high molecular mass. The dispersity index (D) is a measure of the distribution of molecular masses in the polymer and is defined as:

$$D = \frac{M_w}{M_n} \quad (11)$$

3.1.2. Average block lengths of PA66/6HIA copolyamides

It is well known that Nuclear Magnetic Resonance (NMR) is an effective tool to determine the microstructure of organic compound as well as polymers by using a radio-frequency radiation and a magnetic field. At initial state, atomic nucleus presents within the molecule (mainly ^{1}H and ^{13}C) precess normally, essentially spinning in random directions. When these nuclei are placed in a strong magnetic field, they line up, precessing in the direction of the applied field, either lined up with the field (parallel) or against the field (antiparallel). The two orientations have not exactly the same energy and if the nucleus are irradiated with radio-frequency radiation, the lower energy nuclei spin-flip or resonate to the higher state. The corresponding resonance signal is dependent on the electrons surrounding the nucleus, the external magnetic field strength and the radiation frequency. Consequently, the signals are usually reported relative to a reference signal, that of TMS (tetramethylsilane), and their position are converted to "chemical shift" (in ppm). This latter is related to the number and the neighboring of the consistent nuclei [264].

The ^{13}C NMR analysis was performed by Frederic Le-Guyader from the Solvay analysis department. Measurement were carried out on a Bruker AV500 spectrometer at 300°K using deuterated Hexafluoroisopropanol as a solvent for the studied copolymer and as a locking agent. The ^{13}C NMR spectra were recorded with the following acquisition parameters: spectrometer frequency 125.76 MHz, sweep width 261.5 ppm and an acquisition time of 2 s. A pulse width of 9µs and a delay of 3 s were used for about 8200 accumulations. Further details on the analysis methodology are now presented.

It is well accepted that the ^{13}C NMR technique is an effective tool to determine the number-average block length and the degree of randomness of the copolyamides resulting from melt blending [60,61,69,70]. All these works rely on the description of the carbonyl chemical shift in the initial homopolyamide and the produced copolyamide. Indeed, the carbonyl resonances signals of the amide groups are sensitive to chain sequences and chain length. As the homopolyamides used in these studies had two distinct diamine monomers, new carbonyl peaks were observed when the amine linked to the carbonyl was modified, in other words when transamidation reactions occurred between the two homopolyamides. Consequently, the measurements have been done based on the carbonyl signal and the peaks assignments were analyzed in terms of dyads sequence distributions in order to determine the degree of randomness of the copolyamides. However, as in our case the diamine monomer is the hexamethylene diamine for both homopolyamides, the amine linked to the carbonyl remains the same after the exchanges reactions. Accordingly, the chemical shift of the carbonyl

function is unchanged and then the block lengths cannot be determined based on the carbonyl signal.

In the present case, we show that it is possible to perform ^{13}C NMR analysis to determine the composition of the copolyamide sequence by monitoring the methylene region of the diamine as described by Michell et al. [265] . The carbon atom of the methylene group linked with the nitrogen of the aromatic amide and the aliphatic amide functions, i.e., -CH2-NH-C(O)-ϕ- and -CH2-NH-C(O)-(CH2)4- respectively, were monitored in terms of ^{13}C dyads (AA, AB, BA and BB where AA corresponds to PA6HIA block and BB to PA66 block (see Figure 52).

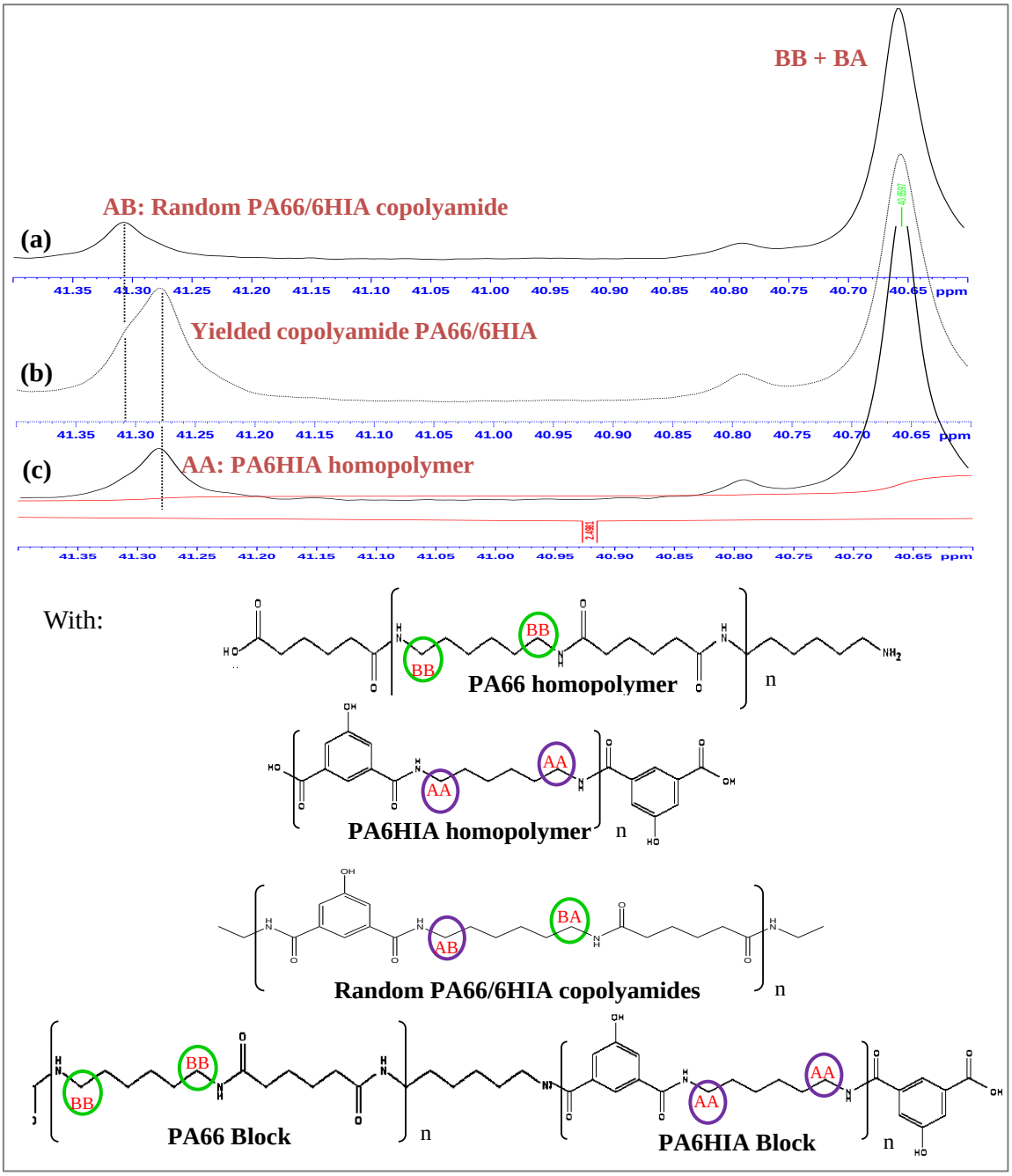

Figure 52: Expanded ^{13}C NMR spectra showing chemical shift range of the CH_2 groups linked with the nitrogen of the amide functions of: (a): Random PA66/PA6HIA; (b):PA66/6HIA copolyamide by reactive blending; (c): non reacted blend of PA6HIA and PA66

Figure 52, represents the chemical structure of PA66, PA6HIA homopolyamides and random copolyamides with their corresponding ^{13}C NMR spectra in the chemical shift of the methylene group (-CH_2-) linked to the nitrogen of the amide function. As polyamide results from the condensation of diamine and diacid, two methylene groups linked to the nitrogen of the amide groups can be identified. In the case of PA66 or PA6HIA, these methylene groups are chemically equivalent resulting in one resonance signal. This signal will be designed by BB in the case of PA66 versus AA for the PA6HIA methylene group as highlighted on their chemical structure in Figure 52. In the case of random copolyamide, two additional dyads corresponding to the methylene groups of the diamine should be considered: The first one, designed BA, corresponds to repeating unit with a methylene group in α position to the nitrogen of aliphatic amide function preceded by an adjacent aromatic amide function. Similarly, the second dyad, AB, corresponds to repeating unit with a –CH_2- in α position to the nitrogen of aromatic amide function preceded by an adjacent aliphatic amide function

Accordingly, two distinct ^{13}C NMR peaks should be expected in the chemical shift rang of methylene signals corresponding to BB and AA dyads respectively. Unfortunately, the chemical shift difference for the dyads resonance (AA,AB) and (BB, BA) was very small and the peaks could not be totally separated as shown in Figure 52-b.

In order to identify the chemical shift matching to the AB and AA dyads respectively, the ^{13}C NMR spectra of random PA66/6HIA copolyamide (Figure 52-a), obtained by copolymerization of adipic acid,1,6-diaminohexane and hydroxyisophtalic acid, and PA6HIA homopolymer (Figure 52-c) were recorded. As PA6HIA homopolymer was partially soluble in the NMR solvent, PA66 was added in order to enhance its solubility. Consequently, the BB dyad of PA66 homopolymer is also highlighted, which explain the resonance signal obtained around 40.56 ppm.

Based on these ^{13}C NMR spectra, the assignment of the chemical shift of the AA and AB dyad in the signal resonance associated to copolyamide prepared by reactive blending was accomplished (see Figure 52-b). Subsequently, the relative area of AA and AB dyads were quantified by deconvolution of the ^{13}C NMR resonance signals into two peaks by using the decomposition package of Dmfit tool.

In order to determine the length of the PA66 block, the relative area of the ^{13}C resonance signals for the dyads BB and BA were measured. Due to the abundant fraction of BB methylene group (PA66) and the small chemical shift difference between the BB and BA dyads, no peak separation was observed in the chemical shift around 40.66 ppm which corresponds to BB signal. Consequently, it was assumed that the area of this signal corresponds to the sum of the BA and the BB dyads (carbon atom linked with the nitrogen of the aliphatic amide). Based on the fact that the BA and AB dyads have the same area (as they are at the same abundance), the relative area of the BB dyads was calculated by simple subtraction.

Finally, the average length of respectively PA66 block ($\bar{L}_{PA66}$) and PA6HIA block ($\bar{L}_{PA6HIA}$), were determined using respectively the relative integrated areas of the ^{13}C diads from the carbon atoms linked with the nitrogen of aliphatic amide (BB and BA) and (AA and AB) from carbon atoms linked with the nitrogen of aromatic amide function. The number-average sequence length was calculated using the following equations:

$$\bar{L}_{PA66} = \frac{1}{P_{BA}} = \frac{[BB]}{[BA]} + 1 = \frac{I_{BB}}{2I_{BA}} + 1 \qquad (12)$$

$$\bar{L}_{PA6HIA} = \frac{1}{P_{AB}} = \frac{[AA]}{[AB]} + 1 = \frac{I_{AA}}{2I_{AB}} + 1 \quad (13)$$

where P_{BA} represents the probability of finding an aliphatic repeating unit (adipic acid linked to 1,6-diaminohexane) with an adjacent hydroxyisophtalic acid: ($P_{BA} = \frac{[BA]}{[BB]+[BA]}$) and P_{AB} represents the probability of finding a semi-aromatic repeating unit (hydroxyisophtalic acid linked to 1,6-diaminohexane) with an adjacent adipic acid: ($P_{AB} = \frac{[AB]}{[AA]+[AB]}$).

Since 1,6-diaminohexane has two methylene atoms linked to the nitrogen of the amide group (see Figure 52), the relative intensity of the AA and BB dyads were doubled. As a consequence, the relative integrated area was divided by two for calculating the concentration of each dyad.

3.1.3. Randomness degree of PA66/6HIA copolyamides

The randomness degree of PA66/6HIA copolyamides was characterized by Matrix Assisted Laser Desorption/Ionization Time-Of-Flight (MALDI-TOF) mass spectroscopy. This technique is widely used for the structural characterization of wide range of polymeric chains. Indeed, it allows the identification, at the femtomole level, of quite large molecules (10^6 Daltons) as well as single oligomers even in complex mixtures. As MALDI-TOF spectroscopy yields information on individual polymer chain, it is usually used in complementary with NMR which is rather an averaging analytical method[266].

The MALDI-TOF mass spectroscopy consists in the production of ions of intact polymer chains, followed by a separation of the produced ions, and finally the collection after different time of flight of the ions by a specific detector. This is schematically illustrated in Figure 53.

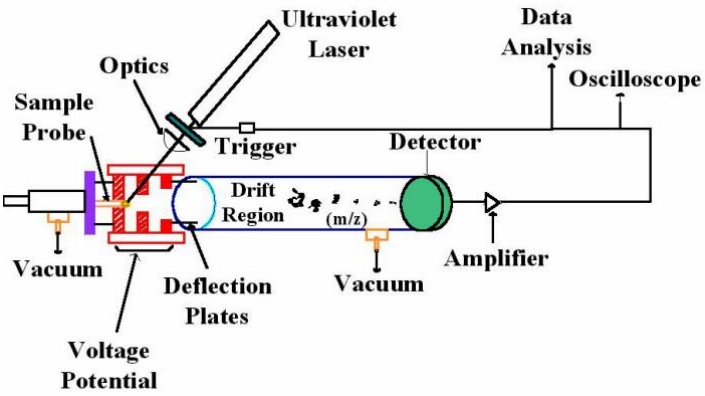

Figure 53: Schematic representation of a MALDI-TOF mass spectrometer

Firstly, the polymer is homogeneously embedded in a large excess of small organic molecules called "matrix". After that, the polymer/matrix mixture is exposed to moderate pulses of laser light in order to get gaseous ions (ionized matrix and polymer). After 300–800 ns of time delay, the packet of ions generated in the process is accelerated by an electric potential, ranging from 15 up to 35 kV. Depending on their mass-to-charge ratio m/z, the ions have different velocities when they leave the acceleration zone and enter a field-free flight

tube (drift-tube) of 1 or 2 m long. After a time-of-flight of the order of 100 ms, the ions impact onto an ion detector, often formed by two microchannel plates connected in series. The oscilloscope connected to the detector, produces a signal (proportional to the number of ions arriving at the detector) as a function of time. This signal is converted by a computer to MALDI-TOF spectrum according to the equation **(14)** that gives the relationship between the flight time and the m/z ratio:

$$\frac{m}{z} = at^2 + b \qquad (14)$$

where m is the mass of the ion, z is the number of charge, t is the ion flight time, a and b are constants that are calculated from the measured flight times of two ions with known masses.

The MALDI – TOF characterization were carried out at the "Institute of Chemistry and Technology of Polymers (ICTP) – UOS Catania" by the Professor Filippo Samperi. The mass spectra were recorded in linear mode using a Voyager-DE STR instrument (Perseptive Biosystem) mass spectrometer equipped with nitrogen laser (emission at 337 nm for 3 ns). To avoid fragmentation of the polymers, the laser irradiance was slightly above threshold (ca. 106 W/cm2). The accelerating voltage was 20 kV, and the grid voltage and delay time were optimized for each sample to achieve the better resolution. Each spectrum was recorded in positive mode using 2-(4-hydroxylphenylazo) benzoic acid (HABA) as a matrix. The concentration of all samples was 5 mg/mL in hexafluoro-2-propanol (HFIP) as solvent. Also HABA was dissolved in HFIP to obtain 0.1 M solution. Appropriate volumes of polymer solution and matrix solution were mixed to obtain a 1:1, 1:2, and 1:3 v/v ratio. About 1µL of each sample/matrix mixture was spotted on the MALDI-TOF sample holder and slowly dried to allow matrix crystallization.

In order to calculate the molar composition, the average sequence lengths of PA66 and PA6HIA and the degree of randomness (DR) of studied PA66/6HIA copolyamides, the relative intensity of the MALDI-TOF mass spectra peaks were processed with a MACO4 program developed by Professor Filippo Samperi.

The degree of randomness illustrates the repartition of PA6HIA and PA66 repeat units along the PA66/6HIA copolyamide. It is admitted that DR=0 corresponds to a completely block copolymer structure, whereas completely random and alternating copolymer structures are respectively characterized by DR=1 and DR=2. It is worth noting that in the case of DR value > 1, the copolymer structure is rather close to alternating copolymer, while it tends toward sequential or block character when DR value is less than unit [60].

3.2. **Multi-scale characterization of the crystalline morphology**

Microscopy techniques provide useful information on the miscibility and morphology of polymer blends as well as on the crystalline features of polymers such as spherulites, lamella and crystal structure. Indeed, microscopy techniques allow reaching various ranges of resolution from macroscopic scale to nanoscopic scale. The resolution of these techniques could be enhanced by the preparation method but it is essentially dependent on the focus, the depth and the brightness of the used source (Light, electron, X-Ray, Neutron). Figure 54 summarizes the different microscopy techniques and their associated objects size range.

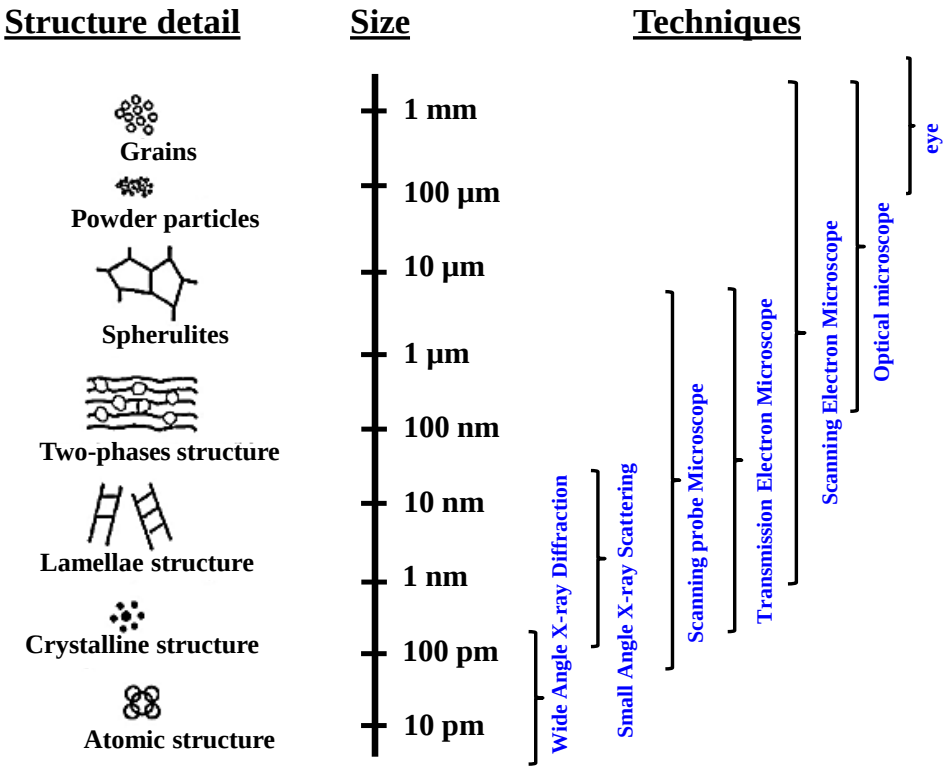

Figure 54: Different experimental microscopy techniques used to characterized the multi-sacle morphology of polymers [267]

Within the framework of this study, Polarized Optical Microscopy (POM) was used for the characterization of spherulites, Transmission Electron Microscopy (TEM) and Small Angle X-ray-Scattering (SAXS) were used for evidencing the crystalline lamellae and finally, Wide Angle X-ray Diffraction (WAXD) was used to characterize the crystalline structure of the studied materials.

3.2.1. Spherulite structure

The size, shape and arrangements of spherulites were characterized by polarized optical microscopy. Figure 55 shows the configuration of polarized optical microscope composed of:

- Illumination system
- Polarizer
- Rotary stage
- Objectives
- Analyzer
- Eyepieces/camera system

The principle of measurement is simple and based on the interaction of microscopic objects with the polarized light, considered as transverse vibration with electric and magnetic field. In the case of birefringent material, the polarized light is split into two plane polarized-waves that vibrate in planes at right angles to one another. For bulk semi-crystalline polymers, a radial "Maltese cross" is observed which is a characteristic of the spherulite organization composed of elements with different refractive indices (crystalline and amorphous phases).

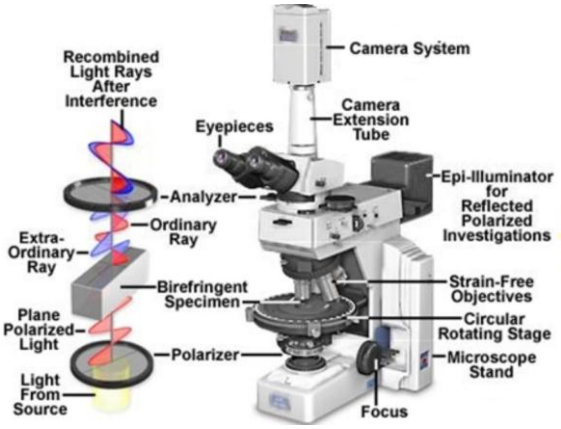

Figure 55: Polarized Light Microscope configuration

In this work, microscopic observations were performed on pellets and injection molding specimens. Concerning the preparation method, the pellets or specimens were first included in Epoxy resin (Araldite) and placed in an oven at 70°C overnight. After that, sections of 2 µm thick were cut at room temperature from the prepared pellets or specimens by using a Reichert Ultracut S microtome equipped with a diamond knife. The sections were analyzed by using a Leica light polarization microscope equipped with video camera Leica DFC420C.

3.2.2. Lamellae organization

Usually, the lamella morphology of semi-crystalline polymers is characterized by Transmission Electron Microscopy (TEM). In this case the specimen is illuminated by an electron beam emitted from an electron gun and accelerated by an anode before being condensed with a lens system. The incident electron beam reacts with the materials and then electrons and photons are ejected from superficial layers or transmitted through the sample with different accelerating energy and wavelength.

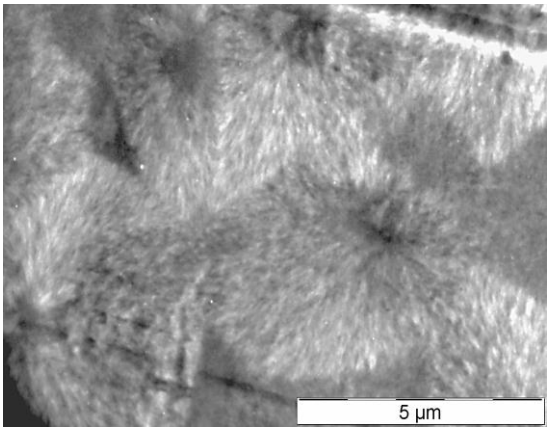

Figure 56: TEM micrographs showing the lamella organization of semi-crystalline polymer

TEM imaging mode is based on the elastic electron scattering from the sample. Thus, measurement should be performed in pronounced vacuum in order to avoid the electron scattering by the air. Amorphous phase scatters electrons in all the directions, and as the objective aperture can collect only a few of them, it results a low intensity. In contrast, the scattered intensity of crystalline phase is concentrated, resulting in a higher intensity which

depends very strongly on the orientation of the crystals and on their thickness. Accordingly, TEM images of semi-crystalline polymers exhibit bright regions corresponding to ordered lamellae that are surrounded by inter lamellar dark zones which correspond to amorphous phase (see Figure 56).

It is interesting to state that polymeric materials scatter electrons weakly, as they have low atomic number, resulting in relatively poor contrast. Consequently, selective staining is often used to enhance the TEM contrast. Increasing the accelerating voltage can also help to improve the contrast. However, high beam may induce sample damage during observation such as loss of crystalline order, mass and dimensional changes. Thus, low accelerating voltage which requires very thin samples is commonly used.

In this study, TEM crystalline lamellar morphology characterizations were performed by Nelly Bulgarelli from Solvay Analysis Department. Pellets were first included in Epoxy resin (Araldite) and placed in an oven at 70°C overnight. After that, samples were cooled to - 40°C and then microtomed using a Leica EMUC6 ultramicrotome with a diamond knife, in order to obtain ultrathin sections (about 100nm thick). After, the sections were stained by phosphotungstic acid $H_3PW_{12}O_{40}$ for 1 hour, and were then observed under the microscope using a Mettecnai 12 Biotwin instrument.

3.2.3. Lamellae thickness

X-ray techniques have now become efficient tools to characterize the polymer microstructure. Indeed, X-Rays photons interact with the matter electrons when passing through it, giving information about the space repartition of the electronic density in the material. Because of the contrast between the electronic densities of the amorphous phase and the crystalline phase, X-ray diffraction technique is widely used to evidence the periodicity in semi-crystalline polymers. Note that Small Angle X-Ray Scattering (SAXS) are designed to highlight structures with a characteristic sizes ranging from few Å to few microns. Accordingly, the thickness of the crystalline lamellae of studied polyamides, which is in the range of few nanometers, was determined by SAXS experiments.

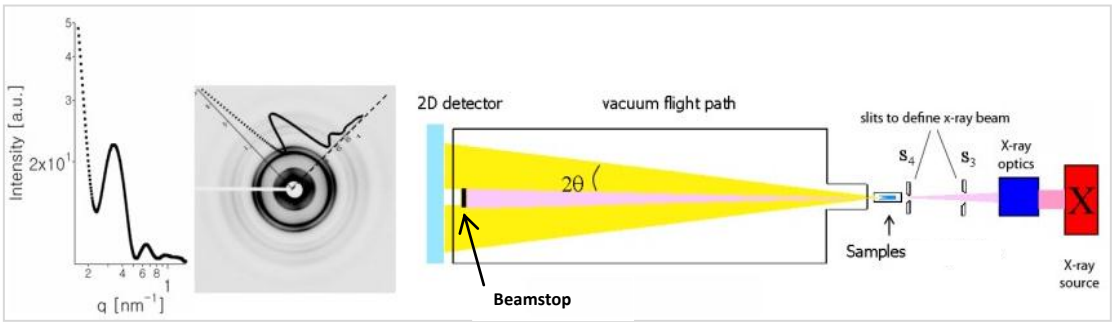

Figure 57: Schema of X-ray scattering experiment

Figure 57 shows a schematic representation of the typical X-ray scattering experiment carried out in the the "Laboratoire Interdisciplinaire sur l'Organisation Nanométrique et Supramoléculaire" (LIONS) in collaboration with Professors O. Spalla and O. Taché. An appropriate copper source (λ=0.154nm) emits a beam of X-rays (E=8Kev) which is focused and monochromated by Xenocs X-ray optics. The size of the beam is adjusted by a system of hybrids slits before hitting the sample. A small part of photon is absorbed by the sample and

the main transmitted is brought to pass immediately through a vacuum flight path in order to reduce the noise due to air scattering. The higher the distance between the sample and the detector (flight path), the smaller the reachable X-ray angle.

The scattered intensity is collected via a 2D detector (Mar300) as a function of the scattering vector q (= $4\pi \sin\theta/\lambda$) in the format of a centric pattern. This pattern was radially averaged using Image J software to get scattered intensity S(q) as a function of the scattering vector q. Since the number of photons scattered in the q direction is dependent of the number of photons transmitted through the sample and the experiment conditions, it was important to normalize the scattered intensity by several parameters (sample thickness (cm), transmission T, incident flux background noise, exposition time) in order to get the absolute intensity Iq(cm^{-1}) . The typical plots of I (q) versus the scattering vectors of semi crystalline polymers, show at least one peak which, accordingly to the Bragg's law, corresponds to an ordered structure with a repeat distance at nanometric scale which is commonly attributed to the lamellae spacing or long period (Lp) calculated as below:

$$L_p = 2\,\frac{\pi}{q_{max}} \tag{15}$$

Where, q_{max} is the scattering vector corresponding to the maximum of scattering intensity

Subsequently the weight average lamella thickness was determined following the equation **(16)**:

$$L_c = L_p * {X_c}^v \tag{16}$$

where L_c is the lamella thickness, L_p the long period and ${X_c}^v$ the volume crystallinity calculated from the crystal weight percentage as below:

$${X_c}^v(\%) = 100\,\frac{\frac{X_c}{\rho_c}}{\frac{X_c}{\rho_c} + \frac{100 - X_c}{\rho_a}} \tag{17}$$

where X_c is the weight crystalline fraction (in our case obtained from the DSC analysis), ρ_c is the crystal density and ρ_a is the amorphous density. The adopted values for the amorphous and crystalline densities are $\rho_c = 1.24$ g/cm^3 and $\rho_a = 1.07$ g/cm^3 [268].

3.2.4. Crystalline lattice

X-rays diffraction techniques can be also used to study the spatial organization of the crystalline phase. As mentioned above an ordered structure with a repeat distance (d) is highlighted by a reflection / scattering peak which could be interpreted by means of the Bragg's approach as shown in Figure 58.

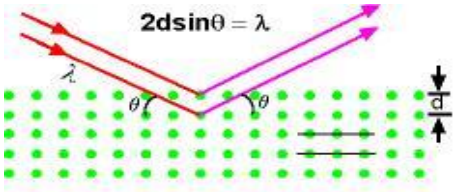

Figure 58: Graphical representation of X-ray diffracting from crystal planes

According to equation (18), d is inversely proportional to sinθ, meaning that the larger the angle at which scattering is observed, the smaller the repeat distance d. Consequently, Wide Angle X-ray Diffraction (WAXD) is ideal for the study of ordered systems at the atomic scale corresponding to crystal lattice.

$$n\lambda = 2\,d\sin\theta \tag{18}$$

where n is an integer which represents the periodicity of the wave, λ the wavelength of the x-ray radiation, and θ the angle at which the scattered beam is observed.

All Wide-angle X-ray Diffraction (WAXD) experiments were carried out at 23°C on rectangular samples of dimensions 2.5mm x 2mm and 0.3 mm thick, using a Bruker D8 Advance diffractometer in the "Centre de Diffractométrie Henri Longchambon" (Erwann Jeannneau).

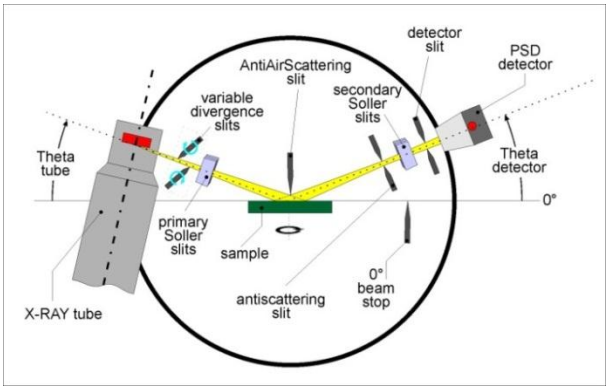

Figure 59: Schematic representation of the experimental WAXD set-up.

The source consisted in a ceramic tube with a copper anode (33 kV & 45 mA) generating Cu Kα radiation. The sample was fixed in the horizontal position, both the X-ray tube and the detector moving simultaneously over the angular theta range. The diffraction measurements were performed in the reflection mode and the diffusion at small angle was suppressed by using Anti Air Scattering slit (Figure 59).

3.3. **Calorimetric measurements**

The melting and crystallization temperatures as well as the crystalline fraction of the prepared materials were determined by Differential Scanning Calorimetry (DSC). Samples (about 8 mg) were put in non-hermetic aluminum pans and analyzed in the DSC under a nitrogen atmosphere. A temperature ramp was applied on the pan containing the sample as well as on an empty pan taken as a reference. The energy required to keep the reference pan and the pan

containing the polymer at the same temperature, called heat flow, was recorded. The crystalline fraction of the sample was then calculated using the following formula:

$$X_{c(sample)} = \frac{\Delta H_f^{measured}}{\Delta H_f^{100\%}} \quad (19)$$

where $\Delta H_f^{100\%}$ is the heat of fusion of a 100% crystalline PA66, taken as 196 J/g [68].
As PA6HIA is amorphous, the crystalline fraction of polyamide 66 was calculated as following:

$$X_{c(PA66)} = \frac{X_{c(sample)}}{w_{(PA66)}} \quad (20)$$

where $W_{(PA66)}$ is the weight fraction of PA66 in the initial blend (0<W<1).

All DSC measurements were performed with a TA Q2000 calorimeter. As shown in Figure 60, the samples were first heated to 300 °C at a heating rate of 10°C/min, and the melting temperature associated to the first heating and defined as the maximum of the endothermic peak was recorded. After that, samples were equilibrated at 300°C during 3 min and then cooled down to 25 °C at a cooling rate of 10°C/min in order to determine the crystallization temperature of the copolymer defined as the maximum of the exothermic peak. After 3 min of thermal stabilization at 25°C, a second heating scan was finally applied from 25 °C to 300°C at 10°C/min, and the melting temperature associated to the second heating was recorded.

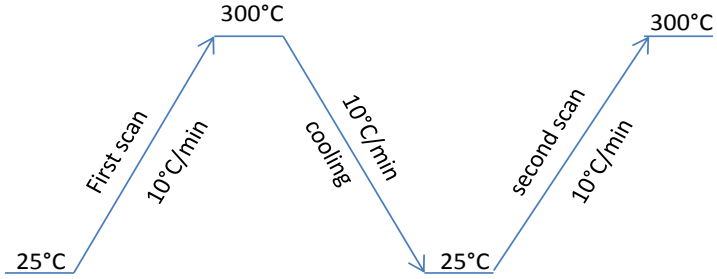

Figure 60: Thermal procedure applied during the DSC measurements

It was difficult to measure the glass transition temperature (Tg) of polyamide by classic DSC, and then DSC measurements were carried out in the temperature-modulated mode (MDSC). Samples were heated up to 200°C at 3°C/min with a temperature modulation of ± 2°C every 60 seconds. The heat capacity which represents the amount of heat needed to change the temperature of polymer sample was then extracted from the total heat flow and the Tg's were taken at the inflexion point of the heat capacity step.

3.4. **Rheological properties**

In order to understand the flow behavior of the prepared material during processing conditions such as extrusion and injection molding, rheological characterizations were performed by Sylvie Ghiringhelli from Solvay ARTI department using a capillary rheometer as schematically presented in Figure 61.

The polymer is first introduced into the barrel of the rheometer and then heated until melting. After that, the molten polymer is submitted to a pressure applied by a movable piston to drive the melt through a capillary die of 1mm of diameter. By measuring the pressure drop DP at the die exit as a function of the fluid volumetric throughput $Q_{v,}$ it was possible to determine the apparent viscosity of the polymer according to equation **(21)**:

$$\eta = \frac{DP\pi(D/2)^4}{8Q_v L} \tag{21}$$

where (η) represents the apparent viscosity in Pa.s, Q_v the volume throughput in Kg/h, L and D represents respectively the capillary length and the capillary diameter in mm.

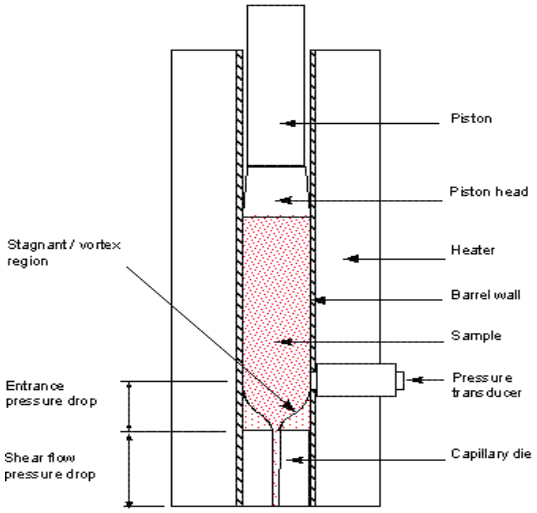

Figure 61: Schematic representation of capillary rheometer

As polyamide viscosity could evolve during the measurement (hydrolysis or post-condensation reactions), a measurement of the viscosity stability at 280°C during ten minutes at a constant shear rate of $200s^{-1}$ was performed on pellets with different moisture contents using a parallel plate rheometer. This operation allowed us to find the moisture level corresponding to a stable apparent viscosity for a given temperature. After that, the rheological characterization were carried out at 280°C with shear rates ranging from 10 to $5000s^{-1}$ on a Göttfert rheograph 2002 using a die 30/1 (length 30mm and diameter 1mm). The shear rate in the capillary rheometer die was calculated according to equation **(22)** which gives the shear rate on the wall of a capillary for a newtonian fluid:

$$\dot{\gamma} = \frac{4Q_v}{\pi(D/2)^3} \tag{22}$$

Where Qv is the volume throughput in Kg/h and D the die diameter in mm

3.5. **Free surface energy**

The free surface energy can be viewed as being the energy required to destroy the intermolecular bonds in order to create a new surface. Different approaches have been developed to measure the free energy of solid surface. Of particular note, the equation expressed by Young in 1805 [269] that gives the relationship between the liquid contact angle and the solid surface energy is given hereafter:

$$\gamma_s = \gamma_{sl} + \gamma_l . cos\theta \tag{23}$$

Where γ_{sl}, γ_l, and γ_s are the interfacial tensions between the solid and the liquid, the liquid and the vapor, and the solid and the vapor, respectively. The equilibrium contact angle that the drop makes with the solid is designated by θ.

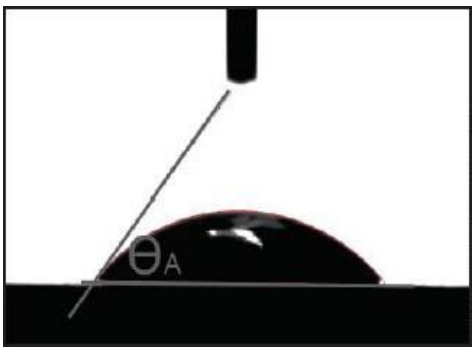

Figure 62: Measurement of contact angle using the sessile drop technique.

In this work, the solid surface energy was calculated using the two-liquid method, as described by Owens and Wendt [270]. Accordingly, the interfacial energy between the solid and the liquid is a function of the geometric mean of the polar and dispersion components of the surface energies of the liquid and the solid as detailed below:

$$\gamma_{sl} = \gamma_s + \gamma_l - 2\left(\gamma_s^d . \gamma_l^d\right)^{1/2} - 2\left(\gamma_s^p . \gamma_l^p\right)^{1/2} \tag{24}$$

Where (γ_s^p , γ_s^d) and (γ_l^p , γ_l^d) are the polar and dispersive components for the solid and liquid surface energy respectively.

By merging (24) with the Young's equation (23) , the following equation is obtained:

$$\gamma_l(1 + \cos\theta) = 2\left(\gamma_s^d . \gamma_l^d\right)^{1/2} + 2\left(\gamma_s^p . \gamma_l^p\right)^{1/2} \tag{25}$$

By measuring the contact angles (θ) of a polar and nonpolar liquid having well-known surface energy, the solid dispersive component (γ_s^d) and polar component (γ_s^p) can be determined according to equation **(25)**. The total solid surface energy is then calculated as below:

$$\gamma_s = \gamma_s^d + \gamma_s^p \tag{26}$$

In this respect, the static contact angle measurements were carried out according to the sessile drop method by using a contact angle analyzer (Kruss, DSA 100). Two liquids, commonly known as the polar and nonpolar liquids for determining solid surface energies [271], were used for these measurements: deionized water and di-iodomethane (DIM). The surface energy of deionized water was determined using the pendant drop method included in the Kruss instrument. The measured surface energy being fully consistent with the surface energy of water from the literature (72.2 mJ/m^2). Also the surface energy of DIM was checked by the same technique and was found equal to 50.8mJ/m^2.

All contact angle measurements were carried out on smooth surface prepared by injection molding with highly polished molds. The surface of injection molding discs was, prior to drop deposit, cleaned with ethanol in order to remove any impurities and then conditioned in controlled temperature and humidity (T=23°C and RH=50). After that, a drop of 4 µl of volume of each liquid was deposited on the horizontal substrate during 60 s, this time seems to be corresponding to equilibrium spreading. The contact angle between the baseline of the drop and the tangent at the drop boundary, as described in Figure 62, was measured using the Kruss integrated CCD camera-controlled software (DSA3 packages). The average contact angle was obtained from at least 10 drops of each liquid (Water and DIM) in different positions on the surface of the sample.

4. Mechanical properties

4.1. Thermo-mechanical properties

Dynamic mechanical properties refer to the response of the material when it is subjected to a periodic force. These properties are dependent on the nature of the material as well as on the experience conditions' such as the temperature, frequency and amplitude of solicitation.

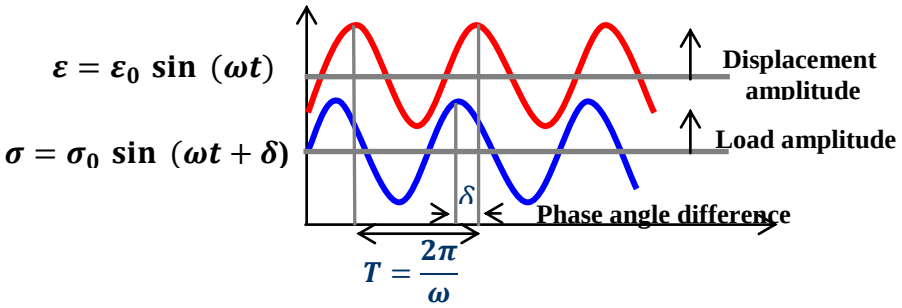

Figure 63: Viscoelastic behaviour of polymer under dynamic stress

It is well known that viscoelastic materials, such as polymers, respond when submitted to a sinusoidal stress with a sinusoidal strain out of phase with the applied stress by a phase angle (δ), as illustrated in Figure 63. This phase difference is generally attributed to the excess time needed for molecular motions and chains relaxations to occur under load. The mechanical response of the sample is generally assumed to be in the linear regime when the amplitude of the applied stress is small. Accordingly, the dynamic modulus is defined by the ratio of the applied stress to the strain as described in Equation (27). It follows that dynamic modulus

consists in a complex value that can be decomposed into two parts, the storage modulus (*E'*) and the loss modulus (*E''*).

$$E^* = \frac{\sigma}{\varepsilon} = \frac{\sigma_0}{\varepsilon_0} e^{i\delta} = \frac{\sigma_0}{\varepsilon_0} (\cos\delta + i\ \sin\delta) = E' + i\ E^{"} \quad (27)$$

where $E' = \frac{\sigma_0}{\varepsilon_0} \cos\delta$ and $E^{"} = \frac{\sigma_0}{\varepsilon_0} \sin\delta$

The storage modulus describes the ability of the material to store potential energy and release it upon deformation. The loss modulus is associated with energy dissipation in the form of heat upon deformation. The loss angle or the out-of-phasing angle between stress and strain represents the energy proportion dissipated as heat by the polymer sample. It is derived from the ratio between the loss and the storage moduli as described in Equation (28).

$$\tan\delta = \frac{E^{"}}{E'} \quad (28)$$

It should be noted that the storage modulus, often associated with the Young's modulus, is commonly related to the stiffness of the material, while the loss modulus is rather associated to relaxation processes. This latter is mainly dependent on molecular motions, intermolecular interactions, morphology and other structural heterogeneities.

As temperature increases, mobility of chains increases, leading to polymer relaxation. Depending on the molecular motion involved in the relaxation process (see Chapter I), relaxations are classified into primary or secondary relaxation. In the case of a secondary relaxation, only a slight drop of the storage modulus is observed. When the main relaxation temperature is reached, E' drops significantly (by 1 or 2 orders of magnitude) and the peaks of loss modulus E'' and tan δ are more pronounced.

In this study, thermo-mechanical characterizations were performed on tensile and impact specimen geometries using a Dynamic Mechanical Analyzer (DMA Q800). The three-point bending method was used, in which the sample is fixed between two supports and the mechanical stress is applied by a cantilever situated at the middle of the sample. The measurements were carried out in a closed furnace; the samples were cooled up to -150 °C and heated up to 250 °C at 2 °C/min. The frequency of the applied stress was fixed at 1 Hz in order to compare the measured α relaxation temperature T_α to the T_g obtained by DSC. The value of T_α was taken at the maximum of tan δ peak.

4.2. Static mechanical properties

4.2.1. Macroscopic tensile tests

The static mechanical properties were explored by carrying out tensile tests on a Zwick/Roell Z020 machine equipped with a temperature chamber and a laser extensometer. All the samples were dried under vacuum at 110°C during 16 hours and then five specimens of each sample were conditioned at least 45 min in the temperature chamber before being tested at

two temperatures: 23°C and 150°C. The geometry used for tensile tests is the ISO-527 standard injection-molded specimen presented in Figure 64.

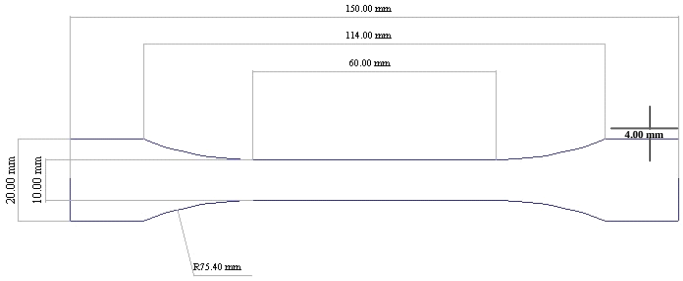

Figure 64: ISO-527-1A standard tensile specimen

Tensile tests were done at a controlled crosshead speed; firstly at 1 mm/min until 0.5% of deformation, to determine the Young modulus E, and then at 5 mm/min until the failure of the specimen. During the experiment, the stress measured with a 20KN cell force and the strain deduced from the laser extensometer were recorded, and a stress-strain curve was plotted. Figure 65 shows an example of typical curves obtained for standard dry PA6,6 at 23°C. The Young modulus E was defined as the slope of the stress-strain curve in the elastic domain (0.05 % < strain < 0.25%) and the yield stress σ_Y was identified as the observed maximum stress.

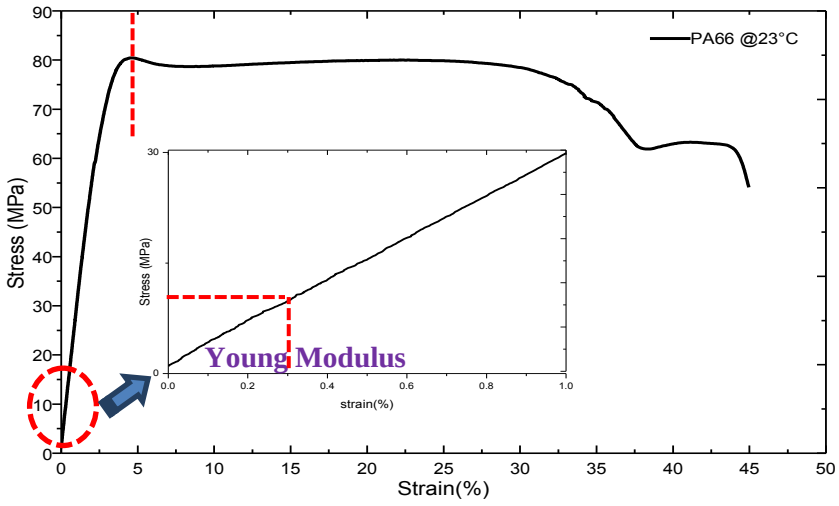

Figure 65: Stress-strain plot, yield stress and Elastic modulus of PA66 at 23°C.

4.2.2. Local deformation

The deformation mechanism at the microscopic scale (cavitation, lamella separation) of samples submitted to static load was explored by in-situ tensile-SAXS experiments. In this respect, a mini-tensile machine equipped with a load cell and a temperature chamber was introduced between the incident beam and the SAXS detector's at the "Laboratoire Interdisciplinaire sur l'Organisation Nanométrique et Supramoléculaire" (LIONS) (see Figure 67). The in-situ tensile-SAXS experiments were done on rectangular samples of 1.5 mm thick submitted to two levels of stress (50 and 70 % of the yield stress) at two temperatures (23 °C

and 150°C). The same SAXS set-up used for lamella characterization (λ=0.154nm, beam characteristics, distance to the detector) was retained for these experiments.

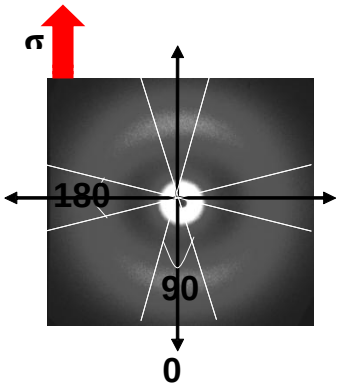

Figure 66: Radially integration of 2-D patterns into 18 azimuthal angles

All recorded SAXS patterns were processed with "Image J" and integrated radially in the azimuthal angular range ($0 \leq Ø \leq 360$) as shown in Figure 66.The scattered intensity as a function of scattering vector was mainly analyzed in two directions: perpendicular and parallel to the load direction. In the results discussion (chapter IV), the azimuthal angular range of ($80 \leq Ø \leq 100$) will be designed by the meridional direction (along the load direction), while the azimuthal range of ($170 \leq Ø \leq 190$) will be called as the equatorial direction.

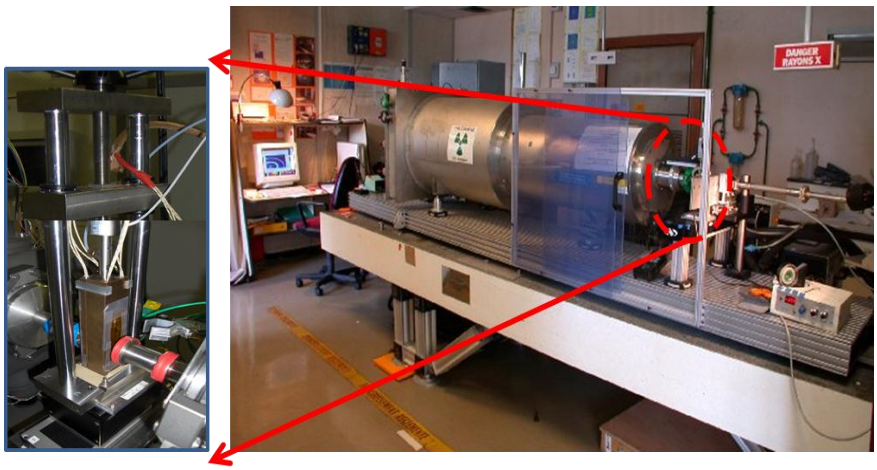

Figure 67: In-situ tensile-SAXS set-up at the LIONS laboratory

The lamellae spacing, determined according to the Bragg's law (see 2.3.1), is expected to vary under the application of stress. So, the local deformation was calculated using the following equation:

$$\varepsilon_{local} = \frac{\Delta L_p}{L_{p(0)}} \tag{29}$$

where $L_{p(0)}$ is the initial long period at the undeformed state and ΔL_p is the additional lamella separation under loading defined as $L_{p(\sigma)} - L_{p(0)}$.

4.3. **Impact resilience**

In order to evaluate the resilience of polyamide based materials at high strain rate, Charpy impact tests, which allow quantitative determination of the dissipated energy upon fracture, were performed. The impact test consists in a conventional pendulum equipped with a hammer of 7.52 J of energy, as shown in Figure 68.

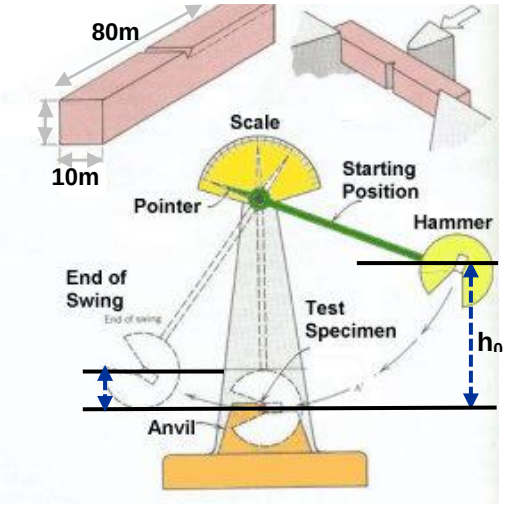

Figure 68: Charpy impact test

The polymer samples, having a dimension of 4x10x80 mm^3 were notched with a notch radius of 0.25 mm and the notch depth was fixed at 2 mm. After that sample were placed beside an anvil and were then hit with the hammer accelerated at 3 m/s as shown in Figure 68.The deformation rates $\dot{\varepsilon}$ corresponding to the Charpy experiment was calculated according to Equation (27) and was roughly equal to 10^4 Hz for samples notched at 0.25 mm.

$$\dot{\varepsilon} \approx \frac{v_{impact}}{r_{notch}} \tag{30}$$

Upon impact, the sample fails, and its resilience was deducted from the change of the potential energy between the initial position of the hammer and the final position after impact. The potential difference defined in equation (31) represents the energy dissipated during the fracture the material.

$$W_d = mg(h_0 - h_f) \tag{31}$$

By knowing the net fracture surface, the impact resilience which represents the material toughness was determined as below:

$$U_r = \frac{W_d}{S} \tag{32}$$

where U_r is the impact resilience in J/m^2 and S is the fracture surface in m^2.

Impact tests were conducted at different temperatures in order to determine the brittle-tough transition temperature. Note that a material is said to be “brittle” when its impact toughness is

low and if it fails completely upon impact. However, a material is said to be “ductile” if it has high impact toughness and if it does not fail entirely upon impact.

Samples were dried under vacuum at 110°C during 16 hours, and were then quickly notched at 0.25 mm before impact test. After that, five samples per formula per temperature were conditioned at temperatures varying from -40°C to 140°C. For temperatures above 23°C, samples were conditioned during 30 minutes at the test temperature. Otherwise, the samples were conditioned during 1 hour at the desired temperature. All the impact tests were done by Sylvie Ghiringhelli from the Solvay ARTI department.

4.4. **Long-term mechanical properties**

4.4.1. Fatigue Life-time assessment

Uniaxial fatigue tests were carried out on a servohydraulic INSTRON 8872 machine, equipped with a cell force of 5KN, at 23 °C in a temperature chamber filled with air at atmospheric pressure and uncontrolled humidity. The geometry of tested specimens corresponded to the standard ISO 527 but in addition, the specimen was notched with a central hole of 1 mm of diameter. This geometry was chosen for having more reproducible failures in the un-filled materials of this study, the stress concentration close to the hole inducing a reproducible damage localisation.

All fatigue tests were conducted in control loading mode with an applied sinusoidal stress, as presented in Figure 69. The maximum of the applied stress was ranging from 50% to 80% of the yield stress determined with static tensile tests. The ratio $R=\sigma_{min}/\sigma_{max}$ between the lowest value of the stress and the highest value was 0.1 in order to prevent buckling of the samples. As the fatigue frequency strongly influences the self-heating of the material, a frequency of 5 Hz which is a good compromise for having a limited temperature rise (about 10°C) and relatively short test durations (from 20 minutes to 1 week, depending on the applied stress) was chosen. Fatigue experiments were repeated 3 to 5 times for each applied stress. The average of number of cycles at failure is then noted and the conventional fatigue S-N (maximum of applied stress versus number of cycles to fail) or Wohler curves are plotted for the studied materials.

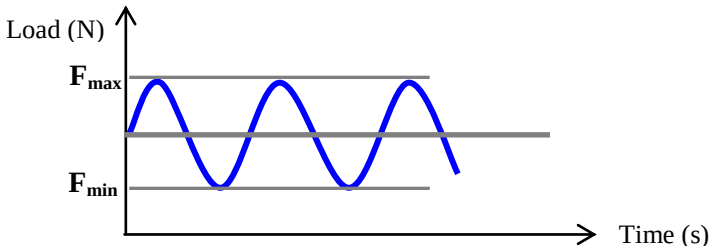

Figure 69: Sinusoidal signal of loading in fatigue tests

4.4.2. Full strain field measurement

The evolution of the deformation under loading was characterized by Digital Image Correlation (DIC) which consists in a full-field image analysis. In this way, the surface of the specimen is marked with a number of small drops of paint, in order to obtain a random

pattern. The pattern quality (speckle size and contrast) was of great importance for carrying out rigorous strain analysis. We present in Figure 70, the possible patterns obtained by black and white powder spraying. In the left image, the contrast difference between the speckles was not good enough to clearly allocate the pixels. The middle image shows large connected spots which are not suitable for fine analysis. The best appropriate pattern was a stochastic pattern with changing gray that provides good contrast, as shown in the right image.

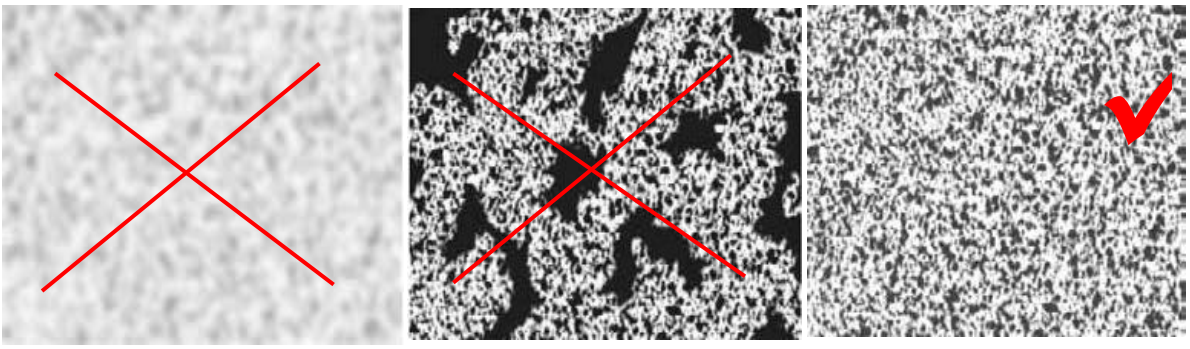

Figure 70: Three kinds of patterns resulting from specimen spraying (a) Unsuitable low contrast stochastic pattern; (b) High contrast stochastic pattern with disturbing large sports; (c) Good stochastic pattern with high contrast

After surface preparation, the specimen was clamped using the fatigue wedge grips of the Instron machine, and consecutive images, using a CCD BOBCAT B6620 camera (29MPixels) equipped with Nikon Telephoto AF Micro Nikkor 200 mm/f4.0 D, were captured before and during the loading test. The camera was also connected with the Instron fatigue machine via a Labview application in order to trigger the acquisition during loading at different fatigue levels (see Figure 71).

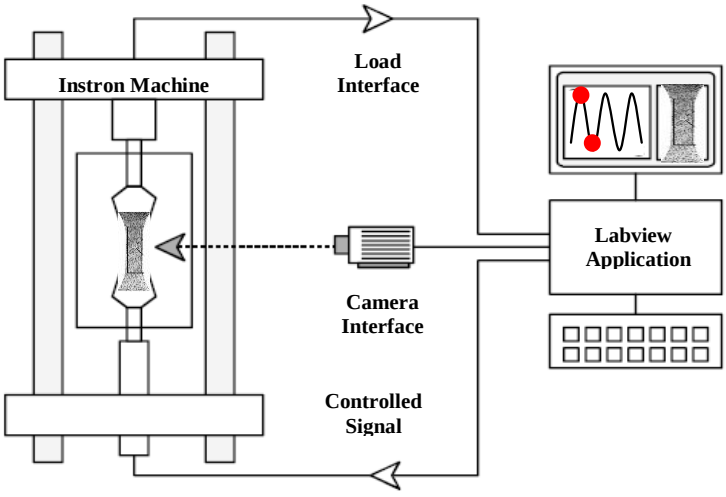

Figure 71: Schematic presentation of interfacing between the CCD camera and the fatigue machine

Dynamic images were acquired every 500 cycles at the frequency of 10 Hz corresponding to two images by cycle taken at the maximum and the minimum of the cycle. After that, the digital camera images were analyzed with ARAMIS system as briefly detailed now:

Firstly, the area to be evaluated (region of interest ROI) is selected, and rectangular images details (facets) with a certain percentage of overlapping (see Figure 72-a) are defined in order to better identify the surface structure and allocates coordinates to the image pixels. The

facets size and number are dependent on the drop pattern quality, the number of pixel and the overall deformation. Once the facets are selected, five to eight facets in different positions of the region of interest were defined as the starting points of analysis. These points are used as reference in order to determine the position of the adjacent facets in the selected image. An example of starting point is presented in Figure 72-b.

By comparing the grey value digital on the next image, it is possible to determine the contour and displacement of all facets under loading in two dimensions and, consequently, the overall displacement field of the specimen surface (see Figure 72-c). By computing the ratio of the displacement field of current image to the facet field of the reference image, the full strain filed is obtained as shown in Figure 72-d.

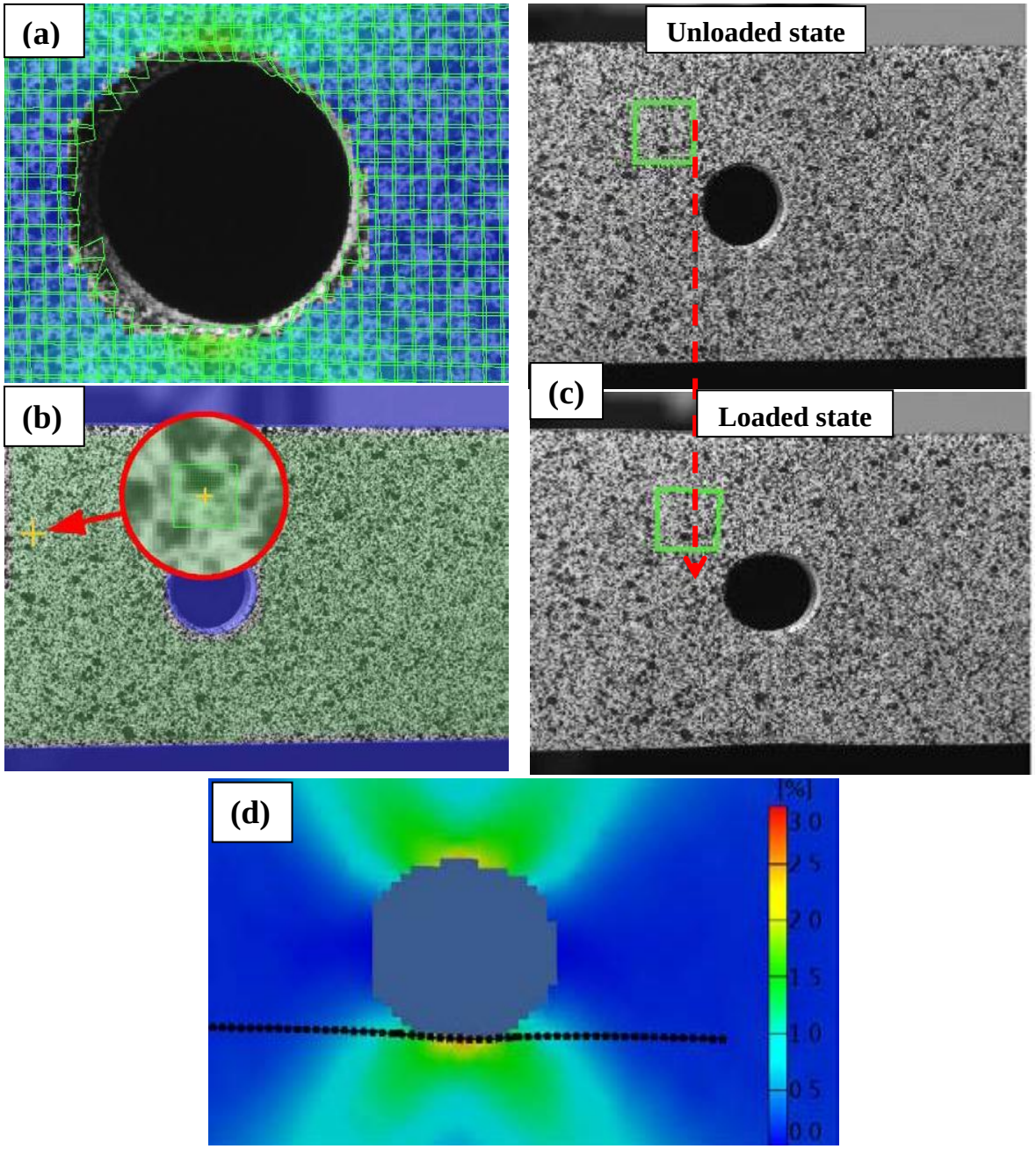

Figure 72: Sequential steps for the strain field analysis using ARAMIS system: (a) ROI and facets definition; (b) example of one selected starting point; (c) facet displacement under load; (d) strain field computation

4.5. Fatigue damage evolution

4.5.1. Dynamic modulus definition

The fatigue tests were performed in controlled loading mode with a load ratio R=0.1. Under cyclic loading, the material is macroscopically deformed and the corresponding stress-strain curves could be considered as cyclic loops. The area of the stress-strain loop (Hysteresis) corresponds to the dissipated energy (W) into the material. In the case of polymeric material, this energy is generally dissipated by inter-chain friction leading to self-heating and internal molecular readjustments. This phenomenon could be highlighted by means of viscoelastic parameters such as the phase angle (δ) between the stress and strain signals.

On the other hand, damage may occur resulting in a reduction of the material stiffness. The evaluation of the stiffness of the material under dynamic loads implies sample unloading after each cycle and the measurement of the Young modulus in the elastic domain, which is experimentally very difficult. An alternative measurement of the Young modulus is the apparent stiffness or the dynamic modulus defined as the slope of the stress-strain curve [233,272]. For a given fatigue cycle (n), the dynamic modulus Ed is determined using the following equation:

$$E_d = \frac{(\sigma_{max} - \sigma_{min})}{(\varepsilon_{\max(n)} - \varepsilon_{\min(n)})} \tag{33}$$

Accordingly, it is possible to evaluate the accumulated damage under periodic loading by normalizing the dynamic modulus at cycle (n) by the initial dynamic modulus at cycle (1). In other words, by calculating the ratio of deformation along the first cycle (1) over that occurred at cycle (n) as described in equation **(34)**.

$$\frac{E_{d(n)}}{E_{d(1)}} = \frac{\frac{(\sigma_{max} - \sigma_{min})}{(\varepsilon_{\max(n)} - \varepsilon_{\min(n)})}}{\frac{(\sigma_{max} - \sigma_{min})}{(\varepsilon_{\max(1)} - \varepsilon_{\min(1)})}} = \frac{(\varepsilon_{max(1)} - \varepsilon_{min(1)})}{(\varepsilon_{max(n)} - \varepsilon_{min(n)})} \tag{34}$$

4.5.2. Experimental methodology

As mentioned in paragraph (II.4.4), the fatigue tests were performed on specimens with a central hole. Consequently, the local stress is heterogeneous due to the presence of a geometrical discontinuity. A finite element stress modeling of 2 mm circular hole notched specimen is presented in Figure 73 [273]. As it can be seen, the stress concentration is located around the hole and then decays rapidly with increasing the distance from the hole. According to Venant's principle, the maximum of the concentration factor (equal to 3) is located at the equatorial edge of the hole while it is close to 1 after 5a distance from the center.

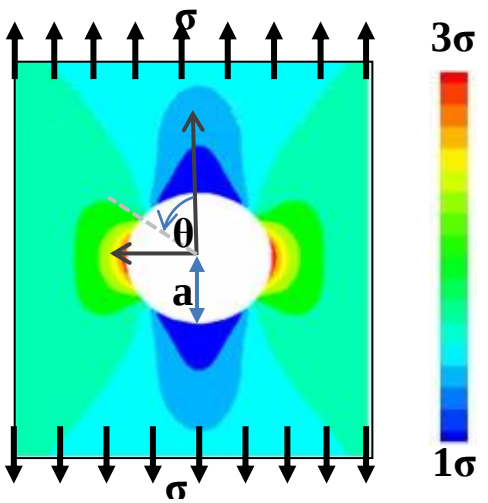

Figure 73: Stress field in hole centered specimen

Note that the stress distribution around a circular hole in infinite thin plate could be determined using the following equations [274]:

$$\sigma_\theta = \frac{1}{2}\sigma\left(1+\frac{a^2}{r^2}\right)-\frac{1}{2}\sigma\left(1+\frac{3a^4}{r^4}\right)\cos 2\theta \quad (35)$$

$$\sigma_r = \frac{1}{2}\sigma\left(1-\frac{a^2}{r^2}\right)+\frac{1}{2}\sigma\left(1-\frac{4a^2}{r^2}+\frac{3a^4}{r^4}\right)\cos 2\theta \quad (36)$$

$$\tau_{r\theta} = -\frac{1}{2}\sigma\left(1+\frac{2a^2}{r^2}-\frac{3a^4}{r^4}\right)\sin 2\theta \quad (37)$$

Where σ is the applied stress, a is the radius of the hole, r and θ are the polar coordinates of a point in the specimen.

In this work, we assumed that damage and then failure were mainly initiated in the highly stressed point. Consequently, the local strain at 300-500µm close to the equatorial edge (perpendicular to the load) was tracked during the fatigue test as shown in Figure 74 .

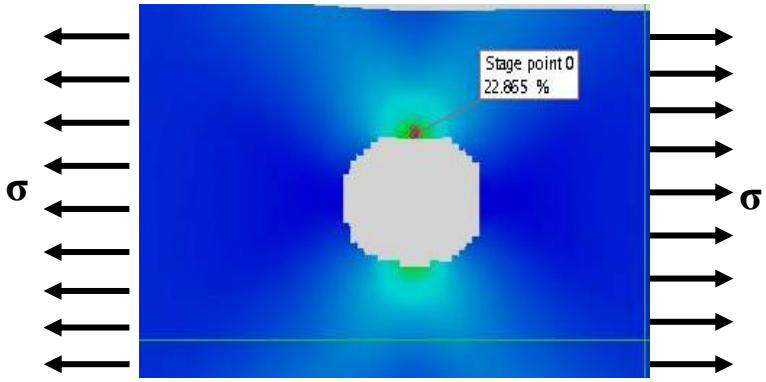

Figure 74: Full strain field and strain value of point located near the hole

Based on the local strain values taken at the maximum and minimum of the cycle, the relative stiffness, at the equatorial edge of the hole, was calculated as a function of the fatigue level using the equation (34). Furthermore, the damage parameter (D) or degree of deterioration suffered by the material after n cycles was quantified as below [275,276]:

$$D = 1 - \frac{E_{d(1)}}{E_{d(n)}} \quad (38)$$

Where 0<D<1; D=0 if no damage is occurred.

4.6. **Fatigue damage characterizations**

In this work, Scanning Electron Microscopy (SEM) and Ultra Small Angle X-ray Scattering (USAXS) are considered as the adequate techniques to characterize the damage that occurs under continuous loading. Fracture surface observations were done by SEM and USAXS experiments were used to investigate the initiation and the growth of damage.

4.6.1. Fractographic analysis

The fracture surface of fatigued specimens was characterized by Scanning Electron Microscopy (SEM). Indeed, the specimen was scanned with a focused electron beam which interacts with a thin surface layer of the specimen (~1µm) as shown in Figure 75. Three signals are then obtained in SEM experiments: backscattered electrons, secondary electrons and X-ray. Usually, only secondary electron imaging is investigated to make very high resolution topographic image of polymer surfaces.

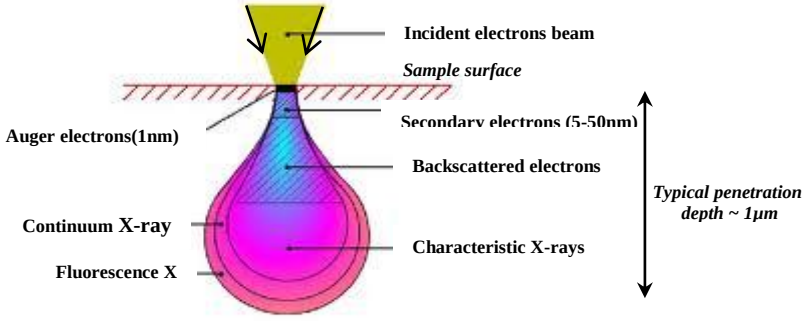

Figure 75: Diagram of interactions between an incident electrons beam and the sample surface

In this study, the fractography surfaces of broken and fatigued specimens at different levels of their lifetime were analyzed by using a Zeiss Ultra 55 microscope. SEM observations were performed on samples taken in the center of specimens across the perpendicular plane to the load direction as presented in Figure 76. All samples surfaces were metallized with a thin Platinum coat of 1µm in order to avoid the electrons accumulation at the sample surface. The observation conditions were set-up in order to limit the sample degradation and to obtain a topographic contrast:

- Accelerating tension: 3keV
- Diaphragm: 20µm
- Secondary electrons detectors (SE2)

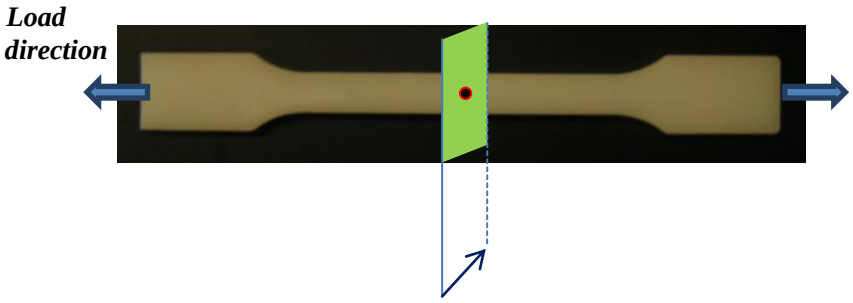

Figure 76: Direction of SEM observation on fatigued specimen

4.6.2. Cavitation analysis

As mentioned earlier, X-ray scattering is commonly used to characterize the structure of semi-crystalline polymers. It is widely admitted that the scattering intensity results from the superposition of two contributions: scattering from periodic structure (crystalline-amorphous) and much more intense scattering from voids. In fact, the electronic density of voids is null as compared to that of polymer. Thus, this electron density difference induces a high diffraction intensity at a given scattering angle.

The changes in the spacing of the periodic crystalline-amorphous structure have been studied in the previous part by SAXS in the q ranging from 2.10-2 to 7.10-1 $A^{\circ-1}$. In this section we will interest to the cavities nucleation under mechanical load by measuring the scattered intensity at ultra-small angle ($10^{-3} < q < 10^{-2}$ nm^{-1}).

Many intensity functions have been established for X-ray scattering by inhomogeneities or particles present in the matrix. These functions take into account the heterogeneity shape (sphere, ellipse, cylinder...), the symmetry center of the particle and more details depending on the particles. An universal approach for all particles shapes, known as the Guinier's approximation, has been also developed [277]. Accordingly, if N groups of voids with different sizes exist in material, the intensity of scattering I(q) may be described by the following formula:

$$I(q) = A\sum_{i=1}^{N} v_i \exp(-q^2\frac{R_i^2}{3}) \quad (39)$$

where A is a constant, R_i the radius of gyration, q the scattering vector and v_i the volume of voids in the i_{th} group which is described as below:

$$v_i = \emptyset\, N_i R_i^3 \quad (40)$$

where N_i in the number of voids and Ø is shape factor of voids in the i_{th} group.

It is important to state that, Guinier's approach is limited to small angle, i.e. when the scattering vector is smaller than the reverse of inclusion gyration radius or in other words, when the size of the void is only in the q range corresponding to q.Rg <1. Otherwise, the Porod's law is applied in the q range ($R_{max}^{-1} < q < 5nm-1$) as highlighted in Figure 77. Indeed, Porod's approach provides information on the surface morphology and on the interface properties between objects having different electronic densities (smooth, fractal surface, and fractal mass).

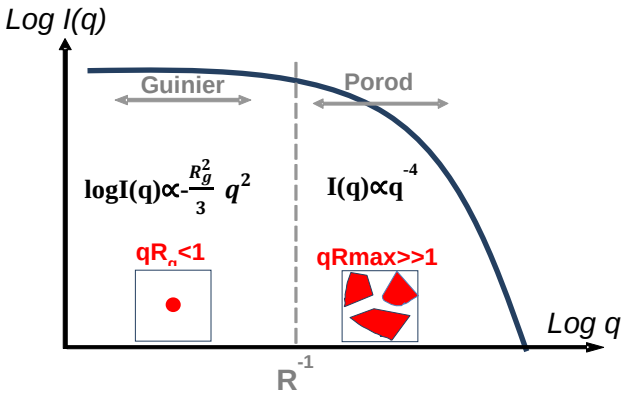

Figure 77: Scattering intensity of voids as a function of scattering vector (q) in Guinier and Porod regime

Within the framework of this study, the absolute intensity of the scattered signal at ultra-small angle was analyzed following the procedure established by Beaucage in the case of polydisperse spherical primary particles [278]. Accordingly, separated spherical voids diffract X-Ray independently and then the scattering intensity is the sum of their individual contributions as described below:

$$I(q) = n(R)\beta^2(\rho - \rho_0)^2V^2P(q) \quad (41)$$

where I(q) is the absolute intensity in cm^{-1}, n(R) is the density of spherical cavity of radius R and volume V in cm^{-3}, β^2 is the electron scattering section (=7.8 10-26 cm^2), ρ is the electronic density of polyamide (cm^{-3}), ρ_0 is the electronic density of void in (cm^{-3}) and P(q) is a global scattering function defined as below:

$$P(q) = \exp(-\frac{(qR^2)}{5}) + \frac{B}{(qR)^\delta}\left[\text{erf}(\frac{qR}{\sqrt{10}})\right]^{12} \quad (42)$$

Where B is a constant related to the void dispersion ($B \geq 4.5$; B=4.5 in the case of monodisperse voids) and δ is a constant related to the curve slope at low q ($\delta \leq 4$; $\delta = 4$ in Porod's regime)

The USAXS measurements were done on rectangular samples of ~1.3 mm of thickness taken from the central part specimens as shown in Figure 78. Specimens fatigued at different levels of their lifetime were used in order to follow the cavitation damage at a distance of 200 µm from the edge of the hole. These experiments were carried out on the ID02 line of the European Synchrotron Radiation Facility (ESRF). The size of the used beam was 200x150 μm^2 and the X-ray incident flux was very bright (3.10^{13} photon/s) with a wavelength of 0.0995 nm. A Bonse/Hart camera which is schematically presented in Figure 79 was used as an USAXS detector.

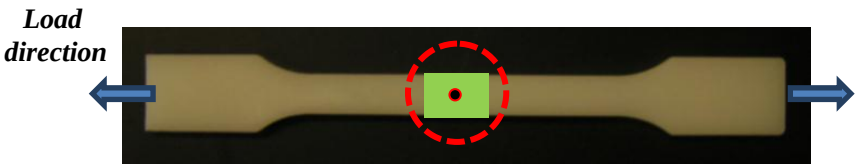

Figure 78: Specimen area analyzed by USAXS.

Two channel-cut Si -220 crystals were used in the Bonse/Hart geometry to collimate the beam and obtain a very high q-resolution. The first one plays the role of a monochromator, selecting the incident wave-vector with high resolution. The second one is used in Bragg geometry as analyzer crystal. The scattered photons were then analyzed by a Si-111 crossed analyzer before being detected by an avalanche photodiode. The resolution of the Bonse/Hart camera, determined by the crystal angular acceptance, is higher than that of the 2D cameras which is defined by the pixel size. However, the acquisition time is longer (5 minutes against 30 s for pinhole SAXS camera) and it is not possible to have 2-D patterns. Consequently, a first measurement was acquired in one direction and then the sample was rotated of 90° to make a second measurement, in order to get the USAXS intensity in the directions parallel or perpendicular to the load. The data reduction process (Air scattering subtraction, absolute intensity calibration and desmearing) was done automatically. The inherent absolute scattering intensity was obtained by normalizing the scattering intensity by the sample thickness using a Matlab tool suite "SAXS utilities" developed by Dr. Michael Sztucki.

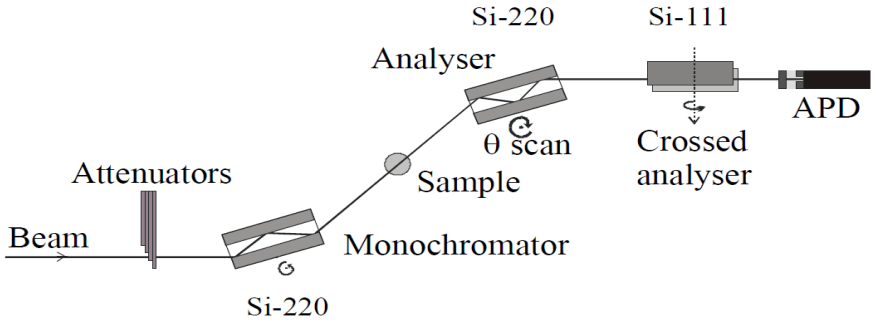

Figure 79: Schematic representation of 1D- USAXS experiments at ESRF

3

Synthesis, preparation and processing of the samples

Chapter III: Synthesis, preparation and processing of the samples

This chapter deals with the preparation of semi-crystalline polyamide materials containing phenolic moieties that are supposed to exhibit a high cohesive energy due to the strong hydrogen bonds between the phenol and the amide groups. In the first chapter, it was proposed to introduce phenolic groups into the polyamide backbone by means of covalent linkage between these groups and the polyamide chains. Accordingly, in this part, the introduction of an amorphous semi-aromatic polyhexamethylene-hydroxyisophthalamide (PA6HIA) bearing phenolic functions into the backbone of polyamide 66 is described.

In a first part, the preparation of aliphatic-aromatic copolyamides by reactive extrusion of carboxyl terminated semi-aromatic polyamide (PA6HIA-COOH) and amine terminated aliphatic polyamide (PA66-NH_2) at the laboratory scale (DSM microcompounder) is detailed. The effect of the processing parameters (temperature, time, catalyst...) on the melt exchange reactions rate between the homopolyamides and on the structure of the resulting copolymer is then studied. The main objective was to define the processing conditions which allow the preparation of PA66/6HIA block copolyamide containing PA66 crystallizable segments sufficiently long to produce an overall crystallinity close to that of the initial polyamide 66. The homopolyamide conversion to copolyamide is highlighted by Gel Permeation Chromatography (GPC) combined to UV-detection while the exchange reactions are estimated from thermal analysis and ^{13}C Nuclear Magnetic Resonance (NMR).

Once the suitable processing conditions are found (temperature, time and catalyst), copolyamides of PA66/6HIA with variable amount of PA6HIA (ranged from 0 to 40 % wt) are prepared. The structure of the prepared copolyamides is characterized by UV-GPC at two wave lengths and NMR experiments, and the morphology is studied by Polarized Optical Microscopy (POM), Transmission Electron Microscopy (TEM) and Wide Angle X-ray Diffraction (WAXD). The crystallization behavior (Crystallization and melting temperatures and crystalline fraction) is studied by DSC.

In a second part, the preparation of PA66/6HIA copolyamides at a larger scale using a Leistritz twin-screw extruder with a tailored screw profile is presented and compared to that realized at the laboratory scale. The molecular weight distribution and the thermal properties of these copolyamides are then discussed. The rheological behavior of block PA66/6HIA copolyamides is also presented and compared to that of random copolyamides PA66/6HIA and two grades of polyamide66 having different molecular weights. Based on these characterizations, the injection parameters suitable to get proper injection molded specimens are listed for each material. Finally, a global conclusion on the preparation of semi-crystalline aliphatic-aromatic copolyamides by reactive blending is outlined.

Part I: Preparation at the laboratory scale

In this part, reactive blending is studied at the laboratory scale in a microcompounder device, the aim being to find the best experimental conditions for preparing block copolyamides with PA66 segments long enough to crystallize into lamellar structure close to that of the hopolyamide PA66. The effect of extrusion time, extrusion temperature and catalyst amount is first studied for a PA66/PA6HIA blend containing 10% in weight of PA6HIA, and then different blends containing between 10% and 40% in weight of PA6HIA are realized in optimized processing conditions and studied.

1. Optimization of processing conditions to enhance copolyamide formation

1.1. Description of the reactions occurring during processing

As mentioned in the first chapter (paragraph 1.4.3), a wide range of possible reactions can occur during the polymers melt extrusion, especially in the case of reactive polymers such as polyamides. Accordingly, three possible reactions occur between polyamide chains at the molten sate : **aminolysis**, **acidolysis** and **amidolysis** [58,67]. Figure 80 highlights the possible exchange reactions, **also called transamidation reactions**, which might occur during the melt blending of PA66 and PA6HIA.

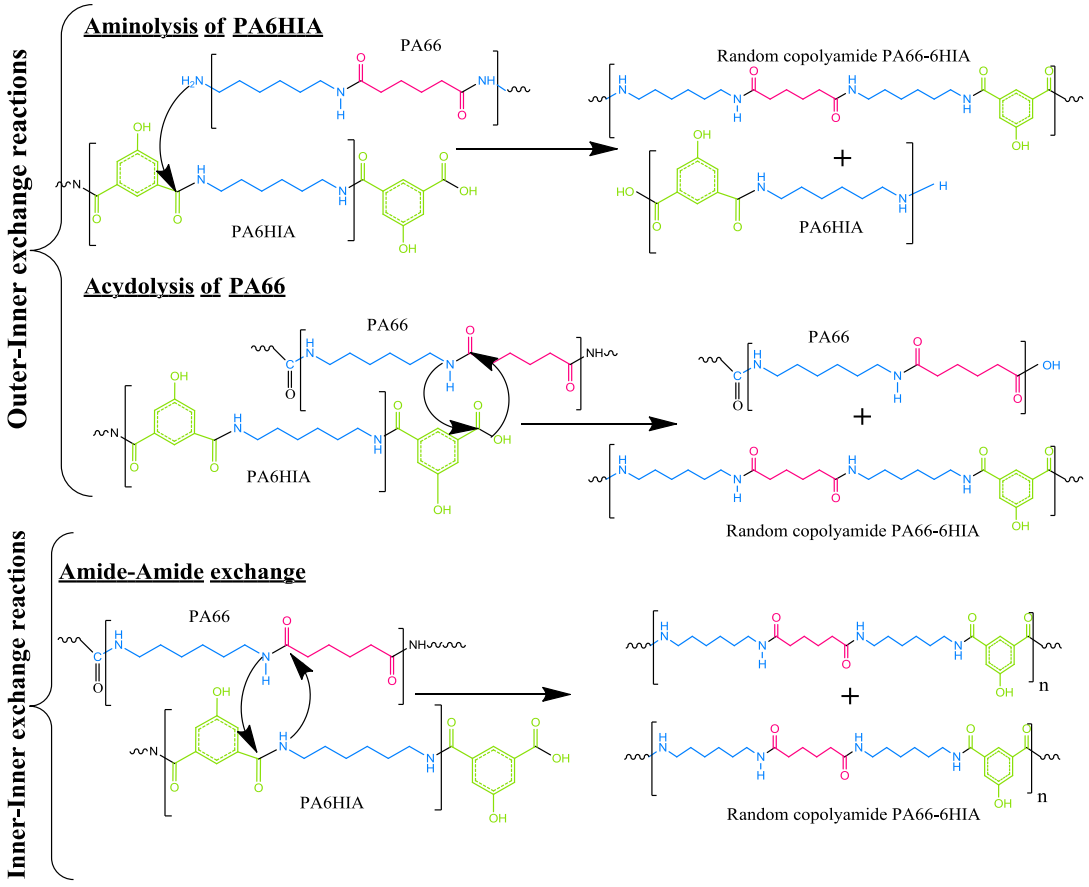

Figure 80: Possible exchange reactions (transamidation) during the melt extrusion of PA66 / PA6HIA blends

Puglisi et al, [63] reported that during reactive blending, when one of the homopolymer has reactive chains ends, the exchange process involves specifically an outer-inner reaction. They also reported that specific outer-outer exchange reaction is possible between carboxylic acid end chains (COOH) and the amine ends chain (NH_2), leading to a **post condensation** at the molten state between the homopolymers. For example, amine ends chain of PA6,6 can react with the carboxylic acid end chains of PA6HIA as presented in Figure 81.

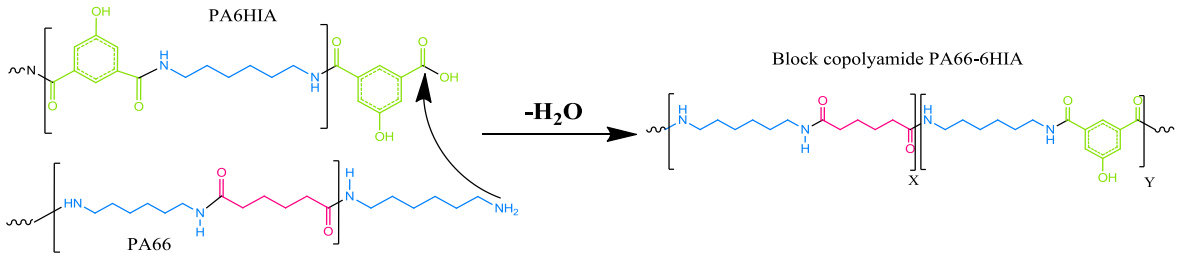

Figure 81: outer -outer exchange reactions (post-condensation) between amine terminated PA66 and carboxyl terminated PA6HIA

These exchange reactions could be likely interesting from the synthesis point of view. In fact, many works reported on the synthesis of copolymers from reactive blending of the homopolymers as an alternative way to the usual copolymerization reactions started from the monomers [39,41,46,279].

In this work, the challenge for enhancing the formation of PA66/6HIA block copolyamides is to favor the outer-outer exchange reaction (post-condensation), and to limit the outer-inner or inner-inner exchange reactions (transamidation). In this respect, low molecular weight acid terminated PA6HIA and amine terminated PA66 were chosen and were extensively dried before processing in order to favor the post-condensation reaction and the associated molecular weight increase. Varying extrusion conditions could alter the extent of the exchange and post condensation reactions and as a consequence the chain microstructure and the thermal behavior of the resulting copolymer. In this section, the effect of processing conditions (extrusion time, extrusion temperature, catalyst amount) on the molecular and structural characteristics of the obtained copolyamide will be discussed in terms of:

- Post condensation extent and rate (axial force evolution)
- Molecular structure (Molecular mass distribution and average blocks lengths)
- Thermal properties (Tg, Tc and Tm)
- Crystalline properties (Fraction, morphology and perfection)

1.2. **Effect of extrusion time**

In this part, the effect of extrusion time in the microcompounder on the microstructural characteristics of copolyamides is studied in the case of the preparation of a PA66/6HIA copolymer from a blend of amine terminated PA66 (PA1 grade) containing 20 ppm of sodium hypophosphite and 10% in weight of carboxyl terminated PA6HIA. In order to avoid thermal degradation at long extrusion times, the extrusion temperature was not too high and set at 290°C.

1.2.1. Axial force evolution

As mentioned in the previous chapter (paragraph 2.1), the force needed for the screw to push the polymer through the circulation channel of the microcompounder is related to the melt viscosity of the system [280]. Taking into consideration that viscosity of the melt is related to the polymer's microstructure (chains length, molecular weight distribution and monomer repartition…), the in-situ reaction between components of reactive blends is qualitatively followed by axial force measurement.

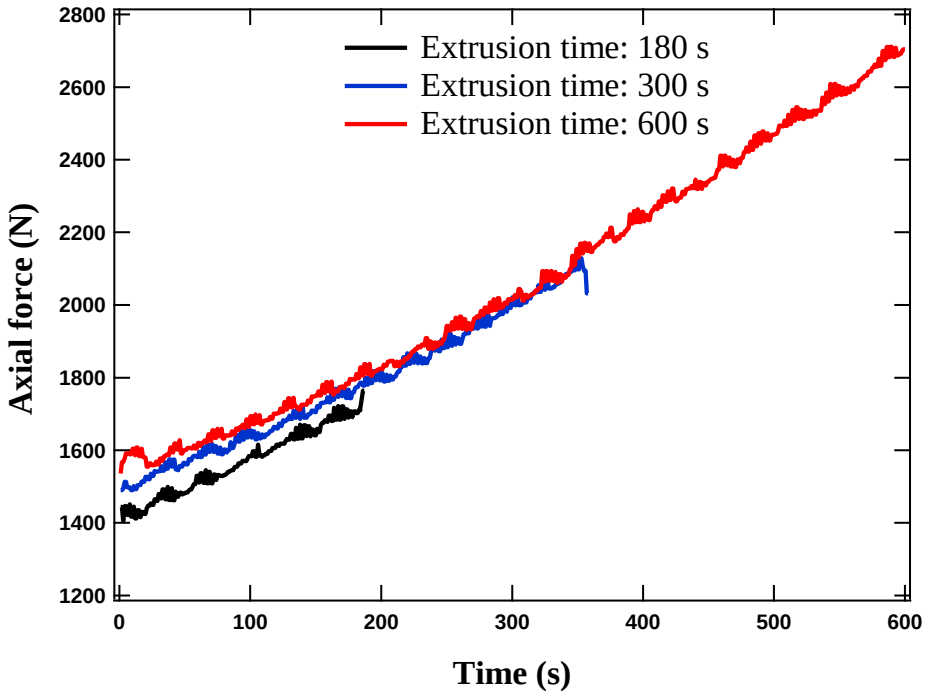

Figure 82: Axial force evolution as a function of residence time of PA66/PA6HIA (90/10 w:w) extruded at 290°C.

The effect of residence time on the copolymerization progress during microcompounding of PA66/PA6HIA blend (90/10 w:w) is illustrated in Figure 82. It clearly appears that melt viscosity increases as residence time increases, reflecting an increase of the molecular weight of the polymer chains during the melt blending. This would be possible only if the two homopolyamides attach mainly end to end to give multiblock copolymers. This suggests that the outer-outer reaction is the primary exchange reaction occurred at the time scale of the microcompounding experiment. Thus, the slope of the axial force evolution with time could be related to the melt polycondensation rate. This latter appears to be independent of the residence time of blend containing 10% in weight of carboxyl terminated PA6HIA at the compounding experiment conditions. It should be noticed, that after 600s of processing at 290°C in presence of 20 ppm of catalyst, the post-condensation reaction is not fully achieved, as evidenced by the absence of a plateau value on the plot of the axial force evolution with time.

1.2.2. Melting and crystallization behavior

The melting and the crystallization behaviors of PA66/PA6HIA (90/10 w:w) blends extruded at 290°C at different times were investigated. As the PA6HIA is amorphous and then does

not crystallize during cooling, a single exothermic peak corresponding to the crystallization of the PA66 component is expected.

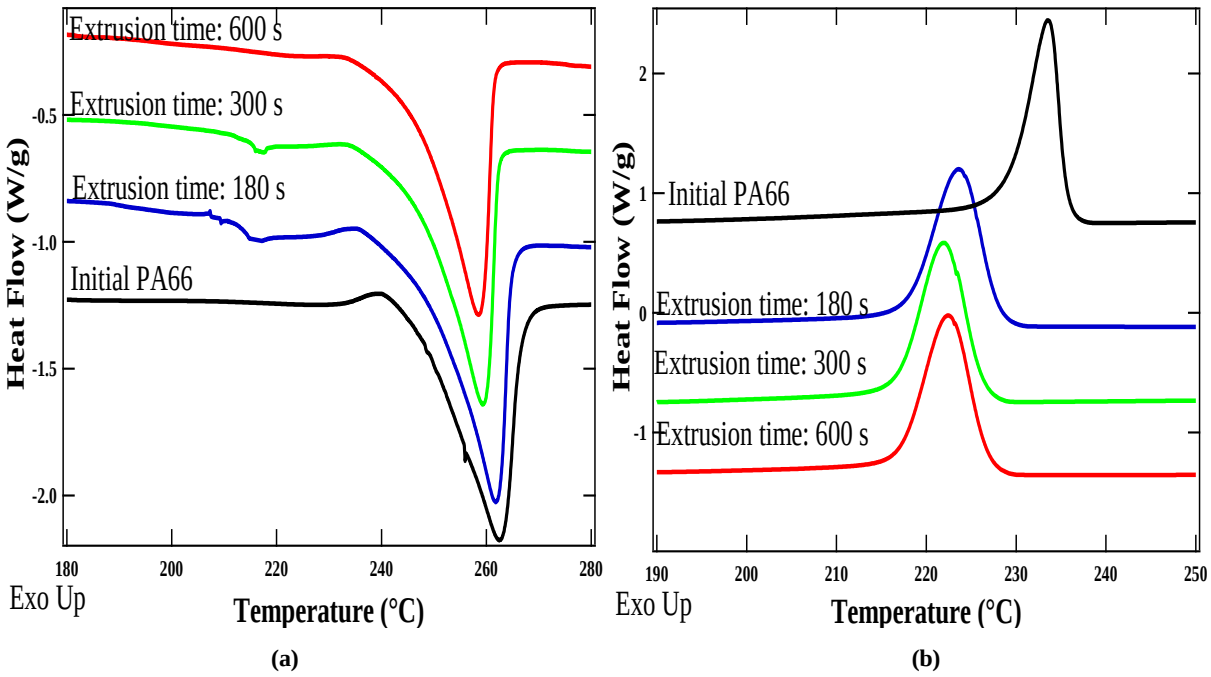

Figure 83: Influence of the extrusion time on the thermal behaviors of PA66/PA6HIA blends (90/10 w:w) extruded at 290 °C: (a) Melting thermograms (first DSC heating); (b) Crystallization thermograms

Figure 83-a shows that the melting temperature of the blends is slightly lower than that of initial PA66 (263°C), and that increasing extrusion time from 180s to 600s slightly reduces the melting temperature from 261°C to 258°C. As the aromatic ring is not incorporated in the crystalline phase, this change could be related to modification of the perfection or the size of the crystallites of polyamide 66.

Figure 83-b shows the crystallization thermograms of PA66/PA6HIA (90/10 w:w) blends extruded during 180s, 300s or 600s in comparison with that of initial PA66. It can be seen that the crystallization temperature of the blend extruded 180s is relatively low (223°C vs 233°C in the case of neat PA66). This observation could be interpreted by the formation of PA66/6HIA copolyamides within the first minutes of blending. It is assumed that the incorporation of non crystallizable PA6HIA segments within the crystallizable domains of nylon 6,6 must hinder the crystallization process of PA66 resulting in lower crystallization temperature.

Increasing the melt mixing time does not further reduce the crystallization temperature. This suggests that a further increase of the extrusion time does not produce a reduction of the PA66 block length sufficiently important to alter the crystallization behavior. So, we expect, at least on the basis of the Tm and Tc values, that the structure of the obtained copolyamides is likely consistent with a block microstructure.

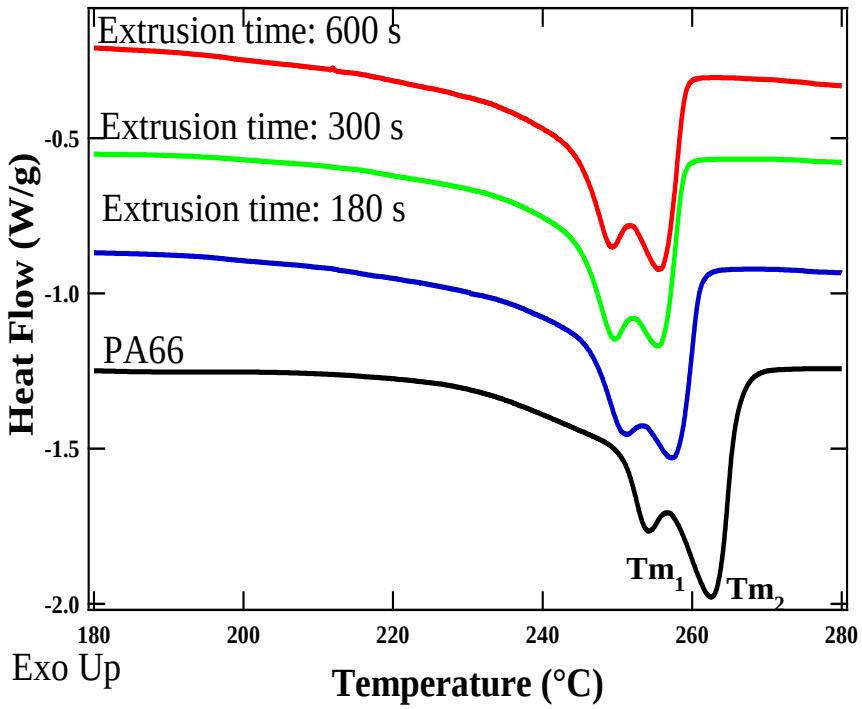

Figure 84: Influence of the extrusion time on the second DSC heating scans at 10°C/min for PA66/PA6HIA blends (90/10 w:w) extruded at 290 °C

In order to more accurately understand the melting behavior of these blends, their second heating scan after DSC cooling is presented in Figure 84. It can be seen that initial polyamide 66 as well as the extruded blends exhibit two melting peaks (Tm_1 and Tm_2). This behavior of double melting endotherm has also been reported in the literature for polyamide processed at different cooling rates or annealing treatments. Some authors discussed it on the basis of two distinct morphological species of PA66: kinetic form I/thermodynamic form II [74]and negative/positive spherulite [281]. They reported that melting temperature of form I is relatively fixed while the form II melting temperature can be either above or below that of form I. The variability in the form II melting point was attributed to variable crystal size and/or perfection. It was also pointed out that negative spherulites melt at higher temperature than the positive ones [48].

Other authors correlated the multi-melting peaks to PA66 crystals thickening upon heating [282,283]. Accordingly, Tm_1 is generally attributed to the thin lamellae formed during cooling, and Tm_2 is attributed to the melting of the crystals thickened during the heating/annealing process.

Similarly to the first heating scan, both melting temperature Tm_1 and Tm_2 of the blends are lower than those of neat PA66 and they are slightly shifted to lower values with increasing extrusion time. This suggests the formation of crystalline structure with thin lamella and /or imperfect crystals. It should be noted that the recrystallization ability of the imperfects crystal/thin lamellae is not enough to get thick lamella having Tm_2 close to that of initial PA66.

1.2.3. Conclusion on the effect of extrusion time

It was observed that post-condensation extent increases as residence time increases, suggesting that reactive blending of PA66 and PA6HIA likely produces copolymer mainly by outer-outer reactions. The crystallization temperature of obtained copolymers is relatively lower than that of initial PA66 while their melting temperatures are very close. This implies the formation of block copolymer having high ability to get crystalline structure close to that of initial PA66. As the extrusion time increases, a slight decrease of the melting and crystallization temperatures is observed, suggesting that PA66 segment of the PA666HIA copolyamides still long enough to retain the block character of produced copolymers. These observations appear to be consistent with the conclusions of Kenney and al. who reported that transamidation reactions take more than 8h at 285 °C to produce completely random copolymers of PA6 and PA66 [284].

1.3. **Effect of a catalyst**

It is clear from the previous results that it is possible to prepare copolyamides by performing reactive melt blending at 290°C with extrusion times as long as 180s-600s. But from an industrial point of view, a shorter blending time is required. The possibility to use a catalyst to accelerate the melt post-condensation process is then investigated. Indeed, in the case of PA66, the post-condensation rate in presence of catalyst appears to be at least three times higher than the post-condensation rate in the uncatalyzed polyamide. Most of the used catalysts for polyamidation reactions are phosphorus compounds [279,285–297]. In the framework of this study, the sodium hypophosphite was chosen. A PA66/PA6HIA (90/10 w:w) blend was extruded at 290°C with different amounts of sodium hypophosphite. It should be noted that sodium hypophosphite offers further benefic effects such as whitening [298] and thermal stabilization during processing of polyamide material [299–301].

1.3.1. Axial force evolution

Figure 85 shows the axial force evolution with time of two PA66/6HIA (90/10 w:w) blends extruded at 290 °C with 20 or 100 ppm of catalyst, being in the form of sodium hypophosphite. The initial melt viscosity of the composition containing 100 ppm of catalyst appears to be slightly higher, which could mean that polycondensation reaction in presence of 100 ppm of catalyst have started before the data recording during the feeding step.

In addition, the slope of axial force evolution with time is more pronounced for the blend containing 100 ppm of catalyst. This result indicates, that catalyst accelerates significantly the polycondensation reaction; it takes 180 s instead of 600 s to produce copolymers with the same melt viscosity. This observation is in agreement with the finding of Zheng et al., who reported that 250 ppm by weight of sodium hypophosphite induces a 50% increase in the polyamidation rate constant at the melt state [302]. So, this result clearly shows that sodium hypophosphite enhances the reaction between the reactive components of the blend and lead to the formation of copolymers with high viscosity in shorter times.

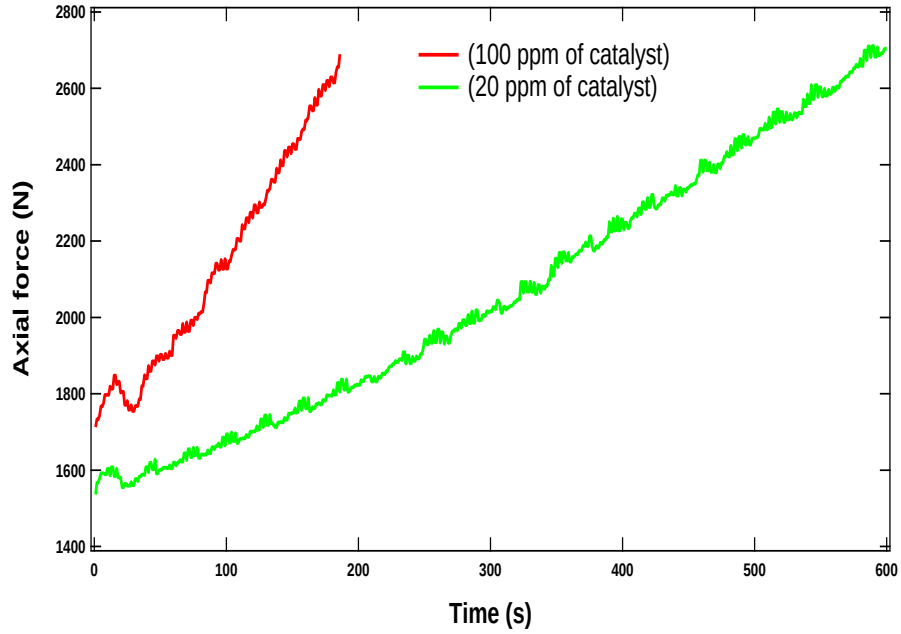

Figure 85: Axial force evolution with time of PA66/PA6HIA blends (90/10 w:w) blends extruded at 290 °C with 20 or 100 ppm of sodium hypophosphite

1.3.2. Molecular structure

The molecular mass distribution of the two PA66/PA6HIA (90/10 w:w) blends extruded at 290 °C during 180s with 20 or 100 ppm of catalyst was characterized by the combination of UV-GPC analyses at two wavelengths detections. It has to be noted that at 254nm, PA66 and PA6HIA are detected, however only the PA6HIA is detected at 310nm. Accordingly, by superposing the chromatograms taken at these two wavelengths, it is possible to differentiate the PA6HIA homoployamide which did not react with PA6,6 from the one attached to the copolyamide.

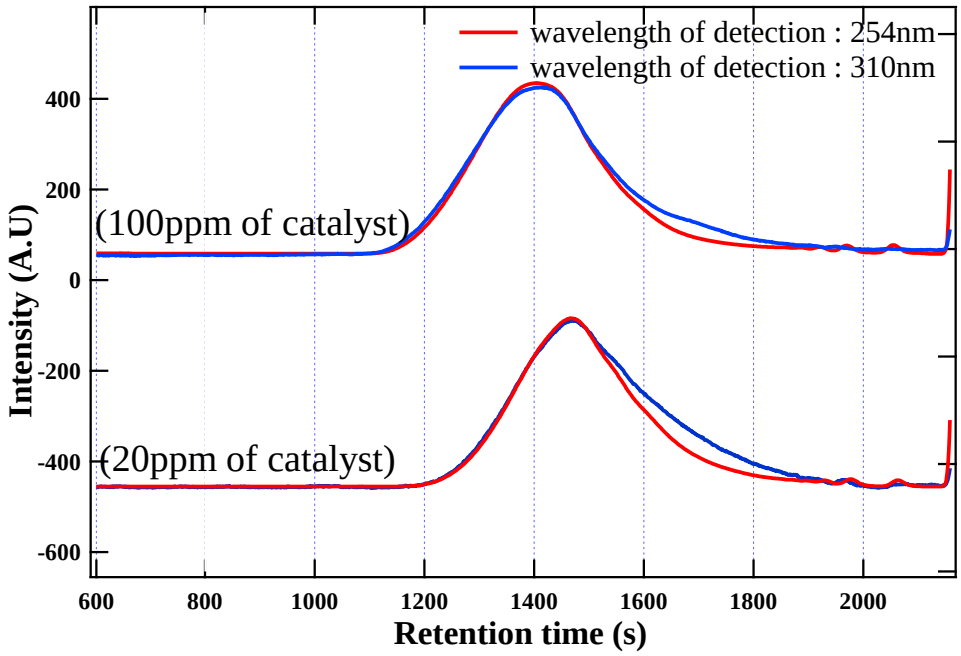

Figure 86 : GPC chromatograms of the PA66/PA6HIA (90/10 w:w) extruded 180 s at 290°C with 20 or 100 ppm of catalyst

A comparison of the GPC chromatograms taken at two detection wavelengths (254nm and 310nm) of the PA66/PA6HIA blends containing 20 or 100 ppm of catalyst is shown in Figure 86. The chromatograms of the blend containing 100 ppm of catalyst is located to lower retention time than that of the blend containing 20 ppm of catalyst, indicating a higher fraction of copolyamides with high molecular weight in the case of 100 ppm of catalyst.

For both catalyst contents, the signal taken at 310 nm is shifted from that taken at 254 nm toward long retention time. This indicates that a small fraction of PA6HIA oligomers has not been converted into copolyamide. But this fraction of PA6HIA oligomer chains that have not reacted with the PA66 appears to be more pronounced in the case of the blend that contains only 20 ppm of catalyst.

Table 3 gives then the absolute molecular weight and the dispersity determined from the GPC chromatograms without oligomers truncation for produced copolyamide as a function of the catalyst concentration. It can be seen that high catalyst concentration produces copolyamide with high weight average molecular mass (Mw). This can be understood based on the higher reactivity of the end groups in the presence of catalyst leading to chains growth by fast combination between the functional PA66 and PA6HIA chains. This difference highlighted by GPC is consistent with the difference in axial force observed previously between samples extruded 180s with 20 or 100 ppm of catalyst. On the other hand, it is believed that catalyst enhances the reaction between the oligomeric (low molecular mass) functions as well as the high molecular chains. This leads to the formation of a broad distribution of molecular mass chains as evidenced by the high dispersity of blends containing 100 ppm of catalyst.

Blends	Mn	Mw	Mz	Dispersity
PA66/PA6HIA with 20 ppm of catalyst	15600	51600	100100	3,3
PA66/PA6HIA with 100 ppm of catalyst	13100	68400	119200	5,2

Table 3: GPC data of the PA66/PA6HIA (90/10 w:w) extruded for 180 s at 290°C containing 20 or 100 ppm of catalyst

To summarize, high molecular weight copolyamides were prepared in short time thanks to the presence of sodium hypophosphite. This latter may also catalyze the transamidation reactions resulting in the formation of random copolymers. In the following, the extent of exchange reactions is qualitatively analyzed in terms of thermal behavior (crystallization and melting processes) of the resulting copolyamides.

1.3.3. Melting and crystallization behavior

Copolyamides having the same melt viscosity may exhibit different degrees of transamidation and then different thermal behaviours. For this reason, we chose to compare the blends containing 20 or 100 ppm of catalyst at the same apparent polycondensation level, i.e. at extrusion times such as the axial force reach a same given value. Thus we present in Figure 87 the melting and crystallization thermograms of PA66/PA6HIA (90/10 w:w) with 100 ppm of catalyst extruded during 180 s and PA66/PA6HIA (90/10 w:w) with 20 ppm of catalyst extruded during 600 s, having the same apparent viscosity (2700N) as previously shown in Figure 85.

For a given polycondensation level, the melting temperature and the melting enthalpy are little affected by the amount of catalyst (see Figure 87-a), indicating that both catalyst contents lead to the same lamella thickness and crystal perfection. This let us to think that the presumed block microstructure for copolymer derived from blend containing 20ppm of catalyst is likely preserved even with addition of 100 ppm of catalyst.

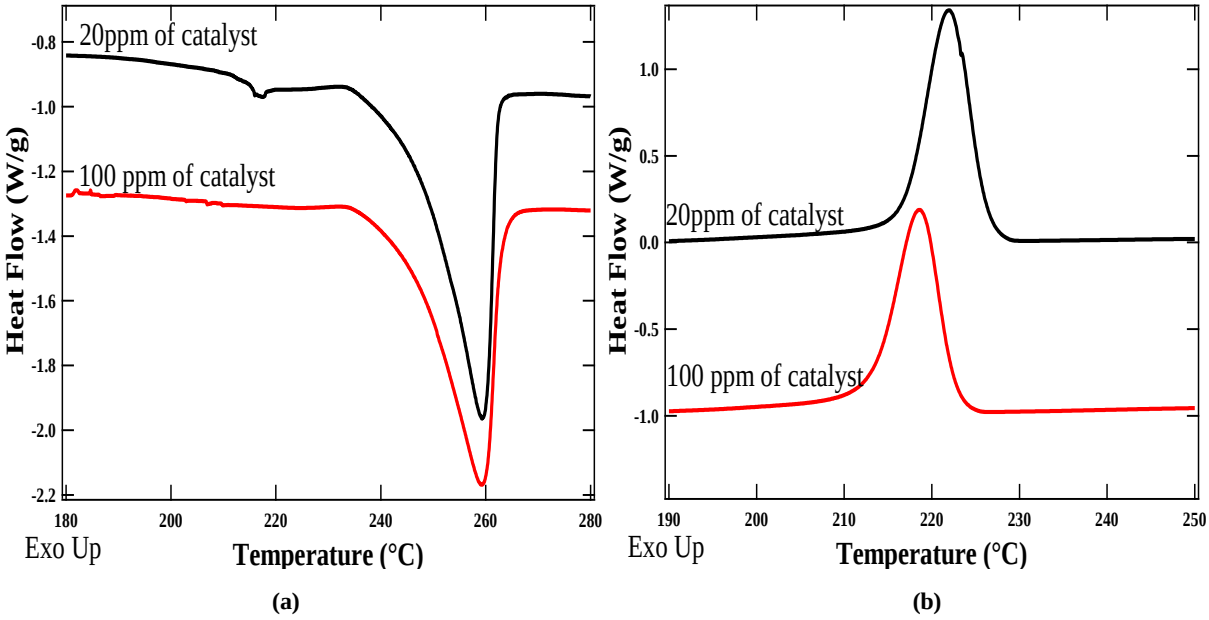

Figure 87: Thermals analysis of the PA66/PA6HIA blends (90/10 w:w) extruded at 290 °C: (a) Melting thermograms; (b) Crystallization thermograms

On the other hand, Figure 87-b shows a slight decrease of the crystallization temperature when the catalyst content is increased. It is widely accepted that addition of catalyst to homopolyamides leads to a higher polyamidation rate by means of activation of the reactive end chains. Therefore, it is expected that high amount of sodium hypophosphite enhances the melt post condensation reactions (outer-outer) as well as the transamidation reactions (outer-inner). This results in an increase of the molecular mass of the copolymers (see GPC data) and/or the formation of shorter crystallisable segments of PA66. Both of these aspects contribute to the observed drop of the crystallization temperature at high catalyst concentration.

1.3.4. Conclusion on the effect of a catalyst

The study of the axial force evolution and the molecular mass distribution shows that a high amount of catalyst enhances the melt condensation reaction and allows to get copolyamide with high molecular weight in shorter time. In spite of minor changes in the crystallization temperature (that may be attributed to a difference in the molecular weight distribution), the melting temperature is unaffected when the catalyst amount is increased. This suggests that in the present experimental conditions, increasing the amount of sodium Hypophosphite does not seem to predominantly activate the outer-inner reactions between the amides groups that would promote the formation of random copolymers.

1.4. **Effect of the extrusion temperature**

It was shown that 100 ppm of catalyst in the form of sodium hypophosphite enhances the formation of copolyamide with high molecular mass without promoting the exchange reactions. However, it was not enough to include all PA6HIA into the copolymer backbone. As extrusion temperature activates the reactive moieties and enhances the condensation and exchanges reactions in the molten state [61], it is important to study the effect of the temperature on copolyamide formation. Thus, the effect of extrusion temperature was examined by extruding PA66/PA6HIA blends containing 100 ppm of catalyst at two different extrusion temperatures (290°C and 310°C). In order to limit polymer degradation at high temperatures, extrusion time was restricted to 180s.

1.4.1. Axial force evolution

Figure 88 shows the axial force evolution with time of PA66/PA6HIA (90/10 w:w) for the two different extrusion temperatures. As already mentioned, the axial force, which represents the melt viscosity, increases with the compounding time as a result of the reaction between the ends groups of PA66 and PA6HIA (post-condensation reaction). It can be also observed that the initial axial force at 310 °C is lower than that observed at 290°C as a consequence of lower melt viscosity at higher temperature. Thus, it is difficult to correlate the axial force and the related viscosity to the structure of the copolyamide and the polycondensation extent. However, the slope of the axial force versus time appears to be roughly independent of the temperature, which suggests that the rate of melt post-polycondensation reactions does not seem to change when temperature varies between 290°C and 310°C.

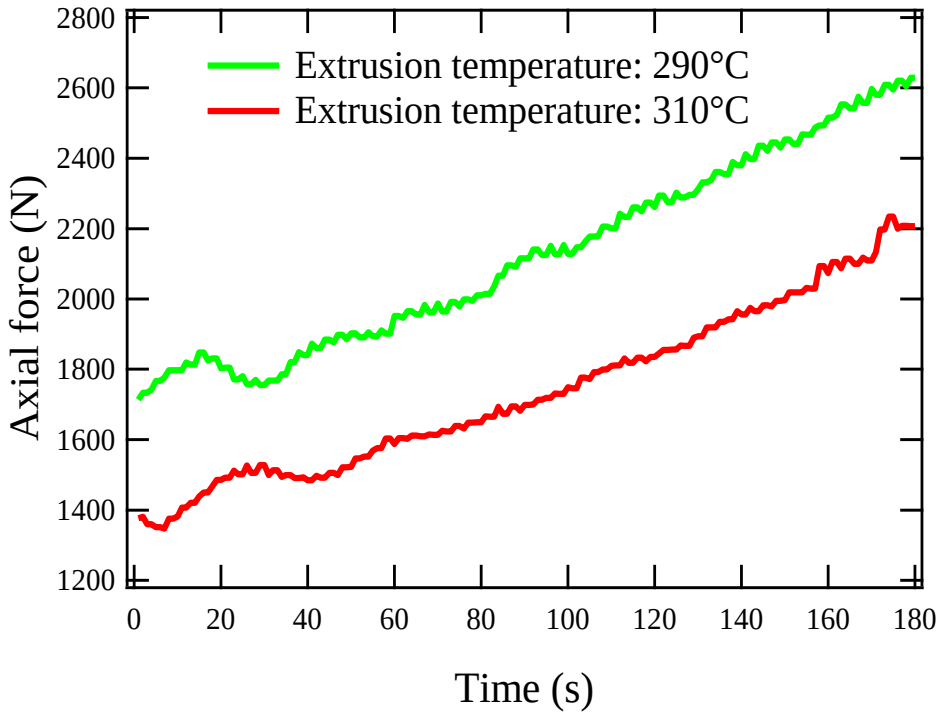

Figure 88: Axial force evolution with time of PA66/PA6HIA (90/10 w:w) extruded during 180s with 100ppm of catalyst at different temperatures

1.4.2. Molecular structure

In order to evaluate the effect of extrusion temperature on the extent of melt polycondensation, UV-GPC analyses were performed on PA66/PA6HIA (90/10 w:w) containing 100 ppm of catalyst extruded 180 s at 290°C or 310°C.

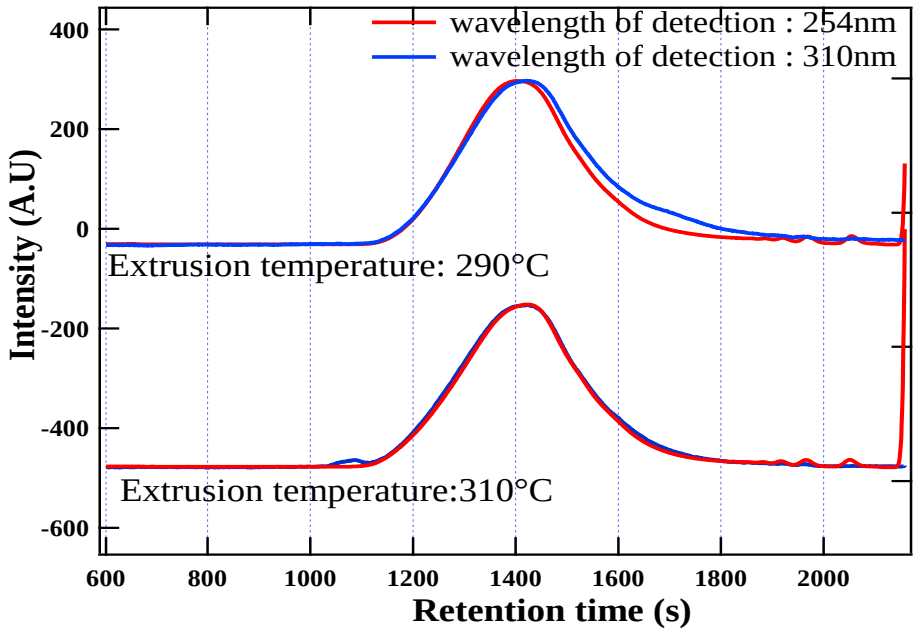

Figure 89: GPC chromatograms of the PA66/PA6HIA (90/10 w:w) containing 100 ppm of catalyst extruded during 180 s at 290°C or 310°C

The GPC chromatograms for PA66/PA6HIA (90/10 w:w) taken at 254nm and 310nm presented in Figure 89 show that the signals at 254 nm and 310 nm are superimposed in the case of the 310°C extrusion temperature, whereas they are not in the case of the 290°C extrusion temperature. The shift of the 310 nm signal to higher retention times at 290°C was already discussed in the previous paragraph, and it suggests that the blend extruded at 290°C consists in a blend of copolyamide and PA6HIA homopolyamide. The superimposition of the signals in the case of the 310°C extrusion temperature suggests a total conversion of PA6HIA into copolyamide.

A second PA66/PA6HIA composition with higher PA6HIA content (77/23 w:w) was extruded in the presence of 100 ppm of hypophosphite of sodium during 180 s at 290°C and 310°C, GPC chromatograms of this blend being shown in Figure 90. Similarly to the (90/10 w:w) composition, the better superimposition of the 254 nm and 310 nm signals show that extrusion at 310°C enhances the conversion of PA6HIA into copolymer in comparison with the 290°C extrusion temperature. If we compare now the (90/10 w:w) composition and the (77/23 w:w) composition at 290°C, we observe a better superimposition of the signals in the case of the (77/23 w:w) blend, suggesting a more efficient incorporation of PA6HIA in the copolymer. This could be explained by a difference in the reaction rate probably correlated to a higher reactivity of the blends containing a large amount of PA6HIA with carboxylic ends groups. This observation is in agreement with the work of Beste et al. [303], who found that acidity catalyzes hydrolysis of the polyamides which will accelerate the exchange transamidation reactions. They reported that the rate of transamidation reaction is proportional to the square root of the carboxyl group concentration.

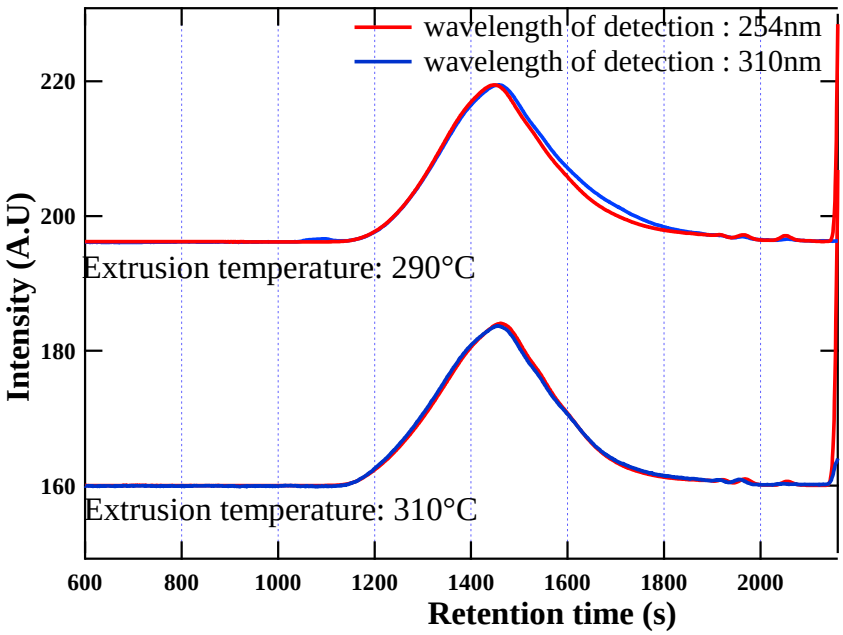

Figure 90: GPC chromatograms of the PA66/PA6HIA (77/23 w:w) containing 100 ppm of catalyst extruded during 180 s at 290°C or 310°C

Increasing extrusion temperature enhances thus the incorporation of PA6HIA into the copolyamide as a consequence of enhanced polycondensation and/or exchange reactions. However, GPC observations do not give information on the transamidation extent during the melt blending which may lead to the formation of random copolymer. In order to quantitatively point out the preparation of block copolymers, number average block length was calculated from the diad sequences of 13C NMR analyses. In Table 4, the average length of PA66 and PA6HIA sequences composing copolymer with 23 % wt of P6HIA is compared as a function of the extrusion temperature.

Homopolymers and copolyamides	$\bar{L}$PA66	$\bar{L}$PA6HIA
Initial PA66	64.1[(a)]	-
Initial PA6HIA	-	17.2 [(b)]
PA66/6HIA(77/23 w:w) 290°C	25	5.9
PA66/6HIA(77/23 w:w) 310°C	16	4.44

Table 4: Number-average sequence lengths of copolymers PA66/6HIA (77/23 w:w) containing 100 ppm of catalyst extruded during 180 s at 290°C or 310°C, (a) determined from the end group concentration (b) determined from 1H NMR spectra

It can be seen that the PA66/6HIA (77/23 w:w) copolymers extruded at 290°C or 310°C have a well-defined block copolymer structure. The block sequences of PA66 and PA6HIA are lower than that of the initial homopolyamides due to possible exchange reactions in the melt. Furthermore, it can be observed that the block length of PA66 and PA6HIA decreases with increasing extrusion temperature. The average size of crystallisable PA66 block decreases from 25 to 16 units likely as a result of more carboxyl attacks of the polyamide 66 backbone. However, the average block length of PA66 remains important enough to retain the block character.

1.4.3. Melting and crystallization behavior

Figure 91 shows the melting and crystallization thermograms of PA66/PA6HIA (90/10 w:w) extruded at different temperatures. It can be seen that the melting temperature is similar for the two extrusion temperatures, whereas a decrease of the crystallization temperature is observed when extrusion temperature increases. In addition, the melting enthalpy and the associated crystalline fraction appear to be not affected by the extrusion temperature increase, as shown in Table 5.

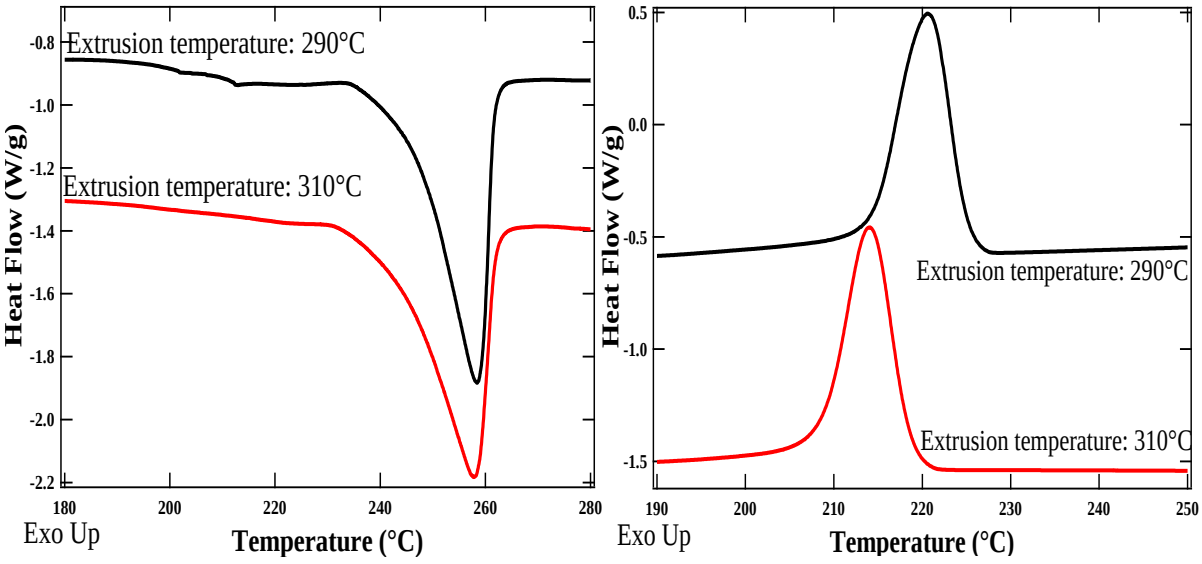

Figure 91: Thermal analysis of the PA66/PA6HIA blends (90/10 w:w) containing 100ppm of catalyst extruded during 180 s at 290°C or 310°C: (a) Melting thermograms; (b) Crystallization thermograms

Eersels et al., [67] reported that increasing extrusion temperature results in lowering the melting and crystallization temperature of PA46/6I as a consequence of an increase of the transamidation extent. In our case, melting temperature is not affected, and the effect of the extrusion temperature on the crystallization temperature is perhaps not only the consequence of an increase of the transamidation extent. Indeed, the composition extruded at 290°C contains a fraction of PA6HIA oligomers that could increases chain mobility in the melt, leading to the observed higher crystallization temperature.

Blends	Extrusion temperature (°C)	T_C (°C)	ΔHc (J/g)	T_m (°C)	ΔHm (J/g)	$Xc_{[sample]}$ (%)	$Xc_{[PA66]}$ (%)
PA66/PA6HIA (90/10 w:w)	290	220.6	49.17	258.4	59.13	30.2	33.5
	310	214	49.02	257.8	59.2	30.2	33.5

Table 5: Thermal Characteristics obtained by DSC for extruded PA66/PA6HIA blends with 100 ppm of catalyst during 180s

It was shown in the previous paragraph that a temperature increase can lead to a reduction of the crystallisable PA66 blocks length, but this length determined by ^{13}C NMR remains important and as the melting temperature was not reduced, it is reasonable to think that the blend extruded at 310°C crystallize into thick lamellae similar to those of the blend extruded at 290°C.

1.4.4. Conclusion on the effect of extrusion temperature

As extrusion temperature increases, a more efficient conversion of PA6HIA into copolymer is obtained. However, the length of the crystallizable PA66 sequence drops slightly as the extrusion temperature increases from 290°C to 310°C, which slightly impedes the crystallization ability of the final copolymers. Such a conclusion was also drawn by Eersels et al. [60], who reported an increase of the degree of transamidation of PA46/6I from 10 % to about 14.5 % when the extrusion temperature was increased from 295°C to 325°C. But the length of the crystallizable PA66 blocks of the copolymer extruded at 310°C appears to be long enough to yield crystals that melt at temperature similar to that of the copolymer extruded at 290°C.

1.5. **Summary of the effect of processing conditions on copolyamide formation**

Aliphatic-semiaromatic copolyamides were prepared by reactive melt extrusion of amine terminated PA66 and carboxyl terminated PA6HIA and the effect of processing conditions on the structure of the resulting copolymer was studied.

Firstly, blends of PA66/PA6HIA (90/10 w:w) were extruded at 290°C during different blending times. It was observed that the viscosity in the melt increases with increasing extrusion time, which indicates the occurrence of polycondensation reactions between the homopolyamides components. DSC analysis showed that incorporation of non crystallizable PA6HIA segments within the crystallizable domains of nylon 6,6 hinders the crystallization process of PA66 resulting in lower crystallization temperature. However, the melting temperature is not considerably affected, suggesting the formation of thick crystalline lamellae. Moreover, it was found that increasing the melt mixing time does not produce a reduction of the PA66 block length sufficiently important to alter the crystallization behavior and the overall crystalline structure of PA66.

In order to avoid long extrusion time, sodium hypophosphite used as a catalyst was added to PA66/PA6HIA blends extruded at 290°C. It was observed that 100 ppm of catalyst increases the melt condensation rate between the end-groups of polyamides, leading to the formation of high molecular mass copolyamide in shorter time in comparison with 20 ppm of catalyst. Furthermore, the thermal behavior of the resulting copolyamide was little affected by the addition of the catalyst, which suggests that catalyst did not promote the exchange transamidation reactions. However, GPC analysis highlighted the presence of a fraction of PA6HIA homopolyamide that was not converted into copolyamide, even with 100 ppm of catalyst.

It turned out that increasing extrusion temperature (from 290°C to 310°C) enhanced the conversion of PA6HIA into copolyamide. It was also observed that the melting behavior of the produced copolyamide was not affected by the temperature increase. However, the crystallization temperature was slightly shifted towards lower temperatures, probably because of the drop of the chain mobility of PA66/6HIA copolyamides and the slight reduction of the PA66 crystallisable sequence as evidenced by NMR experiments.

To sum up, in order to produce PA66/6HIA block copolyamide in a reasonable time and achieve complete PA6HIA conversion into copolyamide, it is proposed to blend polyamides

bearing opposite reactive end-groups at 310°C during at least 180 s in the presence of soft catalyst like sodium hypophosphite.

2. Preparation and characterization of PA66/6HIA copolyamides containing various amounts of PA6HIA

The influence of the blend composition on the reactive co-polycondensation and exchange processes was examined by studying blends having different weight fraction of PA6HIA (between 0% and 40% in weight of PA6HIA). The blends were extruded in the processing conditions established in the first part (100 ppm of catalyst, T°=310°C, t =180s).

Depending on the amorphous polyamide content (PA6HIA) in the blend, it can be expected that the produced copolyamides may exhibit significant differences in their microstructure as well as in their physical transitions such as the glass transition, crystallization and melting temperatures.

2.1. Glass transition temperature

The glass transition temperature can point out different physical characteristics of blends and copolymers such as the miscibility (two Tg's attest of a phase separation) and the chain mobility (Tg value depend on polymer inter-chain interactions). In the case of miscible blends, the Tg can be calculated as a function of the weight composition following the Fox equation:

$$\frac{1}{T_g} = \frac{w_1}{T_{g1}} + \frac{w_2}{T_{g2}} \qquad (43)$$

where w_1 and w_2 are the weight percentages of the components 1 and 2 respectively, and Tg_1 and Tg_2 are the glass transition temperatures of the components in ° K.

Figure 92 shows the glass transition temperatures (Tg) of the copolymers dried in the DSC and measured by modulated Differential Scanning Calorimetry (MDSC) as a function of the blend composition in comparison with the Tg calculated from the Fox equation. For all the compositions except for (60/40), one Tg between the Tg of initial PA66 and the Tg of PA6HIA was observed, indicating full miscibility of these blends on the composition range 0-23% wt PA6HIA. The higher Tg of PA6HIA (162°C in comparison with 65°C for neat PA66) originates from the presence of rigid aromatic rings in the backbone chain and the presence of strong Hydrogen interactions between the Hydroxyl groups and the amide groups. As predicted by the Fox law, the Tg of the blends increases with PA6HIA content but the measured Tg appears to be significantly higher than the Tg calculated with the Fox equation (reaching 95°C instead of 82.5°C for composition containing 23% of PA6HIA). The positive difference between the measured Tg and the Tg predicted by the Fox law could originate from the fact that Fox law does not take into account the effect of crystalline fraction variation, the presence of crystals inducing generally an increase of the glass transition temperature. As PA6HIA is completely amorphous, its Tg value could constitute an underestimated value for the calculation of the semi-crystalline copolymers Tg. Moreover,

the strong H-bonds interactions between the phenolic moieties of the PA6HIA and the amide groups of PA66 contribute to the positive deviation of the measured Tg.

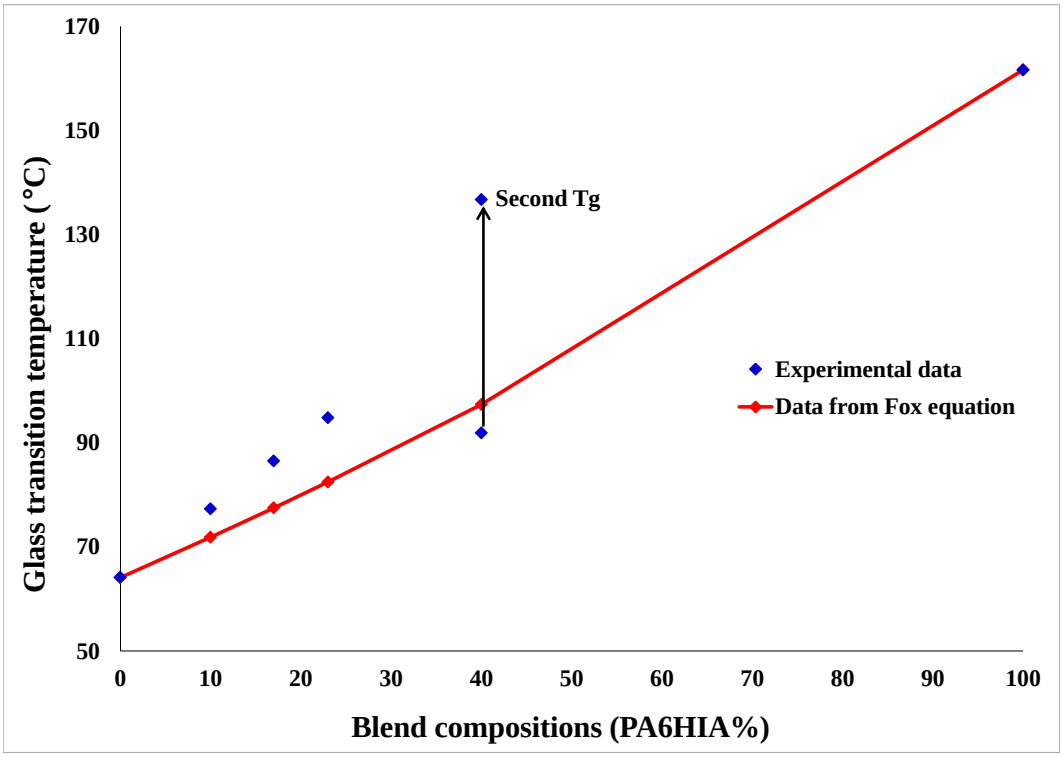

Figure 92: Glass transition temperatures, determined by MDSC on dried samples, of extruded copolyamides (Temperature: 310°C; extrusion time: 180s; 100 ppm of catalyst) as a function of the blends composition

The Blend containing 40% of PA6HIA exhibits two Tg's at 90°C and 135°C, suggesting the presence of two amorphous phases. This apparent immiscibility was interpreted in terms of incomplete reaction: the first Tg measured at 90°C could be attributed to the amorphous phase of a PA66/6HIA copolymer whereas the second Tg at 135°C could be assigned to the presence of residual amorphous PA6HIA resulting from an excess of the carboxyl terminated PA6HIA in comparison with the amine terminated PA66, or attesting of a miscibility limit. But it is important to notice that the second Tg is lower than the Tg of the homopolymer PA6HIA, suggesting that some interactions have taken place between the residual PA6HIA and the PA66/6HIA copolymer.

It has to be noted that after heating at 200°C and subsequent cooling at a rate of 10°C/min, the Tg temperatures determined with the second heating run were 2-5 °C lower than those recorded during the first heating run. This Tg reduction may be correlated to some chains reorganization to equilibrium state in the amorphous phase or crystal thickening during the first heating of fast cooled extruded samples.

2.2. **Molecular structure**

In order to get information on the effect of the blends composition on the molecular mass distribution, the extruded copolyamides, excepted PA66/6HIA (60/40 w:w) which exhibits amorphous phase segregation, were characterized by the GPC technique. In addition, ^{13}C

NMR analyses were performed in order to describe the distribution of the 6HIA comonomers in the copolyamide.

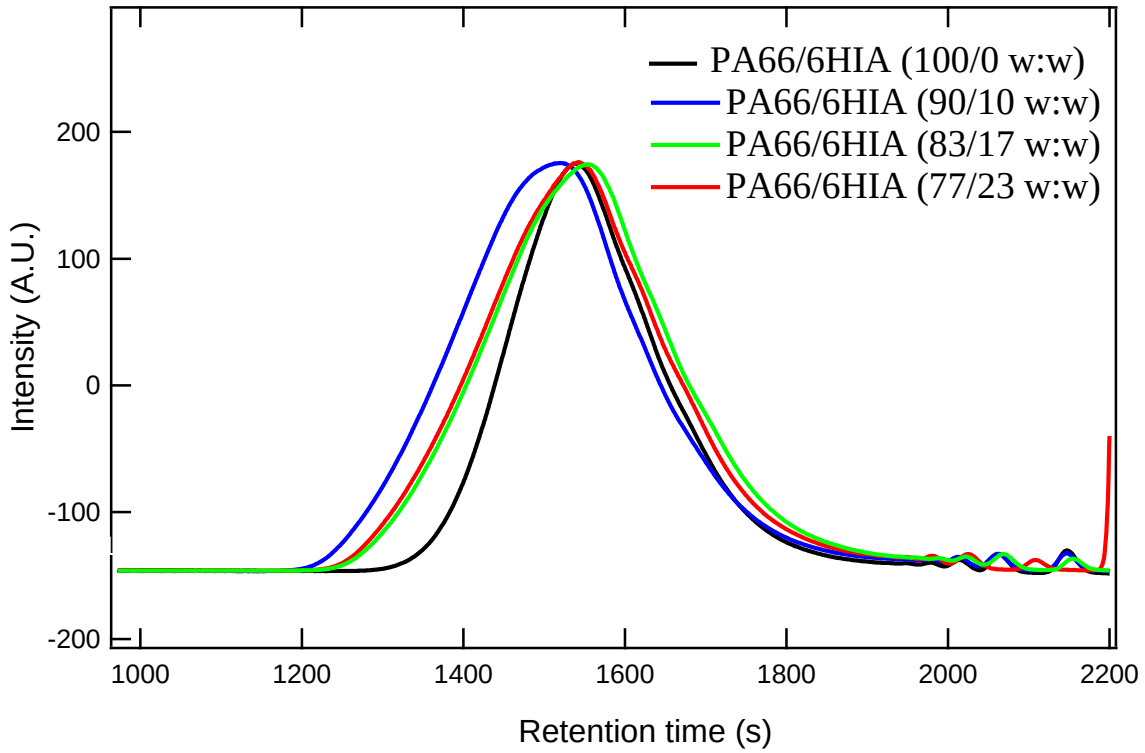

Figure 93: GPC chromatograms of the PA66/6HIA blends containing 100ppm of catalyst extruded during 180 s at 310°C

Figure 93 shows the GPC chromatograms taken at 254 nm (detection of the amide function) of the different blends extruded at 310°C during 180 s. Chromatograms profiles appear to be very dependent on the blend composition. For the PA66/6HIA (90/10 w:w) composition, the peak of the polyamide signal is shifted to shorter retention time in comparison with the PA66 chromatogram, this confirming the formation of a high molecular mass copolymer by melt state condensation between the carboxylic ends groups of PA6HIA and the amine ends groups of PA66.

For the (83/17 w:w) and the (77/23 w:w) compositions, the peaks are broader on the left hand side of the signal (short retention time), indicating also the formation of high molecular mass copolymers. But, simultaneously the peaks are also broadened to long retention times, suggesting the presence of short polymer chains that could be related to PA6HIA chains which did not react with PA66 (PA6HIA homopolyamide).

As mentioned earlier, it is possible to differentiate the PA6HIA homopolyamide from the reacted one into copolyamide by chromatogram superposition at two wavelengths detection. Figure 94 displays the same chromatograms taken at 254 nm (where the PA66 and PA6HIA detected) and at 310 nm (only PA6HIA can be detected) for all the PA66/6HIA compositions. It appears that for all blend compositions, the signal taken at 310 nm and 254nm seems to be very similar. This indicates that PA6HIA is totally converted into the copolyamide by reactive melt blending during few minutes (3min). Therefore, we could assume that the signal broadening to higher retention time observed in the case of (83/17 w:w) and (77/23 w:w) compositions does not correspond to PA6HIA homopolyamide that did not react. But it could

correspond to PA6HIA that did react with PA66 oligomers, forming copolyamides with molecular weight not very different from that of PA6HIA.

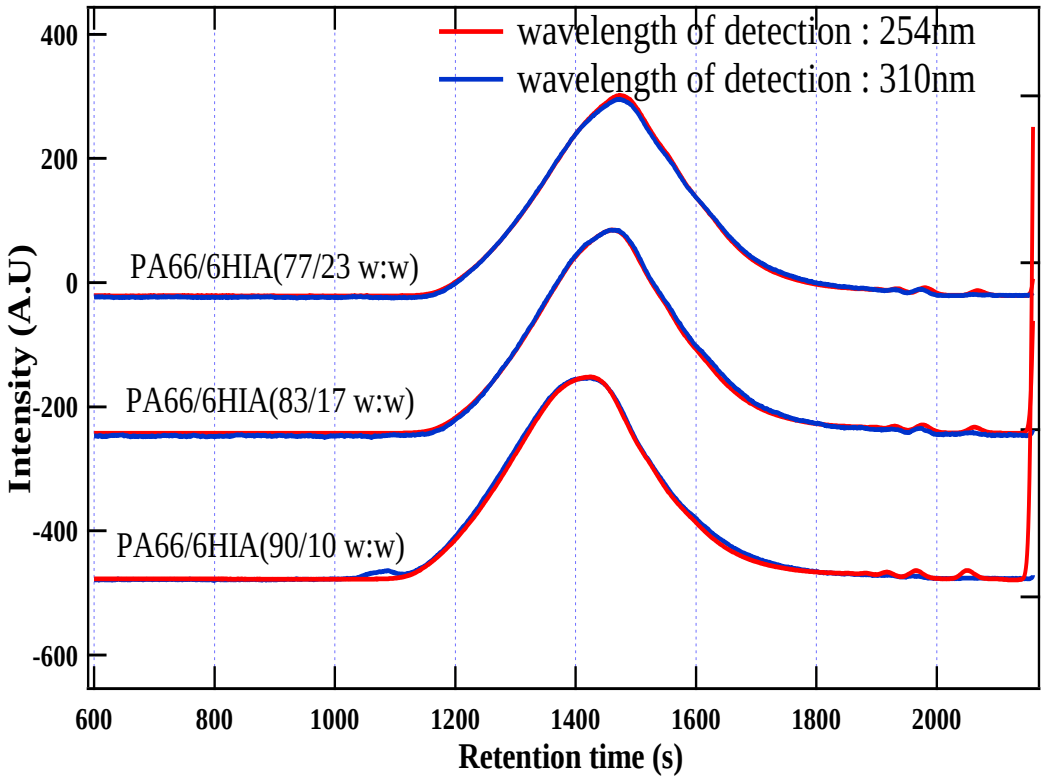

Figure 94: Superposition of the GPC chromatograms taken at two wavelengths of detection (254nm and 310nm)

The molecular characteristics extracted from the GPC chromatograms of the homo and copolyamides are summarized in Table 6. The molecular masses of all the copolyamides appear to be higher than the homopolyamide ones, which confirms the formation of multi-block copolymers. In addition, the weight average molecular mass of the (90/10 w:w) copolyamide is 17% higher than that observed for the other copolymers. The observed difference in the molecular mass as a function of the initial blends composition could be explained by the differences of reactivity and initial stoichiometric ratio of the carboxylic and amine end-groups. This point is now further discussed.

Homopolymers and copolyamides	Mn (g/mol)	Mw (g/mol)	Mz (g/mol)	Dispersity
PA6HIA	6500	13800	23700	2.1
PA66/6HIA (100/0 w:w)	10500	35000	44500	3.3
PA66/6HIA (90/10 w:w)	14800	67500	126500	4.5
PA66/6HIA (83/17 w:w)	15900	57000	107000	3.5
PA66/6HIA (77/23 w:w)	16800	58800	119000	3.5

Table 6: GPC data of PA66, PA6HIA and PA66/6HIA copolyamides extruded during 180 s at 310°C

In the case of the (90/10 w:w) blend composition, the carboxylic/amine end groups ratio is around 0.65, which means that the homopolyamide 66 is in excess. In a first step, the amine end-group recombines with carboxylic end-group to form diblocks copolymers. Then, the amine terminated PA66 in excess will probably react with the diblocks copolymers by outer-

outer reaction, yielding a high molecular mass triblock copolymer as schematically shown in Figure 95.

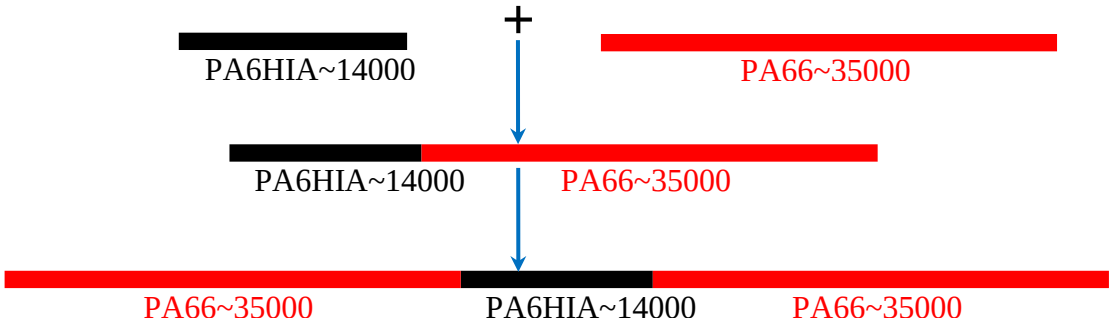

Figure 95: Schematic representation of the structure of copolyamide PA66/6HIA (90/10 w:w)

Consequently, there should be a mixture of diblocks and triblocks copolyamides corresponding to a weight average molecular mass of around 68000.

In the case of the PA66/6HIA (83/17 w:w) copolyamide, the carboxylic/amine end groups ratio is around 0.98, which suggests that the copolyamide will mainly result from of a single outer-inner reaction, leading to the formation of mainly diblock copolymers (see Figure 96) with molecular mass around 50000 g/mol.

Figure 96: Schematic composition of copolyamide PA66/6HIA (83/17 w:w)

In the case of the (77/23 w:w) blend composition, the carboxylic/amine end groups ratio is around 1.24, which means that the PA6HIA homopolyamide is in excess. This carboxylic terminated PA6HIA in excess will probably react with both ends of the amine terminated PA66, yielding a high molecular mass triblock copolymer. Thus, the final product should be a mixture of diblocks and triblocks copolyamides as shown in Figure 97.

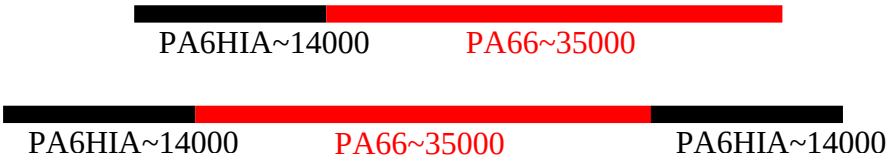

Figure 97: Illustration of triblock structure of copolyamide PA66/6HIA (77/23 w:w)

The simple copolymerization mechanisms described above assume that the polycondensation reactions (outer-outer) are predominant. However, other possible exchange reactions (outer-inner and inner-inner) compete with the main post condensation reaction (outer-outer) in the melt state. Accordingly, PA66/6HIA copolyamides synthesized by reactive extrusion consist in a mixture of multiblock copolymers having different sequence distribution and different block length. The presence of many populations of block copolyamides could be at the origin of the high value of dispersity (about 4.5). The determination of PA66 and PA6HIA sequences and their distribution along the resulting copolyamide was then assessed by ^{13}C NMR analysis.

The results of the number average block length calculated from the diad sequences of the copolymer are listed in Table 7 for the different blends compositions. These data are

compared with the initial values of PA66 and PA6HIA homopolyamides determined from respectively the ends groups concentration and the ^{1}H NMR.

Table 7 clearly shows that the block sequences of PA66 and PA6HIA in the produced copolyamides are lower than the initial homopolyamide block length. The drop of the homopolyamide block length in the copolyamides indicates that transamidation by outer-inner and inner-inner reactions between PA6HIA and PA66 take place during melt blending. Nevertheless, the produced copolyamides are still far from random copolymers indicating that the extent of exchange reactions is very limited in the established conditions of reactive extrusion.

It can be noted also that the block length evolution with PA6HIA content is not the same for PA66 and PA6HIA. As the PA6HIA content increases, the block length of PA66 drops continuously from 46 to 16 for the (77/23 w:w) copolymer composition, whereas the block length of PA6HIA stabilizes at about 5 units on all the PA6HIA contents range. This means that, on average, there are 5 neighboring homologous groups of repeat units of Hexamethylene-hydroxyisophtalic acid in all the copolyamides.

Polymer	Melt mixing conditions	$\bar{L}_{PA66}$	$\bar{L}_{PA6HIA}$
PA6HIA	-	-	17.2 [a]
PA66/6HIA(100/0 w:w)	-	64.1 [b]	-
PA66/6HIA(90/10 w:w)	180 s at 310°C	46	5.11
PA66/6HIA(83/17 w:w)	180 s at 310°C	27.2	4.47
PA66/6HIA(77/23 w:w)	180 s at 310°C	16	4.44

Table 7: Number-average sequence lengths of PA66 and PA6HIA into PA66/6HIA copolyamides; (a) determined from ^{1}H NMR spectra, (b): determined from the end groups concentration.

This difference could be explained by a stoichiometry difference between amine terminated PA 66 and carboxylic terminated PA 6HIA. In the case of the (90/10 w: w) blend composition, the carboxylic/amine end groups ratio is around 0.65, which means that amine ends groups in excess could attack several times the PA6HIA (outer-inner reaction), resulting in a reduction of the PA6HIA block to 5 units. At the same time the carboxylic end functions could attack the inner amide groups of PA66 leading to the reduction of PA66 block to 46 units. When PA6HIA content further increases, the number of carboxylic ends groups increases, favoring more the attack of PA66 segments than the attack of PA6HIA segments, and leading to the formation of block copolyamides with shorter PA66 blocks. The high reactivity of carboxylic ends groups could explain the reduction by 4 of PA66 length with adding only 23% wt of PA6HIA-COOH. These results appear to be in agreement with the finding of Eersels et al. [61]. They showed that the exchange reactions become more important with high semi-aromatic content, as a result of high reactivity of the initial blend, leading to shorter crystallizable segments of PA66.

As a conclusion, the block length of PA66 in the copolyamides and their molecular mass distribution appear to be very dependent of the initial blends composition through the stoechiometry parameter which governs the ability of the reactive components to form diblocks or triblocks copolymers as well as the extent of the transamidation reactions.

2.3. **Melting and crystallization behavior**

Figure 98 shows the melting behavior of the different copolyamides extruded under similar processing conditions. Melting temperature appears to decrease with increasing PA6HIA content, it decreases by 5 °C with adding 10% wt of PA6HIA and and by 10°C in presence of about 25 % wt of PA6HIA (250°C instead of 260°C in the case of neat PA66). The melting temperature depression could be related to lower stacking order or thinner lamellae of polyamide 66 due to the length reduction of the crystallizable PA66 segments which was highlighted by NMR experiments and described in the previous paragraph.

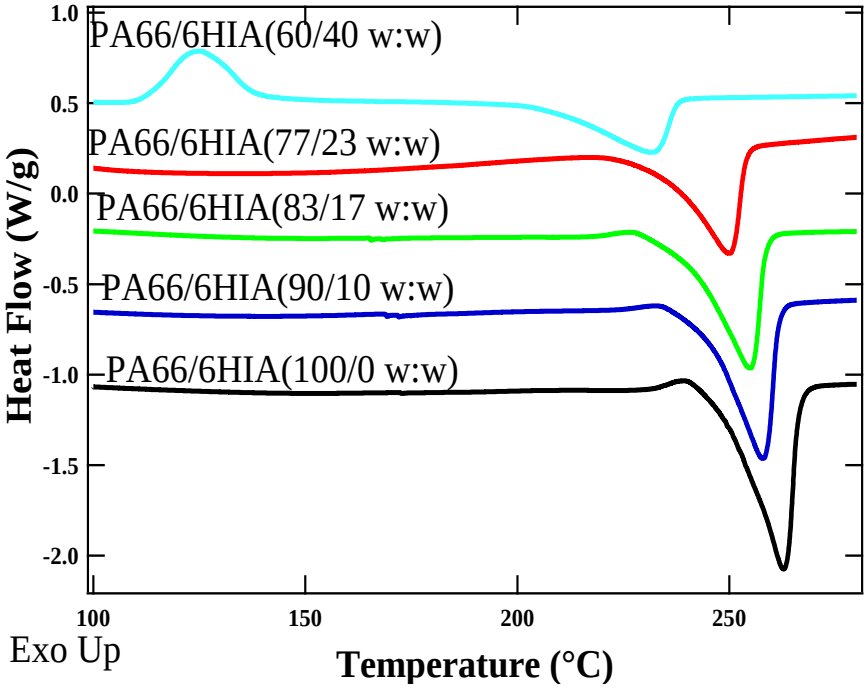

Figure 98: Melting thermograms (first DSC heating) of PA66/6HIA blends extruded during 180 s at 310°C

In the case of the PA66/6HIA (60/40 w:w) blend composition, an exothermic peak above the Tg was observed at 120 °C during the DSC heating scan. This peak should be attributed to cold crystallization and it reflects the poor crystallization ability of the copolyamide that contains a high PA6HIA content.

The cold crystallization peak should be related to the crystallization of the PA66 sequences of the PA66/6HIA copolyamide. By comparing the global melting enthalpy of the PA66 into this composition (36 J/g) with the cold crystallization enthalpy (29 J/g), it can be assumed that the as-extruded PA66/PA6HIA (60/40 w:w) blend is roughly amorphous. In addition, the melting temperature is more than 30°C below the melting temperature of the homopolyamide 66, indicating that crystals formed upon cold-crystallization in the DSC exist in the form of thinner lamellae and/or smaller crystallite.

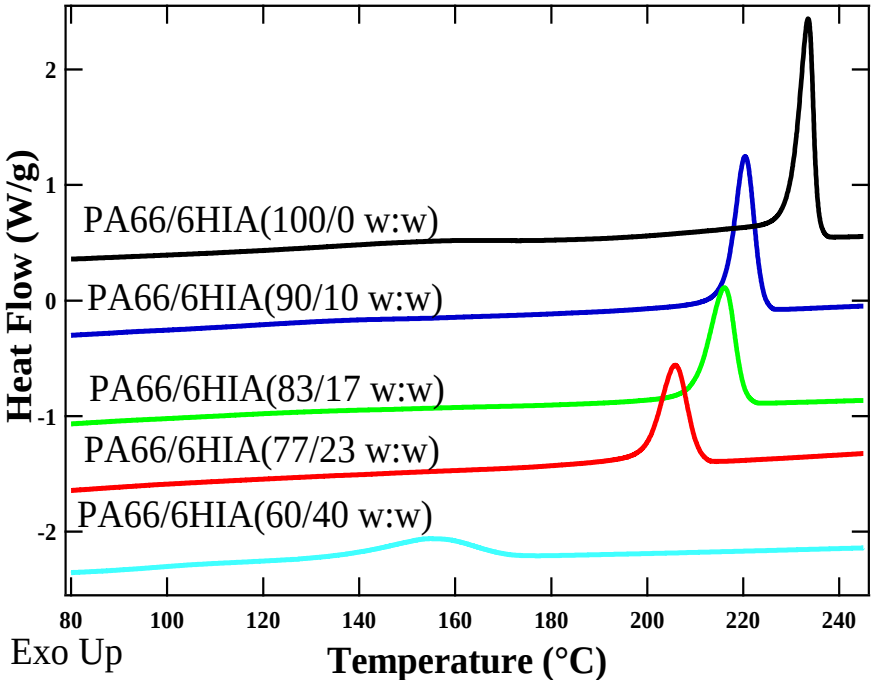

Figure 99: Crystallization thermograms of PA66/6HIA blends extruded during 180 s at 310°C

Figure 99 shows then the thermograms of the different blend compositions obtained upon cooling from the melt. It can be seen that the crystallization temperature decreases as the PA6HIA content increases. For instance, blends containing less than 25 % wt of PA6HIA crystallize around 210 °C (20°C below the crystallization temperature of the homopolyamide 66), whereas the blend with 40% wt of PA6HIA crystallizes more than 70°C below the crystallization temperature of PA66. Increasing PA6HIA content results also in a broadening of the crystallization peaks indicating a lower crystallization rate.

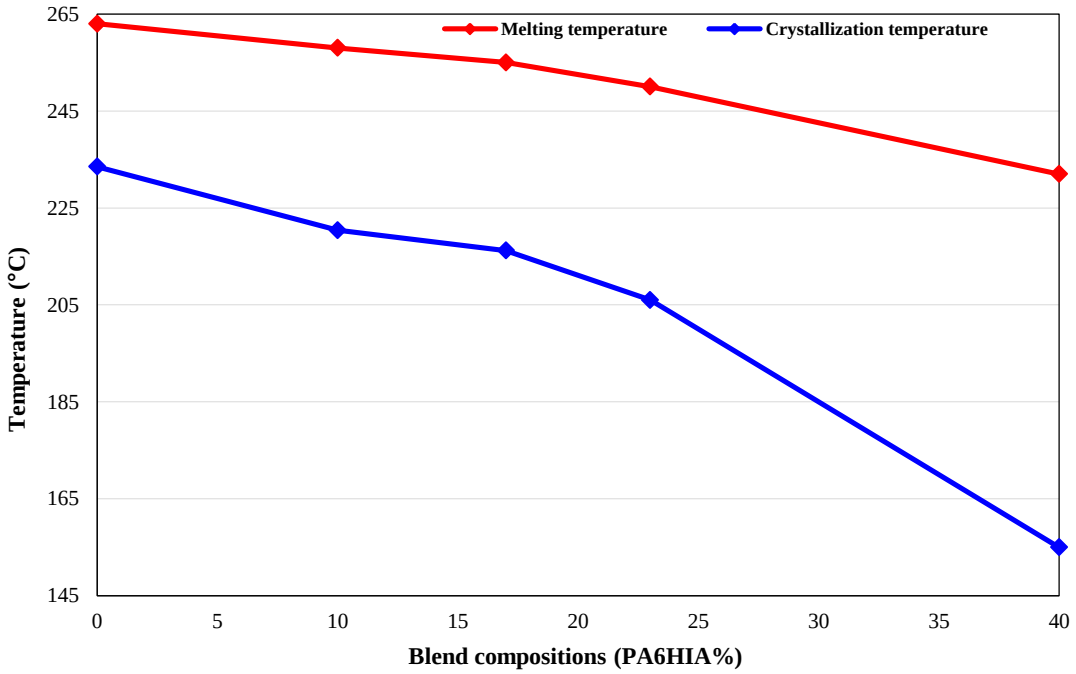

Figure 100: Variation of the melting and crystallization temperatures with the PA6HIA content

Figure 100 summarizes the evolution of the melting and the crystallization temperatures with PA6HIA content, and it is shown that the composition effect is more pronounced on the crystallization behavior than on the melting behavior. Indeed, the lower ability to crystallize as PA6HIA content increases might be explained by the increase of molecular mass and the incorporation of semi rigid aromatic segments that hinder the crystallization process of PA66 sequences. The moderate Tm decrease between 10% and 23% of PA6HIA comonomer suggests that on this composition range, the crystallizable PA66 block length remains sufficiently long to yield crystals of similar size / perfection, which is in accordance with the NMR results.

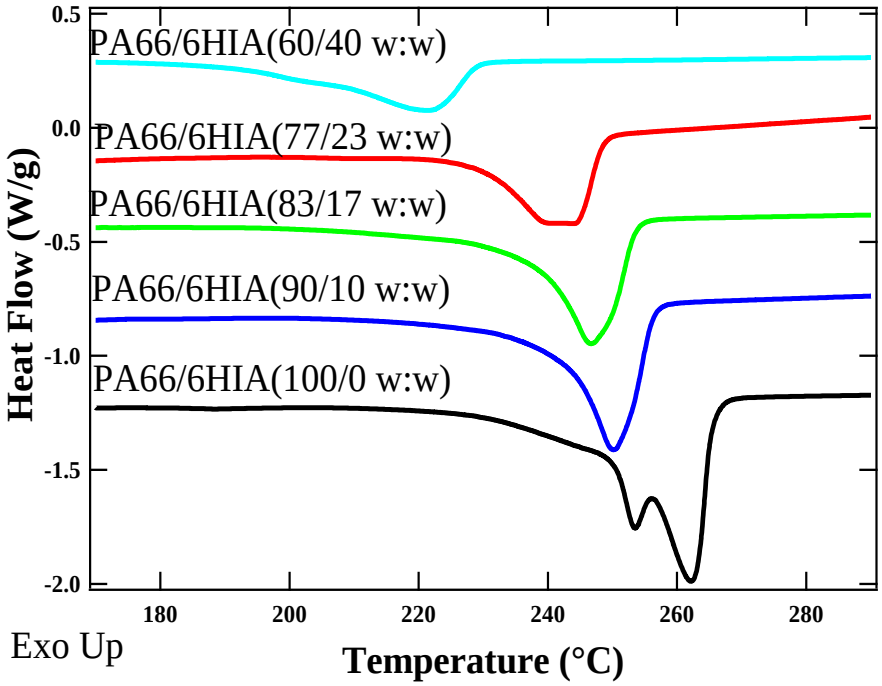

Figure 101 : Second DSC heating scans at 10 °C/min for PA66/6HIA blends extruded during 180 s at 310°C.

Figure 101 shows then the melting thermograms obtained after cooling from the melt at 10°C/min. As previously detailed in section (II.1.2.2), PA66 exhibits two melting peaks at 253 °C (Tm_1) and 262 °C (Tm_2) related to PA 66 crystals thickening upon heating.

In the case of copolyamides, an increase of the melting enthalpy of Tm_1 accompanied by a disappearance of the endotherm associated to Tm_2 is observed as PA6HIA concentration increases. Indeed, PA66/PA6HIA copolyamides reveal a single broad melting endotherm around 250°C for the compositions until 23% wt of HIA. This can be understood in terms of the structure of the block copolymers that are likely to be formed. The addition of non-crystallisable PA6HIA segment results in the formation of imperfect and/or thinner crystals which melt at low temperature. The disappearance of the second melting peak may be a result of poorer recrystallization ability of the imperfect crystals during the melting process. It is worth noticing that double melting peaks of PA66/6HIA (90/10 w:w) extruded at 290°C (see Figure 84) are merged into one single peak when the extrusion is carried out at 310°C(Figure 101). This is probably because of the lower chain mobility in the melt of the resulting copolyamides having higher molecular weight and more incorporated HIA groups.

Table 8 summarizes the thermal characteristics obtained by DSC (T_m, T_c, ΔH_c, ΔH_m and X_c), of extruded PA66/6HIA copolymers. As mentioned previously, the as-extruded PA66/PA6HIA (60/40 w:w) appeared to be roughly amorphous (Xc_{PA66}~5 %). But in the case

of PA6HIA content below 25 %, the melting enthalpy per unit of weight of PA66 and subsequently the crystalline fraction of PA66 are almost constant despite a pronounced slowing of the crystallization kinetics. These results appear to be in accordance with the block microstructure evidenced by ^{13}C NMR analysis which suggests a low transamidation reactions rate. It should be noticed that, because of the amorphous character of PA6HIA, the overall crystalline fraction of the PA66/6HIA copolyamides, determined as detailed in chapter II, is significantly reduced when the PA6HIA content increases.

Homopolymer and copolyamides	Melt blending time (s)	T_C (°C)	ΔHc (J/g)	T_m (°C)	ΔHm (J/g)	$Xc_{[sample]}$ (%)	$Xc_{[PA66]}$ (%)
PA66/6HIA (100/0 w:w)	-	233.5	60.35	263	64.5	33	33
PA66/6HIA (90/10 w:w)	180	220.4	45.4	258	58.3	29.6	33
PA66/6HIA (83/17 w:w)	180	216.2	42.9	255	55.1	28.6	33.8
PA66/6HIA (77/23 w:w)	180	206	35.7	250	50	25.5	33.2
PA66/PA6HIA (60/40 w:w)	180	155	18.2	232	7.1	3.6	6

Table 8: Thermal Characteristics of extruded PA66/6HIA blends at 310 °C obtained by DSC

2.4. Crystalline structure

The effect of copolyamide composition on the crystalline structure was studied at different observation scales (from the crystalline lattice to the spherulite), by using Wide Angle X-Ray Diffraction (WAXD), Transmission Electron Microscopy (TEM) and cross-Polarized Optical Microscopy (POM).

2.4.1. Crystalline perfection

WAXD measurements were conducted in order to characterize the crystalline structure of PA66/6HIA copolyamide at the scale of the crystalline lattice of PA66. Figure 102 shows WAXD patterns of copolyamides containing various amounts of PA6HIA in comparison with the initial homopolyamides PA66 and PA6HIA.

The three distinct peaks observed for polyamide 66 at 2θ of 13.7°, 20.4° and 23.7°, are consistent with the diffraction of the (002), (100) and (010,110) planes of the triclinic α form [72,304]. Changes in the crystal structure were examined through the comparison of the peaks of the (100) plane and the (010,110) plane of the α-form, which are the strongest reflections.

It can be deduced that the crystalline peaks intensity decreases with increasing PA6HIA content. This drop is supposed to be related to the reduction of the global crystalline fraction of PA66/6HIA copolyamides. On the other hand, until 17 % wt of PA6HIA in the blend, the (100) and (010)/(110) peak position as well as their relative magnitude appear to be constant, meaning that the crystalline phase is most likely unchanged.

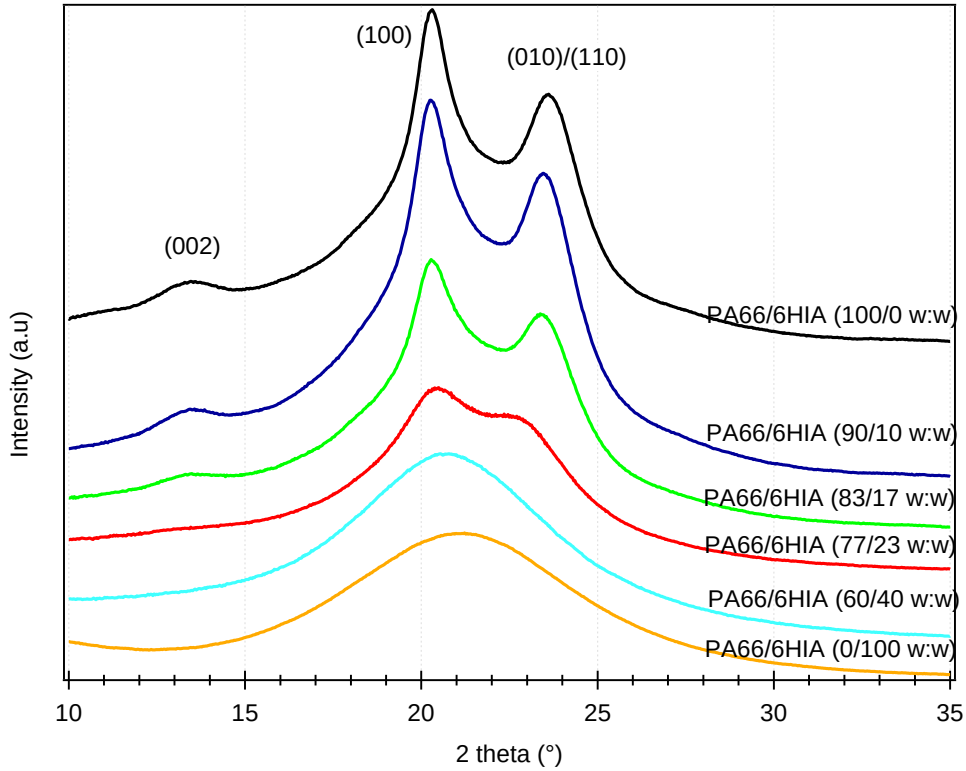

Figure 102:Wide-Angle X-ray Diffraction patterns on PA66/6HIA copolyamides extruded during 180 s at 310°C

For the PA66/6HIA (77/23 w:w), a significant variation of the peak position, peak width and relative peak intensities were observed, indicating a change in the crystalline lattice structure as well as in the crystallite size (also called crystalline size perfection in the case of PA66). In the case of the copolyamide containing 40% wt of PA6HIA, a broad amorphous halo is observed, which is in accordance with the amorphous nature of this composition evidenced by DSC. It should be noted that the amorphous homopolyamide PA6HIA exhibits a much broader amorphous halo centered around 21.3°.

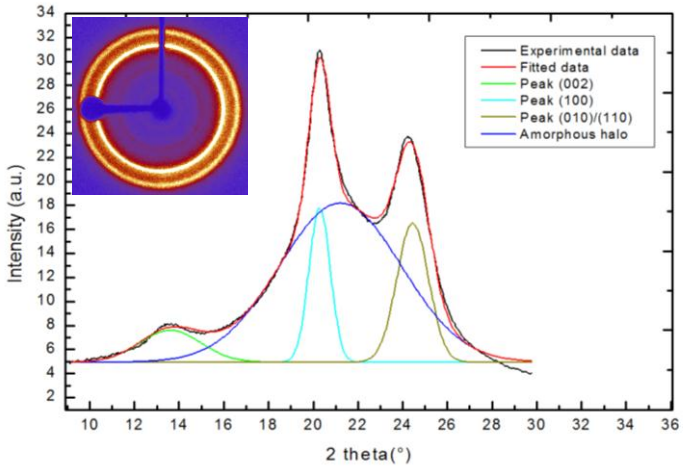

Figure 103: Graphical results of peak fitting analysis for polyamide 66

In order to determine the crystallite size, multiple peak fits were implemented using IgorPro software. WAXD patterns are decomposed into four peaks: three sharp peaks associated to

the (002), (100) and (010,110) planes of the triclinic α form, and one broad peak associated to the amorphous halo as shown in Figure 103. The peak locations in 2θ were roughly held constant (identified at highest intensities), while the peak heights and widths were allowed to vary. The 2θ locations of (100) plane and (010,110) plane of PA66 were identified by peak intensities occurring at approximately 2θ =20.3° and 23.7° respectively [90,305]. The amorphous peak location was generally around 2θ =21.3° [72,306].

The crystallite size perpendicular to the (hkl) diffraction plane was calculated according to the Scherrer's equation [307]:

$$L = \frac{K\lambda}{B\cos\theta}$$

where K is the Scherrer factor which is ~0.9, λ is the X-ray wavelength (=0.154nm), B, in radians, is the full width at half maximum of the diffraction peak and 2θ is the Bragg angle.

Polymer	(100) plane			(010,110) plane		
	2θ (°)	B (°)	L (nm)	2θ (°)	B (°)	L (nm)
PA66/6HIA (100/0 w:w)	20.29	1.03	7.83	23.74	1.42	5.72
PA66/6HIA(90/10 w:w)	20.25	1.09	7.41	23.6	1.41	5.75
PA66/6HIA(83/17 w:w)	20.26	1.13	7.15	23.56	1.44	5.63
PA66/6HIA(77/23 w:w)	20.37	2.11	3.83	22.87	2.1	3.88

Table 9: Peak data and crystallite size of PA66/6HIA copolymers extruded during 180 s at 310°C

Peak data and the corresponding crystallite sizes are listed in Table 9. It appears that the interplanar spacing and the crystallite sizes L associated to the (100) and (010)/(110) planes of copolyamides remain approximately constant with addition of PA6HIA until 17 wt %. This suggests that the crystalline lattice as well as the crystallite size is unaffected in all the crystallographic directions. For the PA66/6HIA (77/23 w:w), the (010,110) peak position is shifted tower lower degree, indicating that the inter H-bonds-sheets spacing is increased while the H-bonds length is slightly reduced ((100) peak is shifted towards higher degree).

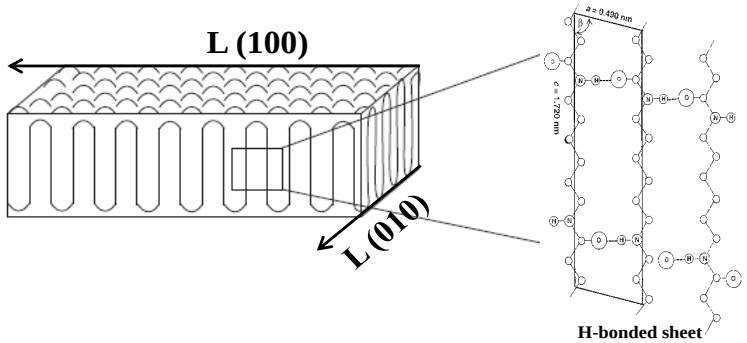

Figure 104:3-D schematic representation of the PA66 crystallite

Since the diffraction comes exclusively from PA66 segments on the basis of the non-crystallization of PA6HIA in the copolyamide, this change could be attributed either to the reduction of the crystallisable block length of polyamide 6.6, evidenced by NMR, or to the restriction of PA66 chains stacking into crystals. It is believed that it is more difficult for the crystallisable PA66 segments to enter the crystal phase with a totally stretched conformation

and they have to adopt a distorted conformation to get into the crystallites, which leads to the formation of imperfect triclinic structure at high PA6HIA content.

It can be also seen that the width of the (100) and (010,110) peaks are dramatically increased, reflecting the occurrence of poor crystalline size perfection. Indeed, the crystallite size is reduced by 50 % in the H-bond direction (crystallographic direction perpendicularly to the (100) plane) and by more than 30 % in the crystallographic direction perpendicularly to the (010) plane (H-bonded sheet) as depicted in Figure 104. This size reduction of the PA66 crystallites of the copolyamide PA66/6HIA (77/23 w:w) could partly explain the depression of its melting temperature as compared to that of the initial PA66 (13°C lower).

2.4.2. Lamellar morphology

Since the electron density of the crystalline phase differs significantly from that of the amorphous phase, Transmission Electron Microscopy (TEM) appears to be a suitable technique to get information on the microscopic packing of the crystalline and the amorphous phases of semi-crystalline polymers.

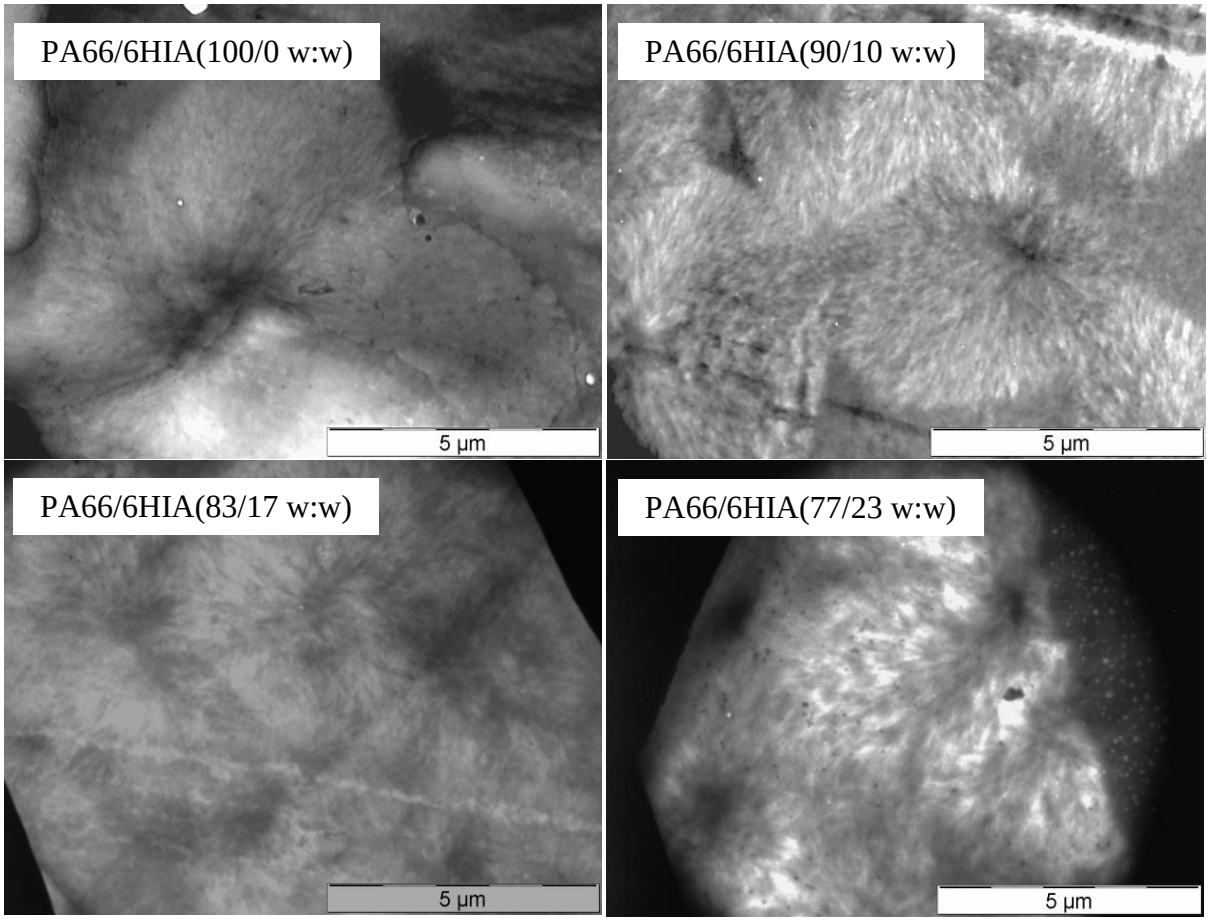

Figure 105: Transmission electron micrographs of PA66/6HIA blends extruded during 180 s at 310°C, showing detailed spherulitic structure.

TEM micrographs presented in Figure 105 show that polyamide 66 chains crystallize into lamellae (white zones) that are surrounded by amorphous interlamellar regions (dark zones that were stained by $H_3PW_{12}O_{40}$). It can be observed also that the lamellae irradiate from a

dark point in all the directions, indicating the formation of an homogeneous spherulitic structure. The morphology observed in the case of the copolymers PA66/6HIA is similar to that observed for PA66. The observation of a lamellar morphology regardless of blend composition confirms that the length of PA66 block in the copolyamides is sufficient to allow crystallization upon cooling from melt.

Unfortunately, the resolution of TEM is not good enough to measure the crystalline lamellae thickness of the examined samples. As a consequence it is difficult to establish a conclusion on the effect of PA6HIA incorporation on the lamellar packing of the obtained copolyamide, and further investigation by Small Angle X–Ray Scattering is needed. Because of the lack of time allowed to SAXS experiments at the "LIONS" laboratory, SAXS characterizations have been done only on injection molded samples. The obtained results will be discussed in the next chapter.

2.4.3. Spherulitic structure

Cross-polarized optical microscopy characterizations were performed on the pellets of the PA66/6HIA copolyamides obtained from the micro-compounder (0-23% of PA6HIA). Figure 106 shows that all copolyamides crystallize in spherulite structure recognizable with Maltese cross pattern. No interspherulitic separated phase of PA6HIA was observed, which is in accordance with the single Tg temperature observed on DSC analysis for the studied range compositions (from 0 to 23%).

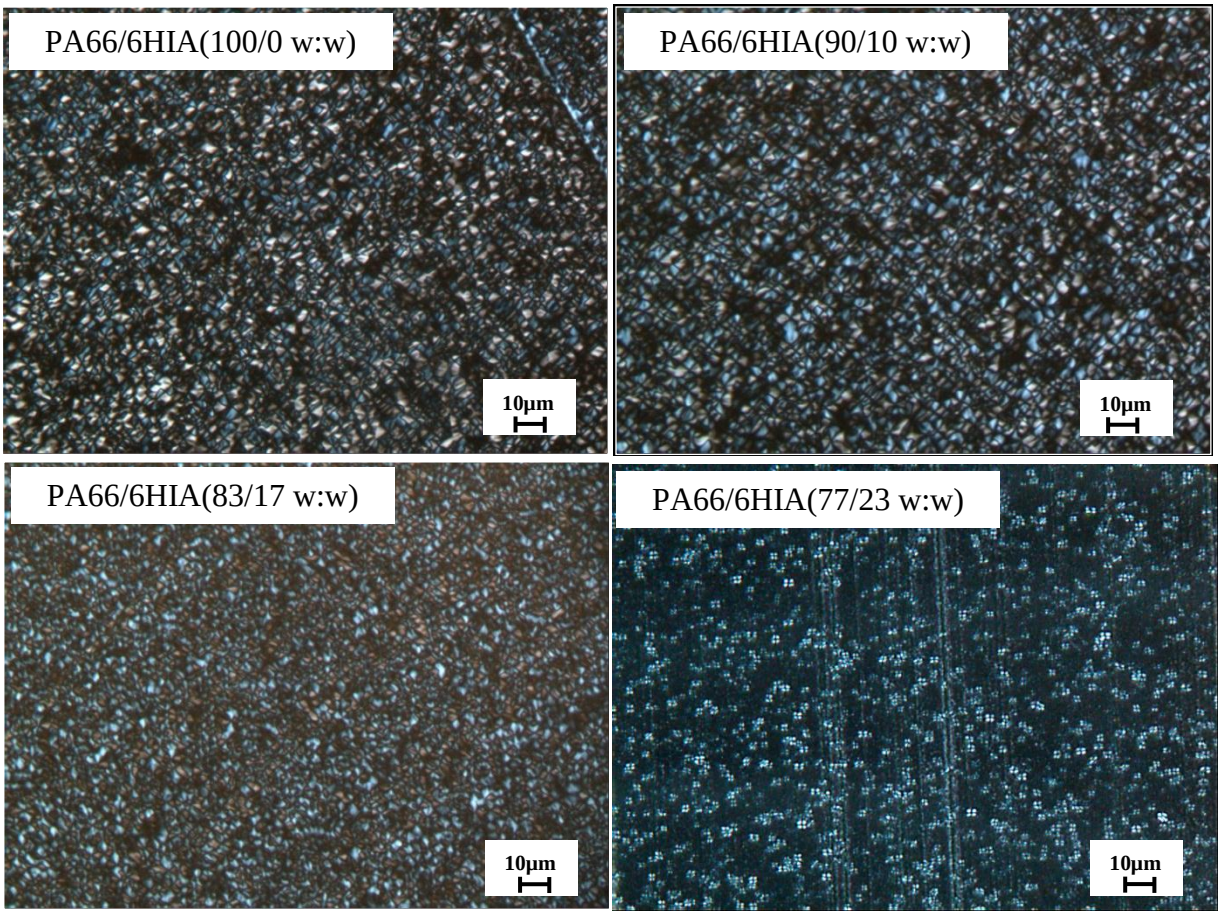

Figure 106: Cross-polarized optical micrographs of PA66 and PA66/6HIA copolyamides

For all the samples, the spherulite structure appears to be homogenous and the diameter of the spherulite was found to be approximately 5-10 µm in the case of the PA66 homopolymer. A slight refinement of the spherulite is observed for PA66/6HIA copolyamides, the spherulite size decreasing to about 3-5 µm in presence of 23% wt PA6HIA. DSC experiments previously showed that the crystallization temperature was reduced when PA6HIA content increased. This could have suggested a lower number of crystals nuclei, and on the basis of this interpretation, larger spherulites should have been expected. The exact reason of spherulite refinement in presence of PA6HIA could be related to a low growing rate of spherulites. As mentioned previously, the incorporation of rigid semi-aromatic segments in the backbone of PA66/6HIA decreases the chain mobility of the copolymer, and this could lead to lower the spherulite growing rate at high supercooling rate from the melt, resulting in the formation of smaller spherulites.

2.5. Conclusion on the effect of PA6HIA content on the structure of PA66/6HIA copolyamides prepared by microcompounding

PA66/PA6HIA copolyamides containing between 0 and 40%wt of 6HIA comonomer have been prepared by reactive blending.

The PA66/PA6HIA (60/40 w:w) blend turned out to be amorphous, as evidenced by the broad halo on WAXS patterns as well as the presence of a cold crystallization peak on DSC thermograms. In addition, two glass transition temperatures were observed, indicating phase segregation in the amorphous phase.

The PA66/6HIA containing between 10 and 23% of PA6HIA turned out to be semi-crystalline, the overall crystalline ratio decreasing as PA6HIA content increased, which is expected because of the amorphous character of PA6HIA. However, the crystalline fraction of the PA66 fraction did not vary with the addition of PA6HIA, suggesting that the presence of PA6HIA comonomer do not significantly hinder PA66 crystallization (a decrease of the crystallization temperature is nevertheless observed, possibly due to both the reduction of PA66 block length as well as the reduced chains mobility associated to high molecular weight and aromatic moieties). For these compositions, the glass transition temperature of the copolyamides increased as PA6HIA content increased, this being due to both the increasing content of semi aromatic segments in the copolyamide backbone and the increasing number of strong amide-phenol intermolecular interactions. Moreover, the molecular weight distribution of the copolyamides was found to be dependent on the stoichiometric ratio of the initial end groups, which governs the ability of the reactive components to form diblocks or triblocks copolymers as well as the length of the PA66 crystallizable sequences. NMR experiments showed that PA66 block length decreases as PA6HIA content increases. However, up to 23% wt of PA6HIA, the transamidation reaction does not seem to be preponderant, and the block length of polyamide 66 is still relatively long (16 units for 23% of PA6HIA according to NMR experiments).

At the end the copolyamides containing 10 and 17% of PA6HIA exhibit a crystalline structure (crystalline lattice, lamellar and spherulitic structure) close to that of PA66, whereas the copolyamide that contains 23% of PA6HIA exhibits a crystalline structure that seems to

be less perfect at the lattice scale, according to WAXS experiments. Table 10 summarizes the main structural and physical properties of PA66/6HIA copolyamides prepared at the laboratory scale in the micro-compounder.

Homopolymer and copolymers	T_g (°C)	T_C (°C)	T_m (°C)	$Xc_{[PA66]}$ (%)	$\bar{L}_{PA66}$	Mw (g/mol)	Cristallite size (nm)
PA66/6HIA (100/0 w:w)	64	233	263	33	64	35000	7.8
PA66/6HIA (90/10 w:w)	77	220	258	33	46	67200	7.4
PA66/6HIA (83/17 w:w)	87	216	255	33.8	27	57000	7.2
PA66/6HIA (77/23 w:w)	95	206	250	33.2	16	58800	3.9
PA66/6HIA (60/40 w:w)	92 and 137	155	232	6	-	-	-

Table 10: Structural and physical characteristics of reactive –extruded PA66/6HIA copolyamides

Part II: Preparation at large scale

The aim of the first part of this chapter was to find the best experimental conditions for preparing block copolyamide with PA66 segments long enough to crystallize into the lamellae structure which is a feature of semi-crystalline polymers. These conditions, established at small scale (micro compounder scale), consist in the blending of ultra-dried (moisture content <400ppm) low molecular weight PA6HIA terminated by carboxyl groups with amine terminated PA66 in the presence of 100 ppm of sodium hypophosphite at 310 °C during at least 180s. In the following, these optimized processing conditions are used to prepare PA66/6HIA block copolyamides using a twin-screw extruder at the pilot scale.

1. Preparation of PA66/6HIA block copolyamide using Leistritz twin screw extruder

In this part, copolyamides preparation was done by reactive extrusion of PA66/PA6HIA blends containing 10, 17 or 23%wt of PA6HIA and 100 ppm of sodium hypophosphite, using a D34 twin screw extruder. The chosen screw profile contained several mixing and reverse elements and the throughput was set to the minimum (8 kg/h) in order to increase the extrusion time. The screw speed was fixed at a standard value of 200 rpm as it should have no effect on the exchange reactions in the case miscible blends as reported by Eersels et al.,[67]. In these conditions, the measured temperature in the molten state was around 308 °C and the extrusion time was approximatively 100s. As this value is about two times lower than the value of 180s set in the microcompounder, it was decided to perform a second extrusion on the extruded copolyamides pellets. In the following, the structure of the copolyamides after the first and the second extrusion are both presented.

1.1. Co-polycondensation progress

The polycondensation reaction between the reactive functions of PA66 and PA6HIA results in an increase of the polymer chains length and subsequently of the melt viscosity. Contrary to the microcompounder, it was not possible to measure the force related to the viscosity that allows to follow the in-situ reaction between the components. Therefore, the polycondensation degree was deduced after extrusion from the molecular masses measurement by gel permeation chromatography.

Figure 107 presents the chromatograms after the first extrusion of PA66/PA6HIA compositions taken at two wavelengths (254 nm and 310 m). Remember that at 254nm, both the PA66 and PA6HIA are detected whereas at 310 nm only the PA6HIA is detected. For all the compositions, the chromatograms taken at the two wavelengths are not superpimposed: the chromatogram taken at 310 nm is shifted to longer retention time indicating the presence of PA6HIA that did not react with PA66.

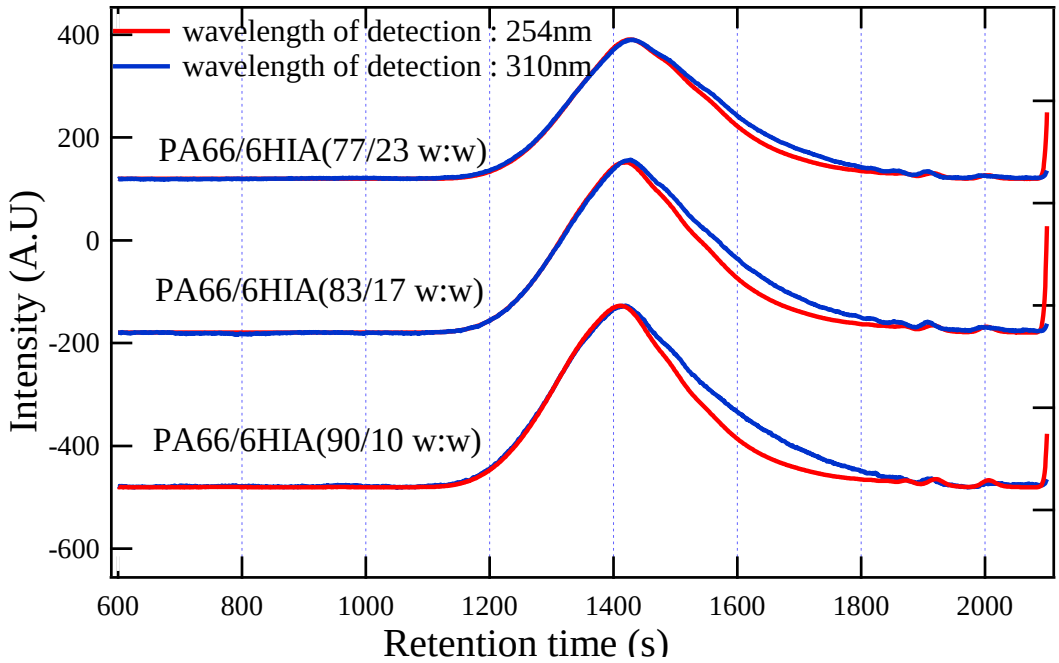

Figure 107: GPC chromatograms of extruded PA66/PA6HIA detected at 254 nm and 310 nm after the first extrusion

The detection of the homopolyamide PA6HIA means that the extrusion time (100 s) was not long enough to convert all PA6HIA into PA66/6HIA copolyamide. In contrast with the microcompounder for which it is possible to reach long residence time thanks to the re-circulation channel, it is not possible to reach extrusion time higher than 100s on the Leistritz extruder. Consequently, we decided to process a second time the extrudates in order to complete the copolymerization reaction. Before the second extrusion, the extrudates were dried under primary vacuum during 12 hours in order to limit the exchange reactions during the second extrusion and to promote the polycondensation reaction.

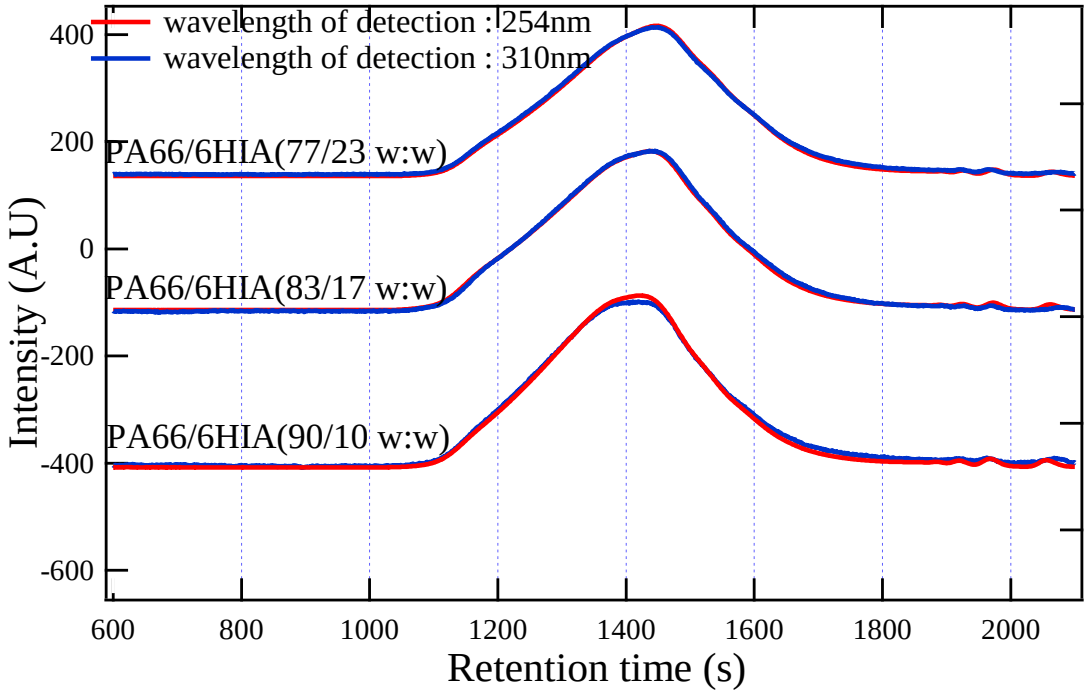

Figure 108: GPC chromatograms of extruded PA66/PA6HIA detected at 254 nm and 310 nm after the second extrusion

The GPC analysis of compositions extruded a second time is given in Figure 108. In comparison with the chromatograms obtained after the first extrusion (see Figure 107), the chromatograms after the second extrusion appear to be shifted to lower retention time, likely as a result of additionally polycondensation reactions between PA66 and PA6HIA. Furthermore, it can be noted that chromatograms taken at 254nm and 310 nm are superimposed, indicating that PA66 and PA6HIA are included in the same polymer chain for the overall mass distribution. Accordingly, it was assumed that after the second extrusion (100s + 100s = 200s residence time), the extruded PA66/PA6HIA blends are fully converted to PA66/6HIA copolyamides having high molecular weight.

In Figure 109, we plot the distribution of the absolute molecular weight determined for PA66/6HIA copolyamides after the second extrusion in comparison with the initial homopolyamide 66. It clearly appears that PA66/HIA copolyamides chains have higher molecular mass than the initial homopolyamide 66. This proves once more that PA66/6HIA copolyamides consist in a multi block structure likely obtained by melt post-condensation.

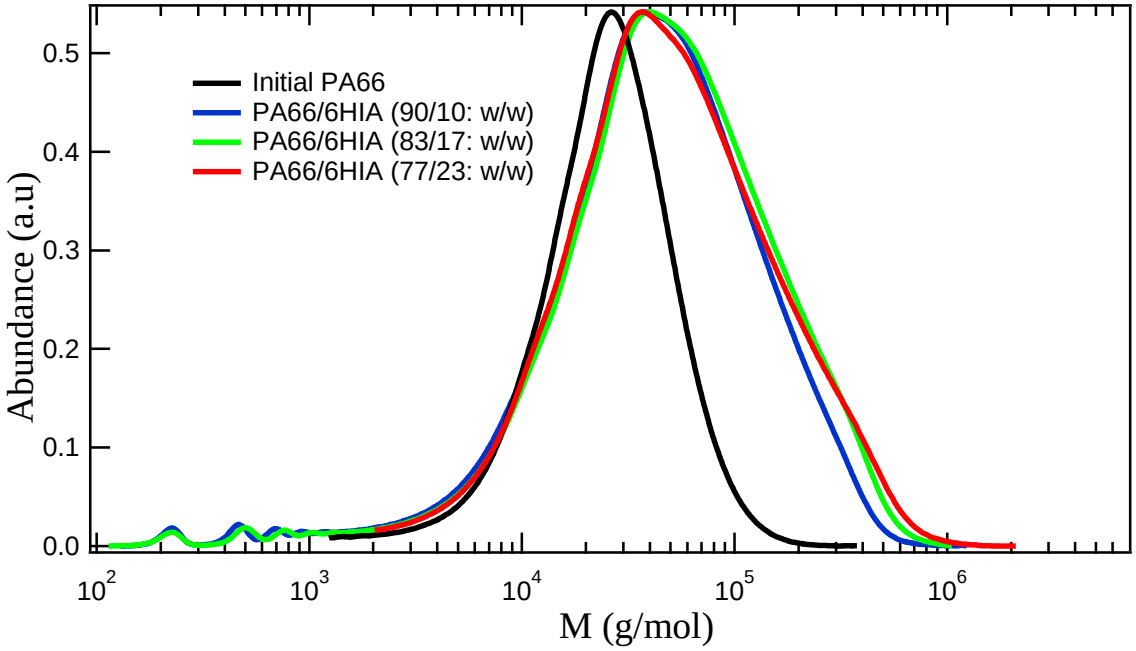

Figure 109: Molecular weight distribution of PA66/6HIA copolyamides after second extrusion

The data obtained by GPC are summarized in Table 11, the data of the 90/10 and the 77/23 compositions prepared with the microcompounder being also included in the table for the comparison. Contrary to the samples processed with the microcompounder, the copolyamide processed with the Leistritz extruder with 10% wt of PA6HIA content has a molecular mass lower than that of the copolyamide containing 23% wt of PA6HIA. This molecular mass difference could be due to the fact that the copolyamide preparation at large scale (Leistritz extrusion) is made of two extrusion steps with an intermediate drying phase while it was continuous (one step) at the laboratory scale (microcompounding). Consequently, the ends functions concentration, the degradation reactions (hydrolyze, decarboxylation...) and the exchange reactions extent could be changed. In other words, the stoichiometry at the beginning of the second extrusion is probably different from that after 100s in the microcompounder. This may alter the polycondensation statistics leading to the formation of copolyamides that have molecular chains distribution entirely different from that obtained by a one-step extrusion.

Copolyamides m-PA66/6HIA	Mn (g/mol)	Mw (g/mol)	Mz (g/mol)	Dispersity (Mw/Mn)
(90/10 w:w) Leistritz	12000	67800	154600	5.7
(90/10 w:w) Microcompounder	14800	67200	126300	4.5
(83/17 w:w) Leistritz	13400	76800	182700	5.7
(100/0 w:w) Microcompounder	15900	57000	107000	3.6
(77/23 w:w) Leistritz	12800	72100	196000	5.6
(77/23 w:w) Microcompounder	16800	58800	119000	3.5
(100/0 w:w) Leistritz	11000	31100	44200	2.8
(100/0 w:w) Microcompounder	10500	35000	44500	3.3

Table 11: GPC data of the PA66/6HIA copolyamides prepared with the Leistritz extruder (200s, 308°C) or with the microcompounder (180s, 310°C)

1.2. Thermal characterizations

DSC experiments were conducted on the samples extruded one or twice in order to determine the crystalline fraction, and the melting and crystallization behaviours.

The crystalline fraction of PA66 as a function of the copolyamide composition is presented in Figure 110. The crystalline fraction in the case of blends of PA66 and PA6HIA (first extrusion) and in the case of copolyamides (second extrusion) are close and not very different from the crystalline fraction measured for neat PA66. This confirms that the progressive integration of PA6HIA in the copolymer does not alter the final crystalline fraction of PA66 segments.

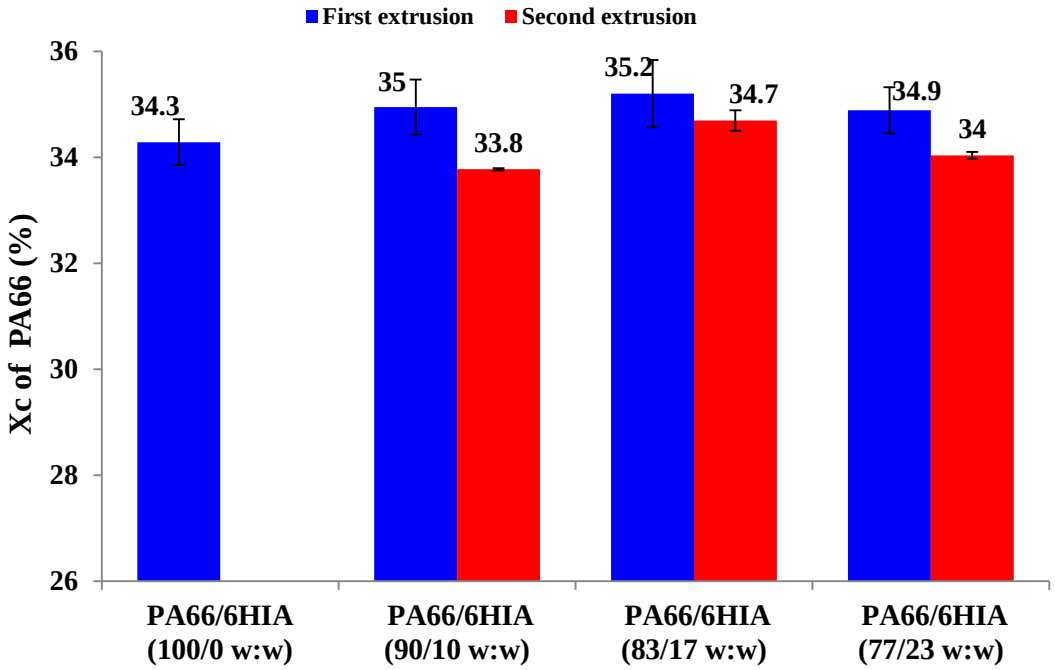

Figure 110: Crystallinity fraction of PA66 as a function of the copolyamide composition

The evolution of the melting temperature with the PA6HIA content for the different preparation setups is then given in Figure 111. As stated in the first part, the melting temperature of PA66/6HIA copolyamides decreases with increasing PA6HIA content and increasing the extrusion time (100s for first extrusion, 200s after second extrusion). It should be pointed out that the melting temperature after the second extrusion is roughly equal to that measured in the case of copolyamides prepared by micro compounding (310°C, 180s), suggesting the formation of similar crystalline structures.

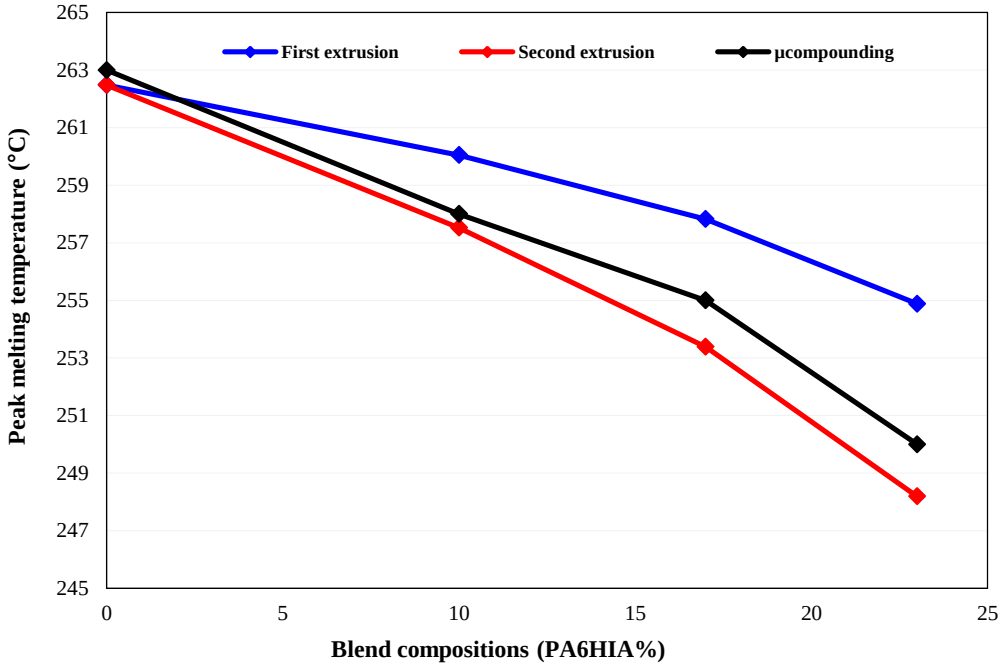

Figure 111: Variation of the melting temperature of P66/6HIA copolyamides with PA6HIA content for different preparation setups

Similarly, the variation of the crystallization temperature with PA6HIA content for the different processing conditions is presented in Figure 112. The same conclusions can be drawn except for the composition with 10% of PA6HIA for which the crystallization temperature is unchanged after the second extrusion and remains above that observed for copolyamide prepared by micro compounding. The lower crystallization temperature after the second extrusion could originate from the disappearance of oligomeric chains (chain mobility reduction) or from the production of shorter crystallisable segments of PA66 (Additional exchanges reactions). The same arguments can be used to explain the drop of the crystallization temperature with PA6HIA comonomer content. In the case of PA66/6HIA (90/10 w:w), the comparison of GPC chromatograms in Figure 107 and Figure 108 suggests that the chains average molecular mass after the first extrusion is not significantly different from that after the second extrusion, which is consistent with the non-variation of the crystallization temperature observed by DSC.

The evolution of glass transition temperature with PA6HIA content is then shown in Figure 113 for extruded and micro compounded compositions. As described in the first part, the glass transition temperature increases with increasing PA6HIA content likely as a consequence of the addition of rigid phenolic moieties which are able to establish strong interchains H-bonds.

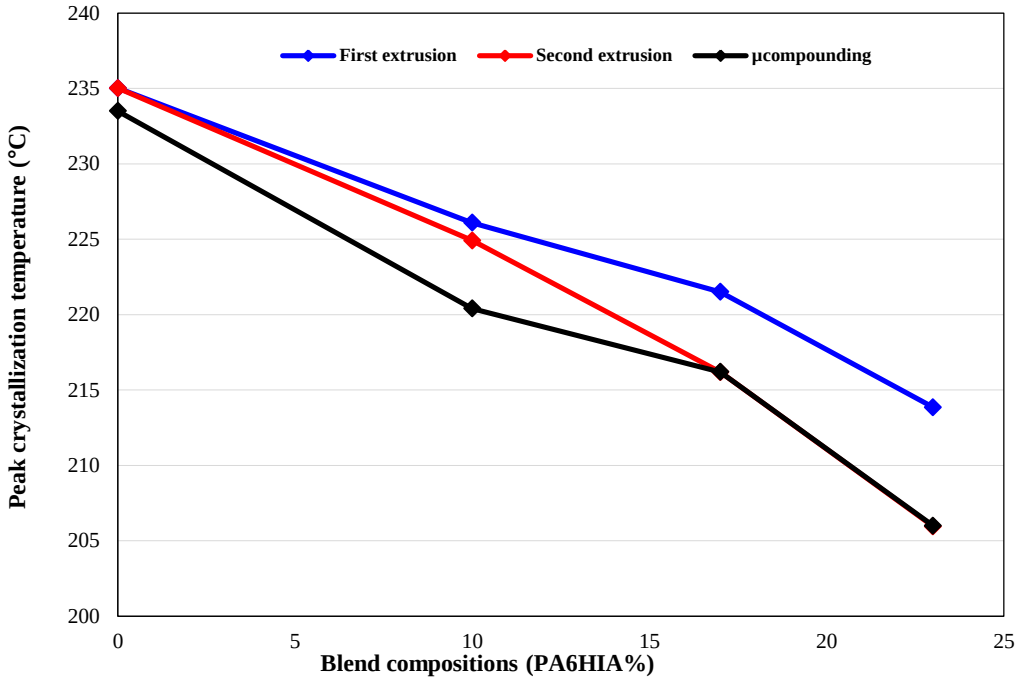

Figure 112: Variation of the crystallization temperature of P66/6HIA copolyamides with PA6HIA content for different preparation setups

It should be noted that the Tg of the extrudates after the first extrusion (partial conversion of PA6HIA into the copolyamide) appear to be slightly higher than that after the second extrusion (full conversion of PA6HIA into the copolyamide). Furthermore, the Tg of copolyamides decreases when their weight average molecular mass increases (77/23 extruded copolyamide exhibits higher molecular weight and lower Tg than that of the 77/23 microcompounded sample). This suggests that amorphous phase molecular dynamics seems to depend on the distribution of the phenolic moieties in the copolymer chains as well as on their chains molecular mass.

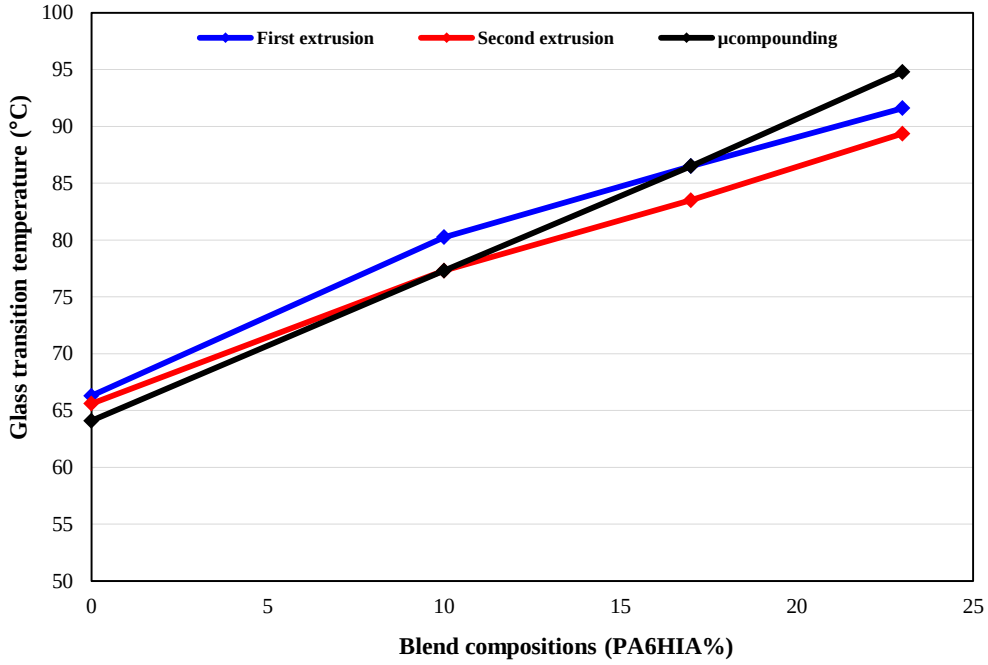

Figure 113: Variation of the glass transition temperature of P66/6HIA copolyamides with PA6HIA content for different preparation setups

Based on these results and assuming that exchanges reactions can be qualitatively highlighted by monitoring the changes in the thermal behavior, it is plausible to say that the copolyamide structure obtained after the second extrusion is quite similar to that of samples prepared at the laboratory scale in the micro-compounder.

1.3. **Summary of the copolyamide's preparation at large scale**

PA66/6HIA copolyamides have been prepared at large scale by reactive extrusion of amine terminated PA66 and carboxyl ended functions PA6HIA using a twin extruder Leistritz. Two-steps extrusion was needed to convert all PA6HIA homopolyamide into copolyamides which appears to be in accordance with the conditions established at the laboratory scale.

The molecular characterizations show once more that PA66/6HIA copolyamides have higher molecular mass than that of homopolyamide 66. We have seen also that the weight average molecular mass of copolyamides varies with PA6HIA content indicating the dependence of the post-condensation extent on the reactive end-groups concentration. The molecular weight of the samples prepared with the Leistritz extruder turned out to be different from that prepared with the microcompounder. This could originate from the fact that the copolyamide preparation at large scale is made of two extrusion steps lasting 100s with an intermediate drying phase, while it was continuous at the laboratory scale (180s). Because of this intermediate drying step, the stoichiometry at the beginning of the second extrusion is probably different from that after 100s in the microcompounder, and this could lead to a different molecular chains distribution.

DSC analysis show that glass transition temperature increases as the PA6HIA content increases while crystallization and melting temperature decrease. In contrast, the crystalline fraction of PA66 seems little affected by the addition of the amorphous PA6HIA. These observations are in good agreement with conclusions drawn from the copolyamides preparation at the laboratory scale, and suggest that it is possible to obtain multiblock semi-crystalline PA66/6HIA copolyamides with a two-steps extrusion on the Leistritz extruder. Concerning the two-steps aspect, as extruded compounds are generally processed a second time (injection molding, blow molding), it could be considered to extrude the copolymer only one time and to achieve the homopolymers conversion during the second processing step. But in the case of injection molding, as water cannot be extracted during processing, the post-condensation reaction could not further progress during the melt residence time associated to injection molding.

2. Mold processing of PA66 and PA66/6HIA copolyamides

In order to evaluate the physical and mechanical properties of prepared copolyamides, tensile and impact specimens were made by injection molding as detailed in chapter II, section.4.2.1. In addition of block PA66/6HIA prepared by reactive extrusion, a random PA66/6HIA copolyamide prepared by in-situ copolymerization was also injection-molded. **Standard PA66** and high molecular weight **HMw PA66** were injection-molded as references. In the following, PA66/6HIA copolyamides prepared by in-situ copolymerization will be designed by **i-PA66/6HIA** so as to differentiate them from copolyamides prepared by reactive extrusion called hereafter **m-PA66/6HIA**.

Rheological characterizations were performed prior the injection molding step on pellets of copolyamides as well as on pellets of standard PA 66 and HMw PA66 in order to find the suitable conditions for injection molding (temperature, moisture level, shear rate...).

2.1. Rheological characterizations

2.1.1. Viscosity stability scanning

As described in the first chapter, the polycondensation reaction is in equilibrium with the hydrolysis reaction. Accordingly, it is of great importance to carry out the rheological characterization at the water equilibrium content since polycondensation or hydrolysis can significantly alter the melt viscosity. Viscosity measurements were then performed during ten minutes at 280°C under a constant shear rate of 200 s^{-1} on samples dried at different levels.

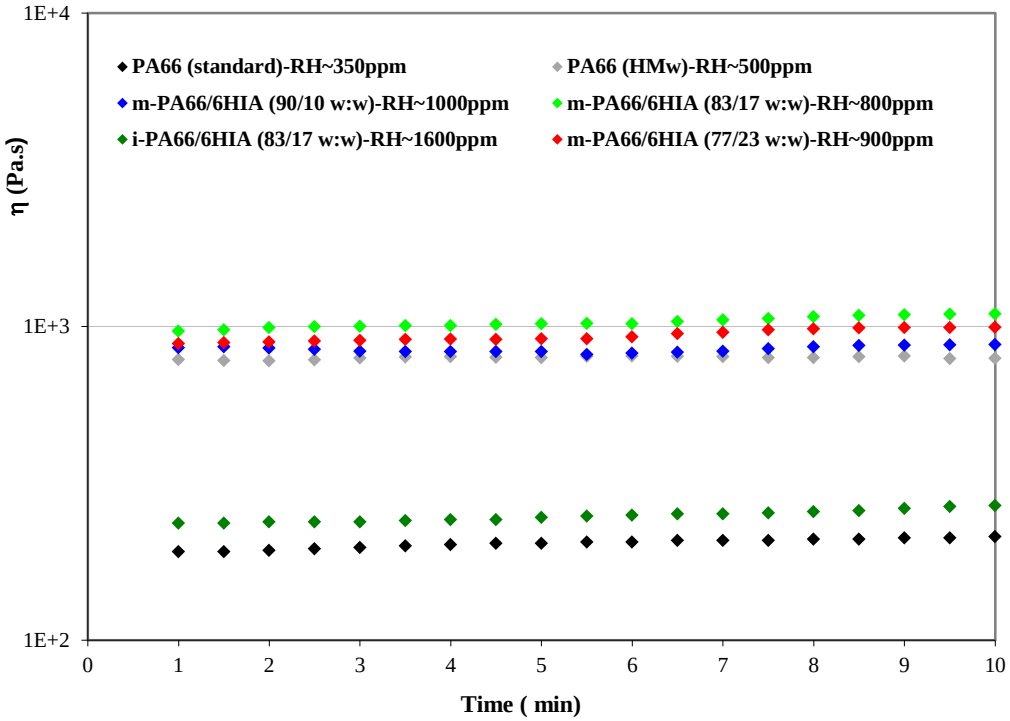

Figure 114: Viscosity stability of PA66 (of standard and HMw) and m-PA66/6HIA copolyamides under shear rate of 200s^{-1} at 280°C

Depending on the water concentration, the viscosity can either increase (polycondensation reaction) or decrease (Hydrolysis reaction). At the water equilibrium content, the chemical structure and the molecular weight of the polymer should not significantly change during the experiment, and this yields a constant viscosity. Figure 114 shows the evolution of the viscosity level in time for the studied materials carried at their respective water concentration corresponding to the equilibrium.

It can be seen that the moisture level corresponding to the equilibrium (constant viscosity) is relatively high in the case of m-PA66/66HIA copolyamides (close to 900ppm versus 350 ppm in the case of standard polyamide 66). This indicates that the ratio of reactive end-groups (amine and acid functions) of m-PA66/6HIA is closer to stoichiometric ratio than that of PA66.

In addition, the viscosity level of m-PA66/6HIA copolyamides turns out to be 150% higher than that of standard PA66 (900 Pa.s versus 350 Pa.s) whereas it is close to that of HMw PA66. The high m-PA66/6HIA's viscosity appears to be in good agreement with the previous GPC analysis showing high polycondensation degree in the case of the extruded m-PA66/6HIA copolyamides. On the other hand, i-PA66/6HIA copolyamide and standard PA66 exhibit similar viscosity levels while their moisture level corresponding to the equilibrium are very different (1600 ppm versus 350 ppm). This suggests that both materials have the comparable polycondensation degree but different reactive end-chains concentration.

2.1.2. Capillary rheometry tests

The evolution of the viscosity versus the shear rate for the PA66 (standard and HMw) and PA66/6HIA copolyamides is plotted in Figure 115. The apparent viscosity of these materials decreases as shear rate increases, showing a typical property of shear-thinning plastics.

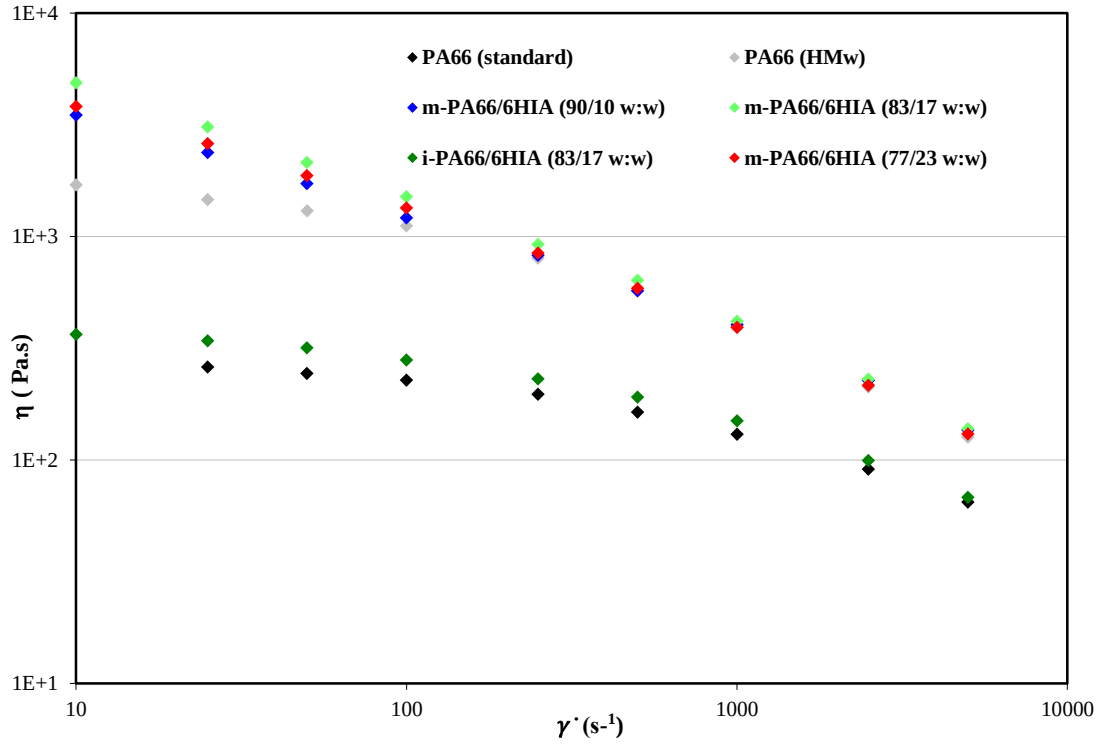

Figure 115: Viscosity of PA66 (standard and HMw) and m-PA66/6HIA copolyamides versus shear rate at 280°C

In the case of standard polyamide 66 and i-PA66/6HIA copolyamide, a Newtonian plateau (constant viscosity) is observed at low shear rate (<200 s^{-1}). After that, viscosity decreases with the shear rate indicating that the polymer chains become oriented in the flow direction. This viscosity drop, commonly known for linear polymers, corresponds to a pseudo-plastic fluid behaviour. By increasing the molecular weight of the polyamide66 (HMw), the apparent viscosity was increased by ~5 times and the same pseudo-plastic behavior was also observed.

Concerning m-PA66/6HIA copolyamides, no Newtonian plateau was identified in the overall tested shear rate range (from 10 to 5000 s^{-1}) and only pseudo plastic behavior is observed. Note that obtained rheological curve is typical of branched polymers. Moreover, the apparent viscosity at this shear rate range is globally higher than that of polyamide 66 having high molecular mass (HMw).

At high shear rate, the viscosity dependence of m-PA66/6HIA copolyamide on shear rate is basically similar to that of HMw polyamide. Moreover, the shear thinning (viscosity drop with the shear rate) is more pronounced, probably due to a particular structuration of copolyamide in the melt (chains configuration), leading to an apparent viscosity equal to that of HMw PA66 at 500 s^{-1}. Note that apparent viscosities of m-PA66/6HIA copolyamides and HMw PA66 at high shear rate (5000 s-1) are close to that of standard PA66. This suggests that these polymers are easily stretchable, under shearing, in the flow direction. A possible explanation for this result could be related to the broad molecular mass distribution (high dispersity) of m-PA66/6HIA copolyamides. In fact, small chains have lower resistance to flow and then facilitate chains alignment in the flow direction resulting in efficient shear thinning.

To summarize, m-PA66/6HIA copolyamides appear to be more viscous than i-PA66/6HIA and polyamide 66 (standard and HMw) at low shear rate which is very suitable for the blow molding operation (high viscosity at low shear rate), while their melt viscosity at high shear rate is close to that of standard polyamide which is very convenient for injection molding process (high shear rate).

2.2. **Injection molding**

In general, injection molding operation requires low viscosity in order to fill correctly the mold. Therefore, high shear rate is usually applied in the case of polyamide having a high viscosity. Based on the above rheological measurements, a power-type law fit of the viscosity evolution in the pseudoplastic behaviour domain ($\dot{\gamma}$ > 250 s^{-1}) was accomplished in order to estimate the shear rate corresponding to a melt viscosity close to 50 Pa.s.

It must be noted that during injection molding, the highest value of shear rate is reached when the polymer passes through the injection die. Assuming that the shear rate into the injection die follows the equation of a Newtonian fluid on the wall of a capillary, the estimated shear rate can be related to the polymer output as below:

$$\dot{\gamma} = \frac{4Q_v}{\pi\left(D/2\right)^3} \tag{44}$$

where Qv represents the volume throughput in cm^3 and D is the Die diameter =0.3cm.

Based on equation (44), volume throughputs corresponding to the requested shear rate were calculated and then the injection speed for each material was determined by using equation (45).

$$Q_v = \pi V (\frac{E}{2})^2 \quad (45)$$

where V is the injection speed in cm/s and E is the Extruder diameter= 3 cm

The injection molding conditions (injection speed and holding pressure) were determined for all PA66 and PA66/6HIA copolyamides. In general, the injection speed must be increased when the molecular weight increases and pronouncedly in the case of PA66/6HIA copolyamides.

Furthermore, the mold temperature was adjusted for each composition in order to properly take out the specimen from the mold. Generally speaking, the mold temperature was reduced at the PA6HIA content increases. This may be understood based on the low crystallization ability of block copolyamides containing high PA6HIA content. In the case of in-situ copolyamide (i-PA66/6HIA), the mold temperature was considerably reduced until 43°C, probably due to a slow crystallization of this copolymer. Details on the structure and physical properties of this copolyamide will be discussed in the next chapter.

2.3. **Summary of PA66/6HIA mold processing**

Experiments of viscosity stability at 280°C show that the moisture level corresponding to the equilibrium of PA66/66HIA is higher than that of PA66 (900ppm for versus 350 ppm).

Flow curves (apparent viscosity versus shear rate) evidence that, in the overall explored shear range, m-PA66/6HIA copolyamides experience pseudo-plastic behavior whereas PA66 (standard and HMw) exhibits Newtonian behavior at low strain rate. This divergence may be related to segment conformation and /or chain interaction in the melt.

Even if extruded copolyamides have higher polycondensation degree than standard polyamide 66, their melt viscosities at high shear rate are very close. Accordingly, the injection speed was adjusted for all copolyamide compositions in order to get proper injection molded specimens. Also the temperature mold was fine-tuned for each composition.

Conclusion

Copolyamide preparation by reactive blending of amine terminated Nylon66 (PA66) with carboxyl terminated Nylon6HIA (PA6HIA) at laboratory scale (micro compounder) was described. It was found that increasing the extrusion temperature and the residence time promotes the copolymerization reaction between the blends components. But it seems that an increase of the temperature appears to be more efficient to achieve a total conversion of the homopolyamides in the copolymer without disturbing the crystallinity, the increase of the extrusion time leading to a slight thinning of the crystalline lamellae. The addition of sodium hypophosphite as a catalyst turned out to enhance the polycondensation extent in shorter time, without favoring the transamidation reactions (no variation of melting temperature). Accordingly, we showed that it was **possible to produce block copolyamides by melt blending of reactive ends-groups polyamides at 310°C during at least 180 s in the presence of a soft catalyst such as sodium hypophosphite.**

The preparation of PA66/6HIA copolyamides was then studied over a wide range of compositions (0 to 40 % by weight of PA6HIA). It turned out that the homopolyamides can be **totally converted into copolymer up to 23% in weight of PA6HIA**, a phase separation suggested by the presence of two Tg's being observed for the 60/40 composition. Until at least 23% of PA6/HIA co-monomer, one Tg is observed and this Tg increases with PA6HIA content, due to the presence of both aromatic moieties and strong phenol-amide interactions. We showed then that the **molecular weight distribution** of the produced copolyamides is very **dependent of the stoichiometric ratio of the initial end groups and their reactivity**. Depending on this stoichiometric ratio, **different configurations of di-blocks or tri-blocks copolymers** are generated with different associated molecular weights. The length of the PA66 segment was determined with NMR, and even if it decreases with increasing PA6HIA content, it seems that the **length of the PA66 segment remains long enough** (16 units for the 77/23 composition) **to yield a crystalline fraction** by unit of weight of PA66 **close to that of the homopolyamide 66**. However, as semi-aromatic PA6HIA is amorphous, a decrease of the global crystallinity was observed. Concerning the crystalline morphology, it turned out that **up to 17% of PA6HIA**, the crystalline structure at the scale of the **crystalline lattice, the lamella or the spherulite is similar to that of the homoplyamide 66.** A modification at the lattice scale is observed for the copolymer with **23% of PA6HIA** (**decrease of the crystalline perfection** evidenced on WAXD patterns). The **crystallization temperature decreases as PA6HIA content increases**, probably due to the increase of the rigid aromatic moieties in the copolymer. But it should be noted that the composition containing 40% of PA6HIA turned out to be almost completely amorphous.

In the second part, three copolyamides compositions (10, 17 and 23% in weight of PA6HIA) were prepared at the **pilot scale** using a **Lestritz extruder with a screw profile tailored** for maximizing the extrusion time. But, as the final residence time could not exceed 100s, a second run in the extruder was necessary to achieve a **complete conversion** of the homopolyamides. This two steps process accompanied by an intermediate re-drying of the extrudates is at the origin of a **small difference in the molecular weight distribution** of the copolymers **in comparison** with that of samples prepared with **the microcompounder** at the same processing temperature during an equivalent total residence time. But the **crystalline morphology o**f the copolymers after the second extrusion appears to **be quite similar** to that of samples prepared at the laboratory scale, as suggested by the similarity of the melting temperatures. At the end, it seems that the **established processing** conditions at **laboratory**

scale are **suitable** for preparation of **block semi-crystalline copolyamides at large scale**. The resulting products exhibit a Tg that increases as PA6HIA content increases, confirming the increase of the cohesion of the amorphous phase that was aimed in the first chapter.

Finally, the **rheological behavior of PA66/6HIA** copolyamides was compared to that of polyamide 66. It was found that extruded copolyamides have **higher apparent viscosity,** likely due to their **higher molecular weight** and the presence of relatively **rigid segment in** their backbone. Moreover, a **pseudo plastic behavior** involving **pronounced shear thinning** was identified at **high shear rate.** Thus, as injection molding requires melt viscosity lower than 100 Pa.s, PA66/6HIA copolyamides were **injected at high injection speed** in order to get proper injection molded specimens.

To sum-up, we **successfully introduced** phenolic moieties that are assumed to offer **strong H-bond** interactions, into the polyamide 66 backbone by means of **a multi-block** structure. The resulting **block copolyamides** have **enough** flexible **segments** of polyamide 66 for yielding a **crystallization close** to that **of genuine polyamide 66.**

4

Impact of the microstructure on the physical and mechanical properties: PA66 versus PA66/6HIA copolyamides

Chapter IV: Impact of the microstructure on the physical and mechanical properties: PA66 versus PA66/6HIA copolyamides

The aim of the previous chapter was to find the appropriate experimental conditions to prepare PA66/6HIA block copolyamides with a well-defined crystalline structure (close to that of PA66). In this chapter, we desire to assess the benefit of associating amorphous PA6HIA, supposed to offer a high cohesive energy thanks to the phenolic functions, on the physical and mechanical properties of the resulting copolymers.

Six materials, presented in chapter III, were considered. They consist in three P66/6HIA copolyamides prepared by reactive extrusion: m-PA66/6HIA (90/10, 83/17 and 77/23 w:w), one copolyamide obtained by in-situ copolymerization i-PA66/6HIA (83/17 w:w) and finally two PA66 homopolyamides (Standard and HMw).

Firstly, the microstructure of the injection molded samples is characterized: The molecular weight distribution is investigated by GPC and the average sequences of PA66 and PA6HIA are determined by MALDI-TOF mass spectroscopy. Then, the thermal characteristics (melting, crystallization behaviour and glass transition) are studied. After that, the morphology and crystalline features of selected materials are described from the spherulite to the crystalline lattice scale.

In the second part, the quasi-static mechanical properties of these samples are presented at two temperatures. Then, the material response, at nanometric scale, upon stretching is investigated through in-situ tensile-SAXS experiments. After that, the impact strength properties of the prepared copolyamides are presented. Finally, the fatigue performance and damage mechanisms of these materials are described.

Part I: Structural and physical characterization

In the framework of this study, all mechanical tests were carried out on injection molded specimens. So, it is of great importance to characterize their microstructure in order to understand their ultimate properties.

It should be noted that theses injected specimens have a skin/core structure, likely resulting from quick solidification of the polymer in contact with the mold surface. It is assumed that the microstructure of the skin region (~100µm) is mainly dependent on the injection molding conditions (mold temperature, mold pressure, cooling rate…) while the core region is rather related to the intrinsic properties of the polymer (crystallinity, crystallization kinetics...). Accordingly, all structural characterizations were performed on the core region taken in the middle zone of tensile specimen as described in Figure 116.

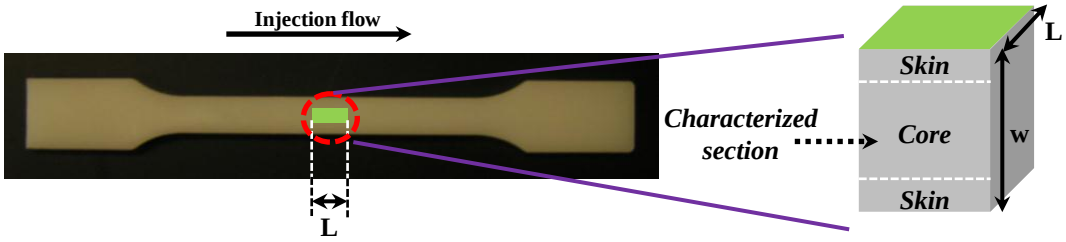

Figure 116: Characterization area of the tensile specimen

In the following, the structure of the injection molded specimen is characterized from the molecular scale up to the micrometric scale.

1. Molecular structure

1.1. Molecular mass distribution

A comparison of the absolute molecular mass distribution of injection molded samples and extruded pellets is given in Figure 117. It can be seen that both standard and HMw injection molded polyamide 66 have a Gaussian distribution of molecular mass chains. As expected the HMw polyamide prepared by solid state post condensation (SSP) exhibits higher molecular weight than standard polyamide 66. For the m-PA66/6HIA copolyamides, prepared by reactive extrusion, an important change in their molecular mass distribution (signal position and shape) is observed when compared with their initial mass distribution before injection. The distribution peak is slightly shifted towards higher molecular mass. Moreover, a shoulder peak is appearing at high molecular mass indicating the formation of second population of copolyamide chains with high molecular weight. These high molecular mass copolyamides probably result from the melt post-condensation between carboxylic and amine terminated copolyamides during the injection step, driven by the low water concentration. It should be kept in mind that water concentration before injection was in the range of 400 ppm for m-PA66/6HIA with 17% and 23 % by weight of co-monomer 6HIA versus 650 ppm in the case

of copolyamide with 10% of 6HIA. This may explain why the shoulder is more prominent for m-PA66/6HIA with high fraction of PA6HIA.

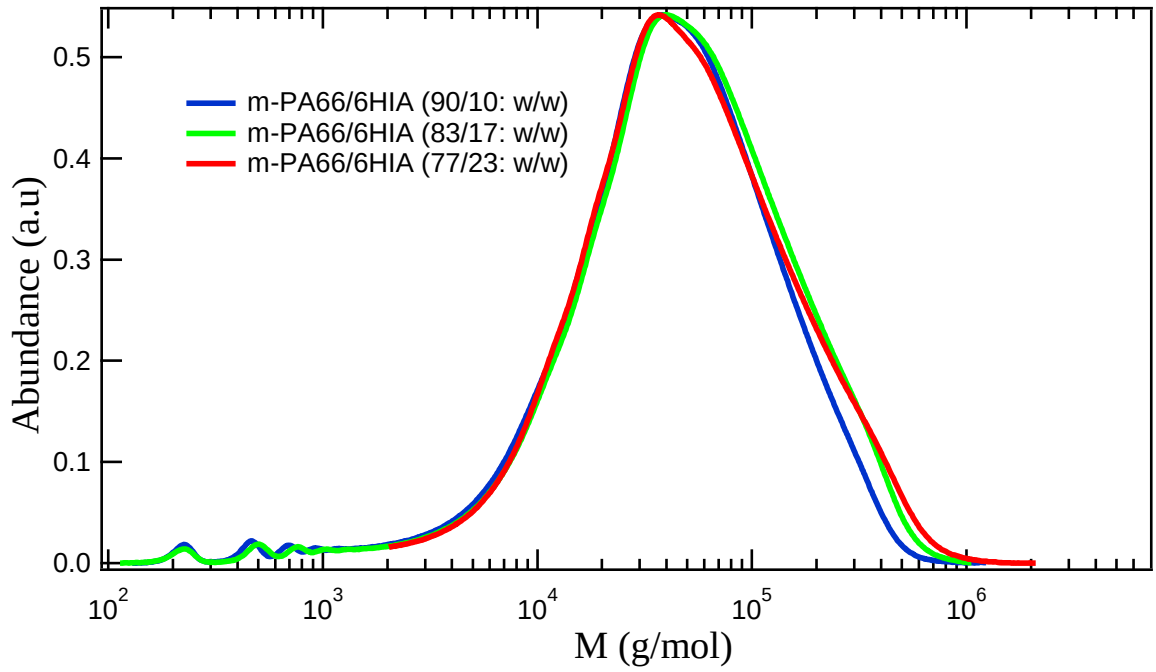

Molecular mass distribution of extruded pellets of PA66/6HIA copolyamides

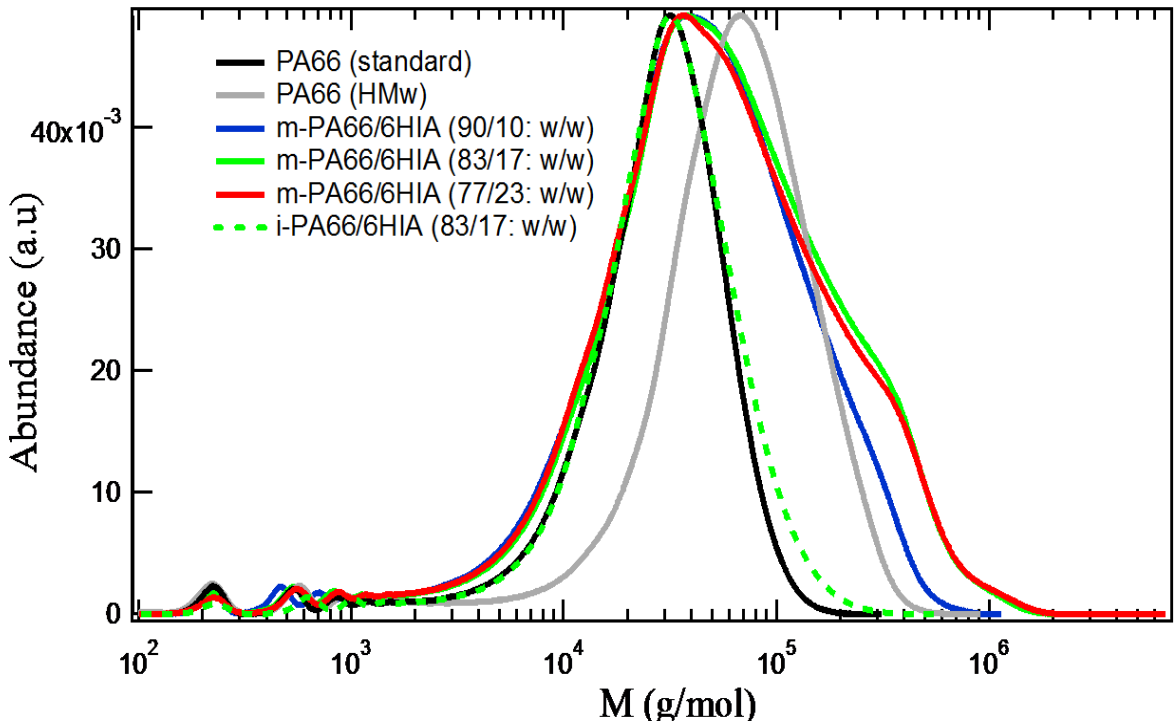

Figure 117: Molecular mass distribution of injection molded specimens of PA66 and PA66/6HIA copolyamides

Similarly to standard and HMw PA66, a Gaussian distribution is also observed in the case of PA66/6HIA copolyamide prepared by in-situ polymerization. Note that standard PA66 and i-PA66/6HIA have similar molecular mass distribution, while m-PA66/6HIA copolyamides

have some fraction of chains having molecular mass close to that of standard PA66 and an important fraction of high molecular mass chain (close to that of HMw).

Polymer sample	Mp (g/mol)	Mn (g/mol)	Mw (g/mol)	Mz (g/mol)	Dispersity
PA66 (standard)	35405	12083	**38189**	54074	3.1
PA66 (HMw)	67575	14706	**80704**	129027	5.4
m-PA66/6HIA (90/10 w:w)	38188	12659	**72459**	163101	5.7
m-PA66/6HIA (83/17 w:w)	37964	14711	**95885**	286412	6.5
i-PA66/6HIA (83/17 w:w)	31330	13465	**35107**	56949	2.6
m-PA66/6HIA (77/23 w:w)	36885	15451	**94069**	292545	6.1

Table 12: GPC data of injection molded specimens of PA66 and PA66/6HIA copolyamides

The molecular characteristics extracted from the GPC chromatograms of the PA66 and copolyamides are summarized in Table 12. The weight average molecular masses (Mw) of all the m-copolyamides appear to be higher than Mw of standard polyamide and in the same range of that of HMw PA66 even if their molecular mass distributions are completely different. The molecular weight of i-PA66/6HIA is obviously lower than that of m-PA66/6HIA containing the same of PA6HIA fraction (15%), but it is quite close to that of standard polyamide 66.

In addition, it is interesting to notice that dispersity of the samples prepared by melt and solid post condensation is relatively higher than that of standard PA66 and i-PA66/6HIA obtained by in-situ polymerization. The observed difference in the dispersity could be related to the mobility difference of reactive chains and consequently to the condensation statistics in solid and melt state.

1.2. **Block length**

Block length and randomness degree of the injection-molded copolyamides have been determined by MALDI–TOF at the “Institute of Chemistry and Technology of Polymers (ICTP) – UOS Catania” by the Professor Filippo Samperi. Unfortunately, the MALDI-TOF mass analyses of m-PA66/6HIA copolyamides, having high molecular weight and high fraction of oligomeric chains (high dispersity), gave unsatisfactory molar composition and chemical microstructural data. Indeed, the related spectra showed intense peaks in the mass range corresponding to oligomers (Mn lower than 8000 g/mol) and weak peaks related to copolymer chains having high molecular mass (higher than 10000 g/mol). Therefore, careful attention must be paid to the analysis outcome (average length and randomness degree) of the reactive prepared copolyamides, since it excludes the copolyamides chains having high molecular weight. However, the mass spectra of the i-PA66/6HIA, having lower molecular mass and narrower molecular weight distribution, luckily displayed mass peaks series corresponding to the overall copolymer chains. Thus, the average sequence length and the degree of randomness could be considered as confident information.

The polycondensation degree of standard and HMw PA66 (calculated on the basis of the end groups concentration) and the number average lengths of PA66 and PA6HIA sequences in PA66/6HIA copolyamides extracted from MALDI-TOF analysis are listed in Table 13. These results are compared with the NMR data, discussed in the previous chapter, of the extruded PA66/6HIA pellets.

It can be seen that block sequences of PA66 in the injection molded PA66/6HIA copolyamides are noticeably lower than the recurrence unit number of standard PA66. MALDI-TOF analysis indicates that the drop of PA66 block length with the PA6HIA content is less important than that observed in the case of extruded pellets, evidenced by NMR. However, the average length of PA6HIA sequences appears to be more reduced (around one unit) in the case of injection molded specimens. An explanation of the observed differences may lie in the fact that NMR analysis was done on extruded pellets prepared by microcompounding while MALDI-TOF analysis was performed on the injection molded specimens. Moreover, the NMR and MALDI-TOF techniques are not absolutely equivalent.

Concerning the randomness degree, the calculated values indicate that the resulting copolymers have a sequential structure character. Reminding that DR=0 corresponds to a completely block copolymer structure whereas DR=1 matches with a completely random structure.

Polymer sample	$\bar{L}_{PA66}$	$\bar{L}_{PA6HIA}$	Degree of randomness (DR)
PA66(standard) specimens	74	-	-
PA66(HMw) specimens	172	-	-
m-PA66/6HIA (90/10 w:w) pellets	46	5.11	-
m-PA66/6HIA (90/10 w:w) specimens	28.1	1.02	0.76
m-PA66/6HIA (83/17 w:w) pellets	27.2	4.47	-
m-PA66/6HIA (83/17 w:w) specimens	25.8	1.04	0.83
i-PA66/6HIA (83/17 w:w) specimens	8.07	1.35	0.86
m-PA66/6HIA (77/23 w:w) pellets	16	4.44	-
m-PA66/6HIA (77/23 w:w) specimens	24.6	1.35	0.85

Table 13: Number-average sequence lengths and randomness degree of PA66 and PA6HIA into PA66/6HIA copolyamides determined by NMR on the pellets (red color) and by MALDI-TOF in the injection molded specimens (green color) in comparison with the repetition unit number of standard and HMw PA66

The PA66 length of the in-situ copolymerized copolyamide i-PA66/6HIAis obviously lower than that of the copolyamide obtained by reactive extrusion m-PA66/6HIA. It is assumed that at 17 % wt of 6HIA content, the 6HIA co-monomer is randomly distributed along the PA66/6HIA backbone. Indeed, during in situ co-polycondensation, there is no selective monomer addition of the adipic acid or Hydroxyisophtalic acid (HIA) and then the 6HIA co-monomer is statistically incorporated, resulting in shorter PA66 segments.

Even if the abovementioned results could not be considered as discriminative evidence of the block character of the injection molded copolyamides, because of the unanalyzed high molecular copolyamides, the average PA66 length variation appears to be in good agreement with the general trend deduced form NMR analyses on the extruded pellets (Table 13). Based on this result, we assume that the multi-block structure of extruded copolyamides is conserved and no additional exchanges reactions occurred during injection molding.

To obtain more reliable information on the chemical composition and on the structure of studied m-PA66/6HIA copolyamides, Professor Filippo Samperi recommended performing SEC/MALDI-TOF coupling method: the copolyamide is fractioned into narrow molar mass fractions by SEC (Size Exclusion Chromatography) and then the molar composition and the sequence length for each SEC fraction are determined by MALDI-TOF analysis. Because of the lack of time, SEC/MALDI-TOF characterizations were not done and only thermal analyses, which could be considered as qualitative discrimination tools of the multiblock structure, were investigated on the injection molded samples.

2. Characteristics of the crystalline phase

2.1. Melting and crystallization behaviour

DSC measurements were carried out in order to obtain the melting and crystallization temperatures as well as the crystalline fraction of the selected samples. The melting thermograms are firstly presented in Figure 118. It can be seen that increasing the molecular mass of polyamide chains induces a little decrease of the melting temperature. Concerning the m-PA66/6HIA copolyamides, the same trend observed on the extrudates is confirmed: melting peaks move steadily to lower temperature as the PA6HIA content increases. Moreover, these melting temperatures are very close to those measured on m-PA66/6HIA pellets before injection which indicates that no additional exchanges reactions occurred during injection molding. This confirms our previous assumption (MALDI-TOF discussion) that the block character of m-PA66/6HIA copolyamides is conserved after injection.

It is interesting to state that i-PA66/6HIA, prepared by in-situ polycondensation, shows a typical thermogram of semi-crystalline polymers even if the HIA monomer is randomly distributed. Similar results are reported in the literature in the case of random copolymers of PA6/66 and PA6/68 [6]. The authors suggest that until certain concentration of the second comonomer, the H-bonds can still be formed between the similar monomers, albeit more irregularly, favoring polyamide chains packing.

The lower melting temperature of i-PA66/6HIA (10 °C lower) in comparison with that of m-PA66/6HIA containing the same 6HIA content suggests that the random copolymer has thinner lamellae and/or smaller crystallite size perfection.

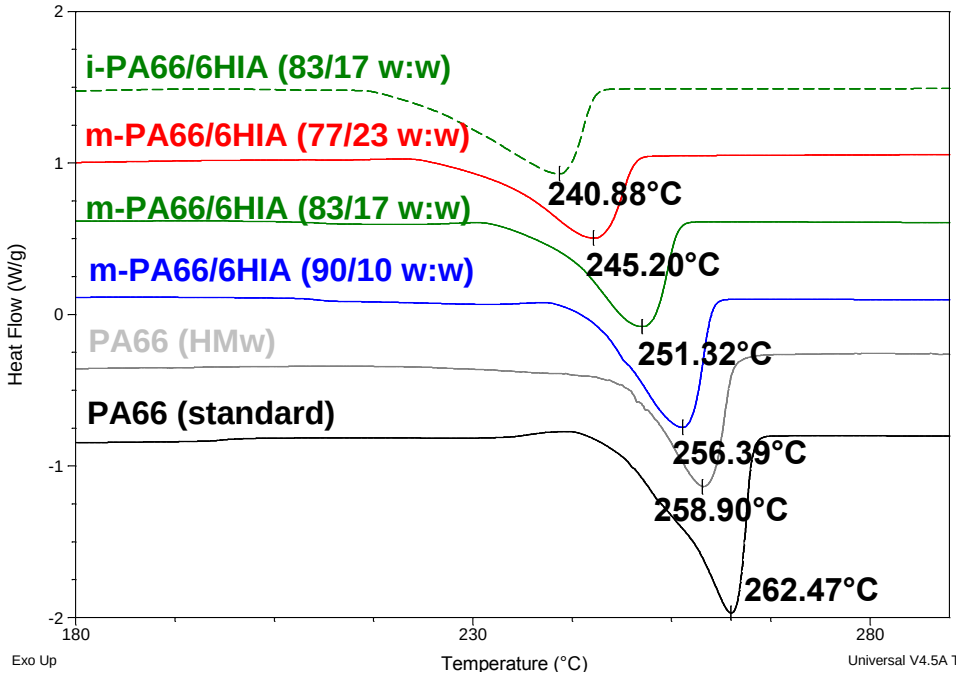

Figure 118: Melting thermograms of injection molded specimens of PA66 and PA66/6HIA copolyamides

The global crystalline fraction of the samples (melting enthalpy divided by the reference enthalpy associated to a 100% crystalline PA6,6) and the corresponding crystalline fraction of PA66 (calculated by taking into account the weight fraction of PA66 - see chapter II), are presented in Figure 119.

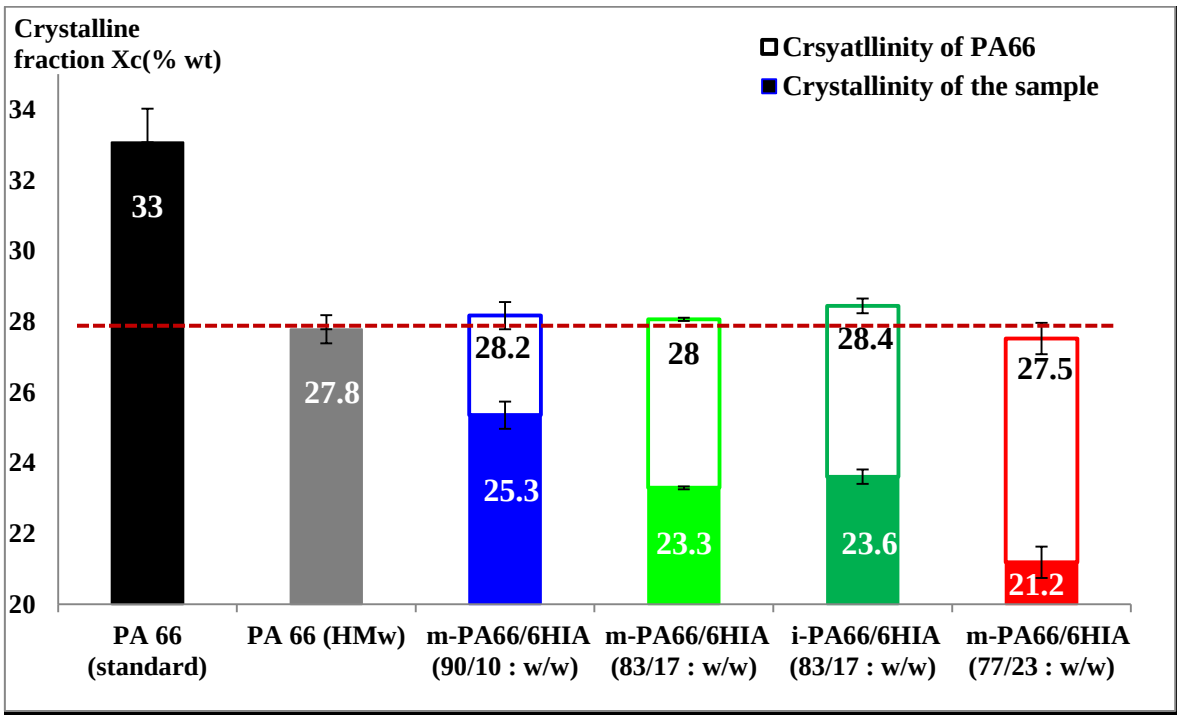

Figure 119: Global crystallinity of the sample (filled) and PA66 crystallinity (empty) as obtained from DSC for PA66 and PA66/6HIA injection molded materials

It turns out that HMw exhibits lower crystalline fraction (- 5%) than standard PA66, probably as a consequence of lower chain mobility in the melt. Moreover, the global crystalline fraction of the copolyamide samples appears to be significantly lower than that of standard P66. However the crystalline fractions of the PA6,6 (corrected by the weight fraction of PA6HIA in the copolyamides) are roughly equal to the crystallinity of HMw PA66 but still below that of standard PA66.

Even if m-PA66/6HIA and i-PA66/6HIA (83/17 w:w) have the same crystalline fraction of PA66 (~ 28%), in-situ co-polycondensation of the 6HIA co-monomer seems to affect more significantly the crystalline fraction of PA66 than the reactive melt co-polycondensation. Indeed, at the same molecular weight the crystalline fraction of PA66 goes down from 33% to 28% when the 6HIA monomer is randomly introduced (Mw of i-PA66/6HIA copolyamide is equal to that of PA66), while it remains constant in the case of block m-PA66/6HIA copolyamides, when compared to that of HMw polyamide having similar molecular weight.

It is worth noting that crystallinity of PA66 of the injection molded samples is 5-6 % lower than that obtained for the corresponding extruded pellets (presented in the previous chapter). This drop of crystalline fraction after injection may originate from difference in processing conditions such as higher shearing and slower cooling rate during the injection molding step.

The crystallization behavior during DSC cooling is now investigated and the thermograms are schown in Figure 120. The crystallization temperature of HMw PA66 was found to be lower than that of standard PA66 which has lower melt viscosity. This observation is in accordance with the literature data showing that lower molecular mass polymers crystallizes faster [6].

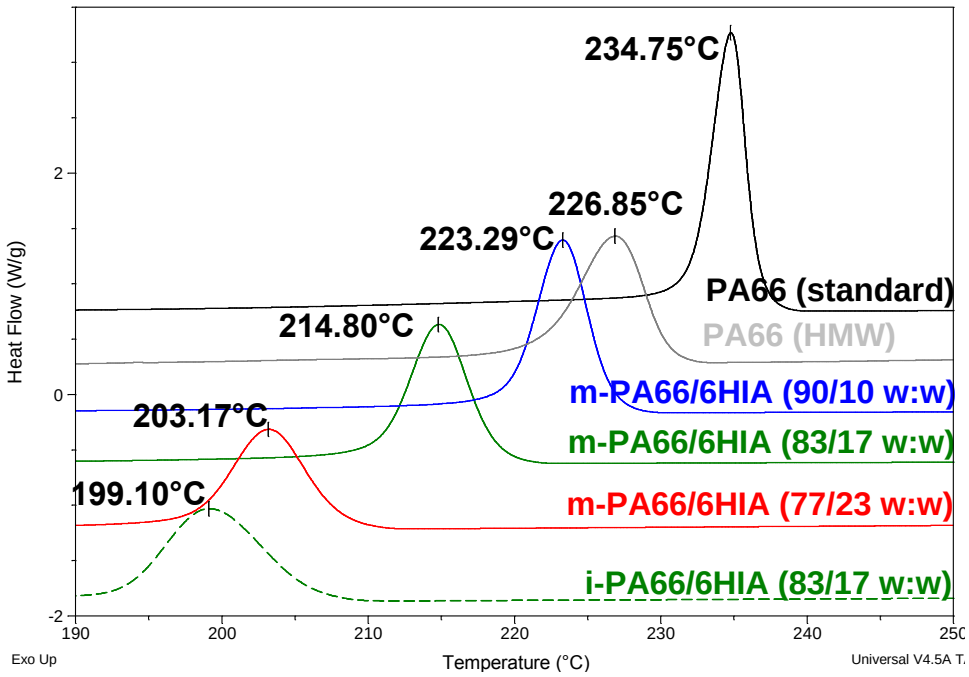

Figure 120: Crystallization thermograms of injection molded specimens of PA66 and PA66/6HIA copolyamides

As already stated in the previous chapter, the crystallization peak of m-PA66/6HIA copolyamides becomes larger and shifts towards low temperature as the PA6HIA content

increases. It should be noted that after injection the crystallization temperature values are reduced by ~ 2-3°C, probably as consequence of the molecular mass increase during injection. In the case of random copolyamide i-PA66/6HIA, having lower molecular mass than its corresponding m-PA66/6HIA, a higher crystallization temperature is expected. However, broader peak of crystallization and lower crystallization temperature (- 15 °C) is observed. Here again, the most plausible explanation for this difference is that random distribution of the 6HIA co-monomer must hinder the crystallization process of the PA66 segments.

To sum-up, increasing the molecular weight and/or adding 6HIA co- monomer reduce the chain mobility in the melt and then hinder the crystallization process of PA6,6 segments. This leads to a reduction of the crystallization temperature as well as of the melting temperature. This reduction is more obvious in the case of in-situ copolyamide. As the molecular weight of this later is close to that of standard PA66, the Tc and Tm drop could be totally related to the incorporation of the 6HIA co-monomer, being randomly distributed along the copolymer chains. Taking it into consideration that the crystalline features at the solid state (spherulite, lamella and crystal lattice) are dependent on the intrinsic properties as well as on the processing conditions, the crystalline morphology (from the micrometric to the nanometric scale) is now investigated.

2.2. **Crystalline structure**

2.2.1. Spherulite morphology

Size and texture of spherulites are dependent on many factors such as chemical structure, cooling rate, crystalline fraction and additives incorporation. Polarized optical micrographs of injection molded specimens, presented in Figure 121, put in evidence the impact of these factors on the spherulitic structure.

Standard polyamide66 exhibits a crystalline structure composed of irregular branched dendrites with some intercalated spherulite of diameter ~10-20 µm. This morphology may be related to the simultaneous nucleation of large number of crystals at fast cooling during injection molding (from 280°C to 80°C in few seconds). With increasing the molecular weight of polyamide, a smaller texture is observed (HMw PA66). For m-PA66/6HIA copolyamides, a crystalline texture similar to that of PA66 (HMw) with some impinged spherulites of a diameter around 5-10 µm can be also identified. The observed spherulite refinement could be related either to a high crystal nucleation or to low growing rate of spherulites. Indeed, the presence of high amount of catalyst can act as crystal nucleus resulting in the formation of smaller spherulites. Moreover, the increase of the molecular mass and the incorporation of rigid semi-aromatic segments in the backbone of PA66/6HIA decrease the chain mobility, and this could lead to lower the spherulite growing rate at high cooling rate from the melt. Note that larger spherulite could be obtained either by annealing solid material below the melting temperature or by slow cooling from the melt.

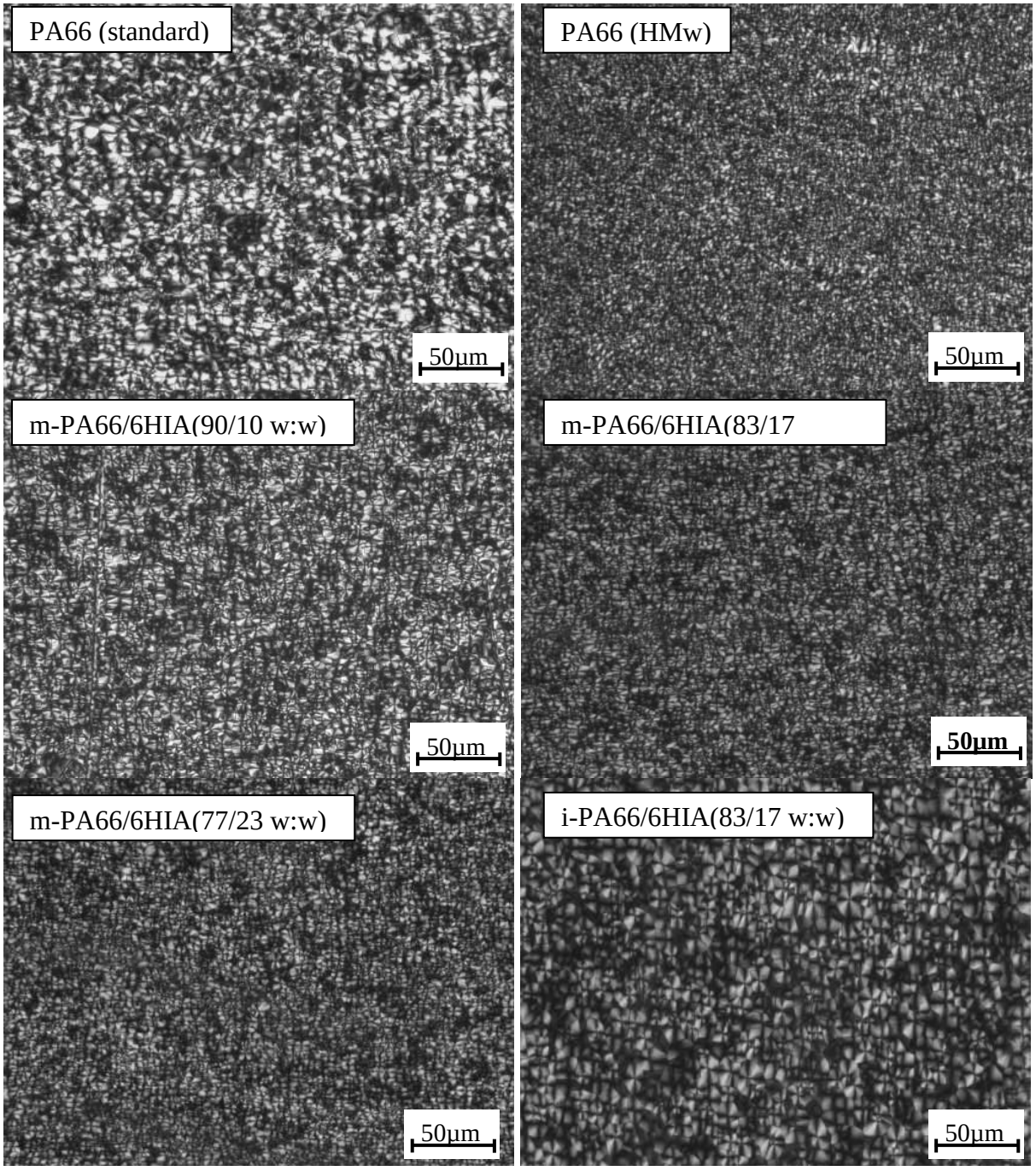

Figure 121: Polarized optical micrographs of injection molded specimens of PA66 and PA66/6HIA copolyamides

Random copolyamide i-PA66/6HIA exhibits well defined spherulites with an average diameter of ~20µm, which is unexpected since it has low crystallization ability. This morphology difference may be related to the absence of catalyst or additives that might act as nucleating agent. In fact, contrary to the HMw PA66 and m-PA66/6HIA containing high amount of catalyst, the in-situ copolyamide does not include catalyst. Thus, the spherulite can irradiate and grow progressively before being blocked by other nucleated crystalline regions.

2.2.2. Crystalline lamella

2.2.2.1. **Lamella thickness at room temperature**

As mentioned in chapter II section 2.3.1, the lamellar structure of semi-crystalline polymer can be highlighted by Small Angle X-ray Scattering (SAXS). The 2-D scattering patterns of PA66 and PA66/6HIA copolyamides taken at 23°C are given in Figure 122. It can be seen that all samples exhibit a high intensity scattering, corresponding to the periodic crystalline-amorphous structure, over the entire azimuthal angles (0°-360°). This shaped-ring scattering indicates that the crystalline lamellae are randomly distributed in the space, which is in full accordance with the crystalline structure identified by POM.

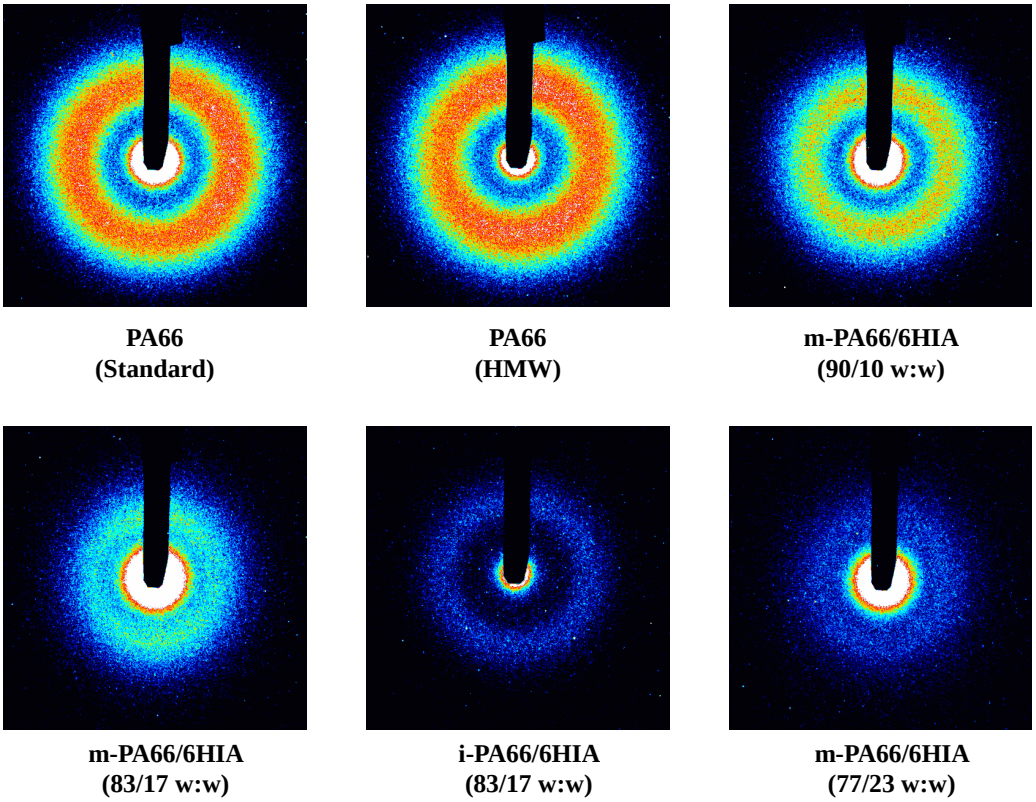

Figure 122: 2-D SAXS patterns of injection molded specimens of PA66 and PA66/6HIA copolyamides performed at room temperature

The scattering ring of HMw PA66 is slightly anisotropic (more intense in the polar region), indicating the presence of a greater fraction of crystalline lamellae oriented perpendicular to the injection direction. A possible explanation of this lamellae orientation could be the chains alignment in the flow direction, during injection at high shear rate (27600 s^{-1}), favoring lamellae growth perpendicularly to the flow direction.

As the PA6HIA content increases, the scattering ring moves towards the center indicating that scattering occurs at lower angle. Moreover, the intensity of scattering ring is reduced which suggests that the crystalline-amorphous structure of PA66/6HIAcopolyamides is likely changed. It is assumed that either the electronic density of the amorphous phase is increased or that of the crystalline phase is reduced.

In the case of i-PA66/6HIA (83/17 w:w), a well-defined isotropic ring indicating the presence of well-developed and randomly distributed amorphous-lamella structure is observed. This result confirms the well-developed spherulite structure previously highlighted by POM.

The average absolute SAXS intensities, extracted from the 2D-SAXS patterns as described in chapter II, are presented in Figure 123 as a function of the scattering vector q. Both PA66 (standard and HMw) have a similar scattering signal in the q range corresponding to the lamellar organization (0.04-01 $A^{\circ -1}$). Concerning the m-PA66/6HIA copolyamides, the scattering signal is shifted towards lower intensity as the PA6HIA content increases. Taking into consideration that the scattering intensity is more related to the crystal packing and lamella ordering than to the crystalline fraction, it can be assumed that these copolyamides have poorly defined lamella and/or less packed crystal. Moreover, in-situ PA66/6HIA copolyamide exhibits much lower scattering intensity than its corresponding m-PA66/6HIA, suggesting that random distribution of the 6HIA co-monomer affects more significantly the crystal packing and lamella ordering of PA66.

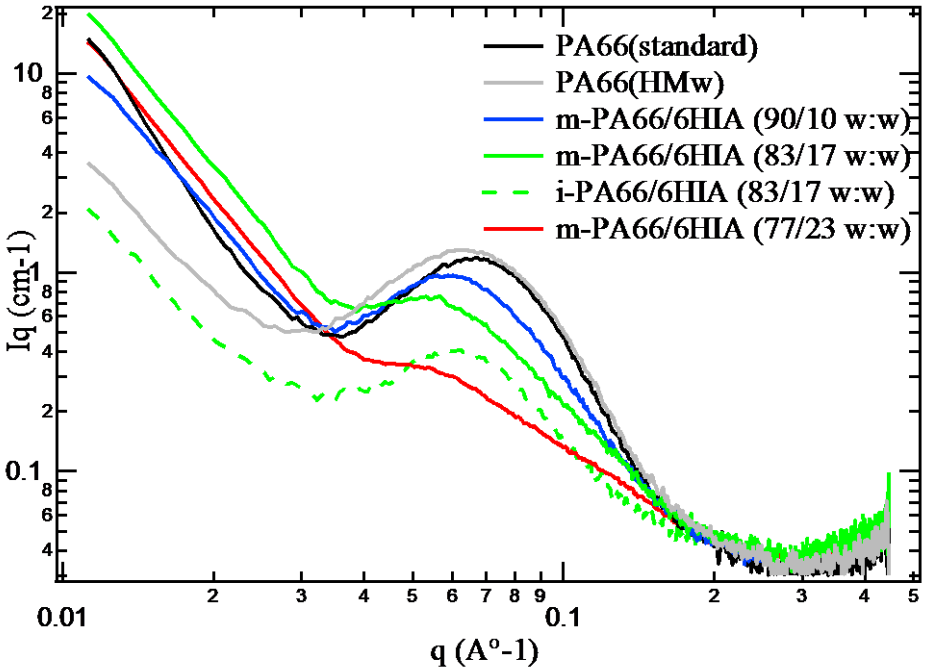

Figure 123: SAXS curves of injection molded specimens of PA66 and PA66/6HIA copolyamides at room temperature

Concerning the position of the maximum of scattering intensity, it can be seen that q_{max} (scattering vector corresponding to the maximum of scattering intensity) related to HMw PA66 is slightly lower than that of standard PA66. In the case of m-PA66/6HIA copolyamides, the position of the maximum of scattering intensity is gradually shifted towards lower values when the PA6HIA content increases. Apparently, we can say that the long period becomes larger as the fraction of amorphous phase increases. On the other hand, at the same crystalline fraction, i-PA66/6HIA shows higher q_{max} than that of m-PA66/6HIA, suggesting that the lamella thickness of i-PA66/6HIA is lower than that of reactive extruded copolyamide.

The long periods, estimated from the application of Bragg's law at the maximum of scattering vectors q_{max} , and the related lamellae thickness, determined as detailed in chapter II section 2.3.1, are given in Table 14. It firstly appears that crystalline lamella of PA66

becomes thinner as the molecular weight increases. Moreover, the lamellae thickness of PA66 crystal drops steadily as the PA6HIA content increases, likely as a consequence of the length reduction of the crystallisable PA66 segments. This drop appears to be more pronounced in the case of random distribution of the 6HIA monomer.

Sample	q_{max} ($A^{\circ -1}$)	L_p (A°)	L_c (A°)
PA66 (standard)	0.0672	93.5	30.85
PA66 (HMw)	0.063	99.7	27.72
m-PA66/6HIA (90/10 w:w)	0.0588	106.86	27.03
m-PA66/6HIA (83/17 w:w)	0.0565	111.21	25.91
i-PA66/6HIA (83/17 w:w)	0.0609	103.17	24.34
m-PA66/6HIA (77/23 w:w)	0.0532	118.11	25.04

Table 14: Long periods and lamellae thickness of injection molded specimens of PA66 and PA66/6HIA copolyamides

To summarize, SAXS measurement put in evidence that all injection-molded samples crystallize in the form of lamellar crystals that are randomly distributed in the space. This organization appears to be slightly anisotropic in the case of HMw PA66. It is shown that increasing the molecular weight and the incorporation of non-isomorphic 6HIA co-monomer lead to the formation of thinner crystalline lamellae. This observation is more obvious at high PA6HIA content and in the case of random distribution of the 6HIA co-monomer.

2.2.2.2. **Lamella thickness at high temperature**

In order to explore the presence of a non-equilibrated crystalline structure due to quick cooling during injection, 2-D SAXS measurements performed on samples heated above the Tg (at 150°C) are presented in Figure 124.

In spite of noticeable increase of the intensity scattering, particularly in the case of random PA66/6HIA copolyamides, no dramatic changes of the SAXS patterns are observed. Keeping in mind that the increase in the scattering intensity is due to either or both an increase in the volume fraction of the crystalline lamellae or increase in the electron density contrast between the crystalline and the amorphous regions. As the crystallinity did not increased during heating, the observed intensity increase may be related to more accurate electron density contrast between the amorphous and crystalline phase. It should be mentioned that at around 160°C (close to the measurement temperature) crystal transition from triclinic to pseudohexagonal phase, commonly known as Brill transition, takes place, resulting in lower crystal density [308]. Therefore, the increase in electronic contrast during heating could not be due to an increase of crystalline density but should be attributed to a decrease of the density of the amorphous phase. Indeed, it is reasonable to think that at 150°C, the interlamellar amorphous chain segments become more mobile and thus less densely packed.

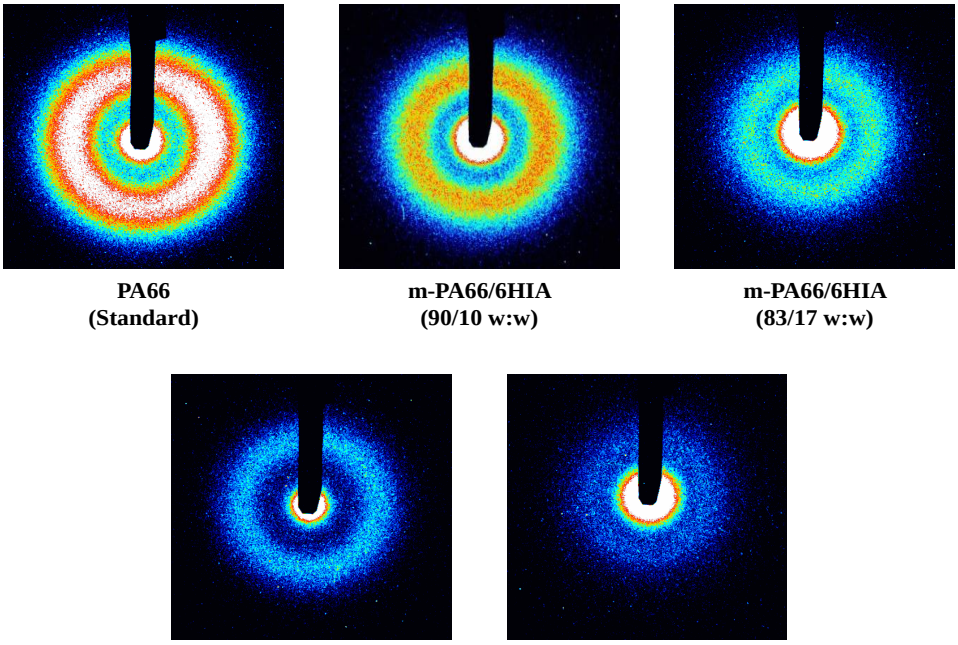

Figure 124:2-D SAXS patterns of injection molded specimens of PA66 and PA66/6HIA copolyamides performed at 150°C

Figure 125 shows the absolute intensity curves extracted from the SAXS experiments carried out at 150°C. It is apparent that at 150°C the scattering peaks are narrower than those observed at room temperature. This suggests the formation of more uniform amorphous-crystalline spacing and more ordered lamella stacking. This homogenization of the amorphous-crystalline structure may originate from chain rearrangement in the amorphous phase and more regular chains folding into the crystalline phase, driven by the chain mobility at high temperature.

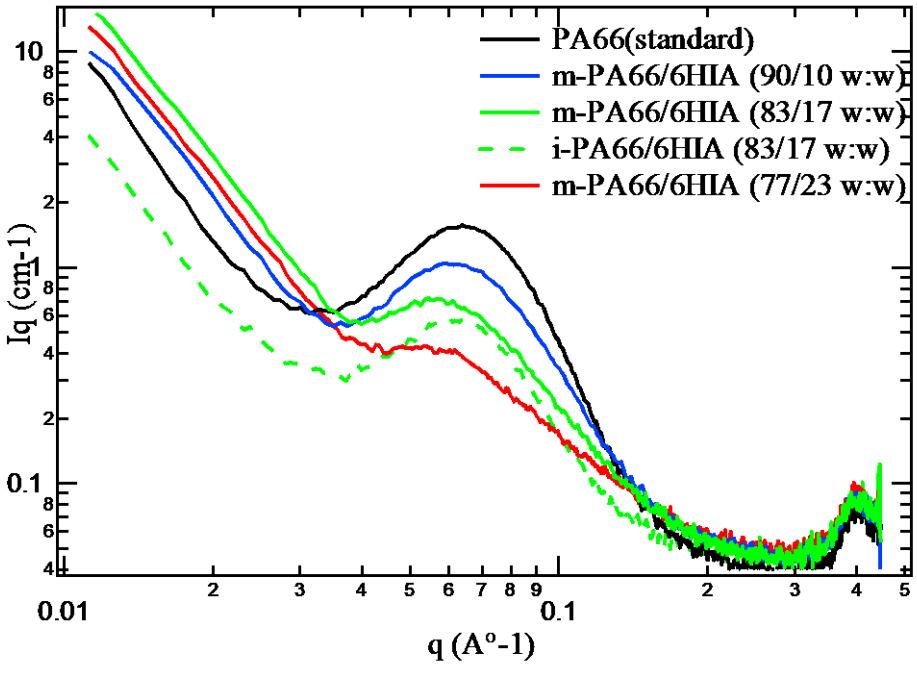

Figure 125: SAXS curves of injection molded specimens of PA66 and PA66/6HIA copolyamides at 150°C

Furthermore, the position of the maximum of scattering intensity appears to be unchanged after heating, suggesting that the long spacing is still constant during SAXS measurement at 150°C, in good agreement with literature results. Indeed, Murthy et al. found that up to 180°C, no significant changes of the long spacing of PA66 occur during heating [309]. Moreover, Koenig et al. reported that melt-crystallized PA66 do not show much increase in fold period at a considerable range of annealing temperature while the long period of solution-crystallized PA66 increases continuously with annealing temperature, particularly at high telperature [310]. However, it should be mentioned that Starkweather et al., [311] pointed out that bulk PA 66 crystals, prepared by ice-water quenching from the melt, exhibit continuous increase of the long period with annealing temperature (from 56 A° at room temperature to 108 A° at 250°C).

Taking the aforementioned results into consideration, we assumed that the injection molded samples have crystalline lamellae in well equilibrium state and that no lamella thickening has occurred during heating.

2.2.3. Crystalline perfection

The WAXD patterns of the injection molded samples are presented in Figure 126. It can be seen that HMw PA66 has diffraction peaks similar to that of standard PA66. Reminding that peak observed at around 23.7° corresponds to the chains distance within the H-bonds sheets, while the second one (around 20.3°) is related to the inter-sheet distance.

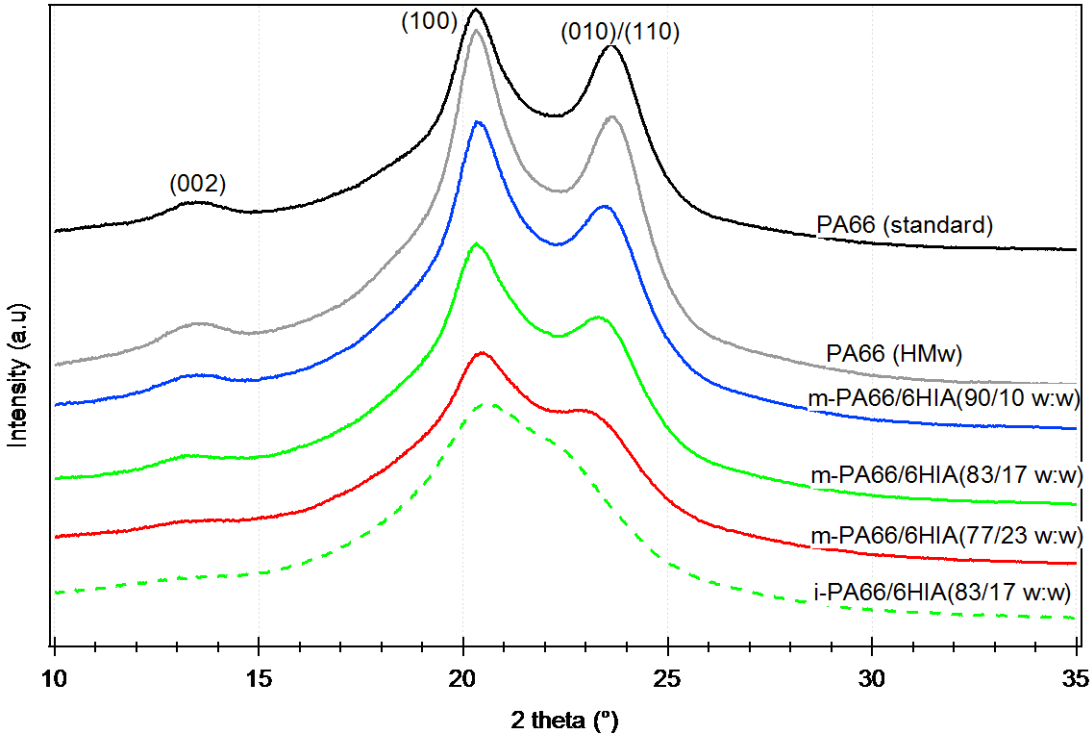

Figure 126: Wide Angle X-ray Diffraction patterns of injection molded specimens of PA66 and PA66/6HA copolyamides

Concerning m-PA66/6HIA copolyamides, the same reported trend, in the previous chapter, for the PA66/6HIA pellets is observed. For i-PA66/PA6HIA, apparently, only one strong (100) peak exists in the diffraction pattern with a very weak (010)/(110) shoulder. This means

that the triclinic structure of PA66 is not conserved when the 6HIA co-monomer is randomly distributed in the copolymer chain, whereas it is not significantly altered in the case of block copolyamide containing the same PA6HIA fraction.

Sample	(100) plane		(010,110) plane	
	2θ (°)	L (nm)	2θ (°)	L (nm)
PA66 (Standard)	20.29	7.28	23.71	6.33
PA66 (HMw)	20.32	7.15	23.75	6.33
m-PA66/6HIA(90/10 w:w)	20.37	7	23.62	6.1
m-PA66/6HIA(83/17 w:w)	20.31	6.5	23.55	6.11
i-PA66/6HIA(83/17 w:w)	20.76	3.24	22.96	4.98
m-PA66/6HIA(77/23 w:w)	20.42	5.5	23.28	5.42

Table 15: Peak data and crystallite size of injection molded specimens of PA66 and PA66/6HIA copolyamides

Peak data and the corresponding crystallite sizes calculated using the Scherrer equation, as detailed in the previous chapter, are listed in Table 15. It appears that the crystallite sizes are independent of the molecular weight and remains approximately constant for m-copolyamides containing until 17 % wt of PA6HIA. This result, already found for the pellets, indicates that no distortion of the crystal lattice occurs during injection molding of these copolyamides. For copolyamide containing 23% wt of PA6HIA, the crystallite size is reduced by 25 % in the H-bond direction (crystallographic direction perpendicularly to the (100) plane) crystallographic directions perpendicularly to the chain axis (100) and by less than 15 % in the crystallographic direction perpendicularly to the (010) plane (H-bonded sheet). It is noteworthy that the drop of the crystallite size is two factors lower after injection molding.

As expected, the random distribution of 6HIA co-monomers restricts the stacking of PA66 segments into crystals, leading to smaller crystallite. Indeed, the crystallite size in crystallographic directions perpendicularly to the chain axis of the in-situ PA66/6HIA copolyamides is two times lower than that of its corresponding m-PA66/6HIA.

2.3. **Relationship between the crystalline features and the melting temperature**

Several works on the correspondence of lamellar thickness to the melting point of single crystal of PA66 were reported [282,312–314]. They concluded that the melting temperature of single crystal of PA66 prepared by crystallization from solution is linearly related to the reciprocal crystal thickness by the following equation:

$$T_m = T_m{}^0 [1 - \frac{2\,\sigma_e}{\Delta H_m\, L_c}] \qquad (46)$$

where T_m is the melting temperature, $T_m{}^0$ is the melting temperature of infinitely-extended crystal, σ_e is the fold surface energy, ΔH_m is the heat of fusion and L_c is the crystal thickness.

In order to examine the validity of this relationship on our results, we plot on Figure 127 the melting temperature of the injection molded samples of PA66 and PA66/6HIA copolyamides as a function of their reciprocal lamella thickness. A linear fit of the experimental data by

using the equation (46) is also presented. The curve slope was defined according to the value reported in the literature while the intercept at origin was allowed to vary.

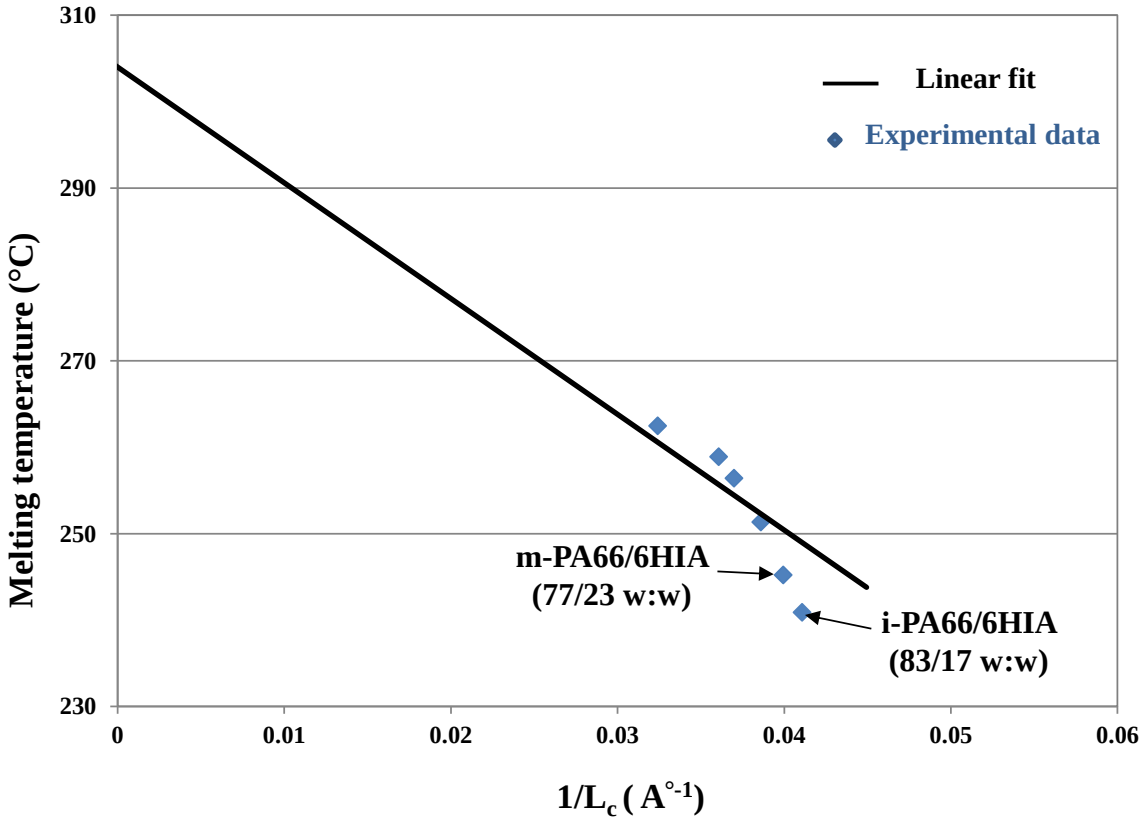

Figure 127: Plot of melting temperature against reciprocal crystal thickness, L_c^{-1}, ($A^{\circ -1}$)

It can be seen that all the Tm values, excepted for i-PA66/6HIA (83/17 w:w) and m-PA66/HIA (77/23 w:w), almost fall in the fit linear curve. In addition, the value of Tm° (304 °C) determined from the interception with X-axis is in good agreement with the values reported by Mitomo et al. [282] (300°C) and by Magill et al (301°C) [313].

The deviation of the melting temperature of random copolyamide and m-PA666HIA (77/23 w:w) from the linear relationship may be related to their small crystallite size perfection detailed in paragraph (II.2.2.3).

Thus, to conclude on the relationship between the melting temperature and the crystalline phase properties, the Tm of our injection-molded samples appears to be directly correlated to the PA66 crystal size, as reported in the literature for solution crystallized polyamides.

3. Molecular mobility of the amorphous phase

3.1. Glass transition temperature

The glass transition temperature (Tg) extracted from modulated DSC measurement on dry samples are presented in Figure 128. It firstly appears that Tg depends upon the molecular weight and the presence of rigid aromatic rings in the polyamide chains. Increasing the molecular weight of PA66 reduces its glass transition temperature by 4°C. As the crystalline

phase restricts the molecular mobility of the amorphous chains close to the crystal[315], this Tg's drop could be related to the lower crystalline fraction of HMw PA66.

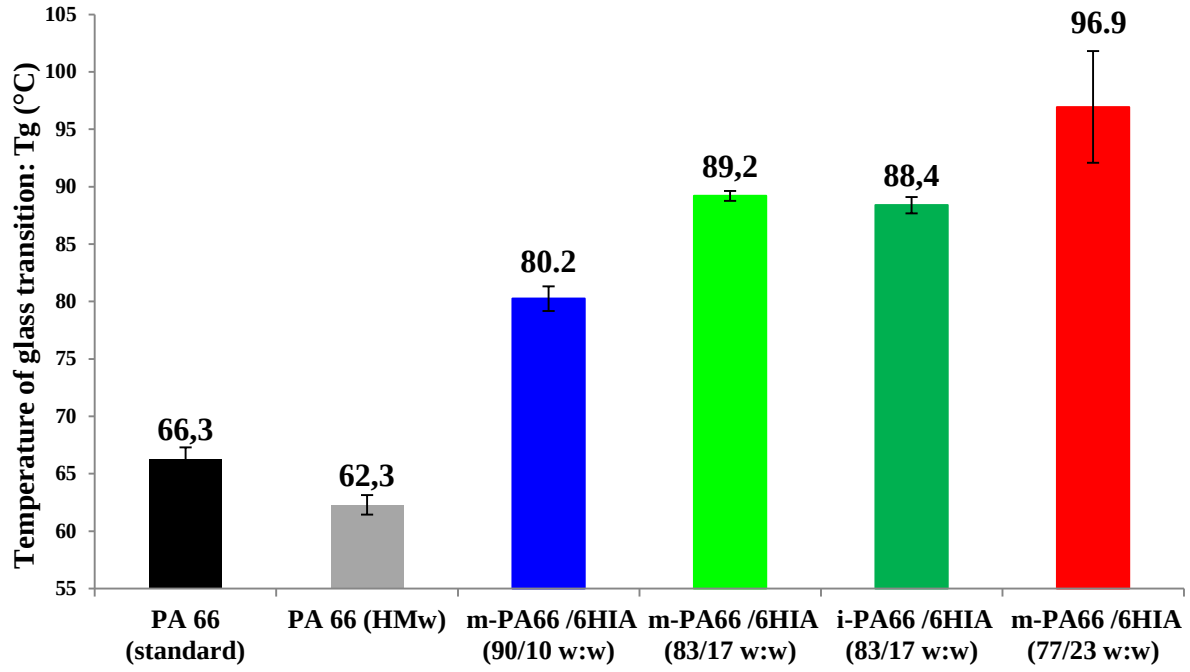

Figure 128: Glass transition temperatures of injection molded specimens of PA66 and PA66/6HIA copolyamides detremined by modulated DSC

Similarly to the extruded pellets (chapter III section 2.1), the Tg of m-PA66/6HIA copolyamides grows up as the fraction of the aromatic co-monomer increases until reaching almost 97°C for copolyamide containing 23% wt of PA6HIA. It should be noted that PA66/6HIA copolyamides prepared by in-situ copolymerization and reactive melt extrusion show comparable glass transition temperature, suggesting that the chains mobility of their amorphous phases is similar.

3.2. **Thermo-mechanical relaxations**

The tangent delta (δ) or the loss damping factor are mainly associated with the main and second relaxations in the amorphous phase. As it can be seen in Figure 129, three peaks of tan (δ) corresponding to molecular relaxations can be identified. The first one occurs at almost -130°C and corresponds to the (γ) relaxation, the second one around -60°C corresponds to the (β) relaxation. The third Peak, the most important, corresponds to the (α) relaxation and it is generally associated with the glass transition temperature.

It seems that (γ) relaxation is not altered by the incorporation of the 6HIA co-monomer or by the increase of the molecular weight as it is related to the vibration of the methylene groups. On the other hand, the (β) relaxation is shifted toward higher temperature with increasing the 6HIA content whereas it is not altered by the molecular weight. Accordingly, we assume that the rotation of the amide groups, which from originates the (β) relaxation, is more difficult when the amide groups is linked to phenolic group (HIA), likely due to strong H-bond interactions.

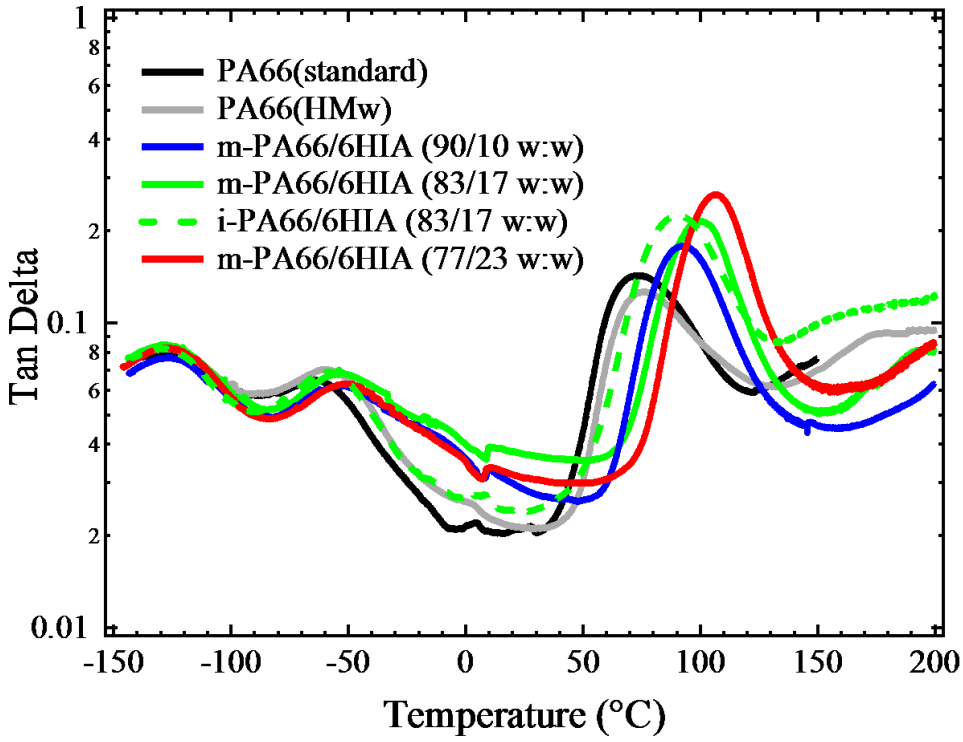

Figure 129: Tans delta evolution for PA66 and PA66/6HIA copolyamides

Concerning the main relaxation associated to the glass transition process, a slight shift of the tangent delta (δ) peak to high temperature (75 °C) is detected when the molecular mass of the polyamide increases (HMw) while the opposite was observed for the glass transition temperature extracted from MDSC measurements. An explanation of the observed difference may lie in the fact that the amorphous chains relaxation is not monitored by the same manner (calorimetric versus mechanic). For PA66/6HIA copolyamides, the (α) relaxation peak is shifted towards higher temperature as the PA6HIA content increases until reaching 115 °C in the case of PA66/6HIA containing 23 % wt of PA6HIA. This finding suggests that the amorphous chain mobility is reduced by the addition of rigid aromatic segments and/or by reinforcing the intermolecular interactions (H-Bonds).

Figure 129 also shows that the T(α) of the random PA66/6HIA copolyamide is 10° C lower than that of the corresponding block copolyamide with 17 % wt of PA6HIA. Similar observations was reported by Wang et al. in the case of PA6/PA6T and PA6/66 copolymers [316,317]. They stated that melt-mixed PA6/PA6co6T and PA6/PA66 exhibit respectively higher Tg that in-situ PA6/6T and PA6/66 copolymers. In related works, it was also found that in-situ PA6/12 [315] and PA6/69 [54] copolymer have lower glass transition temperature than the initial homopolyamide PA6. It was agreed that the Tg drop of random copolymers originates from the decline of crystallinity and the reduction in hydrogen-bonding concentration due to the irregular distribution of amide groups along the copolymer molecules. In our case, both random and block copolyamides have the same crystalline fraction; therefore we suppose that the higher T(α) in the case of m-PA66/6HIA is rather related to the efficient segmental immobilization of the polyamide chains resulting from more regular distribution of the phenolic ring along the copolymer backbone.

The lower chain mobility can be also ascribed to a topologically constrained amorphous region (constrained amorphous phase) between the crystal surface. Reminding that block m-PA66/6HIA has higher crystallite size than the random one which may hinder more significantly the amorphous chains anchored into the crystal.

It is worth noting that, contrary to the (α) relaxations peaks, Tg values (extracted from MDSC measurements) of random and block copolyamide are very close. This observation points out that the signature of the amorphous chains relaxation in these copolyamides is dependent on the way that the cooperative motion is recognized (calorimetric or thermomechanic).

Further information can be deduced from the curves of Tan delta such as the magnitude of the α-relaxation. Thus, we plot in Figure 130 the magnitude of the α-relaxation as a function of the crystalline fraction or the PA6HIA content. It appears that the magnitude of the α-relaxation of PA66 slightly decreases when the molecular weight increases, probably due to the presence of high chain entanglement density. For PA66/6HIA copolyamides, the magnitude increases as the crystallinity decreases or the PA6HIA content increases. This result seems to be reasonable, since the amorphous fraction, from which the alpha relaxation originates, increases. Furthermore, it can be supposed that lamella thickness reduction may favor the relaxation process and then lead to more pronounced tangent delta peaks.

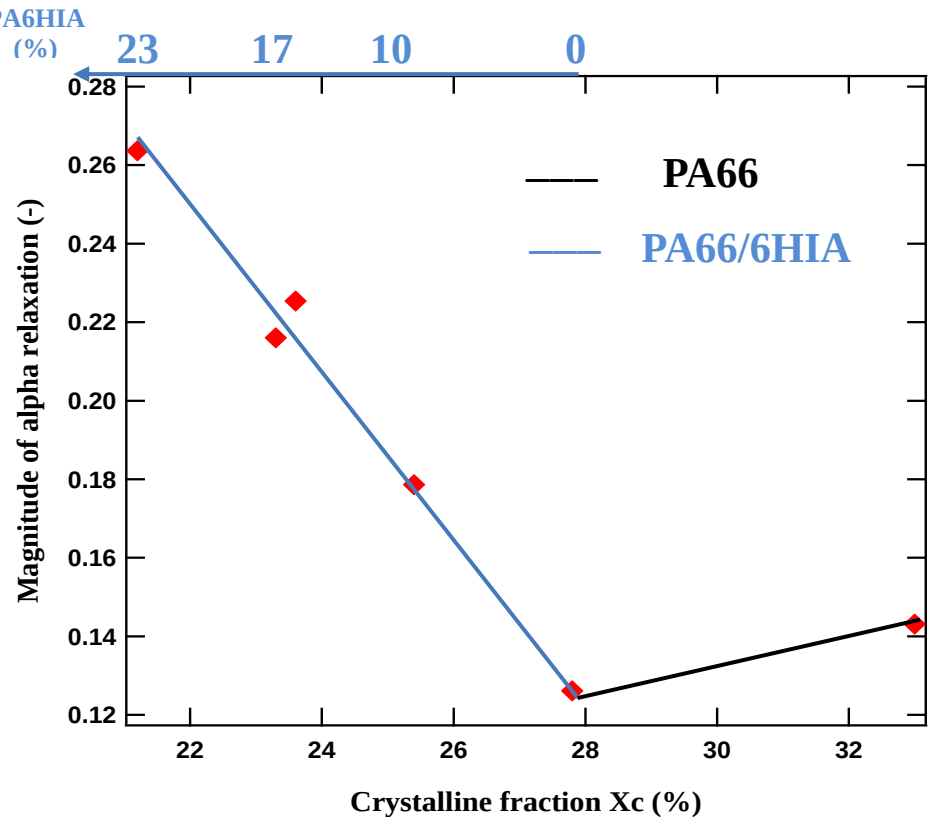

Figure 130: Dependence of magnitude of relaxation on crystalline fraction for PA66 and PA66/6HIA copolyamides

To conclude on the molecular mobility of the amorphous phase, the glass transition temperature appears to be dependent on the crystalline fraction and the intermolecular interaction. It is shifted toward higher temperature when the crystalline fraction or the fraction of rigid phenolic segments increases. The main relaxation (α), commonly associated with the glass transition, further reveals that random introduction of the phenolic function in

the PA66 backbone has lower impact on the chains mobility restriction than segmental incorporation. For instance, i-PA66/6HIA, being random copolymer, shows lower T(α) than it corresponding block copolyamide.

Unfortunately, the divergence between the Tg and the T(α) values is not negligible and then careful attention must be paid to the value taken into consideration. We believe that calorimetric assessment of the molecular chains relaxation is more accurate than the mechanical measurement (DMA). Therefore, the glass transition temperature, extracted form MDSC measurements, will be considered herein after as the physical parameter to monitor the amorphous phase mobility.

4. Free surface energy

As detailed in the first chapter, the introduction of the HIA monomer aims to increase the cohesive energy of the amorphous phase by means of strong intermolecular interactions. One way to assess the cohesive energy consists in measuring the free surface energy. The ideal solution is the quantification of the free surface energy of the amorphous phase where the 6HIA monomer is located. To our knowledge, no experimental technique can provide information on the free surface energy of the interlamellar amorphous phase. Therefore, only the overall free surface energy of the semi-crystalline material was considered.

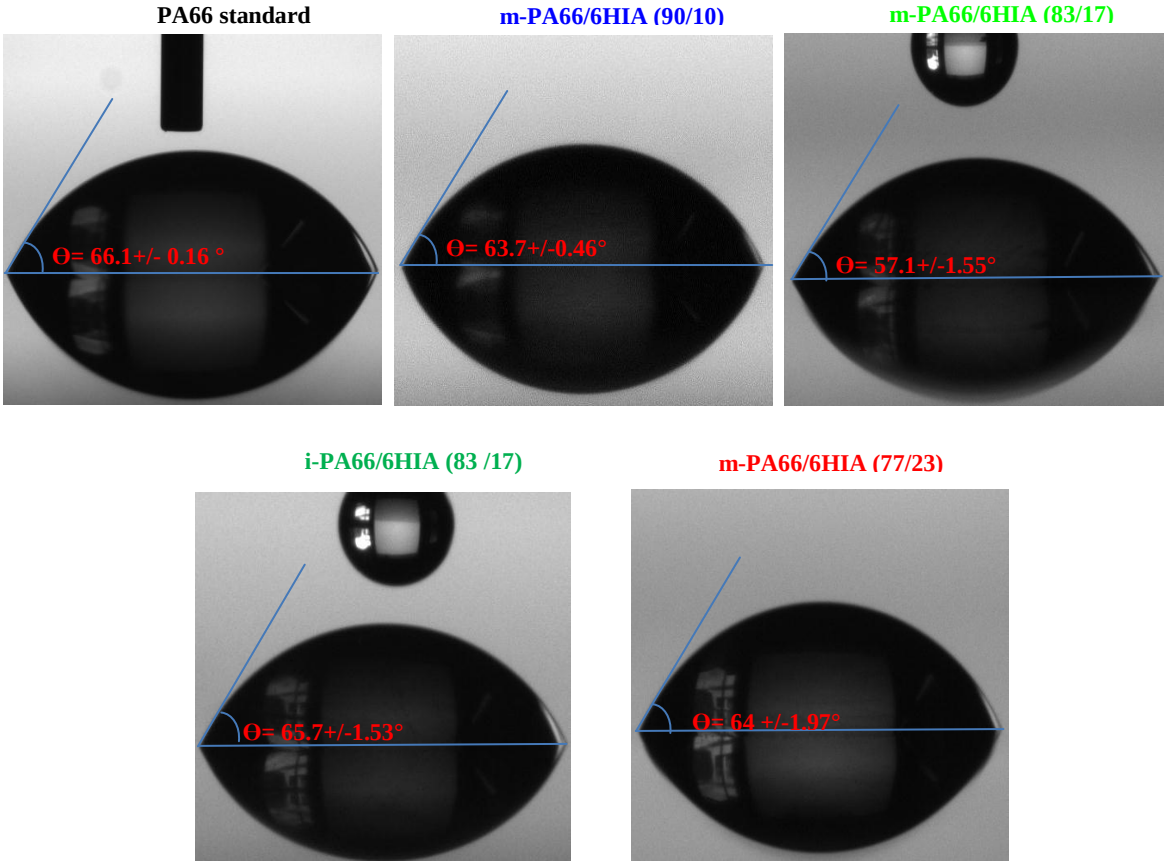

Figure 131: Micrographs of contact angle between a water drop and the solid surface of the studied samples

Solid contact angle measurements, presented in Figure 131, show that contact angle between the water drop and the solid surface of PA66/6HIA copolyamides is lower than that in the

case of standard PA66. This means a higher free surface energy of the copolyamides samples as shown in Figure 132. It is interesting to notice that this increase is nonlinear with the content of PA6HIA. For instance, it is around 6.5% with adding 17% wt of PA6HIA while it does not exceed 2.2 % in the presence of 23 % wt of PA6HIA. In addition, it seems that the free surface energy of random copolyamide i-PA66/6HIA is lower than that of its corresponding block copolyamide m-PA66/6HIA (83/17 w:w).

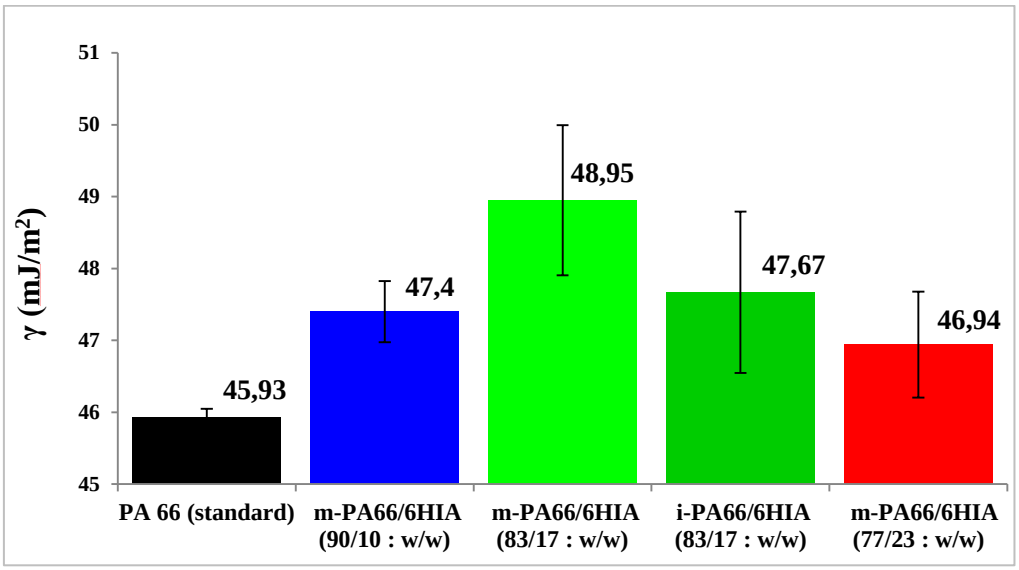

Figure 132: Free surface energy at room temperature of PA66 and PA66/6HIA copolyamides

Even if the properties of the crystalline phase (fraction, perfection...) may have an influence on the above results, these latter could be considered as an indirect evidence of the enhancement of the cohesive energy of the amorphous phase by the HIA monomer.

5. Summary of the microstructure of PA66 and PA66/6HIA copolyamides

The molecular structure of injection molded samples of PA66 and PA66/6HIA copolyamides has been investigated by GPC and MALDI-TOF. It was shown that solid post-condensed PA66 (HMw) has higher weight average molecular mass than that of standard PA66 which has lower dispersity. The average molecular weight of m-PA66/6HIA copolyamides increases after injection, likely due to further polycondensation reactions in the melt. Furthermore, their molecular mass distributions were found to be broader than that of HMw PA66 even if they have comparable weight average molecular mass. It was also observed that in-situ copolymerized PA66/6HIA copolyamide exhibits a Gaussian distribution of molecular mass which is roughly superposed to that of standard PA66. MALDI- TOF analyses revealed that PA66 sequence of block m-PA66/6HIA copolyamides is longer than that resulting from random distribution of the 6HIA co-monomer. Moreover, it is believed that the PA66 sequences of reactive extruded copolyamides are not considerably reduced after the injection molding.

DSC analysis pointed out that increasing the molecular weight reduces both the melting and crystallization temperatures of PA66. Moreover, the crystallization and melting temperatures of injection molded PA66/6HIA copolyamides were found in the same range of those of the pellets, suggesting that no additional exchange reactions were occurred during injection. Concerning the crystalline fraction, it was observed that the crystalline fraction of PA66 decreases when the molecular weight increases and that the crystalline fraction of PA66 in the PA66/6HIA copolyamide is close to that of HMw PA66. However, the global crystalline fraction of the PA66/6HIA samples was found to decrease when the 6HIA co-monomer increases, because of the amorphous character of the PA6HIA component. It was also observed that for a given molecular weight, the addition of 6HIA in the form of block sequence does not alter the crystalline fraction of PA66 while the random incorporation of the 6HIA monomer reduces it.

Morphological characterizations showed that, except for i-PA66/6HIA copolyamide, adding 6HIA co-monomer as well as increasing the molecular weight of PA66 induces a slight refinement of the spherulite structure. This latter consists in randomly oriented crystalline lamellae connected by disordered phase as highlighted by the SAXS experiments. The thickness of the crystalline lamellae was found to decrease when the amount of PA6HIA or the molecular weight increases. Moreover, random distribution of the HIA co-monomer along the chain copolymer reduces significantly the lamella thickness and crystallite size perfection of the resulting crystal.

Based on the aforementioned characterizations, the drop of the melting temperature with the PA6HIA content and the molecular weight increase was successfully correlated to the thickness of the crystalline lamella and the crystalline size perfection of the PA66 crystal.

Finally, the molecular mobility of the studied material was investigated by MDSC and thermomechanical analysis. It was found that glass transition temperature increases when the fraction of rigid phenolic segments increases. Moreover, the cohesion of the amorphous phase was indirectly highlighted by means of free surface energy. It was observed that the free surface energy tends to increase with the incorporation of 6HIA co-monomers, suggesting strong intermolecular interactions.

Part II: Mechanical properties

1. Quasi-static mechanical properties

1.1. Elastic modulus

The elastic modulus of the studied materials was investigated by measuring the dynamic storage modulus E'(elastic modulus under low cyclic deformation) and the Young's modulus (elastic modulus at given strain rate).

The Young's moduli, determined at room temperature and at strain level < 0.5% are listed in Table 16. It can be noted that increasing the molecular weight of PA66 does not alter its elastic modulus. Despite a lower crystalline fraction, the Young's modulus of the HMw PA66 is close to that of standard PA66 (~3100 MPa). It is assumed that the drop of the crystalline fraction is counterbalanced by more resistant amorphous phase. Indeed, the elastic deformation is essentially generated by the interlamellar amorphous region [318] by means of interlamellar separation, interlamellar rotation and interlamellar shear [137]. The magnitude of these processes depends on the crystalline phase, the mobility of the disordered chains as well as on the entanglement chain density and the number of tie molecules. These latter are supposed to be higher in the case of HMw PA66 and may explain its high stiffness (resistance to deformation).

Samples	E(MPa)
PA66 (standard)	3140
PA66 (HMw)	3110
m-PA66/6HIA (90/10 w:w)	2990
m-PA66/6HIA (83/17 w:w)	3190
i-PA66/6HIA (83/17 w:w)	2300
m-PA66/6HIA (77/23 w:w)	3053

Table 16: Tensile strength properties of PA66 and PA66/6HIA copolyamides at 23°C

Despite a more cohesive amorphous phase, Young's moduli of m-PA66/6HIA copolyamides are in the same range of that of PA66. This suggests that the reinforcement of the intermolecular interactions by adding 6HIA co-monomer is balanced by contrary phenomena such as drop of the crystalline fraction and lamella thickness. Moreover, the lower elastic modulus of random i-PA66/6HIA (83/17 w:w) copolyamide compared to that of block m-PA66/6HIA (2300MPa versus 3100 MPa) suggests that reduction of the crystallite size perfection also affects the elastic modulus of the material.

The evolution of dynamic storage modulus of PA66/6HIA copolyamides and polyamide 66 (standard and HMw) as a function of temperature is given in Figure 133. Similarly to the Young's Modulus, the glassy storage modulus temperature (below 50°C) of all compositions, except i-PA66/6HIA which exhibits lower elastic modulus, does not distinguish from each other within the experiment error.

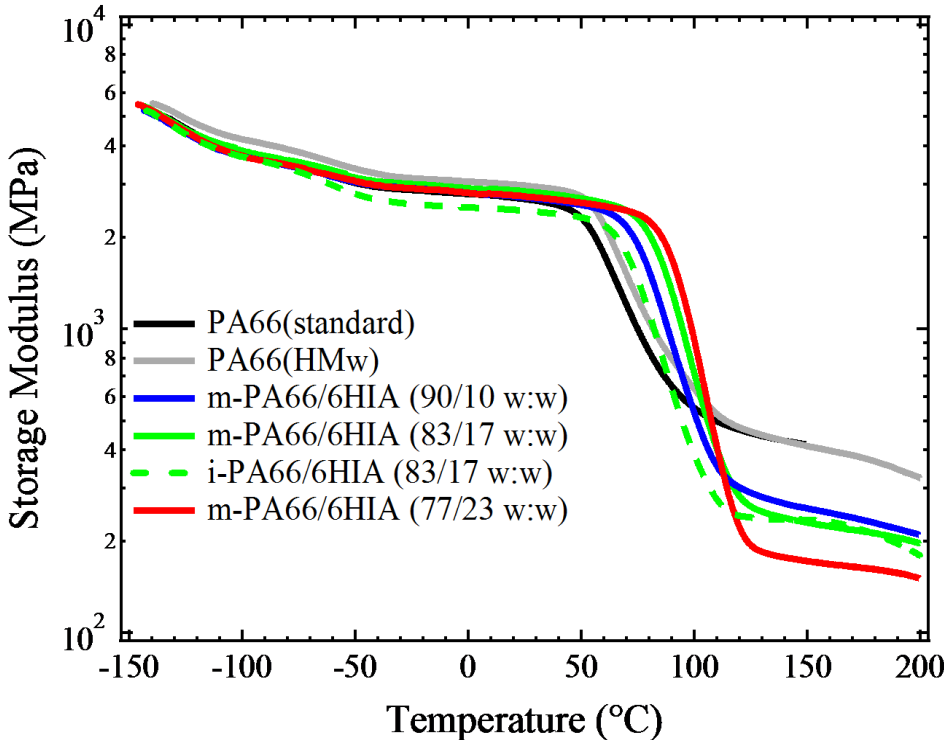

Figure 133: Storage Modulus evolution for PA66 and PA66/6HIA copolyamides

Close to the glass transition temperature (50°C to 100°C), a sharp decline of the storage modulus is observed. This drop is more significant in the case of PA66/6HIA copolyamide and it increases with increasing the PA6HIA content. After that, the elastic modulus reaches a plateau which is roughly constant when increasing the temperature. The low residual storage modulus of PA66/6HIA copolyamides may be related to their lower crystallinity degree. It is of interest to note that random and block PA66/6HIA copolyamide (83/17 w:w) having the same crystalline fraction shows comparable elastic modulus above the glass transition. It appears then that the material response above the glass transition is mainly governed by the crystalline fraction.

To sum up, below the glass transition the elastic modulus of the studied material appears to be mainly dependent on the amorphous chain mobility and the crystalline features (lamella thickness and crystallite size perfection) of the crystalline phase, while it is rather dependent on the crystalline fraction above the glass transition. Moreover, it was found that the molecular weight does not affect the elastic response of the material (at low strain level) over a wide range of temperatures.

1.2. **Tensile strength properties**

In this paragraph the tensile properties of PA66 and PA66/6HIA copolyamides at temperature below and above the glass transition (23°C and 150°C) are studied. Firstly, tensile behaviour at room temperature is discussed and then tensile tests at 150°C are presented.

1.2.1. Below the glass transition

The results of uniaxial tests carried out at 23°C, are presented in Figure 134. The obtained stress-strain curves are typical of thermoplastic materials. At the beginning (small strain), the stress increases linearly with the strain in the elastic regime. As the deformation increases, the stress-strain dependence becomes nonlinear which is considered as a sign of the viscous response of the material. No significant difference, except for the random copolyamide which appears to deform more easily, is noted in the viscoelastic regime. Subsequently, all materials undergo plastic flow facilitated by chain disentanglement via cooperative diffusion and molecular rearrangement along the stress direction. This phenomenon known as yielding process occurs when stress reaches the critical values for crystallographic slip, and plastic deformation. The maximum of stress, called "yield stress", was found at around 4.5% of strain ratio for all materials.

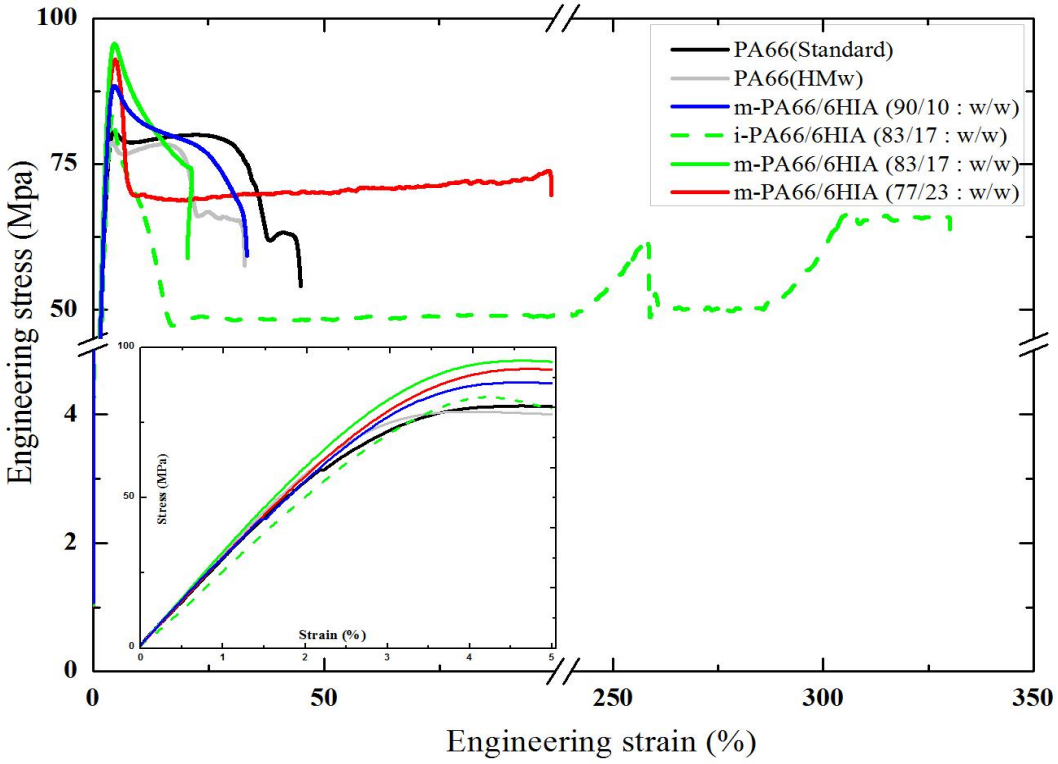

Figure 134: Engineering stress-strain curves from uniaxial tests at 23°C with a crosshead speed of 5mm/min

After the yield, a sharp decrease of the strength, remarkable in the case of copolyamides PA66/6HIA is observed. This stress drop may be related to a local cross-section reduction by necking process. In the case of PA66 (standard and HMw), a steady extension of the neck, known as cold drawing, is observed. The material in the neck stretches slightly and then new material at the neck shoulders necks down resulting in steady propagation of the neck under constant stress. This process, involves lamellae fragmentation and chain orientation parallel to the draw direction.

As HMw polyamide has longer chain than standard PA66, a longer cold drawing step could be expected. However, the failure occurs at lower ultimate strain. This is believed to be due to the presence of smaller spherulites . Indeed, Starkweather et al.,[108] found that decreasing

the size of the spherulites of nylon 66, through increasing nucleation, results in a lower ultimate elongation and a loss of the ductility.

The cold drawing process was not identified for copolyamides containing 10 and 17 % wt of PA6HIA. In these cases, the material in the neck stretches continuously and fails at low strain level. It can be presumed here that necking process produces a microstructure whose breaking load is lower than that needed to induce necking in the untransformed material just outside the neck. As a result, the elongation at break is governed by a competition between plastic stretching and a terminal process of fracture such as a defect inside the neck.

On the other hand, m-PA66/6HIA (77/23 w:w) and random copolyamide have undergone a surprising cold drawing process leading to failure at relatively high strain. It should be noted that in the case of random copolyamide two strain hardening followed by necking processes were observed prior to the final failure, which occurred at 330% of drawing ratio. Taking into consideration that the plastic properties of the crystalline component govern the overall deformation behavior [319], the observed spectacular drawing is assumed to be the result the presence of thinner lamellae and poorer crystal perfection. In fact, it is well established that thinner lamella lowers the restriction to crystallographic slip and then facilitates the plastic deformation of the crystal [317]. Moreover, the crystalline lattice determines the crystal ability to plastic deformation. For example, pseudo hexagonal-γ crystals of PA6 show easier crystal drawing than monoclinic-α crystals as they have smaller interchain interactions and then lower packing density[320–322].

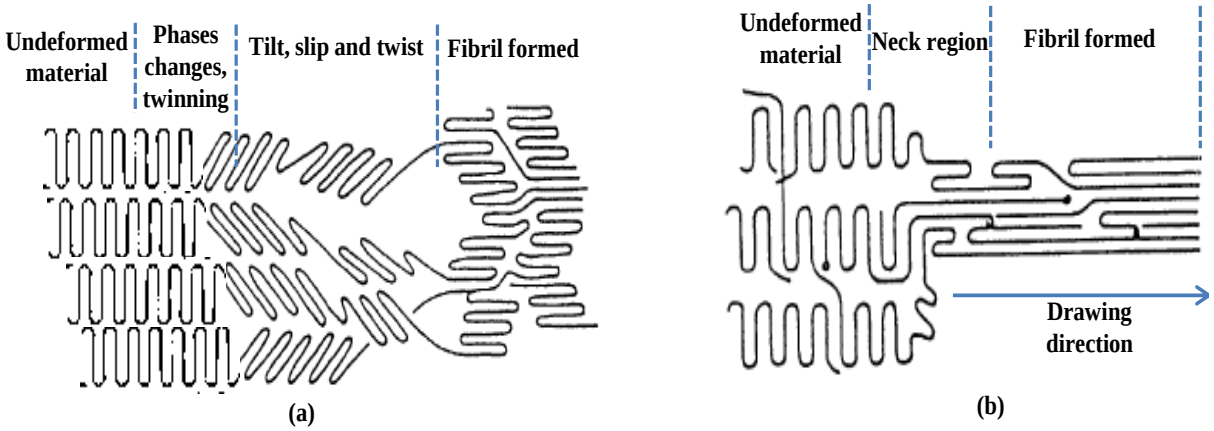

Figure 135: Molecular mechanisms of stretching for stacked lamellar morphology posed by: (a) Peterlin et al. [136] **(b) Petermann et al.**[323]

Accordingly, it is admitted that the crystalline phase of m-PA66/6HIA (77/23 w:w) and random copolyamide is more prone to deform plastically than the PA66 crystal. We presume that the cold drawing of these polymers involves similar molecular processes to that observed in the case of polyethylene such as chain slip, chain tilt and chain pullout. This results in lamella breaking and fibril formation as schematically presented in Figure 135 .

1.2.1.1. Relationship between the tensile strength property and the amorphous phase molecular mobility

In the case of amorphous polymers, the yield stress depends on the temperature test, more likely on the difference to the glass transition (T-Tg); it increases linearly as the chain

mobility decreases [324]. However, for semi crystalline polymers, two contributions should be considered: Firstly the crystalline phase (crystalline fraction and morphology) and secondly the amorphous phase (chain mobility). Several works have been devoted to the study of the contribution of the crystalline phase. They pointed out that the yield stress of semi-crystalline polymers is related to the crystalline phase mobility which is likely dependent on the crystals size. They reported that yield stress increases as the lamellae thickness increases [324–327].

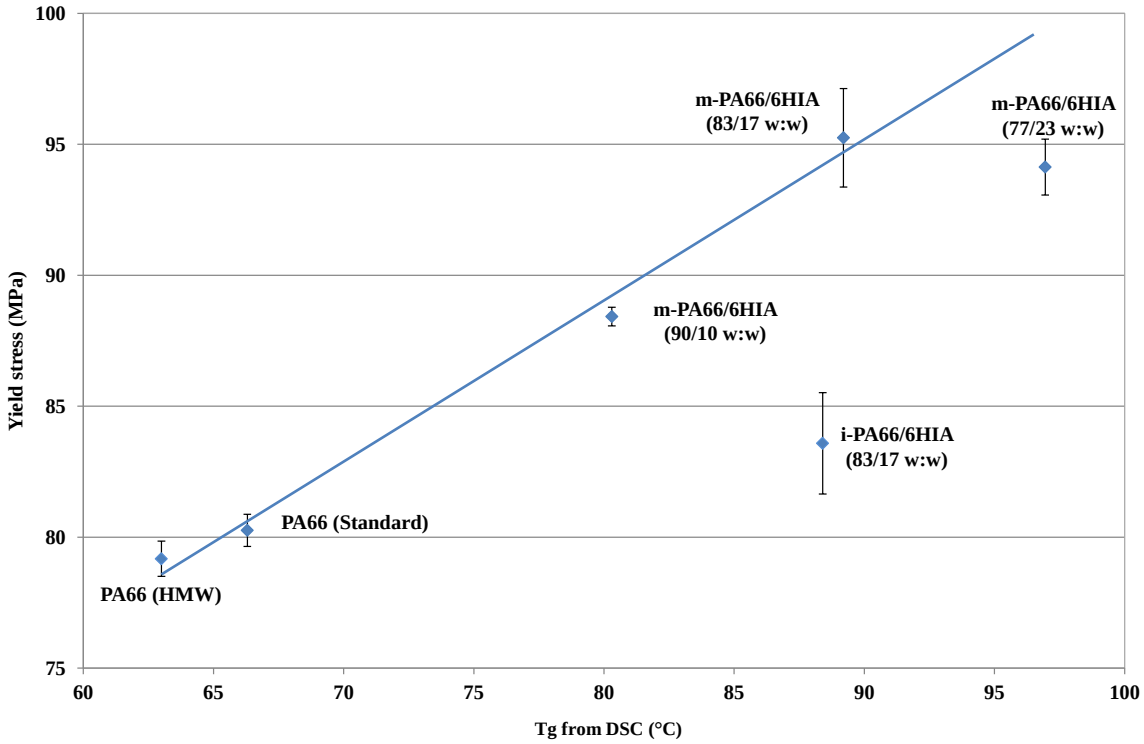

Figure 136: Yield stress plotted as a function of the Tg of studied materials

In the framework of this thesis, we mainly focused on the modification of the amorphous phase, namely on the intermolecular interaction. Thus, the dependence of the yield stress at 23°C on the chain mobility (glass transition) is considered and presented in Figure 136. It can be seen that the yield stress grows up as the glass transition temperature increases following a linear law. Block copolyamide containing high amount PA6HIA (23%) and random copolyamide however diverge from this linear relationship. In both cases, the deviation from the linear dependence could be ascribed to the poorer crystalline packing and the lower crystallites size perfection that should experience easier crystal plasticity (slip and fragmentation). For instance, a lower yield stress is observed for the random i-PA66/6HIA which exhibits chain mobility (Tg) close to that of m-PA66/6HIA copolyamide but poorer crystalline perfection.

To sum up, we can say that for given crystalline features (thickness and perfection), the yield stress of semi-crystalline copolyamides is linearly dependent on the chain mobility (glass transition temperature) of the amorphous phase.

1.2.1.2. **Deformation analysis at the nanometric scale**

The morphological changes at the nanometric scale during the deformation of the studied samples were evidenced by in-situ Small Angle X-ray Scattering (SAXS) experiments on samples submitted to uniaxial loading (~0.5 σ_y). The 2-D patterns at room temperature under two stress level (40 and 55 MPa) in comparison with the SAXS data at the undeformed state are shown in Figure 137. As described in the first part of this chapter, the pattern of the undeformed material appears in the form of an isotropic circle, which is consistent with a random lamellae stacking. Near the center, a high scattering intensity is observed. This is commonly related to preexisting cavities or heterogeneities in the material.

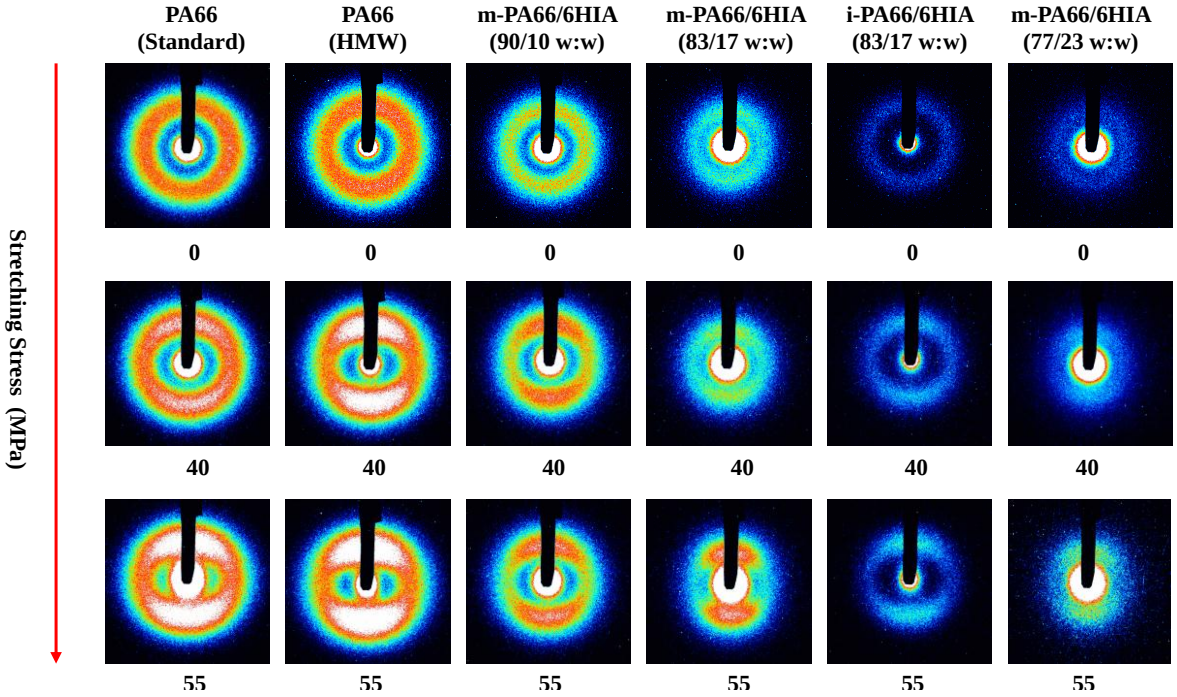

Figure 137: 2-D SAXS patterns for undeformed and uniaxially drawn samples at 23°C. Direction of drawing is vertical. The numbers on the graph indicate stress values in MPa

At 40 MPa (around 50% of the yield stress of standard and HMw PA66), a slight increase of the scattering intensity accompanying by shifting towards lower q in the polar region (parallel to the load direction) is observed. For all material, the isotropic ring is almost conserved which means that neither the lamellar structure nor the random lamella stacking have been destroyed.

This increase of scattering intensity in the polar direction may be correlated to more difference of electron density between crystalline and amorphous phases. In fact, under loading (40MPa), the crystalline lamellae oriented perpendicular to the load direction (mainly located in the equatorial region of the spherulite) are separated. As a consequence, the amorphous phase located in the equatorial region of spherulite will be stretched, mainly by interlamellar slip and interlamellar separation. This results in a volume expansion and then lower electron density of the amorphous phase.

As the deformation proceeds, the scattering intensity becomes more excessive and shifts toward lower q in the polar region while the opposite occurs in the equatorial region (perpendicular to load direction) resulting in an ellipse scattering pattern. For PA66/6HIA

copolyamides, the region of highest intensity becomes roughly separated into two meridional spots, while the equatorial scattering intensity decreases towards the background level. The observation of two point patterns indicates a rise of the number of lamella oriented perpendicular to the load direction. It is assumed that at large stress level, the high stretching of the amorphous chains results in abundant oriented lamellae (perpendicular to the load direction) by means of lamella rotation as schematically presented in Figure 138. Similar observations were also reported for stretched films of PA6 [328].

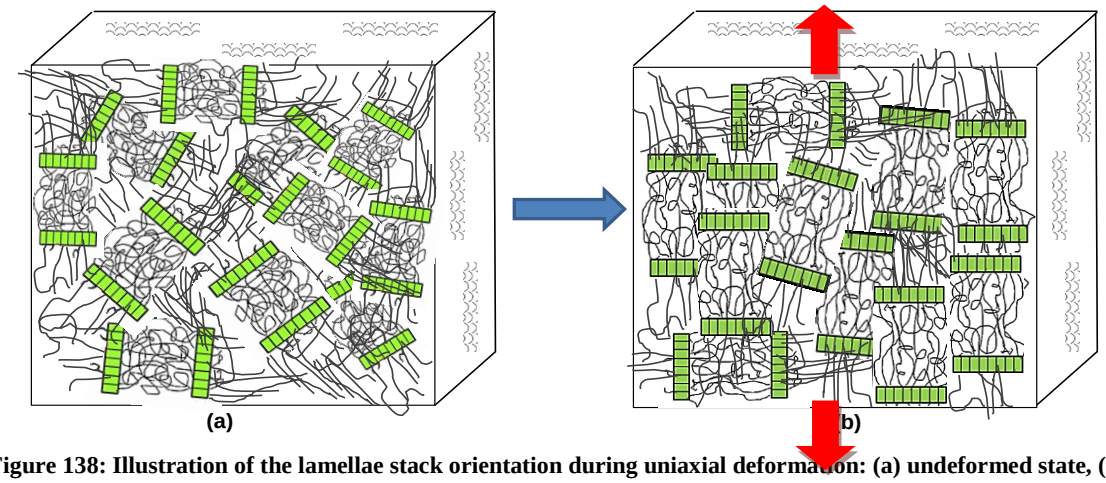

Figure 138: Illustration of the lamellae stack orientation during uniaxial deformation: (a) undeformed state, (b) stretched state, stretching direction is vertical

In order to quantitatively analyze the SAXS data, we have radially integrated the 2-D patterns in the meridional direction (80 ≤azimuthal angular range ≤ 100) and the equatorial direction (170 ≤ azimuthal angular range ≤ 190) as described in chapter II.

The most important changes in the scattering profiles were found to occur in the meridonal direction, corresponding to the equatorial zone of the spherulite. Therefore, the SAXS data for the studied samples are only discussed in the meridional direction. The corresponding absolute intensities (normalized by the samples thickness and experience parameters) at the selected stress levels (40 and 55 MPa) are presented in Figure 139. Changes in the magnitude and position of the scattering intensity can be clearly seen. The long spacing (Lp), estimated from the application of Bragg's law on the maximum of scattering vectors, are given in Table 17.

Sample	σ = 0 MPa		σ = 40 MPa			σ = 55 MPa		
	Q_{max} ($A^{\circ -1}$)	Lp (A°)	Q_{max} ($A^{\circ -1}$)	Lp (A°)	ΔL_P (A°)	Q_{max} ($A^{\circ -1}$)	Lp (A°)	ΔL_P (A°)
PA66 (Standard)	0.0672	93.5	0.0649	96.81	3.31	0.0609	103.17	9.67
PA66 (HMw)	0.063	99.7	0.0609	103.17	3.44	0.0574	109.46	9.73
m-PA66/6HIA (90/10 w:w)	0.0588	106.86	0.057	110.23	3.37	0.055	114.24	7.38
m-PA66/6HIA (83/17 w:w)	0.0565	111.21	0.0535	117.44	6.23	0.0515	122	10.79
i-PA66/6HIA (83/17 w:w)	0.0609	103.17	0.0579	108.52	5.35	0.0567	110.82	7.64
m-PA66/6HIA (77/23 w:w)	0.0532	118.11	0.05	125.66	7.56	0.0487	129.02	10.91

Table 17: Summary of Long spacing for PA66 and PA66/6HIA copolyamides submitted to different stress levels at 23°C

Generally, the maximum of scattering vector is shifted towards lower values as the stress level increases. For instance, Q_{max} of standard PA66 is reduced by 0.007 $A^{\circ-1}$ at 55MPa while that of m-PA66/6HIA(77/23 w:w) is shifted by 0.0045 $A^{\circ-1}$. Moreover, it can be noted that lamella separation ΔL_P, defined as the difference $L_{p(\sigma)} - L_{p(0)}$, increases with increasing the applied stress. It should be noted that at 40 MPa, ΔL_P of PA66/6HIA copolyamides is higher than that of standard PA66 and increases as the PA6HIA content increases (Xc decreases). It is expected that the modulus of the amorphous phase increases with the incorporation of the phenolic ring (HIA) due to strong inter-chains interactions and more rigid moieties. Therefore, lower lamella separation should be observed when the PA6HIA content increases. However, an opposite effect is observed suggesting that lamella separation is rather dependent on the crystalline fraction that on the chain mobility of the amorphous phase. For i-PA66/6HIA copolyamide having similar crystalline fraction to block copolyamide, lower lamella separation than that of m-PA66/6HIA is observed. This suggests that additional microstructural parameters such as lamella thickness and crystallite size perfection may play a role on the lamella separation.

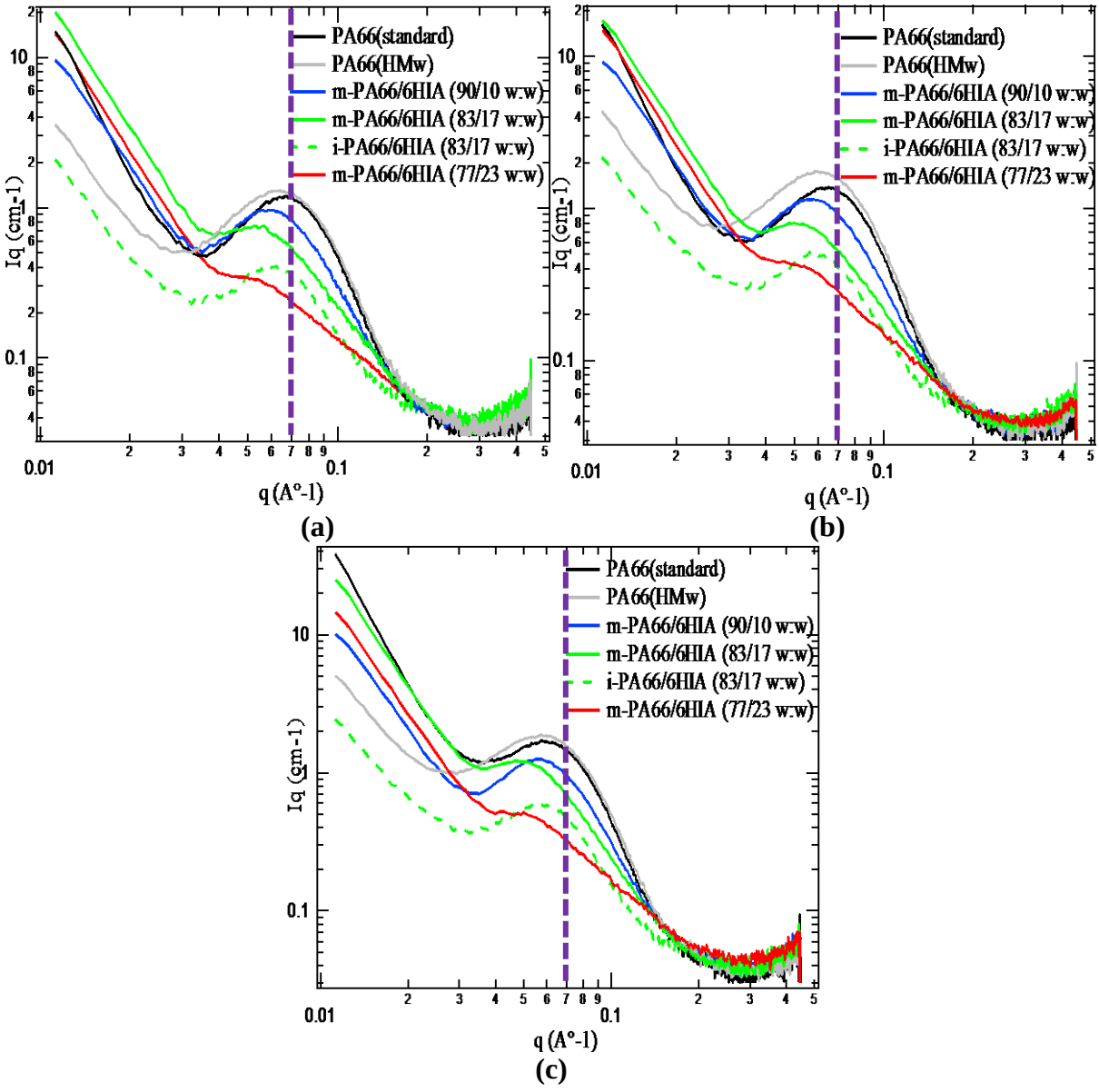

Figure 139: SAXS curves in the meridional direction of PA66 and PA66/6HIA copolyamides at 23°C: (a) undeformed state, (b) applied stress =40MPa, (c) applied stress =55 MPa

At 55 MPa, the lamella separation of standard and HMw PA66 becomes very close to that of PA66/6HIA copolyamides (~9 A°). This observation may be related to the fact that the applied loading level is close to the yield stress of PA66 (0.7 σ_y) where additional processes such as cavitation and crystal slip can be activated.

Furthers information can be deduced from the scattering intensities presented above (Figure 139). Close to the beamstop (q <0.02 $A^{\circ -1}$), a significant difference in the absolute intensity between the un-deformed samples can be noticed. Reminding that high scattering intensity, at low scattering angles is usually attributed to cavities and micro-voids in the materials. By comparing the intensity in this q range, it is appears that in-situ copolyamide has the lowest fraction of preexisting voids followed by HMw PA66, m-PA66/6HIA (90/10 w:w) and then standard PA66 and copolyamide containing 23 % wt of PA6HIA. Surprisingly, m-PA66/6HIA (83/17 w:w) shows the highest scattering intensity which means that it contains the larger fraction of pre-existents voids.

After relatively small stress (σ=40MPa), a slight increase of the scattering intensity can be noted for HMw PA66, whereas at larger stress (σ=55MPa) a significant increase is observed for all samples except copolyamides containing 10 and 23 % wt of PA6HIA. It is speculated that this increase may be related to voids nucleation or to growth of preexisting cavities even if the applied stress is below the yield point. These cavities are supposed to be elongated perpendicularly to stretching direction and are mainly located between the equatorial lamellae of the spherulite.

Finally, it is worth noting that PA66 under 50MPa shows the greater rise of scattering intensity (at least two time higher than I(q) in the un-deformed state).This indicates that the cavitation at this stress level is more abundant in the PA66 than in the PA66/6HIA copolyamides. The aforementioned result suggests that the energy required to nucleate cavities in the amorphous phase of polyamide, under a given stress, is increased by the addition of 6HIA co-monomer, this being precisely what we wanted to obtain.

1.2.1.3. **Local deformation**

From the long period measured along the stretching test at room temperature, the local deformation was calculated using the following equation:

$$\varepsilon_{local} = \frac{\Delta L_p}{L_{p(0)}} \tag{47}$$

where $L_{p(0)}$ is the initial long period at the undeformed state and ΔL_p is the additional lamella separation under loading defined as $L_{p(\sigma)} - L_{p(0)}$.

The local strain ratio is then calculated as below:

$$Ratio = \frac{\varepsilon_{local}}{\varepsilon_{macro}} \tag{48}$$

where ε_{macro} is the applied macroscopic strain during the in-situ SAXS experiments.

In this work, we have been exclusively interested in the visco-elastic behaviour before yielding, where the strain is totally reversible. Thus, we plot in Figure 140, the local strain

ratio (ε_{local} / ε_{macro}), under 40 MPa corresponding to very small strain (<1.5%), versus the crystalline fraction of studied materials. The local strain ratio was only determined for lamellae oriented perpendicularly to the tensile direction (located in the equatorial region of the spherulite) and then submitted to the highest separation.

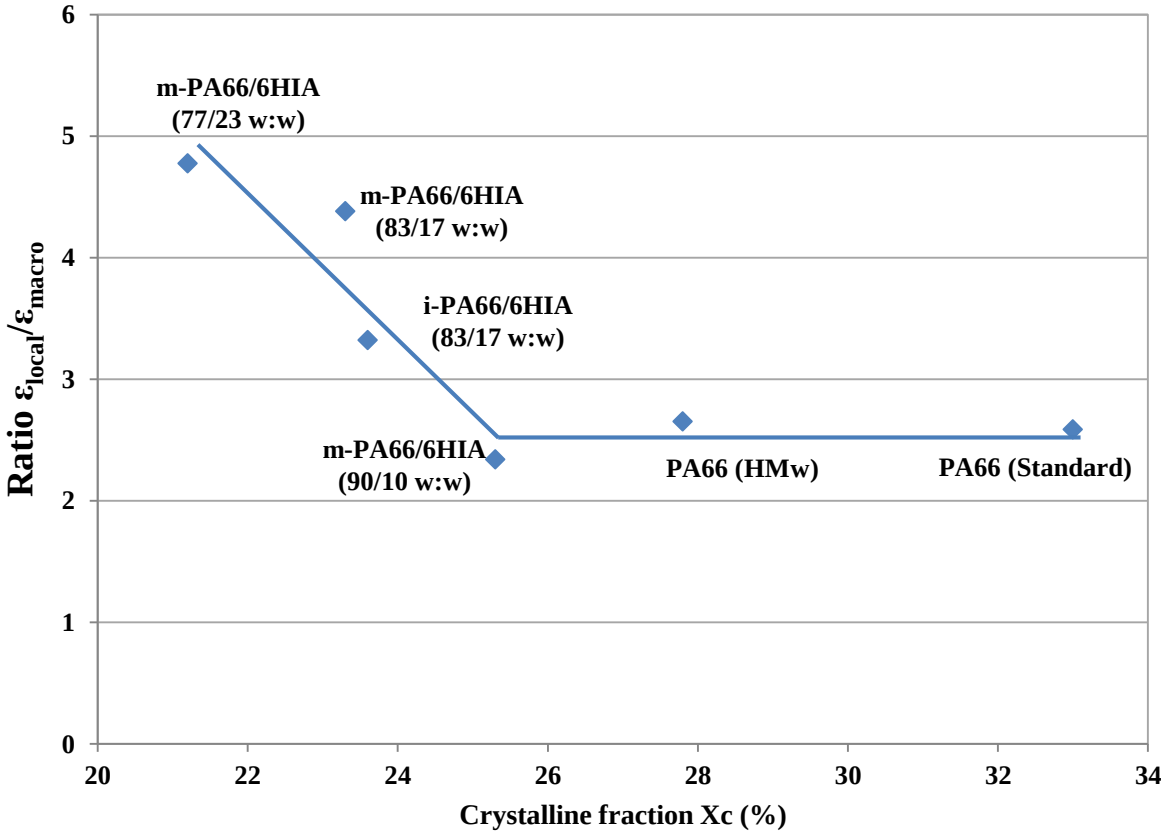

Figure 140: Local strain amplification versus the crystalline fraction of PA66 and PA66/6HIA materials

The ratio $\varepsilon_{local}/\varepsilon_{macro}$ for standard and HMw PA66 is found to be greater than unity (2.5) which means that the equatorial regions are more deformed than the whole sample. For PA66/6HIA copolyamides, a linear dependence of the local strain amplification with the crystalline fraction is observed. The ratio $\varepsilon_{local}/\varepsilon_{macro}$ increases as the crystalline fraction decreases (or the PA6HIA content increases). This means that the equatorial crystalline lamellae of the copolyamides containing high fraction of PA6HIA (lower crystalline fraction) are the most separated. Considering that the equatorial stacks behave approximately as a serie coupling model, it is easy to understand the observed result. In fact, at lower crystalline fraction, the amorphous interlamellar distance is higher and then supposed to be more stretchable. This results in more lamellae separation and then higher local deformation (ε_{local}).

To summarize, in-situ SAXS experiments show that uniaxial load implies local deformation phenomena by means of shearing and lamella separation. This latter, which mainly occurs in the equatorial region of the spherulite, was found to be more noticeable when the crystalline fraction is low (high PA6HIA content).

1.2.2. Above the glass transition

The tensile performance of the studied polymers at temperature above the glass transition (150°C) is illustrated in Figure 141. It can be seen that at the beginning, the stress increases in an approximately linear manner as the applied strain increases. After that, a steadily increase of stress as the drawing evolves, known as strain hardening, is observed at large strain. It is interesting to note that reactive extruded copolyamides shows more noticeable hardening than standard PA66 and in-situ PA66/6HIA copolyamide. Upon straining, polymer chains are aligned in the draw direction, thereby increasing the stress value. The degree of strain hardening depends on the chain mobility and the entanglement density. Taking into consideration that the m-PA66/6HIA copolyamides have higher molecular weight than PA66, it is easy to accept the observed result.

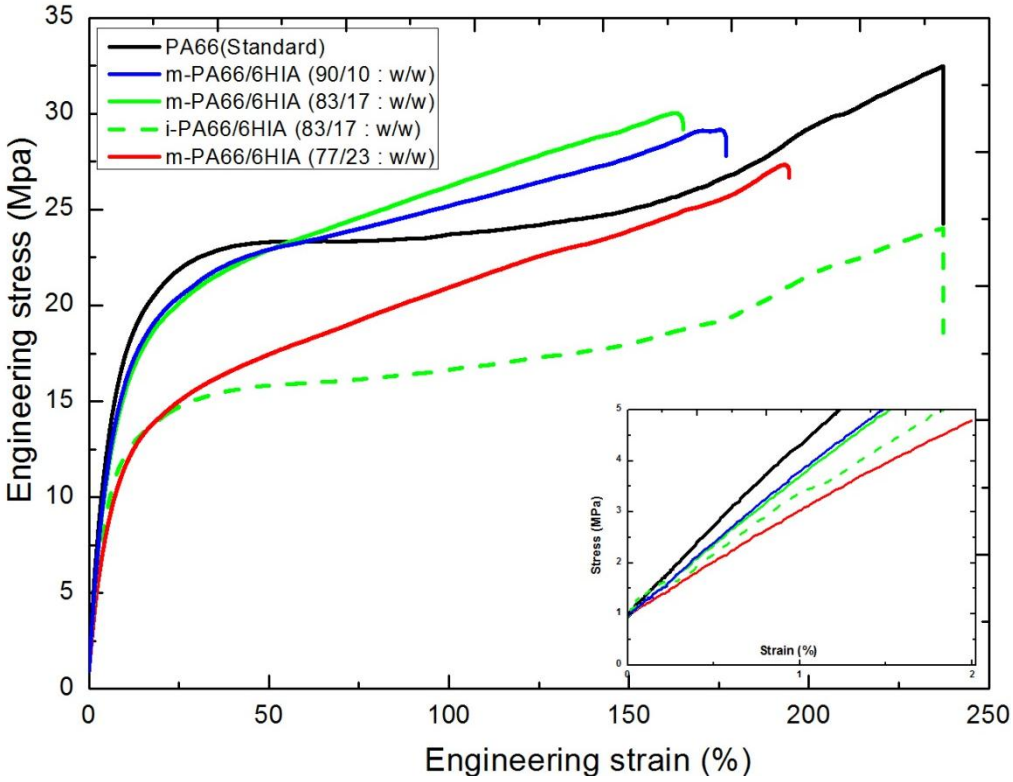

Figure 141: Engineering stress-strain curves from uniaxial tests at 150°C with a crosshead speed of 5mm/min

Strain hardening was not accompanied by macroscopically necking, suggesting that no localization of the stress occurred. In the case of m-copolyamides, the failure took place below 200% strain, whereas standard PA66 and i-copolyamides did not break at the maximum of crosshead displacement of the tensile machine. It is noteworthy that these samples experience an obvious increase of the stress just before the end of the test.

Although the yield stress in not precisely seen, it can be deduced that the yield process for m-copolyamides containing less than 20% of PA6HIA occurs at stress slightly lower than that of PA66 while the yield stress of random and m-PA66/6HIA (77/23 w:w) copolyamides is almost 1.5 factor lower. It is admitted that above the Tg, the lamella is plastically deformed by chain slip as schematically illustrated in Figure 142. Therefore, the lower yield stress of random and m-PA66/6HIA (77/23 w:w), may be related to less resistant crystal (poor crystallite size perfection) to plastic deformation. This may lead to the conclusion that the

Yielding process above Tg is governed by the crystalline phase, mainly by the crystalline perfection and marginally by the lamella thickness.

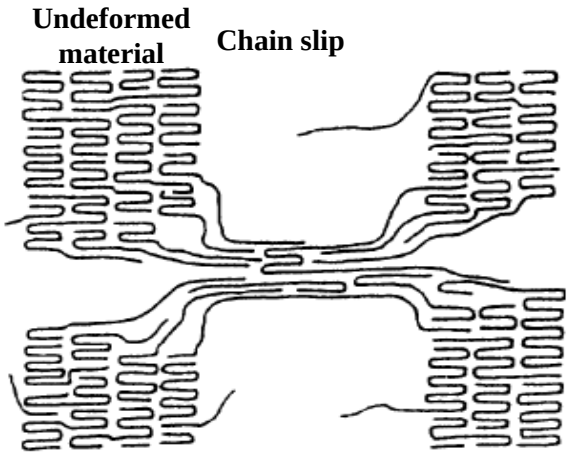

Figure 142: Fragmentation of pilled Lamella into fibrils as proposed by Tagawa et al. [145]

1.2.2.1. **Deformation analysis at the nanometric scale**

The in-situ SAXS experiences were carried out at 150 °C in the same manner as that done at 23°C. The 2-D patterns under 15 MPa in comparison with the SAXS data for the undeformed samples at 150°C are presented in Figure 143.

As described previously, the pattern of the undeformed starting material is in the form of almost isotropic circle, which is a signature of the random spatial organization of the crystalline lamellae. Samples stressed at 15 MPa show comparable changes in the scattering intensity to that stretched at 40MPa at room temperature. Indeed, above the Tg, the polymer chains of the amorphous phase exist at the rubbery state and then they are easily strained at low stress value.

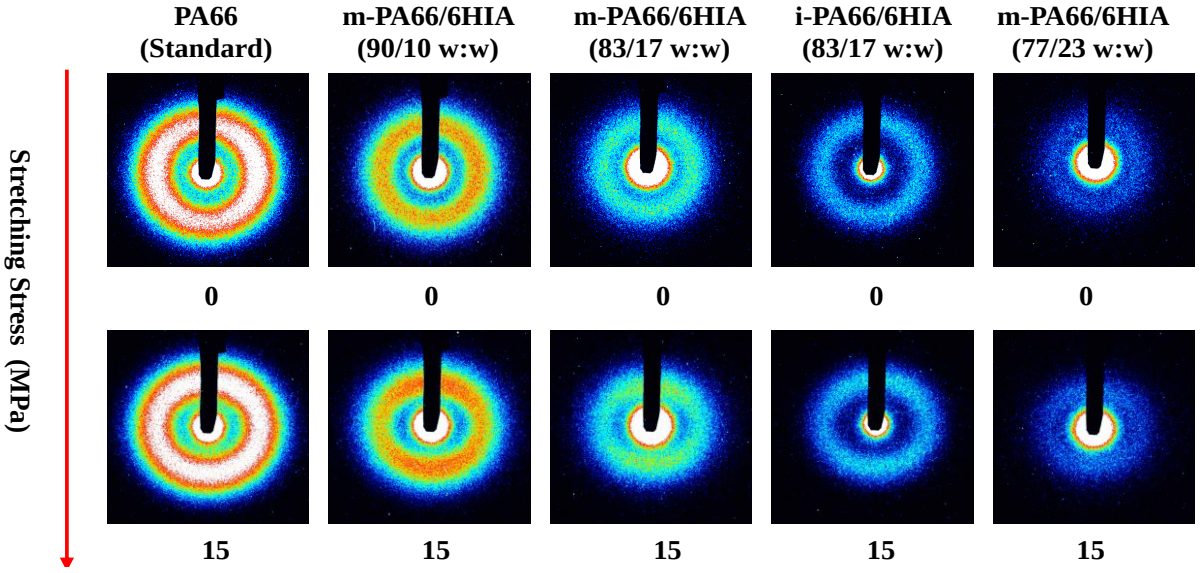

Figure 143: 2-D SAXS patterns for undeformed and uniaxially drawn sample at 150°C. Direction of drawing is vertical. The numbers on the graph indicate stress values in MPa

The analysis of the SAXS profile along the meridional direction for the un-deformed and stretched samples at 150°C is given in Figure 144. A slight increase of the scattering intensity accompanying by shifting towards lower q of the scattering peaks is observed. Apart from these variations, no additional changes can be noted even in the low q range (associated to micrometric voids). This suggests that above the Tg, the sample is mainly deformed by shear and lamella separation and that no cavitation phenomena occurs upon the applied stress.

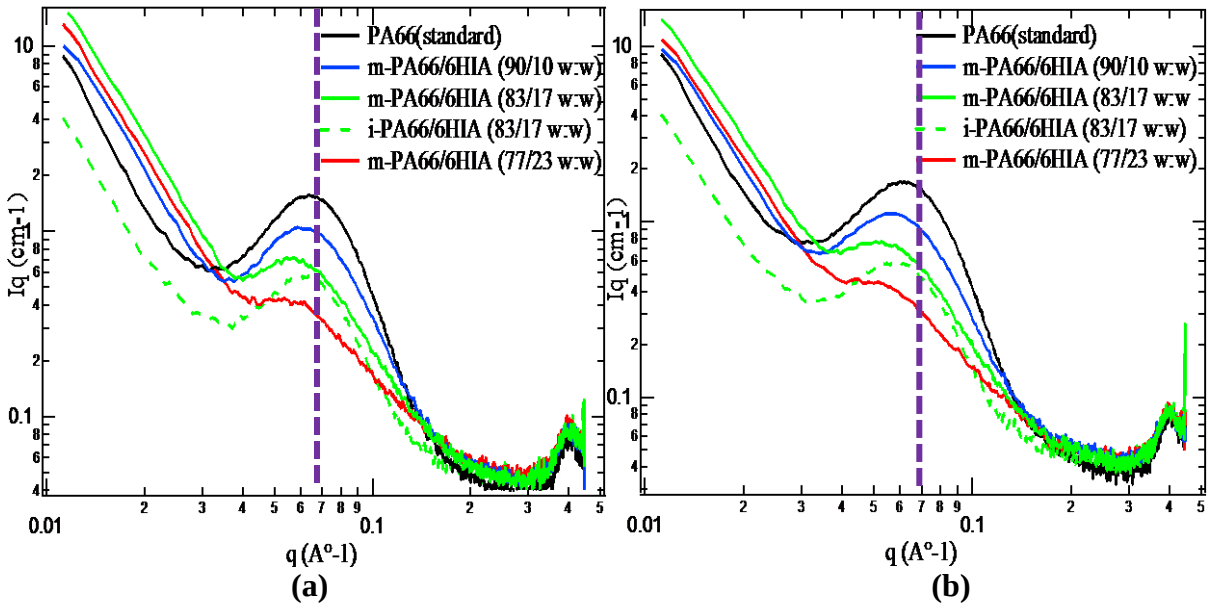

Figure 144: SAXS curves in the meridional direction of PA66 and PA66/6HIA copolyamides at 150°C: (a) undeformed state, (b) applied stress =15MPa

1.3. **Conclusion on the quasi-static mechanical properties**

Tensile tests of PA66 and PA66/6HIA copolyamides were carried out below and above the glass transition temperature (23°C and 150°C). Firstly, it was observed that molecular weight does not significantly affect the elastic modulus of PA66. Moreover, it was found that addition of 6HIA monomer by reactive extrusion does not alter the glassy elastic modulus of the resulting copolyamides while in-situ co-polycondensation of the HIA monomer reduces it. The constant modulus of block PA66/6HIA copolyamides was related to a balance between reinforcing the amorphous phase by the rigid moieties with strong intermolecular interaction and weakening of the crystalline phase. In the case of random PA66/6HIA, the significant drop of the crystalline perfection counterbalances the positive effect of the intermolecular interaction resulting in lower modulus.

It should be noted that above the glass transition, an important drop of the elastic modulus was observed for both random and block PA66/6HIA copolyamides. This stiffness reduction is probably due to the drop of the global crystalline fraction as the PA6HIA content increases.

It was also observed that the yield stress increases as the PA6HIA content increases and that σ_y of block copolyamide is higher than that of it corresponding random copolyamide. However, this latter was found to be more ductile than the block one (high strain level at failure). The evolution of the yield stress with the 6HIA content was correlated to the molecular chain mobility and the crystalline features. It was suggested that block copolyamides containing 23% of HIA and random i-PA66/6HIA copolyamide (83/17 w:w), are less resistant to crystallographic deformation and are then easily stretchable because they have the thinner lamella and the poorer crystallite size perfection.

In-situ tensile SAXS experiments pointed out that uniaxial load implies local deformation phenomena by means of shearing and lamella separation. At higher stress level, lamella separation is more important and further local process such as lamella rotation occurred, resulting in lamella orientation perpendicularly to the draw direction.

Analyses of the long spacing variation in the equatorial region of the spherulite put in evidence that lamella separation is more significant in the case of PA66/6HIA copolyamides having lower crystalline fraction.

At small q range ($q < 0.02\ A^{\circ -1}$), injection molded HMw PA66 and i-PA66/6HIA show the lowest voids scattering intensity, suggesting that these material have the highest density. In addition, it turns out that addition of 6HIA co-monomer reduces the rise of the scattering intensity corresponding to void nucleation or growth. It is presumed that addition of 6HIA co-monomer, offering strong intermolecular interactions, reduces the cavitation under a given applied load.

Finally, the tensile properties above the glass transition temperature were studied. It was found that i-PA66/6HIA and m-PA66/6HIA (77/23 w:w) experiences lower yield stress than the other materials. Here again, it is assumed that crystallite size perfection and lamella thickness have a strong effect on the plastic flow and yielding. SAXS investigations put in evidence once more the separation of the equatorial lamellae, but no cavitation signature was identified at the studied stress level.

2. Impact strength properties

2.1. Brittle-Tough transition

In order to assess the brittle-tough transition temperature ($T_{B/T}$), impact tests were conducted on dry injection-molded specimens of PA66 and PA66/6HIA copolyamides at different temperatures, ranging from -40°C to 150°C.

Figure 145 shows the evolution of the resilience for the studied PA66/6HIA copolyamides as a function of the temperature test. It appears that at low temperature, all PA66/6HIA copolyamides experience small level of resilience corresponding to brittle fracture. As the temperature increases, the resilience level grows up steadily. It should be noted that copolymer containing 10 % wt of PA6HIA exhibits a more pronounced increase of the resilience with the temperature. At around 100°C, a sharp rise of the resilience level is observed accompanying an incomplete failure of the specimen which indicates a tough behaviour. This transition is known as the brittle-tough transition. The brittle-tough transition appears to be shifted toward high temperature as the PA6HIA content increases. This trend will be further explained in the next paragraph. On the other hand, despite similar crystalline fractions and similar phenolic moieties contents, m-PA66/6HIA exhibits lower temperature of brittle-tough transition ($T_{B/T}$) than i-PA66/6HIA. This could be related to the spherulite size difference. In fact, Wright et al., stated that the temperature of impact transition ($T_{B/T}$) of PP was found to decrease with decreasing spherulite size [329].

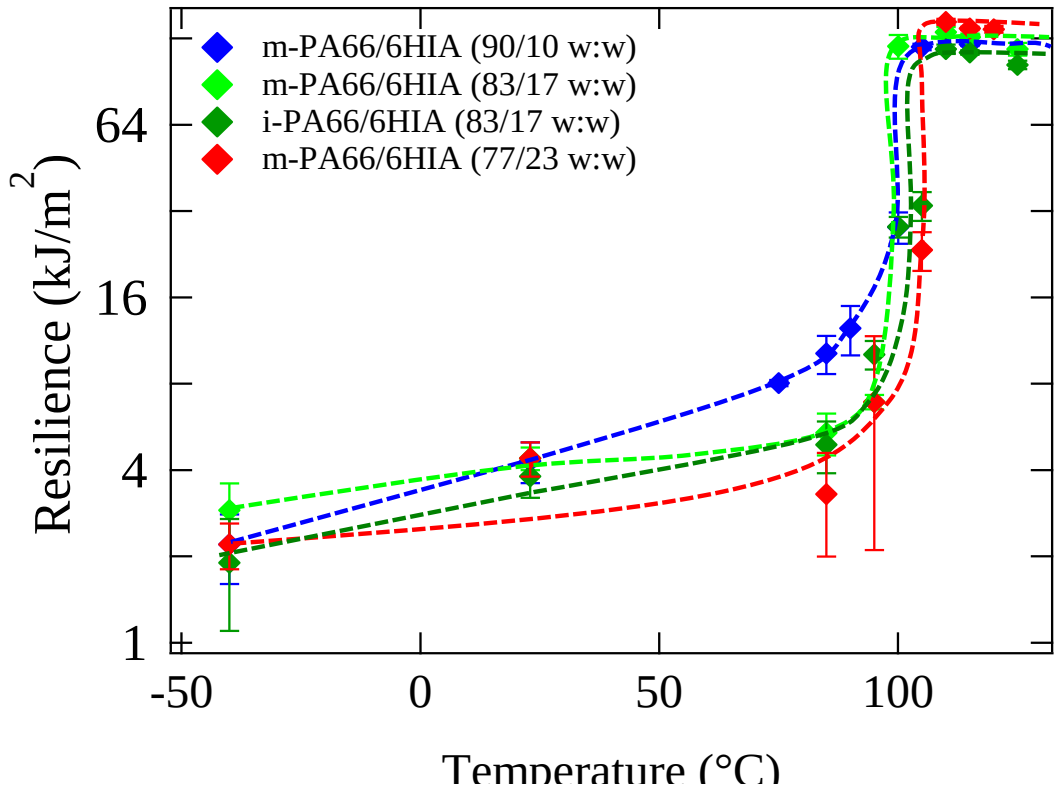

Figure 145: Brittle-tough transition curves of the PA66/6HIA copolyamides. Dashed curves are fitted sigmoids between points

A previous PhD in our lab [81] established that the brittle-tough transition temperature of various polyamides 66 modified at the molecular scale was linearly related to the Tg of the polymer, a wide range of Tg's being obtained by assessing the materials in different hygrometry levels (dry state, conditioned at HR50, conditioned at HR100). These results are plotted in Figure 146, our own results being also reported for the comparison. It can be seen that the $T_{B/T}$ of random and block copolyamides follow the linear relationship obtained by Rios. This confirms that the brittle-tough transition is directly related to the molecular chain mobility of the amorphous phase and it suggests that the crystalline phase (crystalline fraction, lamella thickness and perfection) as well as the molecular weight do not significantly affect this transition temperature.

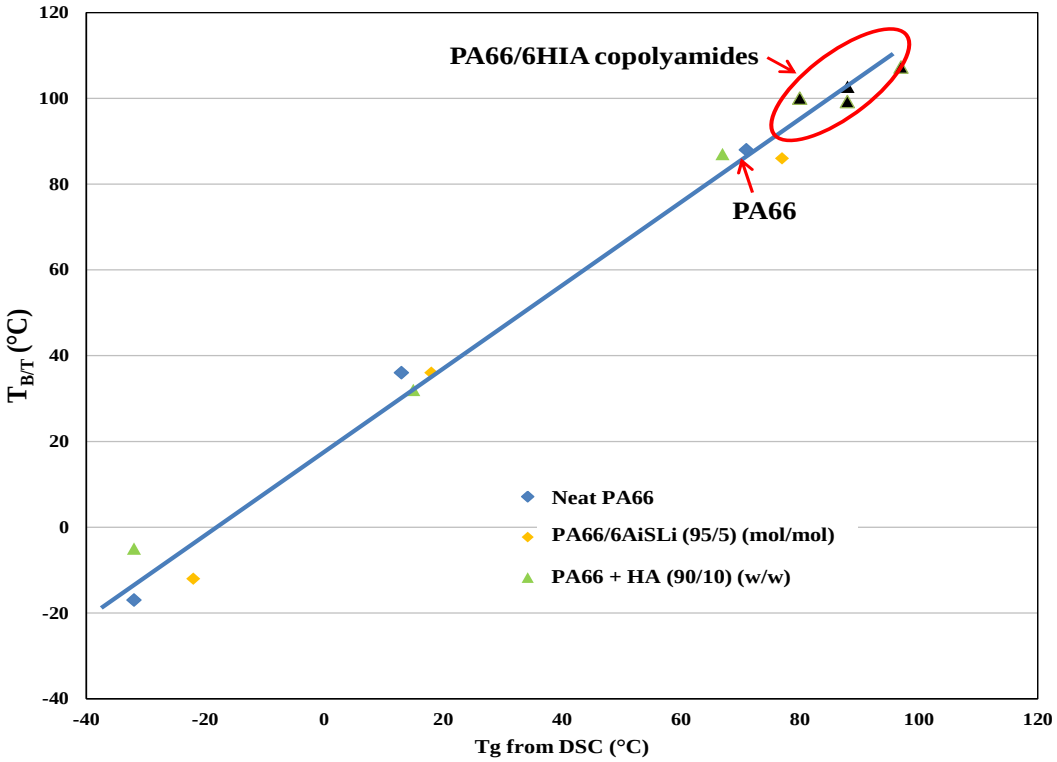

Figure 146: Plot of the brittle-tough transition temperatures of PA66/6HIA copolyamides according to the linear correlation, established by Rios et al., between the $T_{B/T}$ and the Tg of different polyamide 66 formulae [81]

2.2. **Impact resilience**

Figure 147 shows the resilience values taken at room temperature (23 °C) for the studied copolyamides in comparison with that of standard injection-molded PA66. As the brittle-tough transition temperatures of PA66/6HIA copolyamide are higher than that of PA66, at a given temperature (below $T_{B/T}$), the resilience of these copolyamides is expected to be lower than that of PA66, resilience increasing steadily with the temperature on the brittle plateau. However, the resilience of the block m-PA66/6HIA copolyamides is globally 30 % higher than that of standard PA66. This suggests that PA66/6HIA copolyamides are more tough than PA66 upon impact. Although, random copolyamide has higher resilience value than that of PA66, it appears less resilient than block copolyamides.

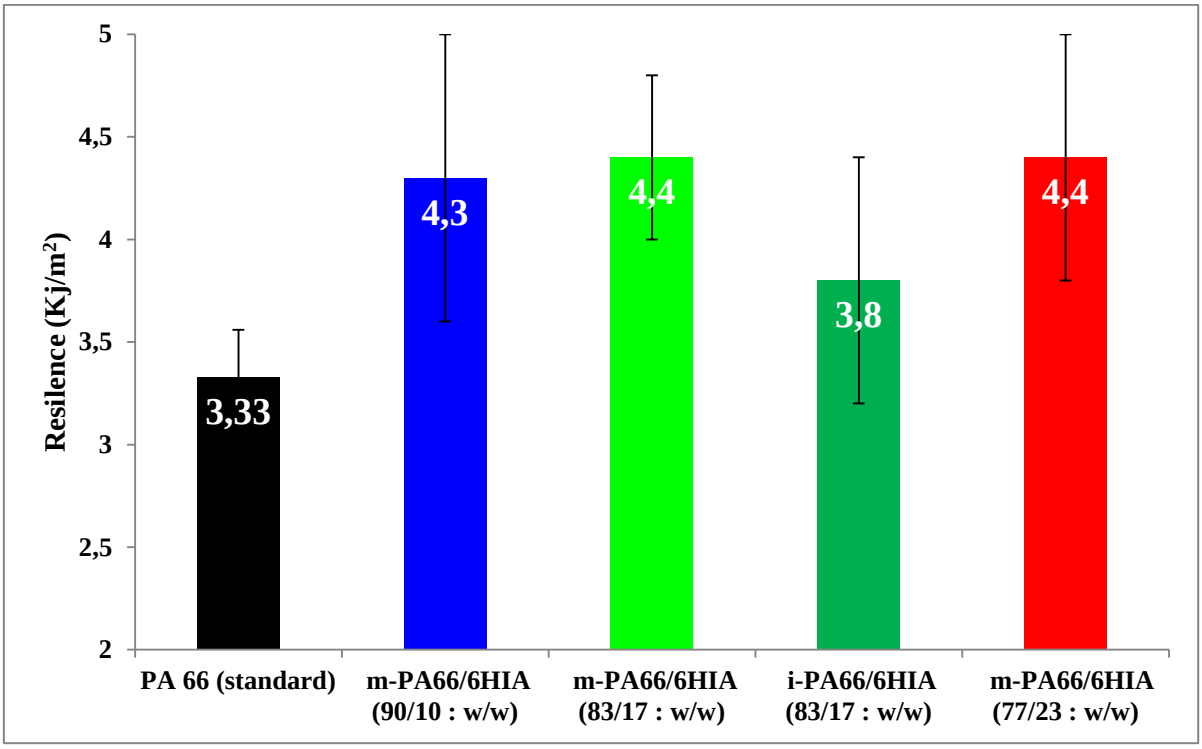

Figure 147: Resilience values at 23°C of the dry state PA66/6HIA copolyamides compared to standard PA66

The high resilience values observed in the case of PA66/6HIA copolyamides might be apparently related to the incorporation of the 6HIA co-monomer. However, further parameters contribute to the obtained result such as the lower crystalline fraction and higher molecular weight. Indeed, Starkweather et al., pointed out that impact strength of PA66 and PA610 drops with increasing sample crystallinity, and that at a constant level of crystallinity, impact resistance increased as the molecular weight increases [104,108].

On the other hand, several works devoted to the relationship between the resilience and the spherulite structure presume that impact resistance is inversely related to spherulite size [105,106,329–331]. Therefore the low resilience value of i-PA66/6HIA copolyamide may originate from the presence of defects between the large spherulites of the material which may have great effect at high strain rate.

3. Long term mechanical properties

3.1. Fatigue lifetime curves

Wöhler (S-N) curves from the tension-tension fatigue tests are presented in Figure 148, where the average of number of cycles at failure (N) is plotted as a function of the maximum of applied stress. It can be noted that the logarithm of fatigue lifetime of PA66 decreases linearly with increasing the maximum of applied stress according to the following equation:

$$\sigma_{max} = -A \log N_F + B \quad (49)$$

where A and B, constants depending on the material and on the experimental conditions.

Figure 148-a shows that HMw has a fatigue lifetime higher than that of standard PA66 under the same applied cyclic stress. This can be understood on the basis of higher chain entanglement and tie molecules density that enhances the endurance of semi-crystalline polymers [175,179]. This benefit is more obvious at high stress regime, approximately above 45MPa. For instance, at σ_{max} = 60 MPa, N_f = 67000 for HMw instead of 8000 in the case of standard PA66. This represents a fatigue lifetime improvement of 700% at high stress level. However, this positive effect on fatigue lifetime does not exceeds 13% at low stress level (σ_{max} = 40 MPa). We suppose that at low loading values, the fatigue lifetime could be more affected by the drop of the crystalline fraction (-5%) than by the molecular weight increase. A similar conclusion was drawn by Niinomi et al. on the effect of molecular weight on fatigue performance of ultra-high molecular weight polyethylene (UHMWPE) [180].

Wöhler curves of m-PA66/6HIA copolyamides, presented in Figure 148-b, show that fatigue lifetime of m-PA66/6HIA (90/10 w: w) is increased by 193 % at σ_{max} = 60 MPa and still increased by more than 170% at low stress (σ_{max} = 40 MPa) compared to the standard PA66. This fatigue lifetime enhancement may originate from the increase of the molecular weight as well as from the introduction of phenol moieties offering strong H-bonds interactions.

As the PA6HIA content increase, the beneficial effect appears to decrease and even a deterioration of the fatigue resistance can be noted. For instance, m-PA66/6HIA copolyamide containing 23% wt of PA6HIA exhibits two fatigue regimes. In the high-stress regime, approximately above 50 MPa, longer fatigue lifetime than that of standard PA66 is obtained while noticeable reduction of the fatigue resistance is observed at low stress values.

As discussed in the case of HMw, the higher lifetime in the high-stress regime may be related to the higher tie molecules density (higher Mw than standard PA66) while the lower fatigue resistance at low stress can be related to the negative effect of the drop of the crystalline fraction. Moreover, the lower lamella thickness and crystallite size perfection in the case of copolyamide containing 23 % wt of 6HIA may considerably reduce the fatigue endurance and then counterbalance the positive effect of tie molecule and strong H-bonds interactions given by the HIA monomer.

It can be seen from Figure 148-c, that the fatigue lifetime of i-PA66/6HIA copolyamide is lower than that of standard PA66 on the whole applied stress range. Reminding that in-situ copolyamide has similar molecular weight to that of standard PA66 but lower crystallinity,

thinner lamella and lower crystal perfection. Consequently, the obvious reduction of fatigue performance may originate from the deterioration of the crystalline features of PA66 in the copolymer.

Figure 148-d highlights the impact of the preparation method of PA66/6HIA copolyamide on its fatigue performance. It clearly appears that fatigue resistance of reactive extruded m-PA66/6HIA (83/17 w:w) copolyamide largely outperforms that of the corresponding in-situ copolymerized copolyamide i-PA66/6HIA (83/17 w:w), even if they similar mobility chains (comparable Tg). This can be understood on the basis of the microstructural characteristics of these copolymers. As far as the former one is concerned, it has an obvious high molecular weight; however, for the latter, remarkable decline of the crystal perfection and a slight thinner lamella are noted.

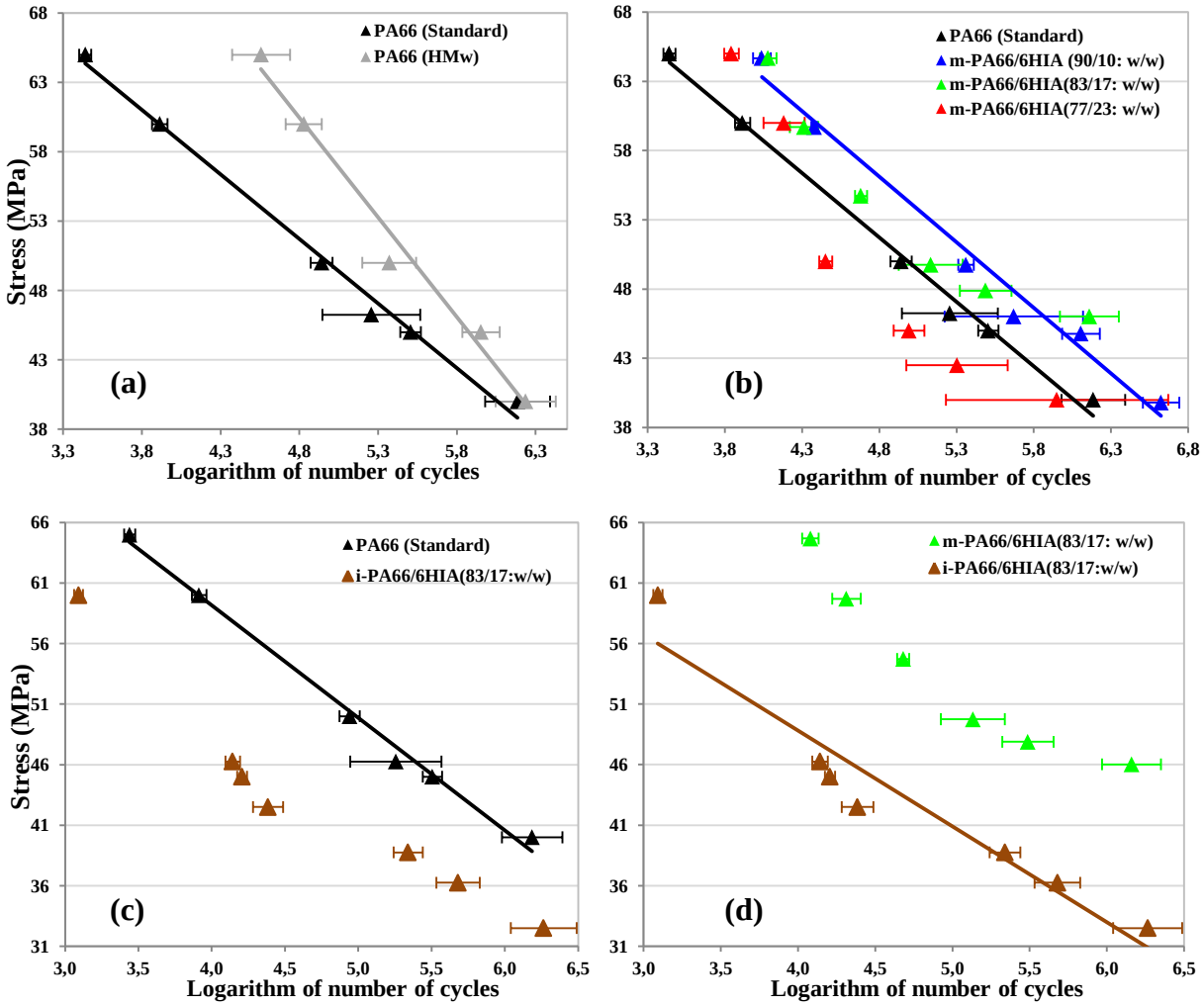

Figure 148: Stress-Fatigue lifetime curves at 23°C, R=0.1, f=5Hz for: (a) standard PA66 vs HMw PA66; (b) m-PA66/6HIA copolyamides vs standard PA66; (c) i-PA66/6HIA copolyamide vs standard PA66; (d) m-PA66/6HIA vs i-PA66/6HIA copolyamides

The maximum of applied stress divided by the elastic modulus (Stress/Young modulus) versus the number of cycles to failure (N_f) for the studied materials are shown in Figure 149. The same conclusions drawn above for m-PA66/6HIA copolyamides can be also noted for the normalized Wöhler curves.

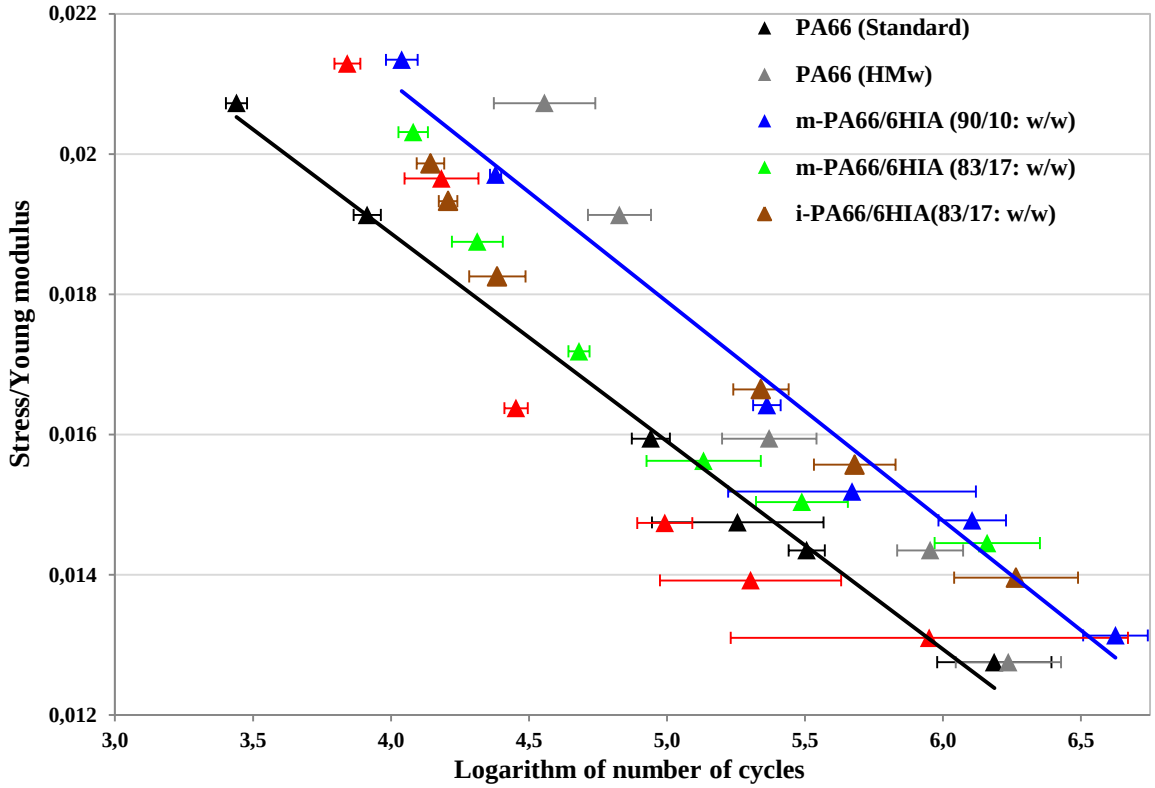

Figure 149: Wöhler curves normalized by Young's modulus at 23°C for PA66 and PA66/6HIA copolyamides, R=0.1, f=5Hz

When comparing the fatigue performance of reactive extruded copolyamide with that of HMw polyamide 66, many factors should be taken in consideration. Firstly, the molecular weight distribution. Even if reactive extruded copolyamides have comparable Mw to that of HMw PA66, their molecular weight distribution are very different. Indeed, m-PA66/6HIA copolyamides have noticeable fraction of chain having low molecular weight (comparable to that of standard PA66) which may reduce the tie molecules density. Moreover, short chains are less resistance to stretching (no entanglement network) and then can be considered as a weakness points under loading. Secondly, the crystalline fraction, lamella thickness and crystallite size perfection are lower in the case of m-PA66/6HIA copolyamides especially at high PA6HIA content (23 % wt). Accordingly, it should be expected that m-PA66/6HIA copolyamides experience lower fatigue resistance than HMw PA66. Surprisingly, m-PA66/6HIA (90/10 w:w) copolyamide shows superior fatigue performance than that of HMw PA66, particularly at low regime stress. This fatigue lifetime enhancement may be related to the modification of the cohesive energy of the amorphous phase containing phenolic functions (HIA) with strong H-bonds interactions. By increasing the PA6HIA content, the enhancement of the cyclic fatigue performance is not observed. It seems that the impact of the deterioration of the crystalline phase (negative effect) overcomes that of the high cohesive energy of the amorphous phase, resulting in lower fatigue resistance.

It is worth to mention that, at given (σ_{max}/E), i-PA66/6HIA copolyamide shows higher fatigue lifetime than the standard PA66 while the opposite trend was identified when comparison was made at the same applied stress (Figure 148-c). This indicates that this copolyamide is more resistant than standard PA66 when stretched at certain macroscopic deformation, whereas it fails quickly when submitted to a given applied stress, probably due to the drop of its elastic modulus.

3.2. **Full strain field**

In Figure 150, we present the axial strain field, characterized by digital image correlation, for specimens fatigued at different levels corresponding to 0; 25; 50 and 75% of the total lifetime, varying between $3x10^5$ and $3x10^6$ cycles, under an applied stress of 45MPa.

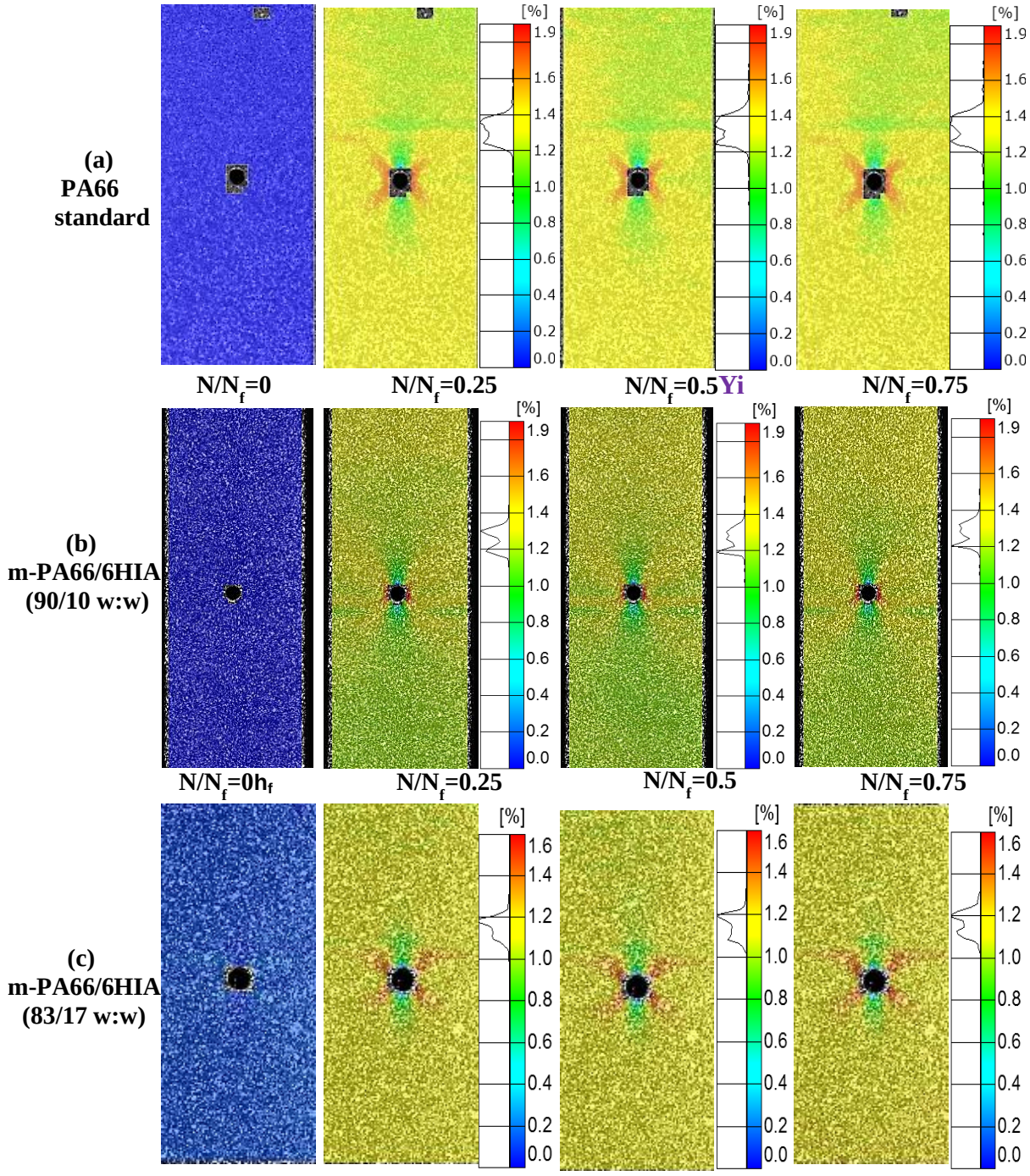

Figure 150: Axial strain filed (%) for specimens subjected to the cyclic fatigue of $N/N_{failure}$=0; 0.25; 0.5 and 0.75 under applied stress of 45 MPa for: (a) PA66 standard; (b) m-PA66/6HIA (90/10) and (c) m-PA66/6HIA (83/17)

It can be seen that the strain field is not homogenous especially in the area close to notch. For example, the overall strain value for standard PA66 specimen is around 1.3% versus 1.9 %

near the hole. This important anisotropy of macroscopic deformation can be related to the heterogeneous stress field in the presence of discontinuity. As presented in the second chapter section 4.5, the stress value at the equatorial edge of the hole is three times higher than the macroscopic applied stress and then decays rapidly with increasing distance from the notch. So, the damage will be probably initiated at the edge of the hole even if it is not obviously clear on the strain field image.

With increasing the number of cycles, the maximum of the axial strain is slightly shifted towards higher value and the distribution becomes broader, suggesting that additional damage generation occurs along the fatigue test. The same trend is observed in the case of PA66/6HIA copolyamides but with lower strain levels than those measured in the case of PA66. For instance, the axial strain distribution in the case of PA66/6HIA (83/17 w:w) is centered around 1.1% instead of 1.3% for standard PA66. This observation is more obvious close to the hole area where the highest axial strain value shifts from 1.9% to 1.6 % after adding 17 % of PA6HIA. This result is quite surprising since the lamella separation in the equatorial zone of PA66/6HIA copolyamides is higher than that of standard PA66. A more detailed analysis of the localized damage near to the equatorial edge of the hole is discussed later.

3.3. **Stiffness evolution**

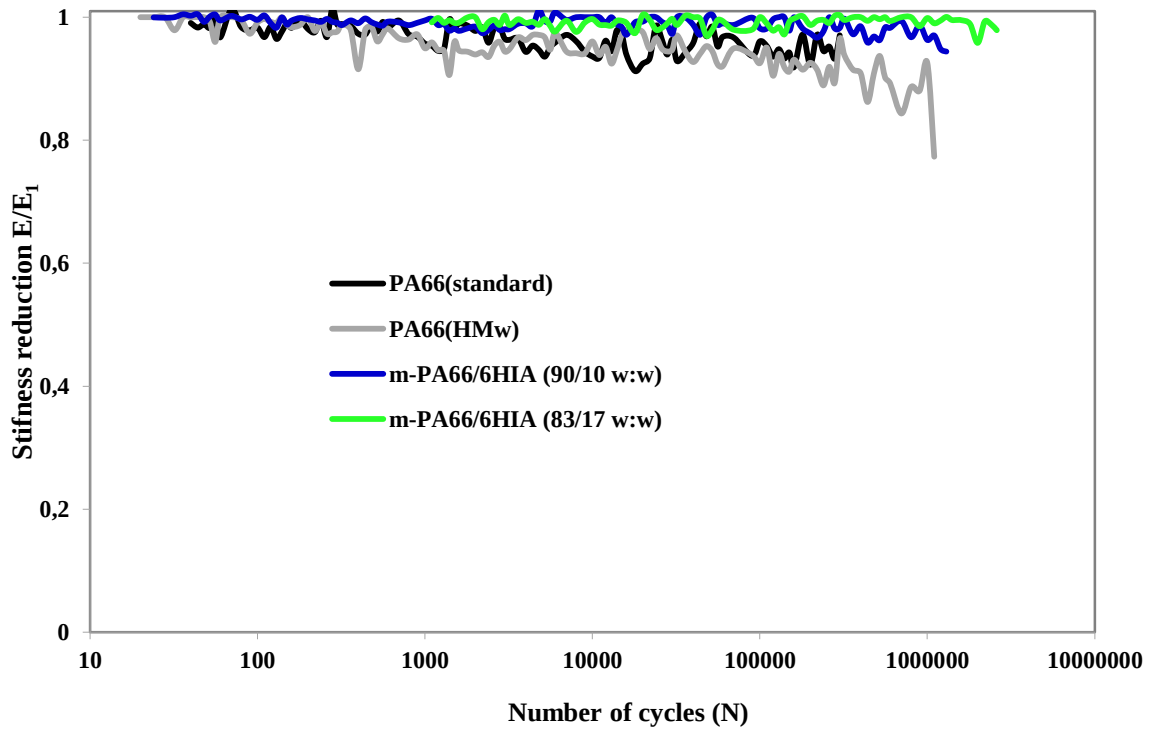

Figure 151: Evolution of damage (E/E_0) with the number of cycles near the equatorial edge of the hole under 45 MPa

The local damage was quantified by means of the relative modulus in the highly stressed point (close to the equatorial edge) as described in the second chapter. Figure 151 shows the damage evolution at around 500µm close the hole as a function of the number of cycles for PA66 and PA66/6HIA specimens submitted to 45 MPa at room temperature. In accordance with the previous work of Mourglia-Seignobos on un-notched PA66 specimens [233], the

modulus ratio (E_n/E_1) decreases roughly linearly with the logarithm of the number of cycles until failure. During the first 1000 of cycle, the ratio (E_n/E_1) is close to unity which indicates that no damage was initiated, then a steadily decrease of the relative stiffness is observed corresponding to damage initiation and growth. The final failure occurred when the stiffness reduction reach a certain critical value.

Apparently, the slope of stiffness decline is sharper for standard PA66 and HMw than in the case of PA66/6HIA copolyamides, suggesting that damage is less pronounced in PA66/6HIA copolyamides. However, this assumption should be confirmed due to low precision of the digital image correlation close to the hole on certain samples. Indeed, the modulus ratio was calculated on the basis of strain value taken, as far as possible, at 500 µm away from the right-hand edge of the hole (see chapter II paragraph 4.5.2). Moreover, the analyses were done only one time because of the lack of time (we have spent a lot of time to put in place this method).

3.4. **Fatigue damage analysis**

3.4.1. Microscopic characterizations

The fatigue damage was first explored through scanning electron microscopy (SEM) observations. SEM micrographs of cryo-fractured specimens fatigued at different levels corresponding to 0, 75 and 100 % of the total lifetime are presented in Figure 152.

It can be seen that all non-fatigued specimens already contain numerous cavities with a diameter varying from few nanometers to 1 micrometer. These cavities are certainly generated during the injection-molding process, likely due to the shrinkage of the polymer during cooling in the mold. In the case of fatigued specimens at 75% of their total lifetime, similar spherical cavities of size ranging from 10 nm up to 1µm can be also identified. It is assumed that cyclic loading results in more voids nucleation and cavities growth; however it is difficult to precisely quantify the fraction of generated damage because of the wide distribution of the cavities size.

Two distinct zones were identified on the fracture surface of broken specimens (N/N_f =1): a ductile area close to the edge of the central hole and a brittle area at around 2mm form the edge of the hole. The brittle zone consist in a smooth fractographic surface while the ductile one is composed of highly deformed polymer containing an array of large voids (around 2µm of diameter), as shown in Figure 152. It is believed that when the ductile zone reaches a certain critical size, the microcrak propagates quickly resulting in brittle surface separation. So, we suppose that the large voids observed in the ductile are formed well before the complete surface separation.

The SEM fractographs of m-PA66/6HIA (90/10 w:w) show that the surface is slightly smoother than that of standard PA66. However, no obvious difference between failure modes of the studied samples is identified.

To sum-up, SEM observations suggests that the failure mode is the same for standard PA66 and PA66/6HIA copolyamides but they do not provides enough information on the damage mechanism, supposed to be at the origin of the fatigue lifetime difference. In this regard,

damage characterizations by Ultra Small Angle X-ray Scattering (USAXS) are now presented.

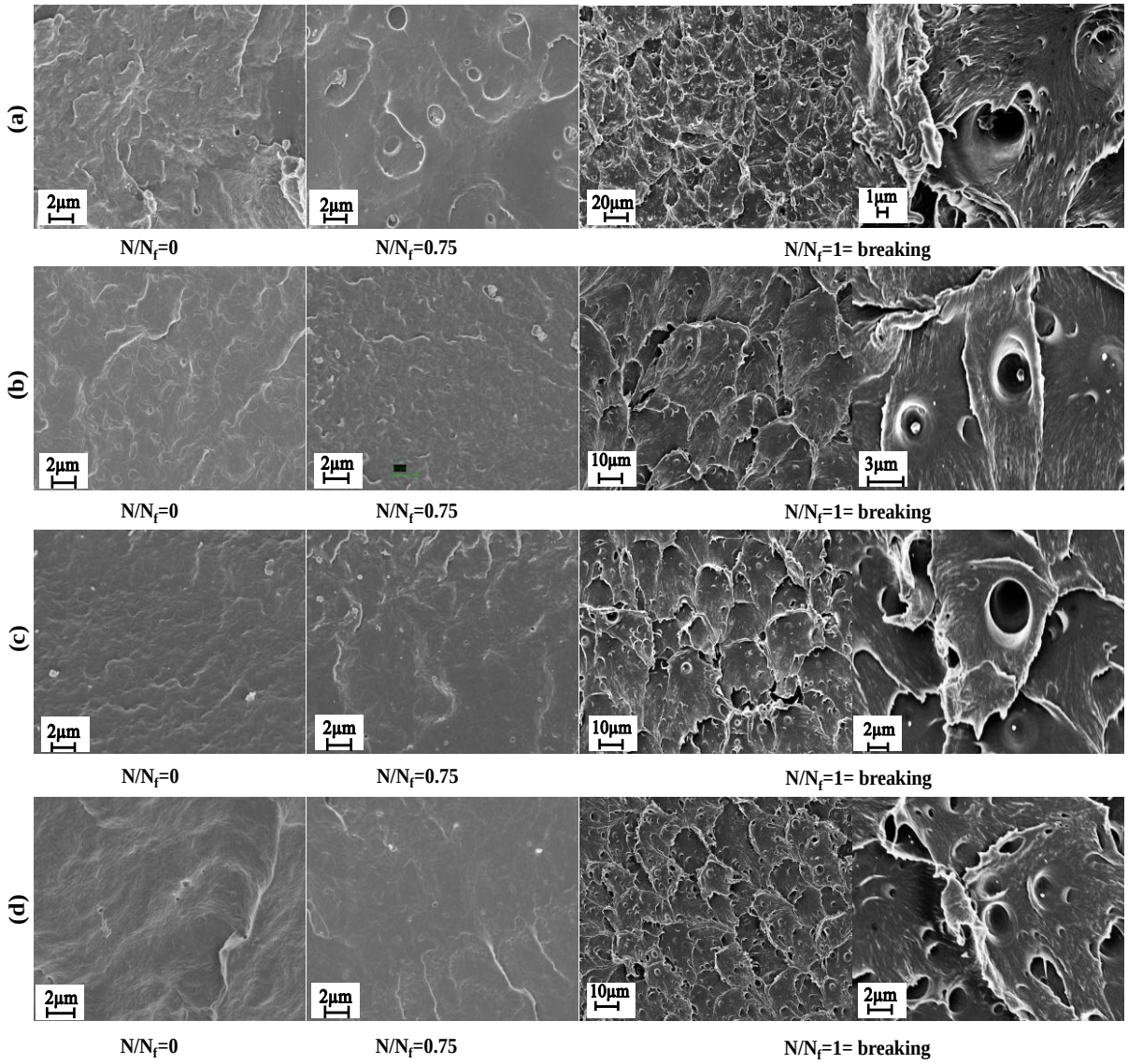

Figure 152: Fracture surfaces of axial fatigued specimens at $N/N_{failure}$=0; 0.75 and 1 (breaking) under maximal stress of 45 MPa for: (a) PA66 (standard); (b) m-PA66/6HIA (90/10 w:w); (c) m-PA66/6HIA (83/17 w:w) and (d) m-PA66/6HIA (77/23 w:w).

3.4.2. Ultra Small Angle X-ray Scattering

Damage or cavitation under cyclic loading was characterized by Ultra Small Angle X-ray Scattering (USAXS) as it gives information on the electron density fluctuations inside the material. As described in the second chapter, specimens fatigued at different level were hit by the X-ray beam at 300 µm away from the equatorial edge of the hole in order to analyze the damage in the highest stressed area. It should be noted that USAXS experiments were equipped with 1-D direction detector and then two measurements have been performed: Firstly the scan direction was parallel to the long axis of the specimens (parallel to load direction) and secondly orthogonally to the long axis of the specimen (perpendicular to load direction).

The variation of scattering intensity for PA66/6HIA copolyamides as a function of scattering vector (q) and the fatigue level are plotted in Figure 153.

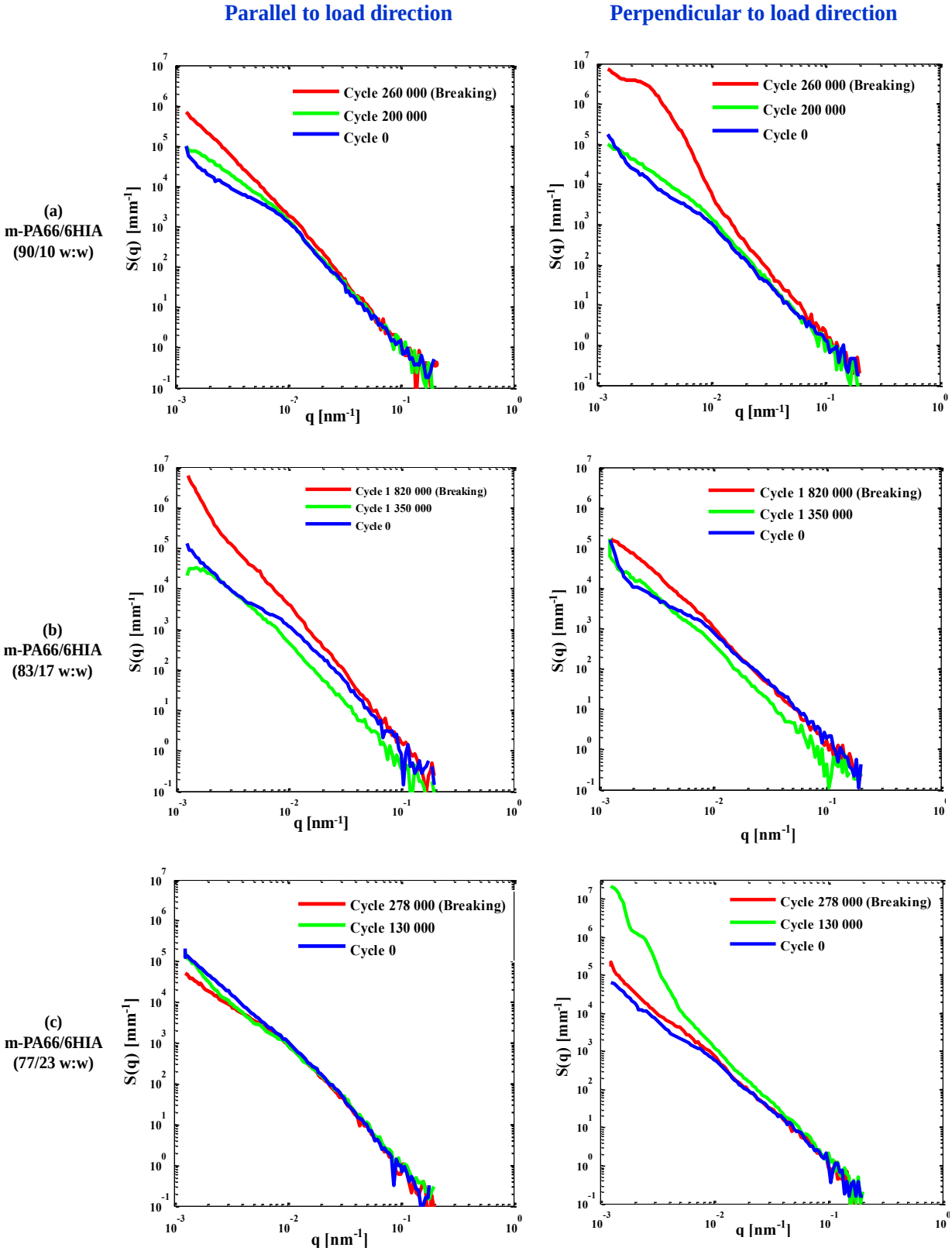

Figure 153: The absolute intensities of USAXS as a function of scattering vectors in the parallel and perpendicular direction to the load, determined at $N/N_{failure}$=0; 0.75 and 1 (breaking) under an applied stress of 45MPa at room temperature for: (a) m-PA66/6HIA (90/10 w:w); (b) m-PA66/6HIA (83/17 w:w) and (c) m-PA66/6HIA (77/23 w:w)

In the scattering vector range from 10^{-2} to 0.2 nm^{-1}, the scattering intensity profiles appear to be relatively identical in both directions (parallel and perpendicular) at the different fatigue levels. However, noticeable differences are observed at low scattering angle. For instance, m-PA66/6HIA (90/10 w:w) shows an increase of the scattering intensity with number of cycle which is more obvious at the failure. It is noteworthy that the intensity increase is almost two decades more important in the orthogonal direction (perpendicular to load direction) than in the parallel direction to the load. This increase of scattering intensity along the fatigue test could be attributed to the formation and/or growth of cavities. In fact, the scattering intensity at cycle 0 mainly originates from the presence of existent cavities formed during the injection molding. As the fatigue test proceeds, new voids nucleate and subsequently grow resulting in higher scattering intensity. The size distribution of these voids can be quantified by using the function model established by Beaucage in the case of polydisperse spherical particles (see second chapter section4.6.2). Figure 154, presents the curves fit of the experimental absolute intensity obtained for m-PA66/6HIA at cycle 0 and at the failure in the orthogonal direction to the load. It can be seen that the fit curves roughly superpose with the experimental data. The estimated average size of the existent cavities (cycle 0) is 300 nm while that of cavities at failure is found to be equal to 800 nm. In the parallel direction, the average size of the voids at failure is very close to the initial size (around 300 nm) which suggests that the nucleated cavities are essentially oriented parallel to load direction as schematically shown in Figure 155.

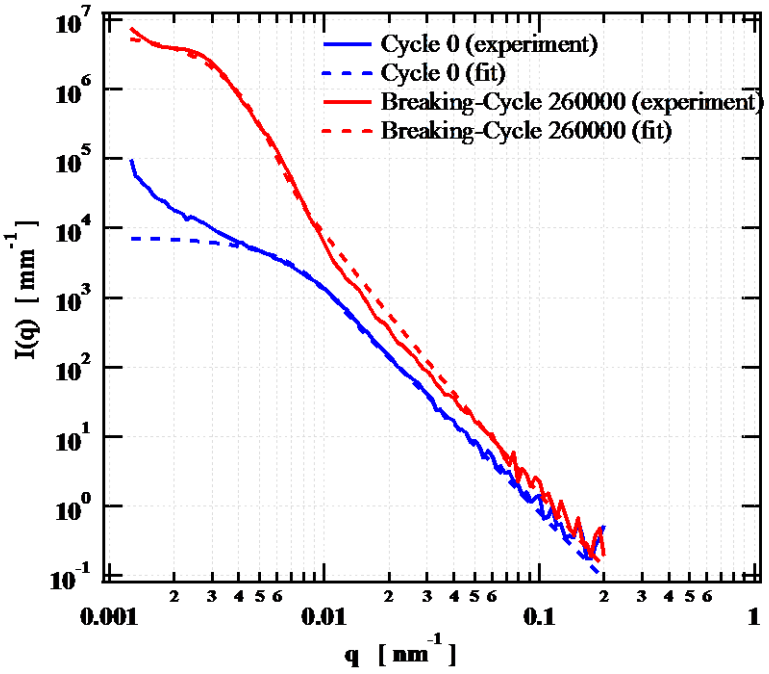

Figure 154: 1-D experimental USAXS data and Beaucage fit curves of the absolute scattering intensity for m-PA66/6HIA (90/10 w:w) submitted to a maximum cyclic stress of 45 MPa

For the copolyamide PA66/6HIA (83/17 w:w), the scattering intensity also increases when the fatigue test proceeds indicating cavities nucleation and growth. However, the intensity increase is more pronounced in the parallel direction (along the load direction) than in the perpendicular direction which suggests that the nucleated cavities are mainly extended perpendicularly to the load direction. This result is in good agreement with the conclusion drawn by Mourglia-Seignobos et al. on standard PA66 [233]. They reported that cyclic

loading of standard PA66 induces significant increase of the scattering intensity in the parallel direction versus negligible changes in the orthogonal direction.

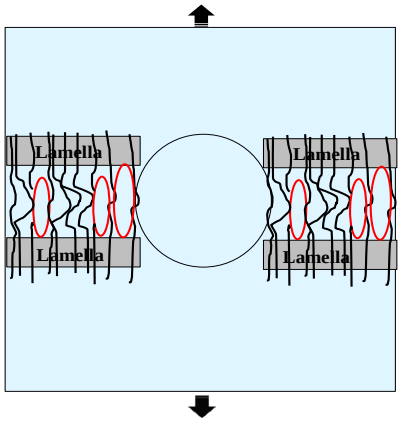

Figure 155: schematic illustration of cavity's location in the amorphous layer at given stretched state.

The same observations noted for the copolyamide m-PA66/6HIA (90/10 w:w) were observed in the case of copolyamide with 23 % wt of PA6HIA. However, the profile of the scattering intensity at ultra-small angle (< $3x10^{-3}$ nm^{-1}) is quietly different. This result let us think that at least two elliptical cavities populations of different size are present in the material. It can also be noted that scattering intensity at failure is lower than that at 75% Nf. An explanation for this difference may be that the analysis was not made at the same distance from the hole edge because of the absence of smooth fracture surface.

Unfortunately, the obtained USAXS data for the standard PA66 samples were not representative because of some irregularity of the surface formed during the sample preparation. Therefore, it is not possible to compare the resulting scattering intensity with that of PA66/6HIA copolyamides and then no clear conclusion on the impact of the HIA monomer on the cavitation mechanism can be drawn.

3.5. **Conclusion on the long term mechanical properties**

Fatigue tensile tests were performed on notched specimens of PA66 and PA66/6HIA at room temperature. It was observed that increasing the molecular weight of PA66 chains results in higher fatigue performance especially under high applied stresses. This improvement is supposed to be a consequence of high chain entanglement and tie molecules density. At low stress value, the benefic effect of the molecular weight is less obvious perhaps because of a concomitant drop of the crystalline fraction.

Concerning the reactively extruded PA66/6HIA copolyamides, it was found that, in spite of their lower crystalline fraction, PA66/6HIA copolymers containing less than 20% of 6HIA monomer have comparable lifetime to that of HMw PA66 and longer fatigue lifetime than the standard PA66. It is assumed that 6HIA co-monomer increases the cohesive energy of the amorphous phase and then overcomes the negative impact of the crystallinity drop and the large molecular weight distribution. Moreover, it was deduced that an important reduction of the lamellae thickness and crystalline perfection, such as those observed for m-PA66/6HIA (77/23 w:w) and i-PA66/6HIA (83/17 w:w), greatly alter the fatigue resistance and may counterbalance the positive effect provided by high molecular weight chains and strong intermolecular interactions.

Strain filed analysis by Digital Image Correlation, showed that for all fatigued specimens the macroscopic deformation is anisotropic particularly near the hole when the stress is highly concentrated. It was found that under the same stress, PA66/6HIA specimens are slightly less deformed than the standard PA66 sample which is quite surprising since they show higher lamella separation. The stiffness evolution curves in the highly stressed point (near the hole) indicate, within the experiment error, that PA66/6HIA copolyamides experience slower drop of the dynamic modulus than the standard PA66. This leads us to believe that PA66/6HIA copolyamides have undergone lower damage accumulation than the un-modified PA66.

Damage characterizations by SEM observations and USAXS experiments suggest that the failure mode is the same for standard PA66 and PA66/6HIA copolyamides. It consists in nucleation of nanocavities between the crystalline lamellae which later grow and become oriented either parallel or perpendicular to the load direction. Unfortunately, the size distribution and fraction of the voids were not quantitatively determined for all the material. Therefore, no clear conclusion on the impact of the HIA monomer on the cavitation mechanism was drawn.

4. Summary of the mechanical properties of PA66 and PA66/6HIA copolyamides

It turns out that storage and Young's modulus originates from the response of both the amorphous phase and the crystalline phase. Below the glass transition, we have seen that the amorphous phase plays a primordial role whereas above the Tg, modulus is mainly driven by the crystalline fraction, an important drop of the elastic modulus at 150°C being observed as the crystalline fraction of copolyamides decreases.

The addition of 6HIA co-monomer reduces the chains mobility of the amorphous phase that was found to primarily determine the yield stress. Otherwise, it is well established that thinner lamellae and poorer crystals perfection are easily plastically deformed, resulting in lower yield stress, which is the case of random i-PA66/6HIA (77/23 w:w) and block m-PA66/6HIA (77/23 w:w) copolyamides.

Morphological changes at the nanometric scale during the deformation process were also investigated. It was observed that lamella stacks oriented perpendicular to the load direction are mainly deformed by shearing and lamella separation. These processes, which occur mainly in the equatorial region of the spherulite, were found to be larger as the crystalline fraction decreases (PA6HIA content increases). At high stress level, lamella rotation along the draw direction was also observed, particularly in the case of PA66/6HIA copolyamides. Furthermore, the variation of the scattering intensity close to the beamstop (low q) with the load level suggests that cavities nucleation and growth are less important in the PA66/6HIA copolyamides, probably due the reinforcement of the intermolecular interactions.

Imapact strength characterizations revealed that the incorporation of 6HIA co-monomer increases by 30% the impact resilience of polyamide at 23°C. This enhancement of the impact resistance may originate from the strong intermolecular interaction but also from the increase of the molecular weight and/or the crystallinity depression. This first contribution (intermolecular interaction) appears to greatly influence the brittle-tough transition ($T_{B/T}$) that was found to linearly increase with Tg.

Finally, fatigue tests pointed out that increasing the molecular weight and incorporating phenolic co-monomers (6HIA) in the amorphous phase of PA66 improve its fatigue endurance, in particular when the crystalline features (lamella thickness and perfection) are not significantly disturbed. In addition, it was observed that random introduction of the 6HIA co-monomer reduces the fatigue lifetime of the resulting copolymer because of the disruption of its crystalline properties. Microscopic characterizations of the fatigued samples suggest that the damage mechanism is the same for all studied samples and mainly involves voids nucleation and growth in the interlamellar phase.

Conclusion

In this chapter, we were interested in the **impact of HIA co-monomer**, which was introduced by two different manners, on the **physical and mechanical properties of prepared copolyamides**. **Three m-PA66/6HIA copolyamides** prepared by reactive extrusion **and one i-PA66/HIA** copolyamide synthesized by in situ copolymerization were considered. Two **PA66** samples (**Standard and HMw**) taken as reference were also studied.

Firstly the microstructure of the injection molded samples was investigated. It was observed that average molecular weight of **m-PA66/6HIA copolyamides** after injection is higher than that of the extruded pellets, likely due to further polycondensation reactions in the melt. Furthermore, their **molecular mass distributions** were found to be **broader** than that of **HMw PA66** even if they have comparable weight average molecular mass. It was also observed that **molecular mass distribution** for **in-situ PA66/6HIA** copolyamide, which has lower average molecular weight than m-PA66/6HIA, **was close to that of standard PA66**.

DSC measurements and MALDI-TOF analysis on m-PA66/6HIA suggest that no further exchange reactions between the PA66 and PA6HIA segments occurred during injection. In the case of in-situ **copolyamide i-PA66/6HIA, a random distribution** of the co-monomer 6HIA is highlighted. Moreover, it was found that HMw PA66 had a lower crystalline fraction, melting Tm and crystallization Tc temperatures when compared to the standard one. This suggests that **increasing the molecular weight** of PA66 chains **impede** their **crystallization** likely due to lower chain mobility in the melt. Furthermore, the melting and **crystallization temperature of i-PA66/6HIA** were found to be lower than those of block copolyamides containing the same PA6HIA content. This suggests that **random distribution** of HIA co-monomer along the PA66 segments **hinders** significantly the **crystallization** process of PA6,6.

Concerning the molecular mobility of the studied material, it was found that **glass transition** temperature **increases when** the fraction of rigid **phenolic** segments **increases**. Moreover, the **free surface energy** of PA66/6HIA **copolyamides** appeared to be **higher** than that of standard PA66, suggesting **higher cohesion** of their amorphous phase.

Secondly, the crystalline morphology of injection molded specimens was characterized. It was observed **that adding 6HIA co-monomer** as well **as increasing the molecular weight** of PA66 induces a slight **refinement of the spherulite** texture. It was deduced from SAXS experiments that the **thickness** of the crystalline **lamellae** also **decreases** when the amount of PA6HIA or the molecular weight increases. **The thickness drop** was found to be more **important** in the case of high PA6HIA content and random **i-PA66/6HIA** copolyamide who also had **poor crystal perfection**. Based on these results, the drop of the melting temperature with the PA6HIA content was successfully correlated to the crystalline lamella thickness and crystal perfection.

In the second part of this chapter, the mechanical properties of these samples were presented. It was observed that molecular weight does not significantly affect the elastic modulus of PA66. The **glassy elastic** modulus (below Tg) of **m-PA66/6HIA** appeared to be **close** to that of **PA66 while** it was **25 % lower** in the case of **in-situ copolyamide** which exhibits poorer crystalline perfection. **Above the glass transition** temperature, the elastic **modulus** of PA66/6HIA copolyamides **drops as PA6HIA increases**, likely as a consequence of the reduction of the crystalline fraction. Concerning the **yield stress**, it was found that it is

linearly **dependent** on the chain **mobility** of the amorphous phase, even if it can be greatly affected by the crystalline perfection. For instance, random i-PA66/6HIA and block copolyamide m-PA66/6HIA (83/17 w:w) have similar chain mobility (same Tg) but exhibit different yield stress: the **σ_y of random i-PA66/6HIA** copolyamide is **lower than** that of **block copolyamide**. It is known that thinner lamella and poorer crystal perfection are easily plastically deformed at low stress by means of chain slipping, tilting and twisting. This is assumed to be at the origin of the lower yield stress of random copolyamide.

In-situ SAXS experiments were also investigated in order to get information on the local deformation during uniaxial tests. It was observed that **equatorial** lamellae are mainly deformed by **lamella separation**, which is clearly **enhanced** in the case of **copolyamides** containing **high fraction of amorphous PA6HIA** (low crystalline fraction). On the other hand, scattering intensity related to **cavitation** was found to be **less important** in the case of **PA66/6HIA copolyamides**. This leads us to believe that addition of **6HIA co-monomer makes cavitation** under uniaxial load more **difficult**. Note, that above the glass transition temperature, no cavitation evidence was identified for all materials at the studied stress level.

We then assessed the impact strength property of these materials. It was observed that **brittle-tough transition** temperatures ($T_{B/T}$) **increases as the PA6HIA** content **increases**, more specifically when the Tg increases indicating that brittle-tough transition depends primarily on the molecular mobility of the amorphous phase, as reported in a previous works done in our labioratory. It was also found that **m-PA66/6HIA** exhibits a **higher resilience** upon notched impact at 23°C (**more than 30%**) than standard PA66 while **i-PA66/6HIA** exhibits only a **14% rise of the resilience**. It is assumed that this enhancement may originate from the strong intermolecular interaction as well as from the increase of the molecular weight and/or the crystallinity depression.

Finally, the long term mechanical properties of the selected materials was studied. It was observed that **increasing the molecular weight** of PA66 chains results in **higher fatigue performance,** likely due to high chain entanglement and tie molecules density. Moreover, it was found that **PA66/6HIA copolymers** containing **less** than **20% of 6HIA** monomer have **comparable lifetime** to that of **HMw PA66** and **longer fatigue lifetime than** the standard **PA66**. It is assumed that **6HIA co-monomer increases the cohesive energy** of the amorphous phase and then overcomes the negative impact of the crystallinity drop. However, m-PA66/6HIA (77/23 w:w) and i-PA66/6HIA (83/17 w:w), having **thinner lamellae** and **lower crystallite size perfection**, exhibit **inferior fatigue performance**. This indicates that the **crystalline features** (lamella thickness, crystal lattice) also **contribute to the fatigue resistance** of semi-crystalline polymers. The damage mechanism of the selected material under cyclic loading involves steady voids nucleation and growth in the amorphous phase. These cavities give later microcraks which propagates rapidly during the final stage leading to failure.

General conclusion

Polyamides are the largest engineering thermoplastics used in the automotive industry because of their excellent chemical resistance, thermal stability, mechanical strength and toughness. Within the general context of developing sustainable polymeric materials, the main objective of this thesis was to enhance the mechanical performance of polyamides, particularly of polyamide 66, in order to get material with longer service lifetime.

The literature underlined that fatigue lifetime of semi-crystalline polymers is largely higher than that of the amorphous ones and that molecular weight and microstructure of the crystalline phase greatly influence the durability of these polymers. In addition, it pointed out the damage under cyclic loading consists in voids nucleation and growth in the interlamellar amorphous phase. In the case of polyamide, it is reported that, up to a certain size, voids quickly close because of the healing action of the surface energy. This latter is supposed to be mainly due to the H-bonds interactions. Therefore, we decided to enhance this self-healing capability of polyamide by introducing phenolic functions, offering strong H-bond interactions with the amorphous polyamide chains. The main challenge was to incorporate these functions in the amorphous phase without altering the coupling between the crystalline and amorphous phases, which has a strong impact on the fatigue resistance of semi-crystalline polymers.

We considered that a block copolymer structure was the appropriate way to efficiently anchor the amorphous phenolic segment (PA6HIA) to the crystalline lamellae without altering the initial microstructure of the modified polyamide. Accordingly, reactive extrusion of PA66-NH2 and PA6HIA-COOH at the dried state (water content < 300 ppm) were carried out at the laboratory and pilot scale in order to prepare block PA66/6HIA copolyamides. It was observed that processing conditions such as extrusion time and extrusion temperature greatly affect the formation of the PA66/6HIA copolyamides. Moreover, addition of catalyst (sodium hypophosphite) appeared to enhance the polycondensation extent in shorter time.

It was concluded that reactive blending at 310 °C during 3 minutes in the presence of 100 ppm of catalyst were the appropriate conditions for the preparation of PA66/6HIA copolyamide. The abovementioned conditions, established at the laboratory scale, were found to be also valid at the pilot scale.

Therefore, three melt blending copolyamides m-PA66/6HIA (90/10; 83/17 and 77/ 23 w:w) were prepared in the first part of this work. In comparison, a fourth copolyamide i-PA66/6HIA (83/17 w:w) prepared by in situ co-polycondensation was also considered

Structural characterizations of the prepared copolyamides were performed on the pellets (after extrusion) as well as on the specimens (after injection). Despite a slight variation of the molecular weight distribution, likely due to drying conditions, the overall microstructure (block structure, crystalline fraction and morphology…) of the extruded copolyamide was conserved during the injection molding process. The main structural features of the prepared materials were then discussed.

Firstly, it was observed that reactive extruded m-PA66/6HIAcopolyamides have higher average molecular weight than the standard PA66. Thus a second grade of PA66 (HMw) having comparable Mw to that of m-PA66/6HIA copolyamide was also studied. It should be noted that reactive extruded copolyamide have broader molecular weight distribution than that of HMw PA66. Fortunately, the averages molecular weight and distributions of in-situ PA66/6HIA copolyamide and standard PA66 were found to be very close.

Secondly, NMR and MALDI-TOF analyses pointed out that pellets and respectively injection molded specimens of m-PA66/6HIA copolyamides have a block structure with PA66 segments long enough to crystallize in a manner similar to that of standard PA66. MALDI-TOF analysis also confirmed that 6HIA co-monomer of the copolyamide prepared by in-situ co-polycondensation is randomly distributed along the copolymer chains.

Thirdly, the molecular mobility of the injection molded materials was studied. It was observed that glass transition temperature increases when the fraction of rigid phenolic segments increases. Moreover, the cohesion of the amorphous phase, highlighted by means of free surface energy, was found to be higher in the case of PA66/6HIA copolyamides.

Fourthly, it was observed that increasing the molecular weight of PA66 reduces its crystalline fraction, crystallization and melting temperatures. The incorporation of rigid aromatic moieties (6HIA) in the form of block sequences reduces the crystallization and melting temperatures as well. This drop appeared to be more significant when the 6HIA is randomly distributed. The crystalline fraction of PA66 into the block copolyamides was found to be comparable to that of polyamide 66 having the same molecular weight, while the overall crystalline fraction of the sample decreases as the fraction of the amorphous PA6HIA increases.

Finally, the morphology was characterized from the microscopic to the nanoscopic scale. It was observed that adding 6HIA co-monomer as well as increasing the molecular weight of PA66 induces a slight refinement of the spherulite texture. Moreover, the thickness of the crystalline lamellae was found to decrease when the amount of PA6HIA or the molecular weight increases. This thickness drop was found to be more important in the case of high PA6HIA content and random i-PA66/6HIA copolyamide who also had poor crystallite size perfection.

In the second part of this work, the mechanical properties of the injection molded specimens were studied. Firstly, it was observed that the glassy elastic modulus (below Tg) of m-PA66/6HIA was close to that of PA66, likely due to a balance between reinforcing the amorphous phase by the 6HIA co-monomer and weakening of the crystalline phase (crystallinity drop). In the case of random PA66/6HIA, the significant drop of the crystalline perfection counterbalances the positive effect of the intermolecular interaction resulting in an elastic modulus 25 % lower than that of standard PA66. Above the glass transition temperature, the elastic modulus of PA66/6HIA copolyamides drops as the PA6HIA increases, likely as a consequence of the reduction of the overall crystalline fraction.

The constant modulus of block PA66/6HIA copolyamides was related to a balance between reinforcing the amorphous phase by the rigid moieties with strong intermolecular interaction and weakening of the crystalline phase. In the case of random PA66/6HIA, the significant drop of the crystalline perfection counterbalances the positive effect of the intermolecular interaction resulting in lower modulus.

Furthermore, the Yield stress was found to be linearly dependent on the chain mobility of the amorphous phase, except for random i-PA66/6HIA copolyamide and block mPA66/6HIA (7723 w:w) which exhibited lower yield stress. This was related to a lower resistance to plastic deformation often associated to small crystallite size and poor perfection. In situ tensile-SAXS experiments pointed out that lamellae separation in the equatorial region of the spherulites was more pronounced in the case of copolyamides containing high fraction of amorphous PA6HIA. Moreover, it was deduced that addition of 6HIA co-monomer makes cavitation under uniaxial load more difficult.

We then studied the impact strength property of the selected materials. It was found that, similarly to common polyamides, the brittle-tough transition temperature ($T_{B/T}$) of PA66/6HIA copolyamides directly depends on the molecular mobility of the amorphous phase. It was also observed that the impact resistance of PA66/6HIA copolyamides at 23°C is 30% higher than that of standard PA66. This benefit was related to strong H-bonds interactions of the 6HIA co-monomer as well as to the lower crystalline fraction and higher molecular weight of these materials.

Finally, the long term mechanical properties of these materials were studied. It was observed that increasing the molecular weight of PA66 chains results in longer fatigue lifetime, likely due to high chain entanglement and tie molecules density. Moreover, it was found that m-PA66/6HIA copolymers containing less than 20% of 6HIA monomer exhibit longer fatigue lifetime than that of standard PA66. This result is quite complex and originates from the increase of the molecular weight as well as of the cohesive energy of the amorphous phase of m-PA66/6HIA copolymers.

In order to interpret this result, the fatigue lifetime of m-PA66/6HIA copolyamides was compared to that of HMw PA66. Taking into consideration that block copolyamides have lower crystalline fraction and contain a large fraction of low molecular weight chains, a shorter fatigue lifetime than that of HMw PA66 is expected. However, a comparable lifetime - if not higher at some stresses - was observed. This demonstrates that reinforcing the amorphous phase by 6HIA co-monomer overcomes the negative impact of the crystallinity drop and short chain segments. Unfortunately, the significant drop of the crystalline fraction, lamellae thickness and crystalline perfection of m-PA66/6HIA (77/23 w:w) and i-PA66/6HIA (83/17 w:w) seem to counterbalance the positive effect provided by the strong H-bonds interactions. Therefore, a reduction of the fatigue lifetime of these copolymers was observed.

To sum up:

1. We showed that it was possible to prepare block PA66/6HIA copolyamides by melt blending of reactive ends-groups of aliphatic polyamide 66 and semi-aromatic polyamide 6HIA at 310°C during at least 180 s in the presence of 100 ppm of sodium hypophosphite.

2. Up to 17% of PA6HIA, the microstructure of the block copolyamide is similar to that of the standard PA66 while that of random copolyamide shows a significant reduction of the crystallite size perfection.

3. In comparison with standard PA66, the reactive-extruded copolyamides exhibit some improvement of the tensile properties (Yield stress and stiffness), while the in-situ random copolyamides demonstrated a deterioration of these properties because of its poor crystalline perfection.

4. This work confirms that molecular weight, crystalline fraction and perfection have an huge influence on the fatigue resistance of the materials, but also demonstrates that intermolecular interactions governs the fatigue lifetime as well:

    - Increasing the molecular weight increases the total fatigue lifetime
    - Reduction of the crystalline perfection results in shorter lifetime
    - Addition of the 6HIA co-monomer enhances the fatigue lifetime

This work could be considered as a basis for the design of new polymer materials with a tailored set of properties, but further complementary researches are needed. For instance, the processing conditions (extrusion and injection) have to be closely controlled in order to get narrower molecular weight distribution. Moreover, in order to separate the contribution of the aromatic moiety from the contribution of intermolecular interactions, it would be interesting to study how the incorporation of aromatic groups without OH functions affects the physical and mechanical properties of the resulting copolymers (for example PA66/6I). In addition, glass fibers reinforced PA66/6HIA copolyamides could be attractive for evaluation as the automotive components are mainly made of glass reinforced polyamide. Finally, it would be interesting to accurately assess the damage cavitation under load in the 3-D dimension, e.g. by using 3-D X-Ray tomography.

Bibliography

[1] Global Industry Analysts, Nylon, a global strategic business report, http://www.strategyr.com/Nylon_Market_Report.asp. (2010) Last consulted on 10 December 2012.

[2] P. Blanchard, Nylon and ABS market overview, http://www.apurchasingd.com/files/CMAI%20-%20Paul%20Blanchard%20-%20Nylon%20ABS%20Review%205.12.pdf. (2011) Last consulted on 10 December 2012.

[3] H.K. Reimschuessel, Nylon 6. Chemistry and mechanisms, Journal of Polymer Science: Macromolecular Reviews. 12 (1977) 65–139.

[4] J. Zimmerman, Equilibria in solid phase polyamidation, Journal of Polymer Science Part B: Polymer Letters. 2 (1964) 955–958.

[5] S.N. Vouyiouka, C.D. Papaspyrides, Solid state polymerization, Encyclopedia of Polymer Science and Technology. (2011) 1–32.

[6] M.L. Kohan, Nylon Plastics Handbook, Munich, 1995.

[7] O.B. Edgar, R. Hill, The p-phenylene linkage in linear high polymers: Some structure–property relationships, Journal of Polymer Science. 8 (1952) 1–22.

[8] T. Yamamoto, S.; Takata, Polyamide and polyamide resin composition, U.S. Patent EU Patent 0449466, 1991.

[9] R.J. Gaymans, S. Aalto, Copolyamides of Nylon • 4,6 and nylon • 4,T, Journal of Polymer Science Part A: Polymer Chemistry. 27 (1989) 423–430.

[10] E. Djodeyre, F. Carrière, H. Sekiguchi, Preparation and some properties of diamine-diacid type alternating copolyamides, European Polymer Journal. 15 (1979) 69–73.

[11] N.-M. Tran, F. Carrière, H. Sekiguchi, Préparation et identification de copolyamides alternés du type ω-aminoacide, Die Makromolekulare Chemie. 182 (1981) 2175–2182.

[12] K. Saotome, K. Sato, Preparation of block copolyamides, Die Makromolekulare Chemie. 102 (1967) 105–114.

[13] J.-C. Bollinger, C. Aubineau, Préparation et Étude Physico-chimique de Quelques Copolyamides Aromatiques Séquencés. II. Preuves de I'Existence de Séquencés dans les Copolycondensats, Journal of Macromolecular Science: Part A - Chemistry. 11 (1977) 1177–1190.

[14] M.B. Polk, K.B. Bota, E.C. Akubuiro, Block copolyamides. 1. Preparation and properties of block copolyamides containing cyclohexane and benzene rings, Industrial & Engineering Chemistry Product Research and Development. 23 (1984) 230–233.

[15] Leszek A. Utracki, Polymer Blends Handbook, Kluwer Academic Publishers, New York, 2003.

[16] Leszek A. Utracki, Polymer Alloys and Blends: Thermodynamics and Rheology, Munich, 1989.

[17] T.S. Ellis, Miscibility of polyamide blends: effects of configuration, Polymer. 36 (1995) 3919–3926.

[18] Y. Liu, J.A. Donovan, Miscibility and crystallization of semicrystalline nylon 6 and amorphous nylon 6IcoT blends, Polymer. 36 (1995) 4797–4803.

[19] G.Z. Zhang, H. Yoshida, T. Kawai, Miscibility of Nylon 66 and Nylon 48 blend evaluated by crystallization dynamics, Thermochimica Acta. 416 (2004) 79–85.

[20] Y.P. Khanna, N.S. Murthy, W.P. Kuhn, E.D. Day, Pseudo super-miscibility: Blends of semi-crystalline nylon pairs exhibiting a single Tg and a single Tm, Polymer Engineering & Science. 39 (1999) 2222–2232.

[21] J. Brisson, B. Breault, Miscibility of polyamide blends. 1. Molecular modeling of poly(n-methyleneisophthalamide)-poly(meta-phenyleneisophthalamide) blends, Macromolecules. 24 (1991) 495–504.

[22] O. Persyn, V. Miri, J. Lefebvre, V. Ferreiro, T. Brink, A. Stroeks, Mechanical Behavior of Films of Miscible Polyamide 6 / Polyamide 6I-6T Blends, Journal of Polymer Science: Part B: Polymer Physics. 44 (2006) 1690–1701.

[23] M. Shibayama, K. Uenoyama, J. Oura, S. Nomura, T. Iwamoto, Miscibility and crystallinity control of nylon 6 and poly(m-xylene adipamide) blends, Polymer. 36 (1995) 4811–4816.

[24] M. Endo, Y. Morishima, S. Yano, K. Tadano, Y. Murata, K. Tsunashima, Miscibility in binary blends of aromatic and alicyclic polyamides, Journal of Applied Polymer Science. 101 (2006) 3971–3978.

[25] T. Ellis, Aromatic polyamide blends: enthalpy relaxation and its correlation with phase phenomena, Macromolecules. 23 (1990) 1494–1503.

[26] T. Ellis, Influence of structure on phase behavior of polyamide blends, Macromolecules. 24 (1991) 3845–3852.

[27] T. Ellis, Miscibility and immiscibility of polyamide blends, Macromolecules. 22 (1989) 742–754.

[28] T. Ellis, mixing relantioship in aliphatic polyamide blends, Polymer. 33 (1992) 1469–1476.

[29] T. Ellis, Miscibiliy in blends of aliphatic polyamides and an aromatic polyamide, nylon 3Me6T, Polymer. 29 (1988) 2015–2026.

[30] T. Ellis, Critical miscibility limits in blends of aliphatic polyamides containing an aromatic polyamide, Polymer. 31 (1990) 1058–1064.

[31] T. Ellis, The role of repulsive interactions in polyamide blends, Polymer Engineering and Science. 30 (1990) 998–1004.

[32] T. Xie, G. Yang, Effects of maleated styrene–(ethylene-co-butene)–styrene on compatibilization and properties of nylon-12,12/nylon-6 blends, Journal of Applied Polymer Science. 93 (2004) 1446–1453.

[33] M. Kyotani, Solution crystallization of blends of nylon 6 and nyoln 12, Journal of Macromolecular Science, Part B: Physics. 21 (1982) 219–230.

[34] M. Wei, I. Shin, B. Urban, A. Tonelli, Partial miscibility in a nylon- 6/nylon- 66 blend coalesced from their common α- cyclodextrin inclusion complex, Journal of Polymer Science Part B. 42 (2004) 1369–1378.

[35] E. Ong, Y. Kim, L. Williams, Dynamic mechanical properties of some nylons and their blends, Journal of Applied Polymer. 31 (1986) 367–383.

[36] J. Brisson, Factors affecting the miscibility of nylon-6I/nylon-6, 6, Macromolecules. 29 (1996) 1839–1841.

[37] T. Ellis, On the Miscibility of Blends of Nylon 66 and Poly (hexamethylene isophthalamide), Nylon 6I, Macromolecules. 29 (1996) 1836–1838.

[38] I. Page, Polyamides as Engineering Thermoplastic Materials, 1st ed., Rapra Review Reports, 2000.

[39] S.M. Aharoni, T. Largman, Process for preparing graft and block copolymers, U.S. Patent 4417031, 1983.

[40] Y.P. Khanna, Process for production of quasi-random copolymers from homopolymers, U.S. Patent 4861838, 1989.

[41] Y.P. Khanna, E.A. Turi, S.M. Aharoni, T. Largman, Quasi-random copolymers from homopolymers, U.S. Patent 4417032, 1983.

[42] M. Evstatiev, J.M. Schultz, S. Petrovich, G. Georgiev, S. Fakirov, K. Friedrich, In situ polymer/polymer composites from poly(ethylene terephthalate), polyamide-6, and polyamide-66 blends, Journal of Applied Polymer Science. 67 (1998) 723–737.

[43] A.C.M. van Bennekom, P.A.A.T. Willemsen, R.J. Gaymans, Amide-modified poly(butylene terepthalate): thermal stability, Polymer. 37 (1996) 5447–5459.

[44] F. Xie, Y.W. Kim, S.A. Jabarin, The interchange reaction between poly(ethylene terephthalate) and poly(m-xylylene adipamide), Journal of Applied Polymer Science. 112 (2009) 3449–3461.

[45] Z. Denchev, H.R. Kricheldorf, S. Fakirov, Sequential Reordering in Condensation Copolymers, 6. Average Block Lengths in Poly(ethylene terephthalate) – Polyamide 6 Copolymers As Revealed by NMR Spectroscopy, Macromolecular Chemistry and Physics. 202 (2001) 574–586.

[46] I.K. Miller, Amide-exchange reactions in mixtures of N-alkyl amides and in polyamide melt blends, Journal of Polymer Science: Polymer Chemistry Edition. 14 (1976) 1403–1417.

[47] F. Samperi, M. Montaudo, C. Puglisi, R. Alicata, G. Montaudo, Essential Role of Chain Ends in the Ny6/PBT Exchange. A Combined NMR and MALDI Approach, Macromolecules. 36 (2003) 7143–7154.

[48] G. Montaudo, M.S. Montaudo, E. Scamporrino, D. Vitalini, Mechanism of exchange in polyesters: composition and microstructure of copolymers formed in the melt mixing process of poly(ethylene terephthalate) and poly(ethylene adipate), Macromolecules. 25 (1992) 5099–5107.

[49] G. Montaudo, C. Puglisi, F. Samperi, Exchange reactions occurring through active chain ends: Melt mixing of nylon 6 and polycarbonate, Journal of Polymer Science Part A: Polymer Chemistry. 32 (1994) 15–31.

[50] G. Montaudo, C. Puglisi, F. Samperi, Mechanism of exchange in PBT/PC and PET/PC blends. Composition of the copolymer formed in the melt mixing process, Macromolecules. 31 (1998) 650–661.

[51] G. Montaudo, C. Puglisi, F. Samperi, Transreactions in Condensation Polymers, Fakirov, S, Wiley-VCH, New York, 1999.

[52] J. Devaux, Transreactions in Condensation Polymers, Fakirov, S, Wiley-VCH, New York, 1999.

[53] F. Pilati, M. Fiorini, C. Berti, Transreactions in Condensation Polymers, Fakirov, S, Wiley-VCH, New York, 1999.

[54] M. Zilberman, A. Siegmann, M. Narkis, The glass transition temperature of 6/6.9 random copolyamides, Polymer. 36 (1995) 5065–5067.

[55] J. Zimmerman, E.M. Pearce, I.K. Miller, J.A. Muzzio, I.G. Epstein, E.A. Hosegood, Reinforcement factors in fibers from block copolyamides and polyamide blends, Journal of Applied Polymer Science. 17 (1973) 849–861.

[56] Y. Takeda, D.R. Paul, Phase homogenization of mixtures of poly(m-xylene adipamide) and nylon 6 by interchange reactions, Polymer. 32 (1991) 2771–2778.

[57] Y. Takeda, D.R. Paul, The effect of physical interactions on melt-phase homogenization of mixtures of poly(m-xylene adipamide) with aliphatic polyamides induced by interchange reactions, Polymer. 33 (1992) 3899–3907.

[58] M. Xanthos, H. Warth, Transreactions in Condensation Polymers, Fakirov, S, Wiley-VCH, New York, 1999.

[59] A.M. Kotliar, Interchange reactions involving condensation polymers, Journal of Polymer Science: Macromolecular Reviews. 16 (1981) 367–395.

[60] A.M. Aerdts, K.L.L. Eersels, G. Groeninckx, Transamidation in Melt-Mixed Aliphatic and Aromatic Polyamides. 1. Determination of the Degree of Randomness and Number-Average Block Length by Means of 13 C NMR, Macromolecules. 29 (1996) 1041–1045.

[61] K.L.L. Eersels, A.M. Aerdts, G. Groeninckx, Transamidation in Melt-Mixed Aliphatic and Aromatic Polyamides. 2. Molecular Characterization of PA 46/PA 6I Blends as a Function of the Extrusion Time, Extrusion Temperature, and Blend Composition, Macromolecules. 29 (1996) 1046–1050.

[62] K.L.L. Eersels, G. Groeninckx, Y. Mengerink, S. Van der Wal, Transamidation in Melt-Mixed Aliphatic and Aromatic Polyamides. 3. Molecular Characterization Using Gradient Elution Chromatography (GEC), Macromolecules. 29 (1996) 6744–6749.

[63] C. Puglisi, F. Samperi, S. Di Giorgi, G. Montaudo, Exchange reactions occurring through active chain ends. MALDI-TOF characterization of copolymers from nylon 6, 6 and nylon 6, 10, Macromolecules. 36 (2003) 1098–1107.

[64] F. Samperi, C. Puglisi, R. Alicata, G. Montando, Essential role of chain ends in the nylon-6/poly(ethylene terephthalate) exchange, Journal of Polymer Science Part A: Polymer Chemistry. 41 (2003) 2778–2793.

[65] F. Samperi, M.S. Montaudo, S. Battiato, D. Carbone, C. Puglisi, Characterization of copolyesteramides from reactive blending of PET and MXD6 in the molten state, Journal of Polymer Science Part A: Polymer Chemistry. 48 (2010) 5135–5155.

[66] F. Samperi, M.S. Montaudo, C. Puglisi, S. Di Giorgi, G. Montaudo, Structural Characterization of Copolyamides Synthesized via the Facile Blending of Polyamides, Macromolecules. 37 (2004) 6449–6459.

[67] K.L.L. Eersels, G. Groeninckx, Influence of interchange reactions on the crystallization and melting behaviour of polyamide blends as affected by the processing conditions, Polymer. 37 (1996) 983–989.

[68] J. Brandrup, E.H. Immergut, E.A. Grulke, Polymer handbook, 4th Editio, John Wiley, New York, 1999.

[69] H.R. Kricheldorf, T. Mang, J.M. Jonté, Polylactones, 2 Copolymerization of glycolide with β-propiolactone, γ-butyrolactone or δ-valerolactone, Die Makromolekulare Chemie. 186 (1985) 955–976.

[70] H.R. Kricheldorf, I. Kreiser, Polylactones, 11. Cationic copolymerization of glycolide with L,L-dilactide, Die Makromolekulare Chemie. 188 (1987) 1861–1873.

[71] N.M. Tran, E. Djodeyre, F.J. Carriere, H. Sekiguchi, Thermal-properties and C-13 nmr-spectra of some alternating and statistical copolyamides, Makromolekulare Chemie-rapid Communications. 1 (1980) 507–512.

[72] C.W. Bunn, E. V Garner, The Crystal Structures of Two Polyamides (’Nylons'), Proceedings of the Royal Society of London. Series A. Mathematical and Physical Sciences. 189 (1947) 39–68.

[73] N.A. Jones, E.D.T. Atkins, M.J. Hill, S.J. Cooper, L. Franco, Chain-Folded Lamellar Crystals of Aliphatic Polyamides. Comparisons between Nylons 4 4, 6 4, 8 4, 10 4, and 12 4, Macromolecules. 29 (1996) 6011–6018.

[74] J.P. Bell, P.E. Slade, J.H. Dumbleton, Multiple melting in nylon 66, Journal of Polymer Science Part A-2: Polymer Physics. 6 (1968) 1773–1781.

[75] N.S. Murthy, Hydrogen bonding, mobility, and structural transitions in aliphatic polyamides, Journal of Polymer Science-B-Polymer Physics Edition. 44 (2006) 1763–1782.

[76] P. Dreyfuss, A. Keller, Chain folding in polyamides - study on nylons 66, 610, and 612 as crystallized from solution, Journal of Macromolecular Science, Part B: Physics. B4 (1970) 811–835.

[77] E. Atkins, M. Hill, S. Hong, A. Keller, S. Organ, Lamellar structure and morphology of nylon 46 crystals: A new chain folding mechanism for nylons, Macromolecules. 25 (1992) 917–924.

[78] S. Havriliak, S. Negami, A complex plane representation of dielectric and mechanical relaxation processes in some polymers, Polymer. 8 (1967) 161–210.

[79] B. Wunderlich, Reversible crystallization and the rigid–amorphous phase in semicrystalline macromolecules, Progress in Polymer Science. 28 (2003) 383–450.

[80] G. Rotter, H. Ishida, Dynamic mechanical analysis of the glass transition: curve resolving applied to polymers, Macromolecules. 25 (1992) 2170–2176.

[81] A. Rios De Anda, Influence of the solvent sorption, additivation, and chemical modification on the molecular mobility dynamics of Polyamide 6,6 amorphous phase and its consequences on the tensile and impact strength properties of this polymer, 2012.

[82] H. Miura, J. Hirschinger, A.D. English, Segmental dynamics in the amorphous phase of nylon 66: solid state deuterium NMR, Macromolecules. 23 (1990) 2169–2182.

[83] G.R. Hatfield, J.H. Glans, W.B. Hammond, Characterization of structure and morphology in nylon 6 by solid-state carbon-13 and nitrogen-15 NMR, Macromolecules. 23 (1990) 1654–1658.

[84] K. Pathmanathan, G.P. Johari, The effect of increased crystallization on the electrical properties of nylon-12, Journal of Polymer Science Part B: Polymer Physics. 31 (1993) 265–271.

[85] J. Varlet, J.Y. Cavaillé, J. Perez, G.P. Johari, Dynamic mechanical spectrometry of nylon-12, Journal of Polymer Science Part B: Polymer Physics. 28 (1990) 2691–2705.

[86] K. Pathmanathan, J.Y. Cavaillé, G.P. Johari, The dielectric properties of dry and water-saturated Nylon-12, Journal of Polymer Science: Part B: Polymer Physics. 30 (1992) 341–348.

[87] A.J. Owen, R. Bonart, Cooperative relaxation processes in polymers, Polymer. 26 (1985) 1034–1038.

[88] R.H. Boyd, Dielectric Loss in 66 Nylon (Polyhexamethylene Adipamide), The Journal of Chemical Physics. 30 (1959) 1276–1283.

[89] N. Murthy, M. Stamm, J. Sibilia, S. Krimm, Structural changes accompanying hydration in nylon 6, Macromolecules. 22 (1989) 1261–1267.

[90] H.W. Starkweather, G.A. Jones, Crystalline transitions in powders of nylon 66 crystallized from solution, Journal of Polymer Science: Polymer Physics Edition. 19 (1981) 467–477.

[91] J. Puffr, R.; Ebenda, On the Structure and Properties of Polyamides. XXVII. The Mechanism of Water Sorption in Polyamides, Journal of Polymer Science Part C: Polymer Symposia. 16 (1967) 79–93.

[92] P. Adriaensens, A. Pollaris, R. Rulkens, V.M. Litvinov, J. Gelan, Study of the water uptake of polyamide 46 based copolymers by magnetic resonance imaging relaxometry, Polymer. 45 (2004) 2465–2473.

[93] L. Lim, I. Britt, M. Tung, Sorption and transport of water vapor in nylon 6, 6 film, Journal of Applied Polymer Science. 71 (1999) 197–206.

[94] Y. Rao, A.J. Waddon, R.J. Farris, Structure-property relation in poly(p-phenylene terephthalamide) (PPTA) fibers, Polymer. 42 (2001) 5937–5946.

[95] M.Z. Elsabee, M.A. Nassar, S.E.M. El-begawy, Preparation and Characterization of Some Aromatic/ Aliphatic Polyamides, American Journal of Polymer Science. 2 (2012) 7–13.

[96] A.J. Uddin, Y. Gotoh, Y. Ohkoshi, M. Nagura, R. Endo, T. Hara, Hydration in a new semiaromatic polyamide observed by humidity-controlled dynamic viscoelastometry and X-ray diffraction, Journal of Polymer Science Part B: Polymer Physics. 43 (2005) 1640–1648.

[97] A.J. Uddin, Y. Ohkoshi, Y. Gotoh, M. Nagura, R. Endo, T. Hara, Melt spinning and laser- • heated drawing of a new semiaromatic polyamide, PA9- • T fiber, Journal of Polymer Science: Part B: Polymer Physics. 42 (2004) 433–444.

[98] A.J. Uddin, Y. Ohkoshi, Y. Gotoh, M. Nagura, T. Hara, Influence of moisture on the viscoelastic relaxations in long aliphatic chain contained semiaromatic polyamide, (PA9-T) fiber, Journal of Polymer Science Part B: Polymer Physics. 41 (2003) 2878–2891.

[99] K. Kudo, T. Suguie, M. Hirami, Melt-Polymerized Aliphatic-Aromatic Copolyamides. I. Melting Points of Nylon 66 Copolymerized with Aromatic Diamines and Teraphthalic Acid, Journal of Applied Polymer Science. 44 (1992) 1625–1629.

[100] J.S. Ridgway, Structure–property relationships of ring-containing nylon 66 copolyamides, Journal of Polymer Science Part A-1: Polymer Chemistry. 8 (1970) 3089–3111.

[101] A. Ballistreri, D. Garozzo, M. Giuffrida, P. Maravigna, G. Montaudo, Thermal decomposition processes in aliphatic-aromatic polyamides investigated by mass spectrometry, Macromolecules. 19 (1986) 2693–2699.

[102] S. Ghosh, J.C. Viana, R.L. Reis, J.F. Mano, Effect of Processing Conditions on Morphology and Mechanical Properties of Injection-Molded Poly (L- • lactic acid), Polymer Engineering & Science. 47 (2007) 1141–1147.

[103] G. Perego, G.D. Cella, C. Bastioli, Effect of Molecular Weight and Crystallinity on Poly(lactic acid) Mechanical Properties, Journal of Applied Polymer Science. 59 (1996) 37–43.

[104] H.W. Starkweather, G.E. Moore, J.E. Hansen, T.M. Roder, R.E. Brooks, Effect of crystallinity on the properties of nylons, Journal of Polymer Science. 21 (1956) 189–204.

[105] C.F. Hammer, T.A. Koch, J.F. Whitney, Fine structure of acetal resins and its effect on mechanical properties, Journal of Applied Polymer Science. 1 (1959) 169–178.

[106] S.M. Ohlberg, J. Roth, R.A. V Raff, Relationship between impact strength and spherulite growth in linear polyethylene, Journal of Applied Polymer Science. 1 (1959) 114–120.

[107] J.L. Way, J.R. Atkinson, J. Nutting, The effect of spherulite size on the fracture morphology of polypropylene, Journal of Materials Science. 9 (1974) 293–299.

[108] H.W. Starkweather, R.E. Brooks, Effect of Spherulites on the Mechanical Properties of Nylon 66, Journal of Applied Polymer Science. 1 (1959) 236–239.

[109] R. Popli, L. Mandelkern, Influence of structural and morphological factors on the mechanical properties of the polyethylenes, Journal of Polymer Science Part B: Polymer Physics. 25 (1987) 441–483.

[110] A. Pawlak, Cavitation during tensile deformation of high-density polyethylene, Polymer. 48 (2007) 1397–1409.

[111] B.A.G. Schrauwen, Deformation and failure of semi-crystalline polymer systems, Eindhoven University of Technology, 2003.

[112] V. Miri, O. Persyn, J.-M. Lefebvre, R. Seguela, Effect of water absorption on the plastic deformation behavior of nylon 6, European Polymer Journal. 45 (2009) 757–762.

[113] C. Stern, A. Frick, G. Weickert, Relationship between the structure and mechanical properties of polypropylene: Effects of the molecular weight and shear-• induced structure, Journal of Applied Polymer Science. 103 (2007) 519–533.

[114] Z. Wang, Y. Zhou, P.K. Mallick, Effects of temperature and strain rate on the tensile behavior of short fiber reinforced polyamide-6, Polymer Composites. 23 (2002) 858–871.

[115] H.K. Reimschuessel, Relationships on the effect of water on glass transition temperature and young's modulus of nylon 6, Journal of Polymer Science: Polymer Chemistry Edition. 16 (1978) 1229–1236.

[116] R.J. Gaymans, R.J.M. Borggreve, a. B. Spoelstra, Ductile transition in nylon-rubber blends: Influence of water, Journal of Applied Polymer Science. 37 (1989) 479–486.

[117] C. Thomas, R. Seguela, F. Detrez, V. Miri, C. Vanmansart, Plastic deformation of spherulitic semi-crystalline polymers: An in situ AFM study of polybutene under tensile drawing, Polymer. 50 (2009) 3714–3723.

[118] C. Thomas, V. Ferreiro, G. Coulon, R. Seguela, In situ AFM investigation of crazing in polybutene spherulites under tensile drawing, Polymer. 48 (2007) 6041–6048.

[119] F. Detrez, S. Cantournet, R. Seguela, Plasticity/damage coupling in semi-crystalline polymers prior to yielding: Micromechanisms and damage law identification, Polymer. 52 (2011) 1998–2008.

[120] P. Bowden, R. Young, Deformation mechanisms in crystalline polymers, Journal of Materials Science. 9 (1974) 2034–2051.

[121] A. Cowking, F. Munro, Deformation and structure of doubly oriented polyethylene, Journal of Polymer Science Part B-Polymer Physics. 17 (1979) 357–370.

[122] A. Keller, D.P. Pope, Identification of structural processes in deformation of oriented polyethylene, Journal of Materials Science. 6 (1971) 453–478.

[123] D.P. Pope, A. Keller, Deformation of oriented polyethylene, Journal of Polymer Science Part B-Polymer Physics. 13 (1975) 533–566.

[124] A. Cowking, J.G. Rider, On molecular and textural reorientations in polyethylene caused by applied stress, Journal of Materials Science. 4 (1969) 1051–1058.

[125] D.A. Zaukelies, Observation of slip in nylon 66 and 610 and its interpretation in terms of a new model, Journal of Applied Physics. 33 (1962) 2797–2803.

[126] J. Preedy, E. Wheeler, A study of twinning in polyethylene, Journal of Materials Science. 12 (1977) 810–815.

[127] P. Allan, M. Bevis, Deformation processes in thin melt-cast films of high-density polyethylene .2. deformation processes in the non-equatorial regions of spherulites, Philosophical Magazine A-physics of Condensed Matter Structure Defects and Mechanical Properties. 41 (1980) 555–572.

[128] T. Seto, T. Hara, K. Tanaka, Phase transformation and deformation processes in oriented polyethylene, Japanese Journal of Applied Physics. 7 (1968) 31–42.

[129] P. Cerra, D.R. Morrow, J.A. Sauer, Deformation of polypropylene single crystals, Journal of Macromolecular Science-physics. B3 (1969) 33–51.

[130] I.L. Hay, A. Keller, Mechanically induced twinning and phase transformations, Journal of Polymer Science Part C: Polymer Symposia. 30 (1970) 289–295.

[131] K. Tanaka, T. Hara, T. Seto, Crystal structure of a new form of high-density polyethylene, produced by press, Journal of the Physical Society of Japan. 17 (1962) 873–874.

[132] J. Steidl, Z. Pelzbaue, Structural changes during deformation of high molecular-weight and low molecular-weight polyethylene, Journal of Polymer Science Part C: Polymer Symposium. (1972) 345–356.

[133] B.A. Newman, S. Song, Gamma-alpha transformation in isotactic polypropylene, Journal of Polymer Science Part A-2: Polymer Physics. 9 (1971) 181–186.

[134] B. Servet, D. Broussoux, F. Micheron, Stretching induced gamma-beta-transition in poly(vinylidene fluoride), Journal of Applied Physics. 52 (1981) 5926–5929.

[135] V. Miri, O. Persyn, J.M. Lefebvre, R. Seguela, a. Stroeks, Strain-induced disorder–order crystalline phase transition in nylon 6 and its miscible blends, Polymer. 48 (2007) 5080–5087.

[136] A. Peterlin, Molecular model of drawing polyethylene and polypropylene, Journal of Materials Science. 6 (1971) 490–508.

[137] A. Pawlak, A. Galeski, Plastic Deformation of Crystalline Polymers: The Role of Cavitation and Crystal Plasticity, Macromolecules. 38 (2005) 9688–9697.

[138] L. Lin, A.S. Argon, Structur and plastic-deformationof polyethylene, Journal of Materials Science. 29 (1994) 294–323.

[139] M. Butler, A. Donald, A. Ryan, Time resolved simultaneous small-and wide-angle X-ray scattering during polyethylene deformation—II. Cold drawing of linear polyethylene, Polymer. 39 (1998) 39–52.

[140] R. Seguela, Plasticity of semi-crystalline polymers: crystal slip versus melting-recrystallization, e-Polymers Journal. (2007) 1–20.

[141] R.J. Young, P.B. Bowden, J.M. Ritchie, J.G. Rider, Deformation mechanisms in oriented high-density polyethylene, Journal of Materials Science. 8 (1973) 23–36.

[142] Z. Bartczak, Influence of molecular parameters on high-strain deformation of polyethylene in the plane-strain compression. Part II. Strain recovery, Polymer. 46 (2005) 10339–10354.

[143] M. Yamada, K. Miyasaka, K. Ishikawa, Rolling of polyethylene single-crystal mats, Journal of Polymer Science Part B: Polymer Physics. 11 (1973) 2393–2401.

[144] G.W. Groves, P.B. Hirsch, Interlamellar slip in polyethylene, Journal of Materials Science. 4 (1969) 929–932.

[145] T. Tagawa, K. Ogura, Piled-lamellae structure in polyethylene film and its deformation, Journal of Polymer Science Part B-Polymer Physics. 18 (1980) 971–979.

[146] W.E. Kaufman, J.M. Schultz, Lamellar and interlamellar structure in melt-crystallized polyethylene .3. effects of small deformation, Journal of Materials Science. 8 (1973) 41–46.

[147] R.G. Quynn, H. Brody, Elastic hard fibers, Ournal of Macromolecular Science, Part B: Physics. 5 (1971) 721–738.

[148] J. Petermann, J.M. Schultz, Lamellar separation during deformation of high-density polyethylene, Journal of Materials Science. 13 (1978) 50–54.

[149] K. Friedrich, Crazes and shear bands in semi-crystalline thermoplastics, Advances in Polymer Science. 52-53 (1983) 225–274.

[150] R.J. Samuels, Structured Polymer Properties: Identification, Interpretation and Application of Crystalline Polymer Structure, John Wiley & Sons Inc, 1974.

[151] P. Allan, M. Bevis, Mechanisms of deformation in cross-linked polyethylene crystals, Philosophical Magazine. 36 (1977) 1121–1129.

[152] A. Galeski, A.S. Argon, R.E. Cohen, Changes in the morphology of bulk spherulitic nylon-6 due to plastic-deformation, Macromolecules. 21 (1988) 2761–2770.

[153] E. Weynant, J.M. Haudin, C. Gsell, In situ observation of the spherulite deformation in polybutene-1 (Modification I), Journal of Materials Science. 15 (1980) 2677–2692.

[154] I.L. Hay, A. Keller, Polymer deformation in terms of spherulites, Kkolloid-zeitschrift and Zeitschrift Fur Polymere. 204 (1965) 43–47.

[155] A. Galeski, A. Rozanski, Flory Prize Lecture: Cavitation during Drawing of Crystalline Polymers, Macromolecular Symposia. 298 (2010) 1–9.

[156] Q. Fu, Y. Men, G. Strobl, A molar mass induced transition in the yielding properties of linear polyethylene, Polymer. 44 (2003) 1941–1947.

[157] G. Capaccio, T.A. Crompton, I.M. Ward, Drawing behavior of linear polyethylene .1. rate of drawing as a function of polymer molecular-weight and initial thermal-treatment, Journal of Polymer Science Part B-polymer Physics. 14 (1976) 1641–1658.

[158] G. Capaccio, I.M. Ward, Effect of molecular-weight on morphology and drawing behavior of melt crystallized linear polyethylene, Polymer. 16 (1975) 239–243.

[159] S. Hobeika, Y. Men, G. Strobl, Temperature and strain rate independence of critical strains in polyethylene and poly(ethylene-co-vinyl acetate), Macromolecules. 33 (2000) 1827–1833.

[160] A. Pawlak, A. Galeski, Cavitation during Tensile Deformation of Polypropylene, Macromolecules. 41 (2008) 2839–2851.

[161] D.A. Opp, D.W. Skinner, R.J. Wiktorek, A model for polymer fatigue, Polymer Engineering & Science. 9 (1969) 121–130.

[162] J.L. Weaver, C.L. Beatty, The effect of temperature on compressive fatigue of polystyrene, Polymer Engineering & Science. 18 (1978) 1117–1126.

[163] A.J. Lesser, Fatigue behavior of polymers, Encyclopedia of Polymer Science and Technology. 6 (2002) 197–251.

[164] A.J. Lesser, Changes in mechanical behavior during fatigue of semicrystalline thermoplastics, Journal of Applied Polymer Science. 58 (1995) 869–879.

[165] Sauer, J. A.; Pae, K. D. Introduction to Polymer Science, John Wiley & Sons, Inc., New York, 1977.

[166] M.N. Riddell, G.P. Koo, J.L. O'Toole, Fatigue mechanisms of thermoplastics, Polymer Engineering & Science. 6 (1966) 363–368.

[167] T.I. Sogolova, Control of the mechanical properties of polymers by modification of their supramolecular structure, Polymer Mechanics. 2 (1966) 395–404.

[168] V.G. Savkin, V.A. Belyi, T.I. Sogolova, V.A. Kargin, Effect of supermolecular structures on the self-Heating of plastics under cyclic loads, Polymer Mechanics. (1966) 501–505.

[169] V.K. Kuchinskas, A.N. Machyulis, Fatigue and fracture of stabilized polycaprolactam, Polymer Mechanics. 3 (1967) 472–477.

[170] I. Bareishis, A. Stinskas, The effect of stabilizers on the fatigue strength of polycaproamide under tension-compression, Mechanics of Composite Materials. 9 (1973) 499–501.

[171] A. Stinskas, Y. Baushis, I. Bareishis, Effect of heat treatment on the static and fatigue strength of polycaproamide, Mechanics of Composite Materials. 8 (1972) 48–51.

[172] J. Sauer, G. Richardson, Fatigue of polymers, International Journal of Fracture. 16 (1980) 499–532.

[173] E. Foden, D.R. Morrow, J.A. Sauer, The effect of molecular weight on the fatigue behavior of polystyrene, Journal of Applied Polymer Science. 16 (1972) 519–526.

[174] R.W. Hertzberg, J.A. Manson, Fatigue of Engineering Plastics, Academic Press, Inc., Orlando, 1980.

[175] J. Sauer, E. Foden, D. Morrow, Influence of molecular weight on fatigue behavior of polyethylene and polystyrene, Polymer Engineering & Science. 17 (1977) 246–250.

[176] S. Wellinghoff, E. Baer, The mechanism of crazing in polystyrene, Journal of Macromolecular Science, Part B. 11 (1975) 367–387.

[177] J.A. Sauer, Static and dynamic properties of monodisperse polystyrenes: influence of molecular weight, Polymer. 19 (1978) 859–860.

[178] S. Warty, J.A. Sauer, A. Charlesby, Effects of radiation and chain ends on fatigue behaviour of polystyrene, European Polymer Journal. 15 (1979) 445–452.

[179] H. Nishimura, I. Narisawa, Fatigue behavior of medium-density polyethylene pipes, Polymer Engineering & Science. 31 (1991) 399–403.

[180] M. Niinomi, L. Wang, T. Enjitsu, K. Fukunaga, Fatigue characteristics of ultra high molecular weight polyethylene with different molecular weight for implant material., Journal of Materials Science. Materials in Medicine. 12 (2001) 267–72.

[181] A. Bernasconi, P. Davoli, D. Rossin, C. Armanni, Effect of reprocessing on the fatigue strength of a fibreglass reinforced polyamide, Composites Part A: Applied Science and Manufacturing. 38 (2007) 710–718.

[182] S. Barbouchi, V. Bellenger, a. Tcharkhtchi, P. Castaing, T. Jollivet, Effect of water on the fatigue behaviour of a pa66/glass fibers composite material, Journal of Materials Science. 42 (2007) 2181–2188.

[183] J.J. Horst, J.L. Spoormaker, Fatigue fracture mechanisms and fractography of short-glassfibre-reinforced polyamide 6, Journal of Materials Science. 32 (1997) 3641–3651.

[184] A. Griffith, The phenomena of rupture and flow in solids, Philosophical Transactions of the Royal Society of London. 221 (1921) 163–198.

[185] P. Paris, M. Gomez, W. Anderson, A rational analytic theory of fatigue, The Trends in Engenieering. 13 (1961) 9–14.

[186] A. Ramirez, J.A. Manson, R.W. Hertzberg, Fatigue crack propagation in amorphous poly(ethylene terephthalate), Polymer Engineering & Science. 22 (1982) 975–981.

[187] R. Hertzberg, H. Nordberg, J. Manson, Fatigue crack propagation in polymeric materials, Journal of Materials Science. 5 (1970) 521–526.

[188] P.E. Bretz, R.W. Hertzberg, J.A. Manson, Fatigue crack propagation in crystalline polymers: effect of moisture in nylon 66, Journal of Materials Science. 14 (1979) 2482–2492.

[189] M.D. Skibo, R.W. Hertzberg, J.A. Manson, Deformation, Yield and Fracture of Polymers, Plastic and Rubber Institute. (1979) 4.1–4.5.

[190] R.W. Hertzberg, J.A. Manson, W.C. Wu, progress in flaw growth and fracture toughness testing, ASTM STP. 536 (1973) 391.

[191] R.W. Hertzberg, M.D. Skibo, J.A. Manson, Fatigue crack propagation in polyacetal, Journal of Materials Science. 13 (1978) 1038–1044.

[192] G.P. Koo, L.G. Roland, Effect of cyclic loading on morphology of Polytetrafluoroethylene, Journal of Polymer Science - Polymer Letters Edition. 10 (1972) 1145–1152.

[193] G.P. Koo, Fluoropolymers, High polymers, 15th ed., Wiley Interscience, New York, 1972.

[194] G. Meinel, A. Peterlin, Plastic deformation of polyethylene.2. Change of mechanical properties during drawing, Journal of Polymer Science - Polymer Letters Edition. 9 (1971) 67–83.

[195] J. Wang, T. Haraguchi, H. Suzuki, M. Omata, The Influence of Crystallinity on Fatigue Crack Propagation Property for the Recycled FRTP, Transactions of the Japan Society of Mechanical Engineers. A. 65 (1991) 2099–2105.

[196] M. Iwamoto, E. Jinen, M. Suzuki, Effect of crystallinity and temperature on fatigue crack growth behavior of polypropylene,Macroscopic considerations, Journal of the Society of Materials Science (Japan). 37 (1988) 807–812.

[197] M. Iwamoto, E. Jinen, M. Suzuki, Effect of crystallinity and temperature on fatigue crack growth behavior of polypropylene,Microscopic considerations, Journal of the Society of Materials Science (Japan). 37 (1988) 1064–1070.

[198] A.F. Laghouati, Ph.D. dissertation, Univ.de Technologie de Compiègne, 1977.

[199] E. Oral, A. Malhi, O. Muratoglu, Mechanisms of decrease in fatigue crack propagation resistance in irradiated and melted UHMWPE, Biomaterials. 27 (2006) 917–925.

[200] F.X. Charentenay, F. Laghouati, J. Dewas, Deformation, Yield and Fracture of Polymers, Institute of Plastics and Rubber. (1979) P.6.1.

[201] J. Runt, M. Jacq, Effect of crystalline morphology on fatigue crack propagation in polyethylene, Journal of Materials Science. 24 (1989) 1421–1428.

[202] J. Strebel, A. Moet, The effects of annealing on fatigue crack propagation in polyethylene, Journal of Polymer Science Part B: Polymer Physics. 33 (1995) 1969–1984.

[203] A. Ramirez, P.M. Gaultier, J.A. Manson, R.W. Hertzberg, Fatigue in Polymer, Plastics and Rubber Institute, London, 1983.

[204] J.T. Yeh, J. Runt, Fatigue crack-propagation in annealed poly(butylene terephtalate), Journal of Materials Science. 24 (1989) 2637–2642.

[205] J.T. Yeh, J. Runt, Fatigue crack propagation in high-density polyethylene, Journal of Polymer Science Part B: Polymer Physics. 29 (1991) 371–388.

[206] K. Friedrich, Proceedings of the 9th Conference on Scanning Electron Microscopy, German Society for Testing Materials (DVM). (1973) 173.

[207] S. Kim, M. Skibo, J.A. Manson, R.W. Hertzberg, Fatigue crack propagation in poly (methyl methacrylate): effect of molecular weight and internal plasticization, Polymer Engineering & Science. 17 (1977) 194–203.

[208] M. Skibo, J.A. Manson, R.W. Hertzberg, E.A. Collins, Effects of molecular weight and plasticizer on fatigue crack propagation in PVC, Journal of Macromolecular Science, Part B. 14 (1977) 525–543.

[209] G. Pitman, I. Ward, The molecular weight dependence of fatigue crack propagation in polycarbonate, Journal of Materials Science. 15 (1980) 635–645.

[210] M. Hahn, R. Hertzberg, Comments on "The molecular weight dependence of fatigue crack propagation in polycarbonate", Journal of Materials Science. 17 (1982) 1533–1537.

[211] J.C. Michel, J.A. Manson, R.W. Hertzberg, Application of a unified theory of fatigue crack-propagation to amoprhous polyemrs, Polym. Prepr. (Am. Chem. Soc., Div. Polym. Chem.). 6 (1985) 141–149.

[212] J. Michel, J.A. Manson, R.W. Hertzberg, A simple viscoelastic model for fatigue crack propagation in polymers as a function of molecular weight, Polymer. 25 (1984) 1657–1666.

[213] Y.-L. Huang, N. Brown, The effect of molecular weight on slow crack growth in linear polyethylene homopolymers, Journal of Materials Science. 23 (1988) 3648–3655.

[214] P.E. Bretz, R.W. Hertzberg, J.A. Manson, The effect of molecular weight on fatigue crack propagation in nylon 66 and polyacetal, Journal of Applied Polymer Science. 27 (1982) 1707–1717.

[215] C. SHEU, R.D. GOOLSBY, Fatigue crack-propagation in high-density polyethylene and polypropylene, Organic Coatings and Applied Polymer Science Proceedings. 43 (1983) 833–838.

[216] A. Lustiger, R. Markham, Importance of tie molecules in preventing polyethylene fracture under long-term loading conditions, Polymer. 24 (1983) 1647–1655.

[217] P.E. Bretz, R.W. Hertzberg, J. a. Manson, Influence of absorbed moisture on fatigue crack propagation behaviour in polyamides, Journal of Materials Science. 16 (1981) 2061–2069.

[218] V. Bellenger, a Tcharkhtchi, P. Castaing, Thermal and mechanical fatigue of a PA66/glass fibers composite material, International Journal of Fatigue. 28 (2006) 1348–1352.

[219] J.J. Horst, N.. Salienko, J.L. Spoormaker, Fibre-matrix debonding stress analysis for short fibre-reinforced materials with matrix plasticity, finite element modelling and experimental verification, Composites Part A: Applied Science and Manufacturing. 29 (1998) 525–531.

[220] J.J. Horst, J.L. Spoormaker, Mechanisms of fatigue in short glass fiber reinforced polyamide 6, Polymer Engineering and Science. 36 (1996) 2718–2726.

[221] K. Noda, Fatigue failure mechanisms of short glass-fiber reinforced nylon 66 based on nonlinear dynamic viscoelastic measurement, Polymer. 42 (2001) 5803–5811.

[222] V. Bouda, V. Zilvar, A.J. Staverman, The effects of cyclic loading on polymers in a glassy state, Journal of Polymer Science: Polymer Physics Edition. 14 (1976) 2313–2323.

[223] L.B. Liu, A.F. Yee, D.W. Gidley, Effect of cyclic stress on enthalpy relaxation in polycarbonate, Journal of Polymer Science Part B: Polymer Physics. 30 (1992) 221–230.

[224] S. Sakurai, S. Nokuwa, M. Morimoto, M. Shibayama, S. Nomura, Changes in structure and properties due to mechanical fatigue for polyurethanes containing poly(dimethyl siloxane), Polymer. 35 (1994) 532–539.

[225] D.G. Legrand, G.R. Tryson, W. V Olszewski, M. Forth, Positional small-angle X-ray scattering, Polymer Engineering & Science. 22 (1982) 928–933.

[226] H. a Hristov, A.F. Yee, L. Xie, D.W. Gidley, Fatigue craze initiation in polycarbonate: study by small-angle X-ray scattering, Polymer. 35 (1994) 4287–4292.

[227] H. Hristov, A. Yee, D. Gidley, Fatigue craze initiation in polycarbonate: study by transmission electron microscopy, Polymer. 35 (1994) 3604–3611.

[228] L.B. Liu, D. Gidley, A.F. Yee, Effect of cyclic stress on structural changes in polycarbonate as probed by positron annihilation lifetime spectroscopy, Journal of Polymer Science Part B: Polymer Physics. 30 (1992) 231–238.

[229] S.N. Zhurkov, V.A. Zakrevskyi, V.E. Korsukov, V.S. Kuksenko, Mechanism of submicrocrack generation in stressed polymers, Journal of Polymer Science Part A-2: Polymer Physics. 10 (1972) 1509–1520.

[230] J. Kallrath, V. Altstädt, J. Schlöder, H. Bock, Analysis of fatigue crack growth behaviour in polymers and their composites based on ordinary differential equations parameter estimation, Polymer Testing. 18 (1999) 11–35.

[231] H.H. Kausch, K.L. Devries, Molecular aspects of high polymer fracture as investigated by ESR-technique, International Journal of Fracture. 11 (1975) 727–759.

[232] N.A. Jones, A.J. Lesser, Morphological study of fatigue-induced damage in isotactic polypropylene, Journal of Polymer Science Part B: Polymer Physics. 36 (1998) 2751–2760.

[233] E. Mourglia Seignobos, Compréhension des mécanismes physiques de fatigue dans le polyamide vierge et renforcé de fibres de verre, Institut National des Sciences Appliquées INSA-Lyon, 2009.

[234] A.A. Griffith, The Phenomena of Rupture and Flow in Solids, Philosophical Transactions of the Royal Society A: Mathematical, Physical and Engineering Sciences. 221 (1921) 163–198.

[235] C. Fouquey, J.-M. Lehn, A.-M. Levelut, Molecular recognition directed self-assembly of supramolecular liquid crystalline polymers from complementary chiral components, Advanced Materials. 2 (1990) 254–257.

[236] M. Kotera, J.-M. Lehn, J.-P. Vigneron, Self-assembled supramolecular rigid rods, Journal of Chemical Society, Chemical Communications. (1994) 197–199.

[237] J.-M. Lehn, Supramolecular polymer chemistry—scope and perspectives, Polymer International. 51 (2002) 825–839.

[238] S. Boileau, B. Laurent, F. Laupretre, F. Lortie, Soluble supramolecular polymers based on urea compounds, New Journal of Chemistry. 24 (2000) 845–848.

[239] V. Simic, L. Bouteiller, M. Jalabert, Highly Cooperative Formation of Bis-Urea Based Supramolecular Polymers, Journal of the American Chemical Society. 125 (2003) 13148–13154.

[240] F.H. Beijer, R.P. Sijbesma, H. Kooijman, A.L. Spek, E.W. Meijer, Strong Dimerization of Ureidopyrimidones via Quadruple Hydrogen Bonding, Journal of the American Chemical Society. 120 (1998) 6761–6769.

[241] R.P. Sijbesma, F.H. Beijer, L. Brunsveld, B.J. Folmer, J.H. Hirschberg, R.F. Lange, et al., Reversible polymers formed from self-complementary monomers using quadruple hydrogen bonding., Science. 278 (1997) 1601–4.

[242] F.M.R. Lange, M. Van Gurp, E.W. Meijer, Hydrogen-bonded supramolecular polymer networks, Journal of Polymer Science Part A: Polymer Chemistry. 37 (1999) 3657–3670.

[243] B.J.B. Folmer, R.P. Sijbesma, R.M. Versteegen, J.A.J. van der Rijt, E.W. Meijer, Supramolecular Polymer Materials: Chain Extension of Telechelic Polymers Using a Reactive Hydrogen-Bonding Synthon, Advanced Materials. 12 (2000) 874–878.

[244] L.R. Rieth, R.F. Eaton, G.W. Coates, Polymerization of Ureidopyrimidinone-Functionalized Olefins by Using Late-Transition Metal Ziegler–Natta Catalysts: Synthesis of Thermoplastic Elastomeric Polyolefins, Angewandte Chemie International Edition. 40 (2001) 2153–2156.

[245] K. Yamauchi, J.R. Lizotte, D.M. Hercules, M.J. Vergne, T.E. Long, Combinations of Microphase Separation and Terminal Multiple Hydrogen Bonding in Novel Macromolecules, Journal of the American Chemical Society. 124 (2002) 8599–8604.

[246] K. Yamauchi, A. Kanomata, T. Inoue, T.E. Long, Thermoreversible Polyesters Consisting of Multiple Hydrogen Bonding (MHB), Macromolecules. 37 (2004) 3519–3522.

[247] F. Tournilhac, C. Soulié-Ziakovic, L. Leibler, L. Lachaize, Supramolecular polymer, U.S. Patent US 20050148760, 2005.

[248] P. Cordier, F. Tournilhac, C. Soulié-Ziakovic, L. Leibler, Self-healing and thermoreversible rubber from supramolecular assembly., Nature. 451 (2008) 977–80.

[249] F. Tournilhac, L. Leibler, P. Cordier, C. Soulié-Ziakovic, Elastic materials, U.S. Patent WO2006087475, 2006.

[250] P. De Groote, J. Devaux, P. Godard, Effect of benzenesulfonamide plasticizers on the glass-transition temperature of semicrystalline polydodecamide, Journal of Polymer Science Part B: Polymer Physics. 40 (2002) 2208–2218.

[251] P. De Groote, J. Devaux, P. Godard, The effect of benzenesulfonamide plasticizers on the glass transition temperature of an amorphous aliphatic polyamide, Polymer International. 51 (2002) 40–49.

[252] P. De Groote, J. Devaux, A.M. Jonas, P. Godard, Melt properties and crystal morphology of polydodecamide plasticized by benzenesulfonamides, Journal of Polymer Science Part B: Polymer Physics. 39 (2001) 2022–2034.

[253] P. De Groote, P.G. Rouxhet, J. Devaux, P. Godard, Infrared Study of the Hydrogen Bonding Association in Polyamides Plasticized by Benzenesulfonamides. Part I: Self-Association in Amide and Sulfonamide Systems; Part II: AmideSulfonamide Interaction, Applied Spectroscopy. 55 (2001) 877–887.

[254] M.W. Huang, K.J. Zhu, E.M. Pearce, T.K. Kwei, The modification of nylon 6 by a phenol-formaldehyde resin, Journal of Applied Polymer Science. 48 (1993) 563–573.

[255] P.T. Huang, J.L. Lee, S.C. Chiu, T.K. Kwei, E.M. Pearce, Modification of Nylon 6 by phenol-containing polymers, Journal of Applied Polymer Science. 73 (1999) 295–300.

[256] P.-T. Huang, T.K. Kwei, E.M. Pearce, S. V. Levchik, Blends of nylon-6 with phenol-containing polymers, Journal of Polymer Science Part A: Polymer Chemistry. 39 (2001) 841–850.

[257] F.-Y. Wang, C.-C.M. Ma, H.-D. Wu, Hydrogen bonding in polyamide toughened novolac type phenolic resin, Journal of Applied Polymer Science. 74 (1999) 2283.

[258] F.Y. Wang, C.C.M. Ma, W.J. Wu, Mechanical properties, morphology, and flame retardance of glass fiber-reinforced polyamide-toughened novolac-type phenolic resin, Journal of Applied Polymer Science. 73 (1999) 881–887.

[259] Z. Zhong, Q. Guo, The miscibility and morphology of hexamine cross-linked novolac/poly(ε-caprolactone) blends, Polymer. 38 (1997) 279–286.

[260] Y. Zhang, Y. Liu, Q. Wang, Synergistic effect of melamine polyphosphate with macromolecular charring agent novolac in wollastonite filled PA66, Journal of Applied Polymer Science. 116 (2010) 45–49.

[261] A.Y.. Hung, F.-Y. Wang, C.-C.M. Ma, H.-D. Wu, Thermodynamic properties affect the molecular motion of novolac type phenolic resin blended with polyamide, European Polymer Journal. 39 (2003) 225–231.

[262] J. Hartikainen, O. Lehtonen, T. Harmia, M. Lindner, S. Valkama, J. Ruokolainen, et al., Structure and Morphology of Polyamide 66 and Oligomeric Phenolic Resin Blends: Molecular Modeling and Experimental Investigations, Chemistry of Materials. 16 (2004) 3032–3039.

[263] F. Wang, C.-C.M. Ma, A.Y.C. Hung, H. Wu, The Interassociation Equilibrium Constant and Thermodynamic Properties of Phenolic Resin/ Polyamide 6 Blend, Macromolecular Chemistry and Physics. 202 (2001) 2328–2334.

[264] J. Keeler, Understanding NMR Spectroscopy, Chapter 2, University of Cambridge, 2002.

[265] R.M. Michell, A.J. Müller, V. Castelletto, I. Hamley, G. Deshayes, P. Dubois, Effect of Sequence Distribution on the Morphology, Crystallization, Melting, and Biodegradation of Poly(ε-caprolactone-co -ε-caprolactam) Copolymers, Macromolecules. 42 (2009) 6671–6681.

[266] G. Montaudo, F. Samperi, M. Montaudo, Characterization of synthetic polymers by MALDI-MS, Progress in Polymer Science. 31 (2006) 277–357.

[267] C.S. Linda, T.G. David, G.F. Meyers, Introduction to Polymer Morphology, in: Polymer Microscopy, Springer New York, 2008: p. 18.

[268] http://www.polymerprocessing.com/polymers/PA66.html, (n.d.).

[269] T. Young, An Essay on the Cohesion of Fluids, Philosophical Transactions of the Royal Society of London. 95 (1805) 65–87.

[270] D. Owens, R. Wendt, Estimation of the surface free energy of polymers, Journal of Applied Polymer Science. 13 (1969) 1741–1747.

[271] F. Garbassi, M. Morra, Polymer Surfaces: From Physics to Technology, Wiley, New York, 1998.

[272] J. a. Casado, F. Gutiérrez-Solana, J. Polanco, I. Carrascal, The assessment of fatigue damage on short-fiber-glass reinforced polyamides (PA) through the surface roughness evolution, Polymer Composites. 27 (2006) 349–359.

[273] D. Hoey, D. Taylor, Fatigue in porous PMMA: The effect of stress concentrations, International Journal of Fatigue. 30 (2008) 989–995.

[274] S. Timoshenko, J.N. Goodier, Theory of elasticity, third edit, McGraw-Hill, New York, 1970.

[275] I. a. Carrascal, J. a. Casado, S. Diego, J. a. Polanco, F. Gutiérrez-Solana, Fatigue damage analysis based on energy parameters in reinforced polyamide, Fatigue & Fracture of Engineering Materials & Structures. 35 (2012) 683–691.

[276] M. De Monte, E. Moosbrugger, M. Quaresimin, Influence of temperature and thickness on the off-axis behaviour of short glass fibre reinforced polyamide 6.6 – cyclic loading, Composites Part A: Applied Science and Manufacturing. (2010).

[277] A. Guinier, La diffraction des rayons X aux très petits angles; application a l'etude de phenomenes ultramicroscopiques, Annal. De Physique (Paris). 12 (1939) 161–237.

[278] G. Beaucage, Small-Angle Scattering from Polymeric Mass Fractals of Arbitrary Mass-Fractal Dimension, Journal of Applied Crystallography. 29 (1996) 134–146.

[279] S.M. Aharoni, M. Plains, T. Largman, Process for Increasing the Melt Viscosity of Polyamide with Aryl Phosphate Compound, U.S. Patent 4,390,667, 1983.

[280] G. Özkoç, G. Bayram, M. Quaedflie, Effects of microcompounding process parameters on the properties of ABS/polyamide- • 6 blends based nanocomposites, Journal of Applied Polymer Science. 107 (2008) 3058–3070.

[281] F. Khoury, The formation of negatively birefringent spherulites in polyhexamethylene adipamide (nylon 66), Journal of Polymer Science. 33 (1958) 389–403.

[282] H. Mitomo, K. Nakazato, I. Kuriyama, Lamellar thickening behaviour of nylon-6,6 crystal by annealing, Polymer. 19 (1978) 1427–1432.

[283] F.N. Liberti, B. Wunderlich, Melting of polycaprolactam, Journal of Polymer Science Part A-2: Polymer Physics. 6 (1968) 833–848.

[284] J.F. Kenney, Properties of block versus random copolymers, Polymer Engineering & Science. 8 (1968) 216–226.

[285] W.B. You, D.T. Su, J.Y. Wu, M.S. Lee, Preparation of Polyamide with Mixture of Phosphorus Catalysts, U.S. Patent 5,298,598, 1994.

[286] R.C. Wheland, Process for Increasing Polyamide Molecular Weight with Organophosphonic Acid or Ester Catalysts on the Presence of Alumina-Containing Titanium Dioxide, U.S. Patent 5,142,000, 1992.

[287] J.F. Buzinkai, M.R. DeWitt, R.C. Wheland, Process for Increasing the Relative Viscosity of Polyamides with Reduced Thermal Degradation, U.S. Patent 5,116,919, 1992.

[288] R.C. Wheland, I.K. Miller, Process for Increasing Polyamide Molecular Weight with P Containing Catalyst, U.S. Patent 4,912,175, 1990.

[289] R.C. Wheland, Process for Increasing the Molecular Weight of a Polyamide with P Containing Catalyst, U.S. Patent 4,966,949, 1990.

[290] R.S. Curatolo, R.C. Sentman, G.P. Coffey, Catalytic Process for the Manufacture of Polyamide from Diamines and Diamides, U.S. Patent 4,543,407, 1985.

[291] H. Hofmann, H.J. Rothe, G. Skupin, K. Wolff, Preparation of Spinnable Polyamide from Dinttrile, Diamine, H2 O with P Containing Catalyst, U.S. Patent 4,436,898, 1984.

[292] G.P. Coffey, R.C. Sentman, R.S. Curatolo, Preparation of Spinnable Polyamide from Dinittle/Diamine/Water with Metal Salt of Oxygenated Phosphorus Compound Catalyst, U.S. Patent 4,490,521, 1984.

[293] W.L. Tomek, Polyamidation Process, U.S. Patent 3,947,424, 1976.

[294] H.G. Burrows, S.J. Hepworth, Polyamides having Improved Dyeability and Thermal Stability, U.S. Patent 3,944,518, 1976.

[295] D.W. Wujciak, Polymerization of Polyamide Precursor Salt in the Presence of a Phosphinic Acid, U.S. Patent 3,365,428, 1968.

[296] W.M. Sum, Polymerization of Polyamide Forming Reactants with Hypophosphite Catalysts,, U.S. Patent 3,173,898, 1965.

[297] M. Genas, Hypophosphorous Acid and Hypophosphites as Catalyzers of Condensation of Monoamino Monocarboxylic Acids, U.S. Patent 2,564,001, 1951.

[298] B.A. Lysek, R.W. Ables, Nucleation of Polyamides in the Presence of Hypophosphite, U.S. Patent 6,197,855, 2001.

[299] K. Kazuhiko, O. Nobuo, I. Masaaki, Resin Composition and its Production, U.S. Patent 7,165,053, 1995.

[300] P. Kelmchuk, Stabilized Polyamide Compositions, U.S. Patent 3,691,131, 1972.

[301] E. Agouri, H. Muller, Improvements in and Relating to the Stabilization of Polyamides, U.S. Patent 1,111,286, 1968.

[302] W. Zheng, B.K. McAuley, E.K. Marchildon, Z. Yao, Melt-•Phase Nylon 612 Polycondensation Kinetics: Effects of Sodium Hypophosphite Catalyst, The Canadian Journal OF Chemical Engineering. 85 (2007) 180–187.

[303] L.F. Beste, R.C. Houtz, Amide interchange reactions, Journal of Polymer Science. 8 (1952) 395–407.

[304] N. Jones, E. Atkins, M. Hill, Investigation of solution-•grown, chain-folded lamellar crystals of the even-•even nylons: 6 6, 8 6, 8 8, 10 6, 10 8, 10 10, 12 6, 12 8, 12 10, and 12 12, Journal of Polymer Science: Part B: Polymer Physics. 38 (2000) 1209–1221.

[305] A. Baji, Y. Mai, S. Wong, M. Abtahi, X. Du, Mechanical behavior of self-assembled carbon nanotube reinforced nylon 6, 6 fibers, Composites Science and Technology. 70 (2010) 1401–1409.

[306] F.L. Beyer, C. Ziegler, Wide-Angle X-ray Scattering Characterization of the Morphology of Nylon 6 6 Obturator Materials, U.S. Army Research Laboratory Report. (2004).

[307] L. Alexander, X-ray diffraction methods in polymer science, Journal of Materials Science. 6 (1971) 93.

[308] R. Brill, Behavior of polyamides on heating, Journal Für Praktische Chemie. 161 (1942) 49–64.

[309] N. Murthy, Interactions between Crystalline and Amorphous Domains in Semicrystalline Polymers: Small-Angle X-ray Scattering Studies of the Brill Transition in Nylon 6,6.pdf, Macromolecules. 32 (1999) 5594–5599.

[310] J.L. Koenig, M.C. Agboatwalla, Infrared studies of chain folding in polymers. v. polyhexamethylene adipamide, Journal of Macromolecular Science, Part B. 2 (1968) 391–420.

[311] H.W. Starkweather, J.F. Whitney, D.R. Johnson, Crystalline order in nylon 66, Journal of Polymer Science Part A: General Papers. 1 (1963) 715–723.

[312] H. Mitomo, Correspondence of lamellar thickness to melting point of nylon-6, 6 single crystal, Polymer. 29 (1988) 1635–1642.

[313] J.H. Magill, M. Girolamo, A. Keller, Crystallization and morphology of nylon-6, 6 crystals: 1. Solution crystallization and solution annealing behaviour, Polymer. 22 (1981) 43–55.

[314] G. Hinrichsen, Untersuchungen zu Struktur und Eigenschaften der Polyamide, Die Makromolekulare Chemie. 166 (1973) 291–306.

[315] I. Goodman, A.H. Kehayoglou, Anionic copolymers of caprolactam with laurolactam (nylon 612 copolymers) II. Crystallisation, glass transitions and tensile properties, European Polymer Journal. 19 (1983) 321–325.

[316] X. Wang, Q. Zheng, L. Du, Influence of preparation methods on the structures and properties for the blends between polyamide 6co6T and polyamide 6: Melt-mixing and in-situ blending, Journal of Polymer Science. (2008) 201–211.

[317] X. Wang, Q. Zheng, G. Yang, Influence of preparation methods on structure and properties of PA6/PA66 blends: A comparison of melt-•mixing and in situ blending, Journal of Polymer Science: Part B: Polymer Physics. 45 (2007) 1176–1186.

[318] H.H. Kausch, G.H. Michler, The effect of time on crazing and fracture, in: Intrinsic Molecular Mobility and Toughness of Polymers, Springer Verlag, 2005: pp. 1–33.

[319] L. Lin, A.S. Argon, Deformation resistance in oriented nylon 6, Macromolecules. 25 (1992) 4011–4024.

[320] V.A. Beloshenko, A.V. Voznyak, Y.V. Voznyak, V.A. Glasunova, T.E. Konstantinova, Polyamide-6 Structure Modification by Combined Solid-Phase Extrusion, Polymer Engineering and Science. 52 (2012) 1815–1820.

[321] M. Ito, K. Mizuochi, T. Kanamoto, Effects of crystalline forms on the deformation behaviour of nylon-6, Polymer. 39 (1998) 4593–4598.

[322] L. Penel-Pierron, R. Séguéla, J.M. Lefebvre, V. Miri, C. Depecker, M. Jutigny, et al., Structural and Mechanical Behavior of Nylon-6 Films. II. Uniaxial and Biaxial Drawing, Journal of Polymer Science: Part B: Polymer Physics. 39 (2001) 1224–1236.

[323] J. Petermann, W. Kluge, H. Gleiter, Electron microscopic investigation of the molecular mechanism of plastic deformation of polyethylene and isotactic polystyrene crystals, Journal of Polymer Science: Polymer Physics Edition. 17 (1979) 1043–1051.

[324] J. Rault, Yielding in amorphous and semi-crystalline polymers: the compensation law, Journal of Non-Crystalline Solids. 235-237 (1998) 737–741.

[325] J. Rault, The alpha c transition in semicrystalline polymers: A new look at crystallization deformation and aging process, Journal of Macromolecular Science-reviews in Macromolecular Chemistry and Physics. C37 (1997) 335–387.

[326] O. Darras, R. Séguéla, Tensile yield of polyethylene in relation to crystal thickness, Journal of Polymer Science Part B: Polymer Physics. 31 (1993) 759–766.

[327] B. Fayolle, a. Tcharkhtchi, J. Verdu, Temperature and molecular weight dependence of fracture behaviour of polypropylene films, Polymer Testing. 23 (2004) 939–947.

[328] B. Yalcin, Z. Ergungor, Y. Konishi, M. Cakmak, C. Batur, Molecular origins of toughening mechanism in uniaxially stretched nylon 6 films with clay nanoparticles, Polymer. 49 (2008) 1635–1650.

[329] D.G.M. Wright, R. Dunk, D. Bouvart, M. Autran, The effect of crystallinity on the properties of injection moulded polypropylene and polyacetal, Polymer. 29 (1988) 793–796.

[330] L. Barish, The study of cracking and fracturing of spherulitic isotactic polypropylene, Journal of Applied Polymer Science. 6 (1962) 617–623.

[331] F.P. Reding, A. Brown, Effect of Spherulites on Physical Properties of Fluorothene, Industrial & Engineering Chemistry. 46 (1954) 1962–1967.

Résumé en Français

Introduction

Ce travail de thèse a été mené au sein du LPMA (Laboratoire Polymères et Matériaux Avancés), unité mixte de recherche entre le CNRS et Rhodia-Solvay. Cette étude s'inscrit dans la thématique de développement des matériaux polymères pour l'allègement de la voiture dans le but de réduire la consommation d'essence et l'émission du CO_2. Les polyamides apparaissent parmi les candidats idéals pour remplacer le métal car ils présentent un bon compromis entre propriétés thermomécaniques et légèreté. A noter que pendant le service d'une véhicule, les pièces de structure sont soumises à des sollicitations mécaniques dans des conditions environnementales très variées (température, humidité, carburant…) et leurs propriétés mécaniques évoluent au cours du temps jusqu'à la ruine du matériau. Ainsi, il nous parait très important d'identifier les mécanismes à l'origine de détérioration de ces matériaux et de les contrôler si c'est possible.

Dans un travail précédent (Thèse E. Mourglia-Seignobos-2009), les mécanismes d'endommagement dans les polyamides semi-cristallines soumis à des chargements cycliques ont pu être identifiées : Il s'agit de mécanismes de nucléation des cavités de taille nanométrique dans la phase amorphe qui croissent jusqu'à atteindre une certaine taille critique causant la rupture finale. Dans le cadre de cette thèse, on va essayer de contrôler les mécanismes d'endommagement de ces matériaux via la modification de la phase amorphe du polyamide 66. Il s'agit d'augmenter l'énergie cohésive de la phase amorphe du polyamide par l'introduction de fonctions polaires (phénol) capables d'établir des liaisons Hydrogènes très énergétiques avec les fonctions amides. Le défi et de réussir à modifier la phase amorphe du polyamide 66 sans trop perturber son organisation cristalline. Ainsi, cette étude s'intéresse plus particulièrement à la relation entre la microstructure (phase amorphe, et cristalline) des matériaux obtenus et leurs performances mécaniques.

Chapitre I : Etude bibliographique

Le premier chapitre de ce manuscrit (page 7) présente une étude bibliographique qui traite l'état de l'art sur la chimie, microstructure, mise en ouvres et propriétés mécaniques des polyamides, notamment celles du polyamide 66.

Les polyamides contiennent des fonctions amides qui résultent souvent de la polycondensation entre groupement amines et acides. Différentes techniques de préparation

sont utilisées : polycondensation en solution, anionique, en masse, interraciale ou post condensation à l'état solide. La polycondensation en masse est la technique la plus répandue. La mise en œuvre des polyamides est comparable à celle d'autres polymères et implique des étapes d'extrusion et d'injection. La particularité des polyamides est que la teneur en eau doit être bien contrôlé afin d'éviter des réactions d'hydrolyse ou de polycondensation (réactions en équilibre) à l'état fondu. Dans le cas des polyamides contenant plusieurs monomères (copolymères) d'autres réactions à l'état fondu pourront avoir lieu. Ces réactions connues sous le nom de « transamidifications » impliquent des échanges de monomères entre les chaînes via trois réactions principales : aminolyse, acidolyse et amidolyse. Cela pourra aboutir à une répartition des monomères tout au long d'une chaîne de copolyamide différente de la distribution initiale.

A noter que les co-monomères peuvent être répartis d'une façon arbitraire (copolymère aléatoire ou statistique) ou par séquences d'homopolymères (copolymère bloc). Ce dernier présente plus d'intérêt que le copolymère statistique du fait qu'il rassemble souvent les propriétés des homopolymères correspondants. Deux voies de synthèses peuvent être identifiées dans la littérature: La polycondensation en deux étapes et la polycondensation à l'état fondue. De point de vue industriel, la deuxième voie est plus attractive et souvent accomplie durant l'étape d'extrusion. Toutefois les conditions d'extrusion doivent être contrôlées très soigneusement afin de limiter les réactions d'échanges citées ci-dessus.
Ensuite la microstructure du polyamide 66 est présente de l'échelle nanométrique (maille cristalline) jusqu'à l'échelle micrométrique (sphérolite). Les caractéristiques de la phase amorphe (mobilité de chaînes et relaxations) ainsi que le mécanisme de plastification par l'eau sont aussi décrits.

Dans une deuxième partie, nous nous sommes plus particulièrement intéressés aux propriétés mécaniques des polymères surtout les polymères semi-cristallins. Il apparait dans la littérature que la microstructure affecte largement les performances mécaniques. Par exemple, la rigidité du matériau ainsi que la résistance à l'écoulement augmentent quand le taux de cristallinité augmente. La taille des sphérolites a une influence aussi sur ces propriétés : quand leur taille diminue, le module de Young augmente. Concernant la résistance à la fatigue, il a été montré que la masse moléculaire influe significativement la tenue en fatigue : La durée de vie augmente quand la masse moléculaire augmente. Plusieurs études signalaient aussi un effet positif du taux de cristallinité sur la tenue en fatigue. La morphologie et la perfection cristalline ont aussi une influence sur les propriétés mécaniques : plus la structure est fine et parfaite, plus les propriétés mécaniques seront bonnes.

L'état de l'art nous a permis de bien établir la relation entre la microstructure et les propriétés ultimes de ces matériaux, toutefois peu d'études sont intéressées à l'impact de la cohésion de la phase amorphe sur les propriétés mécaniques. En se basant sur le modèle énergétique établi par E. Mourglia-Seignobos pour décrire l'endommagement dans le PA66, l'objectif dans ce travail ainsi que la stratégie adoptée pour atteindre cet objectif a été définie. Il s'agit d'augmenter la cohésion de la phase amorphe via l'introduction des groupements à forte interactions intermoléculaire avec les groupements amides. La technique adoptée pour incorporer ces groupements est l'extrusion réactive qui permette d'obtenir des copolymères bloc susceptibles de cristalliser de la même façon que le PA66. L'idée est de faire varier seulement la microstructure de la phase amorphe mais pas celle de la phase cristalline afin d'établir la relation entre les propriétés ultimes du matériau et l'organisation de sa phase amorphe.

Chapitre II : Matériaux et techniques expérimentales

Le chapitre II (page 59) décrit en détail les matériaux étudiés dans ce travail ainsi que les techniques expérimentales utilisées pour préparer et caractériser ces matériaux.

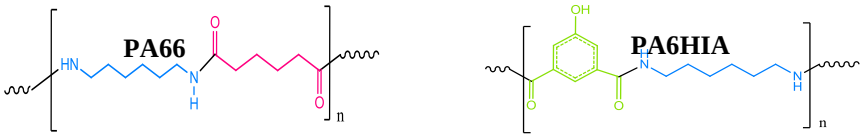

Figure 1: Structure chimique du PA66 et PA6/HIA

Pour préparer les copolyamides bloc, un PA6,6 déséquilibré amine PA66-NH_2 (PA1) et un semi-aromatique PA6HIA terminé acide PA6HIA-COOH ont été utilisés. Les structures chimiques de ces polymères sont montrées sur la Figure 1.

Ensuite un deuxième polyamide PA 2(Mn = 12100 g/mol, Mw = 38200 g/mol) sélectionné comme référence a été utilisé. Pour étudier l'effet de la masse moléculaire sur les propriétés mécaniques du PA6,6, un troisième PA66 (PA3) obtenu par post polycondensation à l'état solide a été choisi.

Les outils de mise en œuvre utilisés pour la réalisation des complymères sont ensuite présentés :

- ✓ Un microcompoundeur (extrudeuse bivis co-rotative discontinue. Cet outil nous a permis de faire varier les paramètres de mise en œuvre (température, temps de séjour) et ajout de catalyseur) dans le but de trouver les conditions expérimentales favorable à la réaction de co-polycondensation.
- ✓ Une extrudeuse Leistritz bivis co-rotative avec un rapport L/D= 35 mm
- ✓ Une presse à injecter Arburg

Les principales méthodes de caractérisation utilisées pendant cette thèse sont également présentées :

- ➢ Chromatographie d'Exclusion Stérique (SEC)
- ➢ Spectroscopie de masse MALDI-TOF
- ➢ Résonnance magnétique nucléaire (RMN)
- ➢ Rhéomètre capillaire
- ➢ Microscopie optique, électronique à balayage (MEB) et transmission (MET)
- ➢ Diffraction des rayons X aux grandes angles (WAXD), petits angles (SAXS) et ultra petits angles (USAXS)
- ➢ Analyse dynamique différentielle DSC classique et DSC modulée (MDSC).
- ➢ Analyse mécanique dynamique (DMA)
- ➢ Mesure d'angle de contact
- ➢ Test de traction, de choc et de fatigue
- ➢ Analyse d'image

Chapitre III : Synthèse, préparation et mise en œuvre des matériaux

Dans la première partie de ce chapitre, des copolyamides blocs avec différents compositions ont été préparés par la technique d'extrusion réactive. Dans un premier temps les conditions expérimentales favorables à la préparation des copolyamides ont été déterminées à petit échelle (microcompoundeur). Nous montrons que le mélange du polyamide66 terminé par des fonctions amines avec du polyamide semi-aromatique terminé par des fonctions carboxyliques permet d'obtenir des copolyamides aliphatique-semi aromatique essentiellement par réaction entre les groupes terminaux comme détaillé dans la Figure 2.

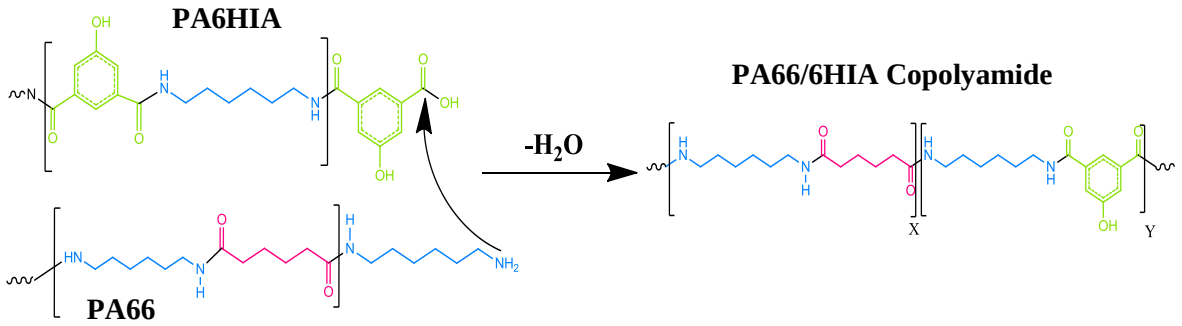

Figure 2: Formation du copolyamide PA66/6HIA par réaction entre les groupements terminaux

Nous avons observé que le degré de conversion des homopolymères (PA66-NH_2 et PA6HIA-COOH) est plus important à des temps d'extrusion très longue. La température de cristallisation de produits obtenus est légèrement plus faible que celle du PA66 de départ. Alors que leurs températures de fusions sont très proches Cela signifie que le composant PA66 du copolymère se cristallise de la même façon que celle du PA66. Ces résultats laissent penser que le copolyamide obtenu existe sous la forme d'un copolymère bloc de PA66 et PA6HIA.

Nous mettons en évidence que l'ajout de catalyseur (hypophosphite de sodium) permet d'atteindre des taux de conversion, des homopolyamides en copolyamides, très élevés pendant un temps court. De plus, les caractéristiques thermiques (température de cristallisation, cristallinité et température de fusion) des produits obtenus ne sont pas largement affectées. Cela signifie que l'ajout du catalyseur accélère les réactions entre groupements terminaux, mais pas les réactions de transamidification ou d'échanges.

Ensuite, l'effet de la température d'extrusion sur la formation des PA66/6HIA copolyamides a été étudié. Nous avons observé que l'augmentation de la température permet de plus incorporer les segments 6HIA dans les copolymères obtenus. Ceci a été mis en évidence par superposition des chromatogrammes de masse moléculaires détectés à deux longueurs d'onde (254 nm: détection des fonctions amides et 310 nm: détection des fonctions HIA) comme montré sur la Figure 3.

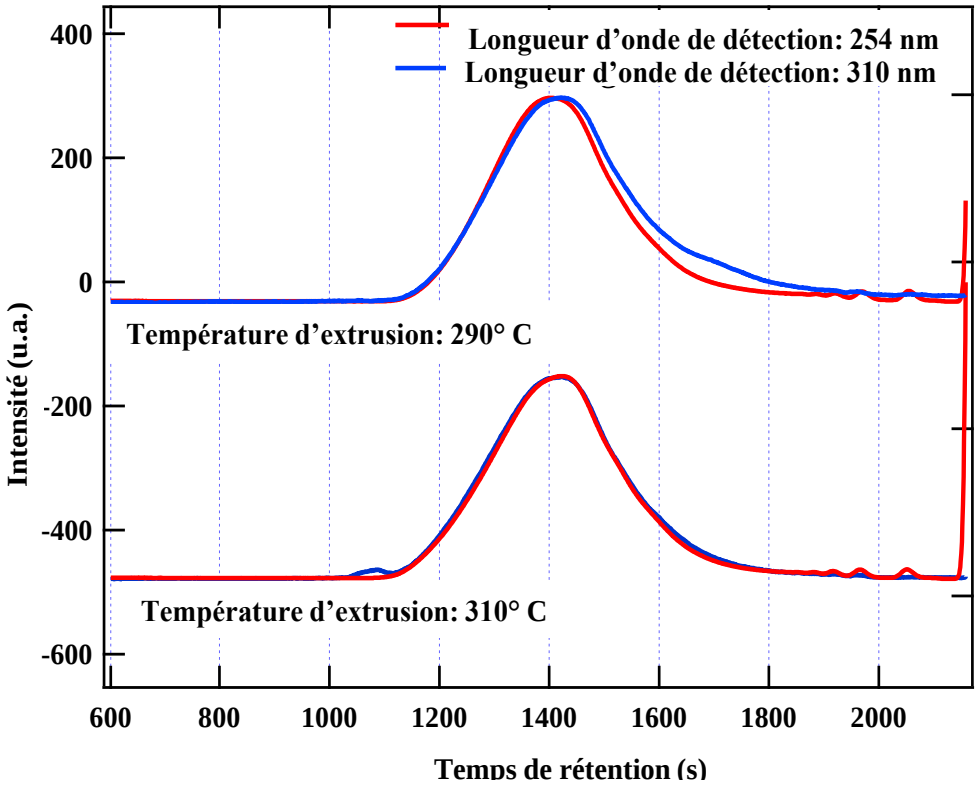

Figure 3:superposition des chromatogrammes obtenus à 254 nm et 310 nm pour le copolyamide PA66/6HIA (90/10 w:w) extrude à deux températures

La longueur de bloc de chaque composant, déterminée par RMN ^{13}C, a été comparé au nombre d'unité de répétition dans les polyamides de départ. On a observé que les séquences du PA66 et PA6HIA sont plus courtes que celles des homopolyamides et que la longueur moyenne de ces blocs diminue quand la température d'extrusion augmente. Il semble que l'augmentation de la température d'extrusion active les réactions entre groupement terminaux ainsi que les réactions d'échanges. Toutefois, la longueur du bloc PA66 dans les copolyamides obtenus reste suffisamment longue pour que les séquences de PA66 cristallisent de la même façon que l'homopolyamide de départ. Cela explique l'invariabilité de la température de fusion et la légère réduction de la température de cristallisation des copolyamides extrudés à haute température (voir Tableau 1).

Mélange	Température d'extrusion (°C)	T_C (°C)	ΔHc (J/g)	T_m (°C)	ΔHm (J/g)	$Xc_{[sample]}$ (%)	$Xc_{[PA66]}$ (%)
PA66/PA6HIA (90/10 w:w)	290	220.6	49.17	258.4	59.13	30.2	33.5
	310	214	49.02	257.8	59.2	30.2	33.5

Tableau 1: Propriétés thermiques obtenues par DSC sur les mélanges PA66/PA6HIA contenant 100 ppm de catalyseur, extrudés pendant 180 s

Après identification de conditions d'extrusion favorables à la formation du copolyamide PA66/6HIA (90/10 w :w), différents mélangés contenant un taux croissant du PA6HIA (de 10 % jusqu'à 40 % en masse) ont été préparés par extrusion à 310°C pendant 180 s en présence 100 ppm de catalyseur.

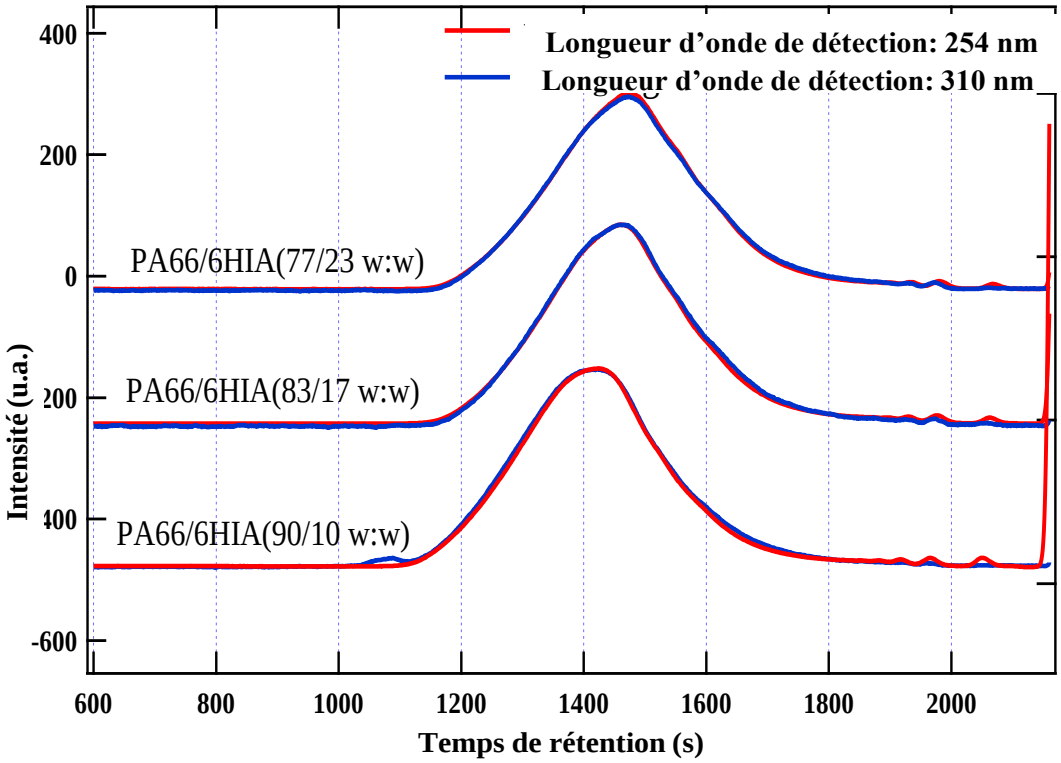

Figure 4: Chromatogrammes GPC du PA66/PA6HIA (90/10 w:w) contenant 100 ppm du catalyseur extrudé pendant 180 s à 290°C ou 310°C

La masse moléculaire des copolymères obtenus a été caractérisée par GPC. On a confirmé que dans les conditions expérimentales citées ci-dessus, le PA6HIA est totalement incorporé dans le copolymère obtenu (voir Figure 4). Nous avons aussi observé que la masse moléculaire du copolymère obtenu est dépendante de rapport entre les fonctions réactives. Un scénario de réactions été proposé afin d'explication les distributions de masse moléculaires obtenues. Ensuite, nous nous sommes intéressés à la longueur de chaque bloc pour les compositions étudiées. Une tendance a été identifiée comme montré dans le tableau 2 : quand la teneur en PA6HIA augmente, la longueur du bloc PA66 et PA6HIA diminue.

Polymère	Conditions d'extrusion	$\bar{L}_{PA66}$	$\bar{L}_{PA6HIA}$
PA6HIA	-	-	17.2 [a]
PA66/6HIA(100/0 w:w)	-	64.1 [b]	-
PA66/6HIA(90/10 w:w)	180 s at 310°C	46	5.11
PA66/6HIA(83/17 w:w)	180 s at 310°C	27.2	4.47
PA66/6HIA(77/23 w:w)	180 s at 310°C	16	4.44

Tableau 2: Longueur moyenne de la séquence PA66 et PA6HIA dans les copolyamides PA66/6HIA; (a) déterminé par ^{1}H RMN (b): déterminée à partir de la concentration des groupements terminaux

L'effet de la fraction du PA6HIA amorphe sur les transitions thermiques (Tg, Tc et Tf) des copolymères a été étudié par DSC. Pour la température de transition vitreuse, on a observé que la Tg augmente avec l'augmentation du taux de PA6HIA et qu'à forte concentration du

PA6HIA (40% w), deux températures de transition vitreuse sont présentes (voir Figure 5). Cela signifie que le mélange contenant 40 % du PA6HIA n'est pas totalement miscible. De plus, on a constaté que la variation de la Tg avec la fraction du PA6HIA ne suit pas la loi de Fox, établie dans les cas de mélanges amorphes.

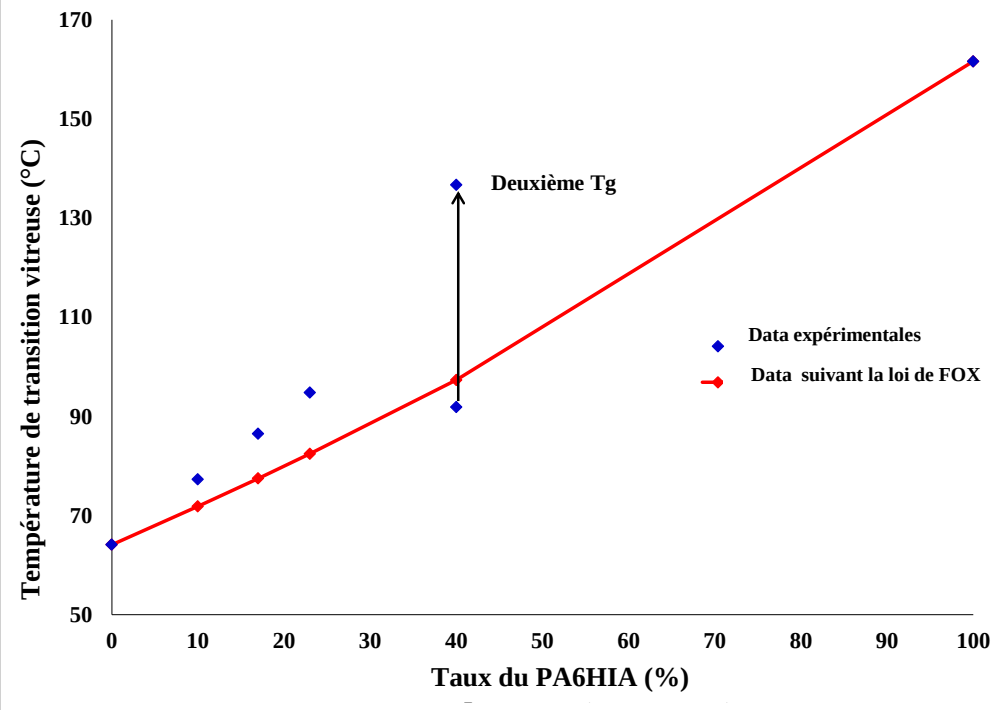

Figure 5: Evolution de la température de transition vitreuse avec le taux du 6HIA

Concernant la température de cristallisation et de fusion, on a observé que l'impact du taux de PA6HIA est plus significatif sur la température de cristallisation comme présentée sur la Figure 6. Il semble que l'aptitude de cristallisation des séquences PA66 est limitée par l'augmentation de la masse moléculaire et l'incorporation des noyaux phénoliques. Ceci apparait sous la forme d'une réduction de la température de cristallisation, surtout à forte teneur en PA6HIA. Toutefois, la fraction cristalline du PA66 ainsi que la morphologie cristalline (sphérolite, lamelle et maille cristalline) des copolymères contenant moins de 20% du PA6HIA est très proches de celle du PA66 de départ, comme l'a montré les analyses microscopique et diffractions de rayons X. Cela pourra explique la fiable décroissance de la température e fusion avec l'augmentation du taux de PA6HIA.

Dans la deuxième partie de ce chapitre, trois compositions of PA66/6HIA copolyamides ont été préparés à grande échelle à l'aide d'une extrudeuse double vis. Les conditions de mise en œuvre ont été adaptées pour mieux correspondre aux conditions expérimentales établies à petit échelle. La microstructure des copolymères obtenus a été caractérisée tout au long des étapes de préparation et comparée avec celle des copolyamides obtenus à petit échelle. Nous montrons que les conditions expérimentales établies à l'échelle du microcompoundeur sont bien transposable à grande échelle et que la microstructure et les propriétés thermiques des copolyamides obtenus sont comparables à ceux trouvés pour les copolymères prépares à petit échelle.

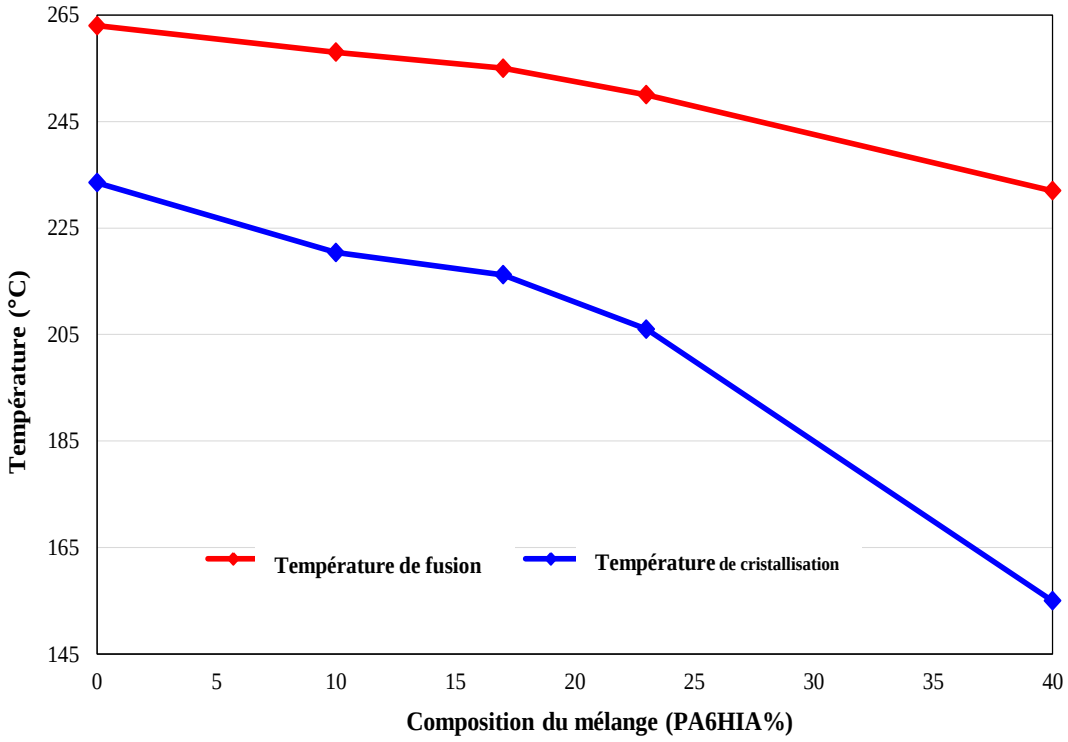

Figure 6: Variation de la température de cristallisation et de fusion en fonction du pourcentage du PA6HIA

Finalement, la rhéologie des copolyamides extrudés a été étudiée afin de trouver les conditions d'injections les plus appropriés pour injecter les pièces finales (barreaux choc et traction). Parallèlement, un autre PA66/6HIA copolyamide préparé par copolymérisation classique (i-PA66/6HIA (83/17 w:w)) et deux autres grades de PA66 (standard et HMw), considérés comme références, ont été étudiés. Les conditions d'injections (température, taux de cisaillement, vitesse d'injection…) ont été déterminées pour tous ces matériaux et rassemblés dans le Tableau 3.

Produit	Taux de cisaillement (s^{-1})	Débit volumique (cm^3/s)	Vitesse d'injection (cm/s)	Pression de maintien (bar)	Température de moule (°C)
PA66 (standard)	20400	60.1	8.5	580	80
PA66 (HMw)	27600	81.2	11.5	1032	80
m-PA66/6HIA (90/10 w:w)	36000	106	15	774	65
m- PA66/6HIA (83/17 w:w)	36000	106	15	645	62
i- PA66/6HIA (83/17 w:w)	23040	67.8	9.6	632	43
m- PA66/6HIA (77/23 w:w)	36000	150	15	929	58

Tableau 3: Paramètres d'injection à 280°C pour les PA66 et PA66/6HIA copolyamides

Chapitre IV : Impact de la microstructure sur les propriétés physique et mécaniques du PA66 et PA66/6HIA copolyamides

Dans ce chapitre on a abordé l'effet de l'introduction du 6HIA co-monomère sur les propriétés physique et mécanique du matériau. Six matériaux ont été considérés : 2 grades de PA66 (standard et HMw), trois copolyamides préparés par extrusion réactives (m-PA66/6HIA (90/10, 83/17 et 77/23) et un copolyamide préparé par in-situ co-polycondensation i-PA66/6HIA (83/17 w : w).

Dans la première partie, la microstructure ainsi que les propriétés physicochimiques des barreaux injectés de ces matériaux sont analysés. Tout d'abord, on observe qu'après injection la masse moléculaire des copolyamides extrudés a augmenté. Ceci est probablement dû à des réactions de polycondensation à l'état fondue soutenus par une teneur en eau très faible.

Les analyses MALDI-TOF mettent en évidences que les blocs de PA66 après injection restent suffisamment longs pour que les séquences de PA66 cristallisent. De plus, il s'avère que ces blocs ne sont pas beaucoup réduits après injection, supposant que peu de réactions de transamidification supplémentaires ont eu lieu pendant l'injection. L'analyse montre aussi que le copolyamide préparé par in-situ copolycondensation i-PA66/6HIA(83/17 w :w) présente une distribution aléatoire du co-monomère HIA tout au long de la chaîne du copolymère.

Figure 7 représente les thermogrammes de fusion et de cristallisation pour les sis matériaux injectés. On observe que l'augmentation de la masse moléculaire du PA66 (HMw PA66) induit une réduction de sa température de cristallisation et de fusion. Egalement, l'ajout du PA6HIA amorphe réduit ces deux températures. Il apparait que l'augmentation de la masse moléculaire et la présence du monomère HIA, particulièrement dans le cas du copolymère statistique, gène la cristallisation des séquences PA66 du copolyamide.

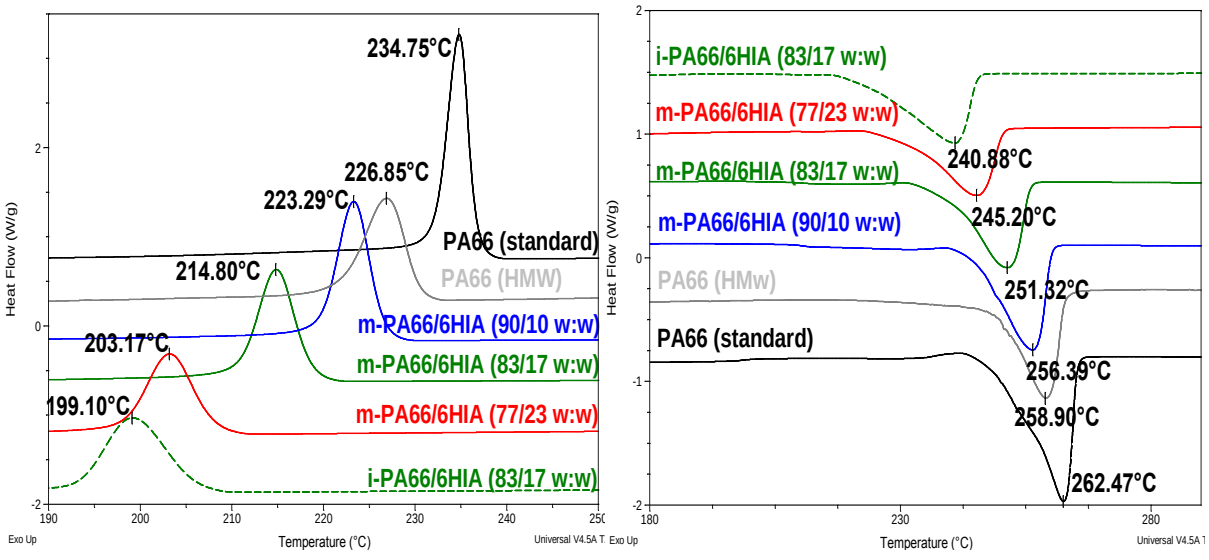

(a) **(b)**

Figure 7: Thermogrammes de fusion (a) et de cristallisation (b) déterminés par DSC sur les barreaux injectés

Toutefois le taux de cristallinité du PA66 (voir Figure 8) décroit avec l'augmentation de la masse moléculaire mais reste constante quel que soit le taux du monomère 6HIA ou la nature

du copolyamide. Il se peut que la longueur des chaînes affecte dans une certaine mesure le taux de cristallinité des segments cristallisable du PA66.

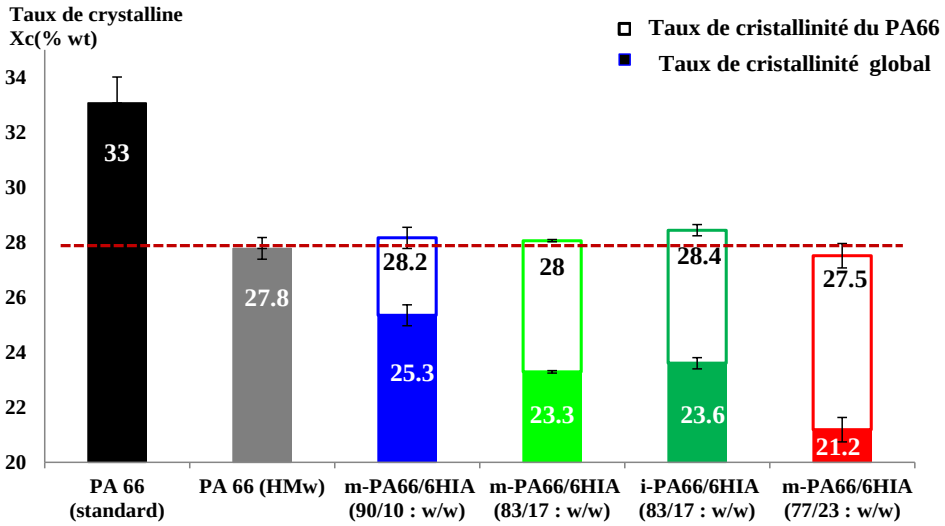

Figure 8 : Taux de cristallinité global et du PA66 (rapporté à la masse du PA66) déterminés par DSC sur les barreaux injectés

La morphologie cristalline des matériaux étudiés a été observée par microscopie optique à lumière croisée. Une réduction de la taille des sphérolites peut être notée dans le cas du HMw PA66 et des PA66/6HIA copolyamides. La structure cristalline a été examinée plus profondément par diffraction des rayons X aux petits et grands angles (SAXS et WAXD). On a observé que l'augmentation de la masse moléculaire induit une légère réduction de l'épaisseur de la lamelle cristalline et que cette réduction est d'autant plus importante avec la croissance du taux de co-monomère 6HIA. De plus, on a trouvé que la perfection cristalline des copolyamides bloc contenant 23 % 6HIA et celle du copolyamide statistique avec seulement 18 % du co-monomère 6HIA est fortement dégradée. En tenant compte de ces observations, une corrélation entre la température de fusion et l'épaisseur de lamelles cristalline a été établie et présentée sur la Figure 9.

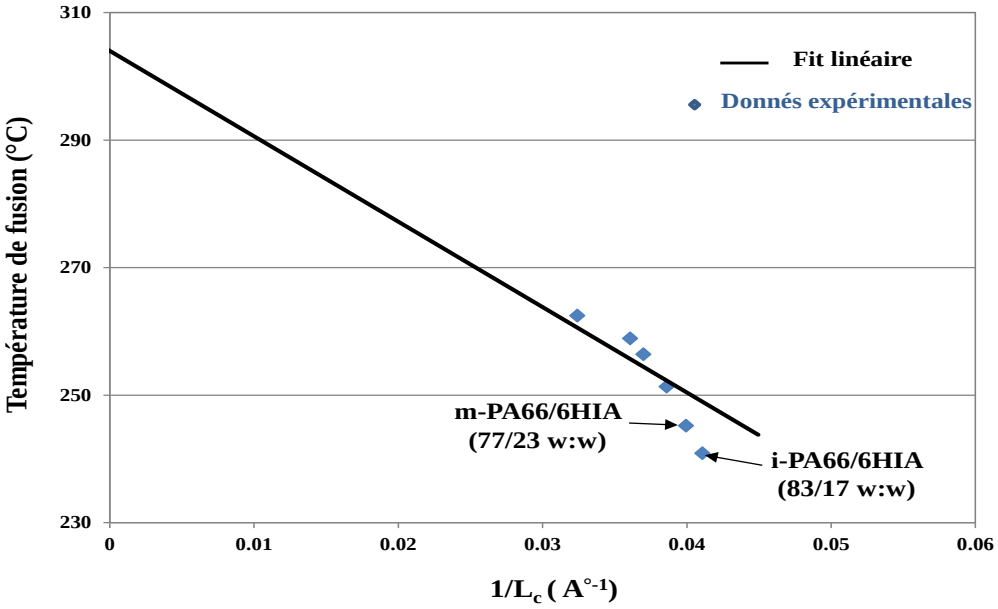

Figure 9: Relation entre la température de fusion et l'inverse de l'épaisseur de la lamelle cristalline

La cohésion de la phase amorphe des copolymères obtenus a été évaluée d'une façon indirecte via des mesures de température de transition vitreuse et des mesures de tension de surface. Il s'avère que l'énergie de cohésion de la phase amorphe augmente avec l'ajout du monomère 6HIA.

Dans la deuxième partie de ce chapitre, les propriétés mécaniques quasi-statiques et dynamiques de ces matériaux ont été étudiées. Il s'avère que le module élastique de ces matériaux est indépendant de la masse moléculaire et de l'ajout du 6HIA co-monomère, sauf dans le cas d'une répartition aléatoire de ce monomère où le module est clairement réduit. On a observé également que la contrainte seuil σ_y augmente avec l'ajout du monomère 6HIA. Une corrélation linéaire entre la contrainte d'écoulement et la mobilité de la phase amorphe est présentée sur la Figure 10.

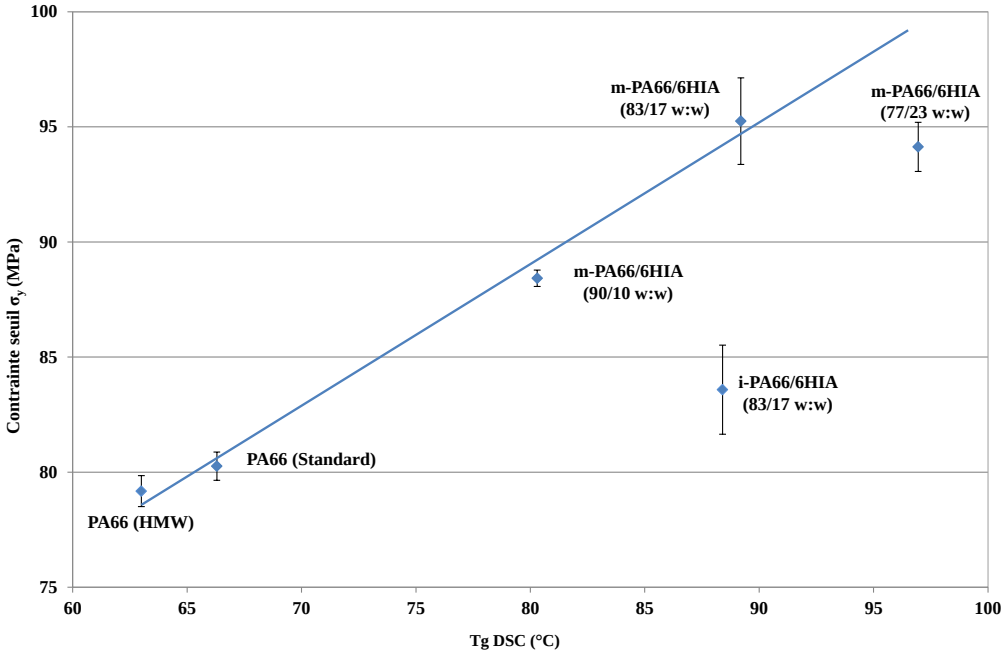

Figure 10: Relation entre la contrainte au seuil et la température de transition vitreuse déterminée par DSC

Nous nous sommes ensuite intéressés à l'analyse de 'écartement lamellaire sous une contrainte donnée. Nous avons observé que les lamelles situés dans l'équateur de la sphérolite (perpendiculairement à la direction de la force) sont les plus sollicitées. La quantification de la séparation lamellaire a été faite sur la base de la variation de la Longue période (ΔLp), calculé à partir du vecteur d'onde correspondant au maximum e diffraction de rayons X. Cette variation ΔLp rapportée à la Longue période initiale (sous contrainte nulle) est appelée déformation locale. Nous montrerons sur la Figure 11, l'évolution du facteur d'amplification, défini comme le rapport entre la déformation macroscopique appliquée et la déformation locale mesurée, en fonction du taux de cristallinité des matériaux étudiés.

On observe que l'ampliation est autour de 2 dans le polyamide PA66 standard, HMw et dans le copolyamide contenta 10 % du 6HIA. Cela signifie que l'équateur de la sphérolite est deux fois plus déformé que la totalité de l'échantillon. Ensuite, le facteur d'amplification augmente avec la chute de la cristallinité surtout à forte taux du 6HIA. Ceci indique que les copolyamides contenant un taux élevé du PA6IA sont les plus déformés localement.

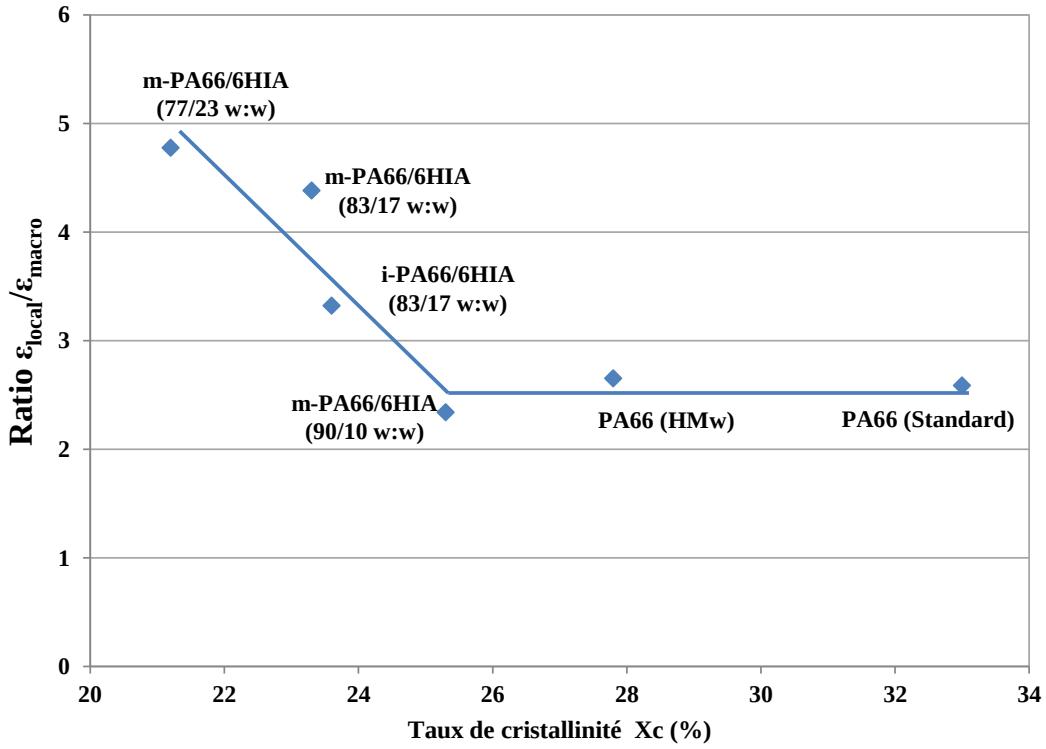

Figure 11: Variation du facteur d'amplification avec le taux de cristallinité global des matériaux étudiés

Concernant la résistance au choc de ces matériaux, une augmentation de la résilience à température ambiante par rapport au PA66 standard a été constatée dans le cas PA66/6HIA copolyamides. De plus une corrélation linéaire entre la $T_{F/D}$ et la Tg de ces matériaux a été identifiée, comme reporté dans la littérature.

Finalement, la tenue en fatigue de ces matériaux a été étudiée. Nous montrons que l'augmentation de la masse moléculaire du polyamide 66 permet d'améliorer sa résistance sous chargement cyclique. De plus nous mettons en évidence que les copolyamides bloc contenant moins de 23 % du PA6HIA présente une durée de vie fatigue nettement plus longue que celle du PA66 standard. Cette amélioration de durée de vie est attribuée d'une part à l'augmentation de la masse moléculaire et d'autre part à l'introduction des noyaux phénoliques offrant des interactions intermoléculaires très fortes.

Conclusion

Pour conclure, les fonctions HIA ont été correctement incorporées dans les chaînes du PA66 par voie d'extrusion réactive. La microstructure de ces matériaux a été bien caractérisée et comparée avec celle d'autres polyamides de référence. Les propriétés mécaniques de ces matériaux ont été évaluées et corrélées avec succès à la microstructure, particulièrement à la cohésion de la phase amorphe et aux caractéristiques de la phase cristalline. Pour résumer, on peut dire qu'on a réussi à augmenter la durabilité du polyamide 66 via le renforcement des interactions intermoléculaires dans sa phase amorphe. Il serait maintenant intéressant de développer de nouveaux matériaux avec d'autres fonctions offrant la possibilité de renforcer à la fois la phase amorphe et la phase cristalline. Cette étude pourra donc constituer une base pour le design de nouveaux matériaux présentant une microstructure contrôlée en fonction des propriétés visées.